8-2014

Spatial Dynamic Models for Fishery Management and Waterborne Disease Control

Michael Robert Kelly Jr.
University of Tennessee - Knoxville, mkelly14@vols.utk.edu

To the Graduate Council:

I am submitting herewith a dissertation written by Michael Robert Kelly Jr. entitled "Spatial Dynamic Models for Fishery Management and Waterborne Disease Control." I have examined the final electronic copy of this dissertation for form and content and recommend that it be accepted in partial fulfillment of the requirements for the degree of Doctor of Philosophy, with a major in Mathematics.

Suzanne Lenhart, Major Professor

We have read this dissertation and recommend its acceptance:

Lou Gross, Yulong Xing, Tuoc Phan

Accepted for the Council:
Dixie L. Thompson

Vice Provost and Dean of the Graduate School

(Original signatures are on file with official student records.)

8-2014

Spatial Dynamic Models for Fishery Management and Waterborne Disease Control

Michael Robert Kelly Jr.
University of Tennessee - Knoxville, mkelly14@vols.utk.edu

To the Graduate Council:

I am submitting herewith a dissertation written by Michael Robert Kelly Jr. entitled "Spatial Dynamic Models for Fishery Management and Waterborne Disease Control." I have examined the final electronic copy of this dissertation for form and content and recommend that it be accepted in partial fulfillment of the requirements for the degree of Doctor of Philosophy, with a major in Mathematics.

Suzanne Lenhart, Major Professor

We have read this dissertation and recommend its acceptance:

Lou Gross, Yulong Xing, Tuoc Phan

Accepted for the Council:
Carolyn R. Hodges

Vice Provost and Dean of the Graduate School

(Original signatures are on file with official student records.)

Spatial Dynamic Models for Fishery Management and Waterborne Disease Control

A Dissertation Presented for the

Doctor of Philosophy

Degree

The University of Tennessee, Knoxville

Michael Robert Kelly, Jr.

August 2014

I dedicate this dissertation and completion of the doctorate program to my parents, Michael and Linda Kelly. I will never be able to thank them enough for their support, love, and encouragement throughout my life. I would not be who I am today if not for their guidance, sacrifice, and care.

Acknowledgements

First and foremost, I must thank my advisor, Dr. Suzanne Lenhart. I cannot thank her enough for her encouragement over the years. With her countless hours and energy devoted to her students, her dedication to research, and her service to this university, she has inspired me greatly as a mathematician and a professor. I am grateful for her support and sound advice, without which this dissertation would not have been accomplished.

I would like to thank the other members of my committee, Dr. Lou Gross, Dr. Yulong Xing, and Dr. Tuoc Phan for their time in reviewing my work and for offering invaluable feedback. I would further like to thank Dr. Lou Gross and Dr. Yulong Xing for their advice and input over the years that has helped develop my research.

I would also like to thank my collaborators, Drs. Joseph Tien and Marisa Eisenberg for their input on my work. My project was motivated by, and is an extension of, the work they have conducted over the past several years. Their involvement has been indispensable.

I was supported during my graduate career by a teaching assistantship in the Department of Mathematics at the University of Tennessee and by a research assistantship with the National Institute for Mathematical and Biological Synthesis (NIMBioS). I am very grateful for the department and staff that has taught and supported me over the years. They have made my years at the university very enjoyable. I am also thankful for NIMBioS for the opportunities they have provided me in furthering my education and growing my love for mathematical ecology.

Abstract

As the human population continues to grow, there is a need for better management of our natural resources in order for our planet to be able to produce enough to sustain us. One important resource we must consider is marine fish populations. We use the tool of optimal control to investigate harvesting strategies for maximizing yield of a fish population in a heterogeneous, finite domain. We determine whether these solutions include no-take marine reserves as part of the optimal solution. The fishery stock is modeled using a nonlinear, parabolic partial differential equation with logistic growth, movement by diffusion and advection, and with Robin boundary conditions. The objective for the problem is to find the harvest rate that maximizes the discounted yield. Optimal harvesting strategies are found numerically.

Infectious diseases are another area of concern for the human population. Recently, questions have been raised as to the importance of spatial features on disease spread and how movement patterns affect management strategies. The role of spatial arrangements in a metapopulation on the spread and management strategies of a cholera epidemic is investigated. We consider how the movement of individuals and water affects the optimal vaccination strategy. For each metapopulation, the model has an Susceptible-Infected-Recovered (SIR) system of differential equations coupled with an equation modeling the concentration of *Vibrio cholerae* in an aquatic reservoir. The model is used to compare spatial arrangements and varying scenarios to draw conclusions on how to effectively manage outbreaks. The work is motivated by the recent cholera outbreak in Haiti.

Table of Contents

List of Tables

List of Figures

Chapter 1

Introduction

Mathematical models help us understand the dynamics of biological systems. The role of spatial features are important when building and analyzing models [61, 44, 45]. The motility of a species or pathogen could affect population dynamics and potentially alter management strategies. Spatial features can be introduced in mathematical models in varying ways. This dissertation includes metapopulation modeling using a system of ordinary differential equations (ODEs) in discrete space and a partial differential equation (PDE) to describe population dynamics in continuous space.

Within both systems, methods of management are modeled as control functions whose values affect the state differential equations. We formulate goals we hope to achieve that depend on the controls and corresponding states. We then use mathematical analyses and numerical simulations to find the optimal control that achieves the desired goals. We here introduce the two problems considered in this dissertation, the management of a natural resource and optimal intervention strategies in controlling a waterborne disease. Later, we provide a brief background on optimal control theory and its application to ordinary and partial differential equations.

1.1 Mathematical Models for Resource Management

As the human population continues to grow, there is need for better management of our natural resources in order for our planet to be able to produce enough to sustain us. One important resource we must consider is marine fish populations. Fisheries provide an important source of food to people across the world. However, many marine populations are severely overfished [29]. The overexploitation of fisheries has called for an improved understanding of spatiotemporal dynamics of resource stocks as well as their harvesters.

We investigate a nonlinear, parabolic partial differential equation (PDE) that models fish stock on a heterogeneous spatial domain. We extend previous work by Joshi *et al.* [31] by incorporating an alternative boundary condition to represent a more realistic habitat. The fishery stock is modeled on a multidimensional, smooth, bounded domain $Q = \Omega \times (0, T)$ with Robin boundary conditions:

$$u_t = \sum_{i,j=1}^{n} (a_{ij}(x,t)u_{x_i})_{x_j} + \sum_{i=1}^{n} b_i(x,t)u_{x_i} + f(u) - h(x,t)u \qquad \Omega \times (0,T) \tag{1.1}$$

$$\frac{\partial u}{\partial \nu}(x,t) + qu(x,t) = 0 \qquad \partial\Omega \times (0,T) \tag{1.2}$$

and initial condition:

$$u(x,0) = u_0(x) \qquad x \in \Omega \tag{1.3}$$

where $u(x,t)$ is the fish stock density. The conormal derivative is given by $\frac{\partial u}{\partial \nu} = \nabla_x u \cdot \nu$ with $\nu = (\nu_1, ...\nu_n)$ and $\nu_i = \sum_{j=1}^{n} a_{ij}(x,t)\eta_j$, with η_j being the outward normal unit vector. The nonlinear growth term is given by $f(u)$ and $h(x,t)$ is the harvest rate. The diffusion and advection coefficients are heterogenous functions of space and time, $a_{ij}(x,t)$ and $b_i(x,t)$, respectively.

We investigate yield maximizing strategies and whether these solutions contain no-take marine reserves, or areas that prohibit fishing effort. We investigate how the boundary

condition, together with the advection and diffusion coefficients, affect optimal harvesting strategies.

1.2 Metapopulaton Model for Waterborne Diseases

Infectious diseases create a terrible burden on society, which can be devastating both in terms of deaths and cost. Waterborne diseases are a major concern worldwide [50]. For the purpose of this project, we classify a waterborne disease as one where transmission by water is possible. Although there are many known waterborne diseases, we focus our study on cholera, which is caused by infection of the intestine with the aquatic bacterium, *Vibrio cholerae*.

Human movement has influenced the spread of infectious disease by bringing more people into contact with the pathogen. Waterborne diseases are a bigger threat since both human and water movement contribute to disease spread. When an outbreak occurs, there is a need to find intervention strategies that control the disease while also optimizing resources available. This strategy needs to consider the effect of population and pathogen movement. We seek to answer the question of how the spatial arrangement of populations, waterway connectivity, and movement patterns affect dynamics and intervention strategies in disease outbreaks.

We extend the Susceptible-Infected-Recovered-Water (SIRW) ordinary differential equation model of Tien and Earn [59], to a metapopulation with both human and pathogen mobility. We use connectivity matrices to account for movement. Also, because of the potential for high mortality rates, we include a death due to disease term. There are varying intervention strategies to consider in attempts to control waterborne disease outbreaks. For cholera, three common approaches are vaccination, sanitation, and the provision of clean water [46]. For this project, we consider vaccination as the only intervention. There are several reasons for this including the short timeframe of an epidemic and the cost of vaccination compared to the other options.

We investigate the following SIRW model, for patches $i = 1, \ldots, n$, with vaccination terms $v_i(t)S_i$ moving susceptible individuals immediately to the recovered class:

$$\frac{dS_i}{dt} = \mu_i N_i - \beta_I^i S_i I_i - \beta_W^i S_i w_i - \mu_i S_i + d_S \sum_{k=1}^{n}(M_{ik}S_k - M_{ki}S_i) - v_i(t)S_i \quad (1.4)$$

$$\frac{dI_i}{dt} = \beta_I^i S_i I_i + \beta_W^i S_i w_i - (\gamma_i + \mu_i + \delta_i)I_i + d_I \sum_{k=1}^{n}(M_{ik}I_k - M_{ki}I_i) \quad (1.5)$$

$$\frac{dR_i}{dt} = \gamma_i I_i - \mu_i R_i + d_R \sum_{k=1}^{n}(M_{ik}R_k - M_{ki}R_i) + v_i(t)S_i \quad (1.6)$$

$$\frac{dW_i}{dt} = \xi_i[I_i - W_i] + d_W \sum_{k=1}^{n}(H_{ik}W_k - H_{ki}W_i) - \phi_i W_i \quad (1.7)$$

with some initial conditions and on a finite time interval. The model includes compartments for pathogen in the aquatic reservoir. The model also includes two modes of transmission of the disease: transmission from person-person contact and from contact with the water compartment. They are referred to as direct (fast) and indirect (slow) transmission. The structure of the connectivity matrices, $M = \{M_{ij}\}$ and $H = \{H_{ij}\}$, representing human and water movement, respectively, determines the spatial arrangements of the model. The goal of the project is to characterize the control that minimizes the number of infected individuals in the network and the cost of the intervention strategy over some finite time period.

1.3 Optimal Control Theory

Optimal control theory is an approach to solving dynamic optimization problems. An optimal control problem consists of an objective that is constrained by a system of state equations, whose dynamics are captured by variables influenced by control functions. The state system can have deterministic or stochastic dynamics of various types. The control variables can be adjusted in the system to achieve the desired objective. See [39] for a detailed introduction to optimal control theory, especially with application to biological problems. We will discuss the theory when applied to ordinary differential equations and partial differential equations.

1.3.1 Optimal Control Theory of Ordinary Differential Equations

Along with the state system, we have an objective functional, which is typically an integral expression formulated in terms of the state and control variable. We seek to find the optimal control, with corresponding states, that achieve the maximum/minimum of the objective functional. When the dynamics of the system are modeled by ordinary differential equations (ODEs), we will use Pontryagin's Maximum Principle [52] to find the necessary conditions for the optimal control problem. Pontryagin and his collaborators developed the theory for ordinary differential equations around 1950. They developed the idea of introducing adjoint functions, which attach the differential equations to the objective functional. We assume our controls are in a subset of Lebesgue measurable functions.

Pontryagin's Maximum Principle (PMP) converts the problem of maximizing (or minimizing) the objective functional subject to the state ODEs with initial conditions to the problem of maximizing (or minimizing) the Hamiltonian pointwise with respect to the controls. To use PMP, the existence of an optimal control and corresponding states must be proven.

The characterization of the control will be in terms of the optimal states and adjoint functions. In many biological applications, there will be bounds on the controls [1, 34]. The optimality system for the problem includes the state equations, adjoint equations, and control characterization. Often, solutions to the optimality system cannot be be solved explicitly so numerical approximations are used. Numerical methods for approximating solutions are discussed in Section 1.4.

1.3.2 Optimal Control Theory of Partial Differential Equations

Although a full generalization of Pontryagin's Maximum Principle does not exist for problems of infinite dimensions, there are aspects of the techniques used in the principle that can be applied to systems of partial differential equations. The book by Li and Yong [41] gives results on PMP for specific types of second order partial differential equations (PDEs).

Starting with a state PDE with initial conditions, boundary conditions, and control terms, we choose an appropriate weak solution space and control set. An objective functional is chosen depending on the goal desired. After formulating the weak solution to our state PDE, the existence and uniqueness of the solution to the state equations, given a control, are proven. In our work, the existence and boundedness of a state solution is obtained through an iteration scheme.

For our work on a parabolic PDE, we use a maximizing sequence argument, continuous dependence of the state on the control, and *a priori* estimates on state solutions to prove the existence of an optimal control. To obtain the necessary conditions for the optimal control, the objective functional is differentiated with respect to the control. Since the objective functional usually contains the state variable, the state must first be differentiated with respect to the control. We call this derivative the sensitivity function, which solves the linearized version of the state equation.

We use the sensitivity PDE with its initial and boundary conditions to find the adjoint PDE and final time condition. The right-hand side of the adjoint equation is found from the derivative of the integrand of the objective functional with respect to the state variable. Lastly, the characterization of the control is formulated by differentiating the objective functional with respect to the control and using the relationship between the sensitivity and adjoint equations. As in the ODE case, the optimality system consists of the state equation, adjoint equation, and the control characterization. The uniqueness of the solution to the optimality system, which gives uniqueness of the optimal control, can be shown for sufficiently small time. Exact solutions to the optimality system usually cannot be solved explicitly, so numerical approximation to solutions are found to illustrate various scenarios. Details on the numerical methods used are found in Section 1.4.

1.4 Numerical Approximations to Solutions

Approximate solutions to the optimality system are obtained using numerical methods. The optimality system, with initial conditions for the state equations and final time conditions for the adjoint equations, is solved using an iteration method. Due to the structure of the optimality system, a forward-backward sweep method is used to solve the systems. See Hackbusch for convergence of this method [26]. For systems of ODEs, we use a fourth-order Runge Kutta method to solve the state and adjoint systems. For systems of PDEs, we use an explicit finite difference method with appropriate unwinding schemes for first order time derivatives. An Euler method is used for the time derivative while a first order upwind scheme is used for first spacial derivatives. The methods and schemes used are described in detail in [30] and in Appendix A.

An iterative forward-backward sweep method [39] is described below:

1. Initiate a guess for the control variable.

2. The state system, given the initial conditions, is solved forward in time, using either the Runge Kutta method or finite-difference method.

3. The state solutions found, as well as the final time conditions, are used to solve the adjoint system backward in time, again using either a Runge Kuta or finite-difference method.

4. The control variable is then updated using a convex combination of the previous value and the new value determined using the control characterization.

5. Steps 1-4 are repeated until successive values of all states, adjoints, and control(s) are sufficiently close, i.e. there is convergence of the optimality system.

Convergence is checked using the relative errors of the optimality system, shown in the relation:

$$\frac{||\mathbf{v} - \mathbf{v}_{old}||}{||\mathbf{v}||} \leq \epsilon$$

where ϵ is the accepted tolerance, $\mathbf{v}$ is the vector of current state, adjoint, or control values, $\mathbf{v}_{old}$ is the vector of values from the previous iteration, and $||\cdot||$ is the sum of the absolute values of the components of the vector.

Chapter 2

Optimal fish harvesting for a population modeled by a nonlinear parabolic partial differential equation

2.1 Background

There is growing concern over natural resource management and how best to use resources to sustain the world's growing population. An important resource to consider is fisheries, which are a source of food for people across the globe. However, many marine populations are severely overfished [29].

In addition to the overexploitation of fish stock, there are threats of habitat degradation and destruction, pollution, and climate change impacts affecting the world's oceans [47, 29]. Researchers must understand what is necessary for assuring a stable supply of fish under environmental stressors of various kinds, while also considering the impact of human behavior on the environment [31]. This is a difficult task given the large variability associated with fishery ecosystems yet there is continual pressure to find methods for optimally solving these management problems.

There has been work investigating various ways to help restore fish populations and protect marine ecosystems, such as time-area closures, limiting the fishing season, as well as the implementation of catch quotas. Another way to help protect fish populations from overexploitation is the inclusion of no-take marine reserves. These reserves are categorized as areas of the ocean completely protected: removal or destruction of natural resources is prohibited [29]. They offer protection for both marine fish populations and the ecosystems of which they are a part.

The establishment of no-take reserves is beginning to receive more attention on the global scale. The total amount of ocean set as marine protected areas (MPAs) has risen by over 150% since 2003. However, only 1.17% of the marine area of the world is protected as MPAs and only a small portion of MPA coverage is designated as fully protected, no-take areas [62]. This may be because marine reserves are a controversial fishery management tool. Some believe that no-take marine reserves actually reduce the yield [14, 66].

The spatial structure of a renewable natural resource is important to consider when determining management strategies. Spatial heterogeneity and dynamics can affect management outcomes. When spatial dynamics of a resource are ignored, management strategies generally produce suboptimal results [28]. There have been many approaches to modeling spatial dynamics. Early harvesting models involving bioeconomics and optimal yield were done using ordinary differential equations. Clark's work provided a foundation for using optimal control theory as a tool in fishery management [15, 16].

Metapopulation models are a common spatial modeling approach, which divides the environment into a collection of patches. Tuck and Possingham used coupled spatially-explicit difference equations to model a single-species, two-patch metapopulation. They considered the problem of optimally exploiting the single species local population that is connected by dispersing larvae to an unharvested second population [63]. They showed that the closed areas had positive net benefits in terms of both stock abundance and economic rents.

Sanchirico and Wilen studied a series of differential equation metapopulation models with logistic growth and density-dependent dispersal between patches coupled with a spatially

explicit harvesting model [56, 55]. They investigated different scenarios, exploring the impacts of a reserve on biomass and effort distribution. Results showed that, under certain conditions, reserves increase both stock abundance and harvest effort [55]. Brown and Roughgarden formulated an optimal control problem for maximizing the discounted profit, using a metapopulation ODE model (continuous in time, discrete in space) for an age-structured fish stock. Their results demonstrate that closed patches can be part of the optimal solution [11].

There have been studies that sought yield maximizing strategies without imposing no-take reserves in the model. Neubert investigated the steady-states of a fish stock in a spatially explicit harvesting model, ignoring the dependence of the stock on time [47]. His model is a second order ODE in space. The benefits of using a spatially explicit model include a more realistic marine reserve in a fixed area of space through which fish move, rather than a fixed harvesting rate across the domain. His objective functional sought to find the fishing effort that maximizes the yield. His model did not incorporate reserves into the model yet they were shown to be part of the resulting optimal harvesting strategy (depending on the length of domain). Neubert also found "chattering" in the optimal control in some cases, which are infinite sequences of reserves alternating with areas of intense fishing.

Ding and Lenhart [19] extended Neubert's work to a multidimensional spatial domain, considering different types of objective functionals. They sought to find an optimal fishery harvesting strategy with fish stock modeled by a semilinear elliptic partial differential equation with Dirichlet boundary conditions. One of their objective functionals was similar to that of Neubert but considered the difference between the yield and a nonlinear cost. Ding and Lenhart [19] also included the minimization of the variation in the control (with H^1 controls) to avoid "chattering." Both functionals result in a reserve as part of the optimal harvesting strategy.

DeLeenheer also investigated a steady-state, parabolic PDE model, rewritten as a system of two first-order ODEs, to address the problem of where exactly to establish marine protected areas (MPA) [36]. His objective involved maximizing fishing yield as well as fish densities.

His results concluded that the location of the MPA was determined by the length of spatial domain and average fish density. This work also did not investigate the role of time in the model.

To include time-varying scenarios, Joshi *et al.* [31] built a nonlinear parabolic PDE model for the growth, movement and harvesting of a renewable resource. This work considered yield maximizing solutions, but in a dynamic fishery system, investigating the spatiotemporal distribution of harvesting effort and the existence of no-take marine reserves that arose as part of the harvesting strategy. Their non-steady state equation also included an advection term. This work was concerned not only with the existence of reserves, but the time of their establishment and the evolution of its size over time.

The PDE models of Joshi *et al.*, Ding and Lenhart, and Neubert [31, 19, 47] for optimal fish harvesting had Dirichlet boundary conditions, representing a lethal domain boundary. This would occur if you had a habitat imbedded into a larger, uninhabitable region. Although many fisheries are not found in such conditions, the impact of alternative boundary conditions was not addressed. Most fisheries occur on open ocean where these artificial boundaries do not exist. The implementation of an alternative type of boundary condition, Robin boundary conditions, deemed more favorable to the fish stock by acting as a resource constraint, could produce an alternative optimal harvesting strategy.

Optimal control of parabolic PDEs with Robin boundary conditions has been successfully used for other applications. Previous work on these boundary conditions was done by Lenhart and Wilson [38] in investigating optimal control of a heat transfer equation with a convective boundary condition. There has also been work done with these boundary conditions in biological applications. Lenhart and collaborators [37] considered boundary habitat hostile in a parabolic system of interacting species, using Robin boundary conditions. We extend the application to fisheries.

Ocean environments are subject to varying currents throughout space and time. In numerical simulations with constant advection, Joshi *et al.* [31] concluded that the location

of reserves shifted in the opposite direction of advection of the fish stock. We will include non-constant advection terms in our numerical simulations to compare results.

Modeling these dynamic systems can help predict the impact of fishing regulations. A heterogenous, spatiotemporal domain with more realistic boundary conditions will help to model the habitat and the fish movement and gain important insights on optimal harvesting strategies. These models provide guidance that could help make decisions to improve our marine resources without compromising the economic yield.

In the next section, we formulate the problem in an appropriate weak solution space and describe the spatiotemporal model for the fish stock and assumptions. We then prove existence and uniqueness of our state solution using an iteration scheme and *a priori* estimates. The proof for the existence of an optimal control is given. Next, we derive the optimality system consisting of the state system coupled with the adjoint system and an optimal control characterization. We prove the uniqueness of the optimality system, guaranteeing the uniqueness of the optimal control solution. Finally, we illustrate some examples by approximating our solutions using numerical methods, and give some conclusions.

2.2 Problem Formulation

The focus of the project is on optimal harvesting strategies of a fish population in a heterogeneous, finite domain. We develop resource management strategies, specifically yield-maximizing solutions, and determine whether these solutions include no-take marine reserves as part of the optimal solution.

The fishery stock is modeled using a nonlinear, parabolic partial differential equation with both diffusion and advection on a multidimensional, smooth, bounded domain $Q = \Omega \times (0, T)$

with Robin boundary conditions:

$$u_t = \sum_{i,j=1}^{n} (a_{ij}(x,t)u_{x_i})_{x_j} + \sum_{i=1}^{n} b_i(x,t)u_{x_i} + f(u) - h(x,t)u \qquad \Omega \times (0,T) \tag{2.1}$$

$$\frac{\partial u}{\partial \nu}(x,t) + qu(x,t) = 0 \qquad \partial\Omega \times (0,T) \tag{2.2}$$

and initial condition:

$$u(x,0) = u_0(x) \qquad x \in \Omega \tag{2.3}$$

where $u(x,t)$ is the fish stock density. The conormal derivative is given by $\frac{\partial u}{\partial \nu} = \nabla_x u \cdot \nu$ with $\nu = (\nu_1, ...\nu_n)$ and $\nu_i = \sum_{j=1}^{n} a_{ij}(x,t)\eta_j$, with η_j being the outward normal unit vector. The nonlinear growth term is given by $f(u)$ and $h(x,t)$ is the harvest rate. The diffusion and advection coefficients are heterogenous functions and given by $a_{ij}(x,t)$ and $b_i(x,t)$, respectively. Also, the initial population $u_0(x) \in L^\infty(\Omega)$ is nonnegative. For this application, our spatial domain Ω is a smooth, bounded open set in $\mathbb{R}^n$, $n = 1, 2,$ or 3, although the theorems are true for multidimensional domains for any integer $n \geq 1$. The Robin boundary condition constant, q, is nonnegative.

Movement of the fish stock is modeled using diffusion and advection. Diffusion forces the stock to not congregate to one centralized area, while advection accounts for currents and drifts in the domain. Robin boundary conditions, where the flux at the boundary is proportional to the stock density at the boundary, are more favorable to the fish stock than Dirichlet boundary conditions, which represent a lethal domain surrounding our spatial domain. We investigate population dynamics with logistic growth. The goal for our problem will be to find the harvest rate, $h(x,t)$, that maximizes the discounted yield. Let P be the price constant, which we will set to $P = 1$, and think of the J as money. The objective functional is:

$$J(h) = \int_0^T \int_\Omega P e^{-\mu t} hu \; dxdt, \tag{2.4}$$

which is maximized over the set of admissible controls:

$$\mathcal{H} = \{h \in L^\infty(Q) \ : 0 \leq h(x,t) \leq h_{max}\}.$$

Given $h \in \mathcal{H}$, we denote by $u = u(h)$, the corresponding state solution, with the state u satisfying (2.1)-(2.3). We make the following assumptions:

1. Uniform ellipticity on the diffusion coefficient:
   There exists $\theta > 0$ such that

$$\theta \sum_{i=1}^{n} \xi_i^2 \leq \sum_{i,j=1}^{n} a_{ij}(x,t)\xi_i\xi_j \quad \text{for all } (x,t) \in Q,\ \xi \in \mathcal{R}^n.$$

2. Symmetry in the diffusion coefficients:

$$a_{ij} = a_{ji} \qquad \text{for} \quad i,j = 1,\ldots,n.$$

3. Bounded coefficients:

$$a_{ij}, b_i \in C^1(\bar{Q}) \ \text{ for all } \quad i,j = 1,\ldots,n.$$

4. The growth term can be written as $f(u) = ug(u)$ where $g \in C^1(\mathbb{R})$ for all $u \geq 0$.

5. There exists $r > 0$ such that $r \geq g(u)$ for all $u \geq 0$.

6. For $M > 0$, there exists $C_1 > 0$ such that for $0 \leq u \leq M$, $g(u) \geq -C_1$

7. For $0 \leq u \leq M$, there exists C_2 such that $f'(u) \geq -C_2$.

8. The Robin boundary condition constant, q, is nonnegative.

9. The discount factor, μ, is a nonnegative constant.

10. The initial condition $u_0(x) \in L^\infty$ and is nonnegative.

Remark 2.0.1. *Two examples of $f(u)$ functions that satisfy the above assumptions are*

$$f(u) = ru\left(1 - \frac{u}{K}\right),$$

where $r \geq 0$ is the growth rate and $K \geq 0$ is the carrying capacity of the population, and

$$f(u) = ru(1-u)(u-a),$$

with $0 < a < 1$.

2.3 Existence of an Optimal Control

The underlying solution space for our state system is given by $V = L^2((0,T); H^1(\Omega))$ and the dual space for the time derivative of the solution is given by $V^* = L^2((0,T); H^1(\Omega)^*)$.

Definition 2.0.1. *The function $u \in V$ with $u_t \in V^*$ is a weak solution to our problem (2.1)-(2.3) if:*

$$\begin{aligned}\int_0^T \langle u_t, \phi\rangle \, dt = \int_Q (f(u) - hu)\phi \, dxdt - \int_Q \sum_{i,j=1}^n a_{ij}(x,t) u_{x_i}\phi_{x_j} \, dxdt \\ - \int_{\partial\Omega\times(0,T)} qu\phi \, dsdt + \int_Q \sum_{i=1}^n b_i(x,t) u_{x_i}\phi \, dxdt\end{aligned} \tag{2.5}$$

for all test functions $\phi \in V$, where $\langle \ , \rangle$ is the duality between $(H^1(\Omega))^*$ and $H^1(\Omega)$ and $u(x,0) = u_0(x)$ for $x \in \Omega$.

Remark 2.0.2. *Since $u \in V$ and $u_t \in V^*$, due to the results of Evans [22],*

$$u \in C([0,T]; L^2(\Omega)),$$

and the initial condition makes sense in $L^2(\Omega)$.

To find the weak solution format to our system, we formally begin by multiplying the state equation by a test function $\phi \in V$ and integrating over the domain, Q:

$$\int_0^T \langle u_t, \phi \rangle \, dt = \int_Q (f(u) - hu)\phi \, dxdt + \int_Q \sum_{i,j=1}^n (a_{ij}(x,t)u_{x_i})_{x_j}\phi \, dxdt + \int_Q \sum_{i=1}^n b_i(x,t)u_{x_i}\phi \, dxdt$$

for all test functions $\phi \in V$. Integration by parts gives,

$$\begin{aligned}
\int_Q \sum_{i,j=1}^n \left(a_{ij}(x,t)u_{x_i}\right)_{x_j} \phi \, dxdt &= -\int_Q \sum_{i,j=1}^n a_{ij}(x,t)u_{x_i}\phi_{x_j} \, dxdt \\
&\quad + \int_{\partial\Omega\times(0,T)} \sum_{i=1}^n \left(\sum_{j=1}^n a_{ij}(x,t)\eta_j \right) u_{x_i}\phi \, dsdt \\
&= -\int_Q \sum_{i,j=1}^n a_{ij}(x,t)u_{x_i}\phi_{x_j} \, dxdt + \int_{\partial\Omega\times(0,T)} \frac{\partial u}{\partial \nu}\phi \, dsdt \\
&= -\int_Q \sum_{i,j=1}^n a_{ij}(x,t)u_{x_i}\phi_{x_j} \, dxdt - \int_{\partial\Omega\times(0,T)} qu\phi \, dsdt
\end{aligned}$$

using the Robin boundary conditions. When we show existence of weak solutions, we will verify that the terms, $\int_Q f(u)\phi \, dxdt$, $\int_Q hu\phi \, dxdt$, are finite.

2.3.1 A Priori Estimates

We first show *a priori* estimates that will be used in the proofs of theorems for existence and positivity of the state solution.

Theorem 2.1. *Suppose* $u \in V$ *with* $u_t \in V^*$ *is a weak solution of (2.1)-(2.3) corresponding to control* $h \in \mathcal{H}$*, and* $u \geq 0$ *a.e. in* Q*. Then there exists positive constants,* K_1,K_2*, and* K_3*,*

such that $\forall h \in \mathcal{H}$,

$$||u(h)||_V \leq K_1 \tag{2.6}$$

$$||(u(h))_t||_{V^*} \leq K_2 \tag{2.7}$$

$$\int_{\partial\Omega\times(0,T)} u^2 \, dsdt \leq K_3. \tag{2.8}$$

Proof. Using u as the test function in the weak formulation on $Q_s = \Omega \times (0, s)$:

$$\begin{aligned} \int_{(0,s)} \langle u_t, u\rangle \, dt + \int_{Q_s} \sum_{i,j=1}^{n} a_{ij}(x,t) u_{x_i} u_{x_j} \, dxdt + \int_{\partial\Omega\times(0,s)} qu^2 \, dsdt \\ = \int_{Q_s} (f(u) - hu)u \, dxdt + \int_{Q_s} \sum_{i=1}^{n} b_i(x,t) u_{x_i} u \, dxdt. \end{aligned} \tag{2.9}$$

Using $hu^2 \geq 0$, we get the inequality:

$$\begin{aligned} \int_{(0,s)} \langle u_t, u\rangle \, dt + \int_{Q_s} \sum_{i,j=1}^{n} a_{ij}(x,t) u_{x_i} u_{x_j} \, dxdt + \int_{\partial\Omega\times(0,s)} qu^2 \, dsdt \\ \leq \int_{Q_s} f(u)u \, dxdt + \int_{Q_s} \sum_{i=1}^{n} b_i(x,t) u_{x_i} u \, dxdt. \end{aligned}$$

By uniform ellipticity on the diffusion coefficients, we have the following:

$$\begin{aligned} \int_{(0,s)} \langle u_t, u\rangle \, dt + \theta \int_{Q_s} \sum_{i=1}^{n} (u_{x_i})^2 \, dxdt + \int_{\partial\Omega\times(0,s)} qu^2 \, dsdt \\ \leq \int_{Q_s} f(u)u \, dxdt + \int_{Q_s} \sum_{i=1}^{n} b_i(x,t) u_{x_i} u \, dxdt. \end{aligned}$$

We can rewrite the time derivative term

$$\int_{(0,s)} \langle u_t, u\rangle \, dt = \frac{1}{2} \int_{Q_s} \frac{d}{dt} u^2 \, dxdt$$

which gives:

$$\frac{1}{2}\int_{Q_s}\frac{d}{dt}u^2\,dxdt = \frac{1}{2}\int_{\Omega\times\{s\}}u^2(x,s)\,dx - \frac{1}{2}\int_{\Omega\times\{0\}}u^2(x,0)\,dx.$$

Then we have the following, using our initial conditions:

$$\begin{aligned}&\frac{1}{2}\int_{\Omega\times\{s\}}u^2(x,s)\,dx + \theta\int_{Q_s}\sum_{i=1}^{n}(u_{x_i})^2\,dxdt + \int_{\partial\Omega\times(0,s)}qu^2\,dsdt\\ &\leq \int_{Q_s}f(u)u\,dxdt + \int_{Q_s}\sum_{i=1}^{n}b_i(x,t)u_{x_i}u\,dxdt + \frac{1}{2}\int_{\Omega}u_0^2(x)\,dx.\end{aligned}$$

Using Cauchy's Inequality, we can rewrite the inequality:

$$\begin{aligned}&\frac{1}{2}\int_{\Omega\times\{s\}}u^2(x,s)\,dx + \theta\int_{Q_s}\sum_{i=1}^{n}(u_{x_i})^2\,dxdt + \int_{\partial\Omega\times(0,s)}qu^2\,dsdt\\ \leq \int_{Q_s}f(u)u\,dxdt + C_{\theta,b}\int_{Q_s}u^2\,dxdt + \frac{\theta}{2}\int_{Q_s}\sum_{i=1}^{n}(u_{x_i})^2\,dxdt + \frac{1}{2}\int_{\Omega}u_0^2(x)\,dx\end{aligned}$$

where $C_{\theta,b}$ depends on θ and the advection coefficients. The structure assumption on $f(u)$ gives us:

$$\begin{aligned}&\int_{\Omega\times\{s\}}u^2(x,s)\,dx + \theta\int_{Q_s}\sum_{i=1}^{n}(u_{x_i})^2\,dxdt + 2\int_{\partial\Omega\times(0,s)}qu^2\,dsdt\\ &\leq 2\int_{Q_s}g(u)u^2\,dxdt + 2C_{\theta,b}\int_{Q_s}u^2\,dxdt + \int_{\Omega}u_0^2(x)\,dx.\end{aligned}$$

After rewriting and using assumption (5),

$$\begin{aligned}&\int_{\Omega\times\{s\}}u^2(x,s)\,dx + \theta\int_{Q_s}\sum_{i=1}^{n}(u_{x_i})^2\,dxdt + 2\int_{\partial\Omega\times(0,T)}qu^2\,dsdt\\ &\leq 2(C_g + C_{\theta,b})\int_{Q_s}u^2\,dxdt + \int_{\Omega}u_0^2(x)\,dx.\end{aligned}\tag{2.10}$$

Using $q \geq 0$, we have:

$$\int_{\Omega\times\{s\}} u^2(x,s)\,dx \leq 2(C_g + C_{\epsilon,b})\int_{Q_s} u^2\,dxdt + \int_\Omega u_0^2(x)\,dx.$$

Let $\xi(s) = \int_{\Omega\times\{s\}} u^2(x,s)\,dx$ and we obtain:

$$\xi(s) \leq G_1 \int_0^s \xi(\tau)d\tau + G_2$$

where $G_1 = 2(C_g + C_{\theta,b})$ and $G_2 = \int_\Omega u_0^2(x)dx = ||u_0||^2_{L^2(\Omega)}$, which is bounded by assumptions. Then by Gronwall's Inequality,

$$\xi(s) \leq ||u_0||^2_{L^2(\Omega)}(1 + G_1 e^{G_1 s}s).$$

Taking the maximum over time, we obtain the following:

$$\max_{0\leq t\leq T} ||u(\cdot,t)||_{L^2(\Omega)} \leq ||u_0||^2_{L^2(\Omega)}(1 + G_1 e^{G_1 T}T). \tag{2.11}$$

Using $\hat{G} = ||u_0||^2_{L^2(\Omega)}(1 + G_1 e^{G_1 T}T)$ in (2.10), we have:

$$\begin{aligned}\theta\int_Q \sum_{i=1}^n (u_{x_i})^2\,dxdt + 2\int_{\partial\Omega\times(0,T)} qu^2\,dsdt \\ \leq 2T(C_g + C_{\theta,b})\hat{G} + \int_\Omega u_0^2(x)\,dx\end{aligned} \tag{2.12}$$

Combining (2.11) and (2.12) gives the estimate of $||u(h)||_V$. This estimate gives estimate (2.8) by a trace result in the spatial derivatives.

For the time-derivative estimate, we start with the PDE:

$$u_t = f(u) - hu + \sum_{i,j=1}^n (a_{ij}(x,t)u_{x_i})_{x_j} + \sum_{i=1}^n b_i(x,t)u_{x_i}$$

By the previous estimate, the right-hand-side of the PDE is bounded in $L^2((0,T);H^1(\Omega)^*)$. Given our assumptions on $f(u)$, every term on the right hand side is in L^2 or is the derivative of an L^2 function. Thus we have the right hand side of the PDE bounded in the dual space, which implies

$$||u_t||_{V^*} \leq K_2.$$

□

2.3.2 Existence and Positivity of the State Solution

To carefully formulate our problem, we first must prove the existence of a state solution, i.e. given a control, h, there exists a state solution $u = u(h)$, showing the dependence on h. Also, we need to prove that there exists a C such that $0 \leq u(h) \leq C$, for all $h \in \mathcal{H}$. Since the controls are bounded above and below, we are able to get corresponding bounds in our solution space for our state, u. We will prove existence and obtain bounds for our state solution using an iteration scheme.

Theorem 2.2. *There exists a supersolution, U, being the solution of the problem:*

$$U_t - \sum_{i,j=1}^{n} (a_{ij}(x,t)U_{x_i})_{x_j} - \sum_{i=1}^{n} b_i(x,t)U_{x_i} = rU \qquad \Omega \times (0,T) \tag{2.13}$$

$$\frac{\partial U}{\partial \nu}(x,t) + qU(x,t) = 0 \qquad \partial\Omega \times (0,T) \tag{2.14}$$

$$U(x,0) = u_0(x) \qquad x \in \Omega \tag{2.15}$$

such that

$$0 \leq U(x,t) \leq ||u_0||_{L^\infty} e^{\lambda t} \tag{2.16}$$

for all $(x,t) \in Q$, where λ is a constant such that $\lambda > r$.

Proof. Let $\lambda > r > 0$. By Evans [22], there exists a classical solution U to (2.13)-(2.15). Let $v = Ue^{-\lambda t}$. Then, we can rewrite the PDE in terms of v:

$$\begin{aligned} v_t - \sum_{i,j=1}^{n} (a_{ij}(x,t)v_{x_i})_{x_j} - \sum_{i=1}^{n} b_i(x,t)v_{x_i} + (\lambda - r)v = 0 \qquad & \Omega \times (0,T) \\ \frac{\partial v}{\partial \nu}(x,t) + qv(x,t) = 0 \qquad & \partial\Omega \times (0,T) \\ v(x,0) = u_0(x) \qquad & x \in \Omega \end{aligned}$$

Claim 2.2.1. *The solution v satisfies*

$$0 \leq v \leq ||u_0||_{L^\infty}.$$

1. Suppose there exists a positive maximum of v at $(x_1, t_1) \in \bar{Q}$.

   Case 1: $(x_1, t_1) \in Q$

   Since $0 < t_1 < T$ and v is maximized at (x_1, t_1), $v_t = 0$ and $v_{x_i} = 0$ at that point. We can rewrite the term, $\sum_{i,j}(a_{ij}v_{x_i})_{x_j}$, using a product rule:

   $$\sum_{i,j}(a_{ij}v_{x_i})_{x_j} = \sum_{i,j} a_{ij}v_{x_ix_j} + \sum_{i,j}(a_{ij})_{x_j}v_{x_i}.$$

   Through a linear change in spatial variables, the matrix $(a_{i,j})$ can be diagonalized with positive entries on diagonal at the point (x_1, t_1), which give the non-positivity of the first term. The second term at (x_1, t_1) is zero due to the first derivative terms. Thus $-\sum(a_{ij}v_{x_i})_{x_j} \geq 0$ at (x_1, t_1). Since $(\lambda - r) > 0$ and $v(x_1, t_1) > 0$, by assumptions on λ, we have:

   $$v_t - \sum_{i,j=1}^{n} (a_{ij}(x,t)v_{x_i})_{x_j} - \sum_{i=1}^{n} b_i(x,t)v_{x_i} + (\lambda - r)v > 0 \text{ at } (x_1, t_1)$$

which leads to a contradiction of the PDE.

Case 2: $(x_1, t_1) \in \Omega \times \{t = 0\}$

Then the maximum would occur at the initial condition, i.e.

$$v(x_1, 0) = u_0(x_1) \leq ||u_0||_{L^\infty}$$

Case 3: $(x_1, t_1) \in \Omega \times \{t = T\}$

From Protter and Wienberger [53], if the maximum occurred at the final time, then in order to have:

$$v_t - \sum_{i,j=1}^{n} (a_{ij}(x,t)v_{x_i})_{x_j} - \sum_{i=1}^{n} b_i(x,t)v_{x_i} + (\lambda - r)v = 0$$

we need $v_t < 0$, since a similar argument as in Case 1 can show that the sum of the other three terms is positive. That would mean that the function v is strictly decreasing in time, so the maximum could not occur at the final time. Thus, the case fails.

Case 4: $(x_1, t_1) \in \partial\Omega \times (0, T)$

Using

$$\frac{\partial v}{\partial \nu}(x,t) + qv(x,t) = 0 \qquad\qquad \partial\Omega \times (0,T)$$

and that $\frac{\partial v}{\partial \nu}(x,t) \geq 0$ at a maximum on the boundary, we have $qv \leq 0$ there. Since $q > 0$ and $v > 0$ at (x_1, t_1), we have a contradiction.

Thus, we have an upper bound on v, i.e.

$$v(x,t) \leq ||u_0||_{L^\infty}$$

2. Suppose there exists a negative minimum of v at $(x_1, t_1) \in \bar{Q}$. We can rewrite our equation using $(-v)$:

$$(-v)_t - \sum_{i,j=1}^{n} (a_{ij}(x,t)(-v)_{x_i})_{x_j} - \sum_{i=1}^{n} b_i(x,t)(-v)_{x_i} + (\lambda - r)(-v) = 0,$$

with initial condition and boundary condition:

$$-v(x,0) = -u_0(x) \text{ and } \frac{\partial(-v)}{\partial \eta} + q(-v) = 0.$$

Using a similar approach as before, we can show that a positive maximum of $(-v)$ satisfies

$$\max(-v) \leq \max(-u_0, 0) = 0.$$

Thus we have a lower bound on v, i.e.

$$v \geq 0$$

The bounds on v,

$$0 \leq v \leq ||u_0||_{L^\infty},$$

give bounds on the supersolution:

$$0 \leq U(x,t) \leq ||u_0||_{L^\infty} e^{\lambda t}.$$

□

Next, to obtain the existence of the state solution, we use an iteration method.

Theorem 2.3. *Given a control $h \in \mathcal{H}$, there exists a unique, weak solution u to (2.1)-(2.3) satisfying*

$$0 \leq u(x,t) \leq U(x,t)$$

a.e. on Q, where U is the supersolution from Theorem 2.1

Proof. From Theorem 2.1, we have bounds on the supersolution, found from maximum principle arguments:

$$0 \leq U(x,t) \leq ||u_0||_{L^\infty} e^{\lambda t}.$$

We initiate an iteration scheme, letting $u^1 = U$, and then use a PDE linear in u^i at each step. Then building the iteration scheme [22, 42], there exists a weak solution u^i for i = 2,3,... such that

$$u_t^i - \sum_{i,j=1}^{n} (a_{ij}(x,t)u_{x_i}^i)_{x_j} - \sum_{i=1}^{n} b_i(x,t)u_{x_i}^i + Ru^i = G(u^{i-1})$$

with the boundary and initial conditions (2.2)-(2.3),

$$\frac{\partial u^i}{\partial \nu} + qu^i = 0$$

$$u^i(x,0) = u_0(x),$$

where $R > h_{max} + C_1 + C_2$, where C_1, C_2 are the bounds from our assumptions, $g(u) \geq -C_1$ for $u \geq 0$, $f'(u) \geq -C_2$, and $G(u^{i-1}) = Ru^{i-1} + f(u^{i-1}) - hu^{i-1}$.

Claim 2.3.1. *For i=1,2,3...,*

$$0 \leq u^i \leq U.$$

We show the claim by induction, and for i=1,

$$0 \leq u^1 = U \leq U.$$

Assume $0 \leq u^j \leq U$, $1 \leq j \leq i-1$ for some $i > 1$.

By choice of R, we have $R \geq h - g(u^{i-1})$. Thus, for u^i,

$$\begin{aligned} u_t^i - \sum_{i,j=1}^{n} (a_{ij}(x,t)u_{x_i}^i)_{x_j} - \sum_{i=1}^{n} b_i(x,t)u_{x_i}^i + Ru^i &= G(u^{i-1}) \\ &= Ru^{i-1} + g(u^{i-1})u^{i-1} - hu^{i-1} \\ &= u^{i-1}(R + g(u^{i-1}) - h) \\ &\geq 0. \end{aligned}$$

Thus, by induction and the parabolic maximum principle for weak solutions [35]

$$u^i \geq 0 \quad \text{for all } i.$$

We then need to show the upper bound on u^i, i.e. $u^i \leq U$. We do so again by induction. First, we must show $u_2 \leq u_1$. We use the equations:

$$\begin{aligned} u_t^2 - \sum_{i,j=1}^{n} (a_{ij}(x,t)u_{x_i}^2)_{x_j} - \sum_{i=1}^{n} b_i(x,t)u_{x_i}^2 + Ru^2 &= Ru^1 + f(u^1) - hu^1 \\ u_t^1 - \sum_{i,j=1}^{n} (a_{ij}(x,t)u_{x_i}^1)_{x_j} - \sum_{i=1}^{n} b_i(x,t)u_{x_i}^1 + Ru^1 &= Ru^1 + ru^1 \end{aligned}$$

where $u^1 = U$, the supersolution. Forming the difference between the equations and by the assumptions on $g(u)$ and the fact that $u^1, h \geq 0$, we have

$$\begin{aligned} (u_t^1 - u_t^2) - \sum_{i,j=1}^{n} (a_{ij}(x,t)(u_{x_i}^1 - u_{x_i}^2))_{x_j} - \sum_{i=1}^{n} b_i(x,t)(u_{x_i}^1 - u_{x_i}^2) + R(u^1 - u^2) \\ = u^1(r - g(u^1)) + hu^1 \geq 0, \end{aligned}$$

giving $u^1 \geq u^2$ on Q.

Now, we assume $u^j \leq U$ for all $1 \leq j \leq i-1$ for some $i > 1$. Then we must show $u^i \leq U$. Again, we consider the equations,

$$\begin{aligned} u_t^i - \sum_{i,j=1}^{n} (a_{ij}(x,t)u_{x_i}^i)_{x_j} - \sum_{i=1}^{n} b_i(x,t)u_{x_i}^i + Ru^i &= Ru^{i-1} + f(u^{i-1}) - hu^{i-1} \\ u_t^1 - \sum_{i,j=1}^{n} (a_{ij}(x,t)u_{x_i}^1)_{x_j} - \sum_{i=1}^{n} b_i(x,t)u_{x_i}^1 + Ru^1 &= Ru^1 + ru^1 \end{aligned}$$

where $u^1 = U$, the supersolution. Using the difference:

$$\begin{aligned} (u_t^1 - u_t^i) - \sum_{i,j=1}^{n} (a_{ij}(x,t)(u_{x_i}^1 - u_{x_i}^i))_{x_j} - \sum_{i=1}^{n} b_i(x,t)(u_{x_i}^1 - u_{x_i}^i) + R(u^1 - u^i) \\ = R(u^1 - u^{i-1}) + ru^1 - g(u^{i-1})u^{i-1} + hu^{i-1}, \end{aligned}$$

and again using assumption (5), we have

$$\begin{aligned} R(u^1 - u^{i-1}) + ru^1 - g(u^{i-1})u^{i-1} + h(u^{i-1}) \\ \geq R(u^1 - u^{i-1}) + r(u^1 - u^{i-1}) + hu^{i-1}. \end{aligned}$$

By assumptions, we have $u^1 - u^{i-1} \geq 0$ as well as $R, h, r \geq 0$ and $u^{i-1} \geq 0$, which gives

$$\begin{aligned} (u_t^1 - u_t^i) - \sum_{i,j=1}^{n} (a_{ij}(x,t)(u_{x_i}^1 - u_{x_i}^i))_{x_j} - \sum_{i=1}^{n} b_i(x,t)(u_{x_i}^1 - u_{x_i}^i) + R(u^1 - u^i) \\ = R(u^1 - u^{i-1}) + ru^1 - g(u^{i-1})u^{i-1} + hu^{i-1} \\ \geq 0. \end{aligned}$$

Thus, by the maximum principle, we have:

$$u^1 - u^i \geq 0,$$

which implies

$$0 \leq u^i \leq U \leq ||u_0||_{L^\infty} e^{\lambda t}.$$

Claim 2.3.2. *By our choice of R, for $i = 1, 2, ...$, $G(u^{i-1})$ is monotone increasing in u^{i-1}.*

We have chosen R such that,

$$\begin{aligned} \frac{\partial G}{\partial u^{i-1}} &= R + f'(u^{i-1}) - h \\ &\geq R - C_2 - h \\ &> 0. \end{aligned}$$

We now must show that for any $i = 1, 2, ...$, we have $u^{i+1} \leq u^i$.

Claim 2.3.3. *The state sequence has a monotone property, i.e. $u^{i+1} \leq u^i$.*

We have already shown above that $u^2 \leq u^1$. Again, we use induction as well as the fact that $G(u^{i-1})$ is monotone increasing in u^{i-1} to prove this claim.
Our hypothesis is that $u^i \leq u^{i-1}$. We then use the equations:

$$\begin{aligned} u_t^i - \sum_{i,j=1}^{n} (a_{ij}(x,t)u_{x_i}^i)_{x_j} - \sum_{i=1}^{n} b_i(x,t)u_{x_i}^i + Ru^i &= G(u^{i-1}) \\ u_t^{i+1} - \sum_{i,j=1}^{n} (a_{ij}(x,t)u_{x_i}^{i+1})_{x_j} - \sum_{i=1}^{n} b_i(x,t)u_{x_i}^{i+1} + Ru^{i+1} &= G(u^i) \quad . \end{aligned}$$

Forming the difference, we have

$$\begin{aligned} (u_t^i - u_t^{i+1}) - \sum_{i,j=1}^{n} (a_{ij}(x,t)(u_{x_i}^i - u_{x_i}^{i+1})_{x_j} - \sum_{i=1}^{n} b_i(x,t)(u_{x_i}^i - u_{x_i}^{i+1}) + R(u^i - u^{i+1}) \\ = G(u^{i-1}) - G(u^i) \geq 0 \end{aligned}$$

since $G(u^i)$ is a monotone increasing function. By induction, $u^{i+1} \leq u^i$.

Lastly, using the *a priori* bounds from Theorem 2.1 on u^i,

$$||u^i||_V \leq K_1 \text{ and } ||u_t^i||_V^* \leq K_2,$$

and the monotone property, we have weak convergence on the sequences (not just on subsequences):

$$u^n \rightharpoonup u \text{ in } L^2(Q) \tag{2.17}$$

$$u_t^n \rightharpoonup u_t \text{ in } L^2(Q). \tag{2.18}$$

By trace results [22],

$$u^i \rightharpoonup u \text{ in } L^2(\partial\Omega \times (0,T)). \tag{2.19}$$

This weak convergence gives

$$\lim_{i\to\infty} \int_Q hu^i\phi \, dxdt = \int_Q hu\phi \, dxdt,$$

since $h\phi \in L^2(Q)$ since h is bounded and $\phi \in L^2(Q)$. Using the result of Simon [58] and the monotone property of u, we obtain the strong convergence,

$$u^i \to u \text{ in } L^2(Q) \tag{2.20}$$

on the sequence, which gives

$$\lim_{i\to\infty} \int_Q f(u^i)\phi \, dxdt = \int_Q f(u)\phi \, dxdt$$

since f is continuous and $u^i \to u$ pointwise a.e. Lastly, by (2.19), we have

$$\lim_{i\to\infty} \int_{\partial\Omega\times(0,T)} qu^i\phi \, dsdt = \int_{\partial\Omega\times(0,T)} qu\phi \, dsdt.$$

Then, passing the limit in the weak formulation of the PDE, we obtain:

$$\begin{aligned}\int_0^T \langle u_t, \phi\rangle \, dt = \int_Q (f(u) - hu)\phi \, dxdt + \int_Q \sum_{i,j=1}^n (a_{ij}(x,t)u_{x_i})_{x_j}\phi \, dxdt \\ - \int_{\partial\Omega\times(0,T)} qu\phi \, dsdt + \int_Q \sum_{i=1}^n b_i(x,t)u_{x_i}\phi \, dxdt.\end{aligned}$$

We conclude that u is a weak solution of (2.1)-(2.3).

To show that the state solution is unique, let $u, \bar{u}$ be solutions to the weak formulation, (2.5), with initial conditions:

$$u(x,0) = \bar{u}(x,0) = u_0(x).$$

Multiplying each formulation by the test function, $u - \bar{u}$, then taking the difference, we have

$$\begin{aligned}\int_0^s \langle u_t - \bar{u}_t, u - \bar{u}\rangle \, dt \quad + \quad & \int_{\Omega\times(0,s)} \sum_{i,j=1}^n a_{ij}(x,t)\,(u-\bar{u})_{x_i}\,(u-\bar{u})_{x_j} \; dxdt \\ & + \int_{\partial\Omega\times(0,s)} q(u-\bar{u})^2 \, dsdt \\ = \quad & \int_{\Omega\times(0,s)} f(u-\bar{u})(u-\bar{u}) \, dxdt - \int_{\Omega\times(0,s)} h(u-\bar{u})^2 \, dxdt \\ & + \int_{\Omega\times(0,s)} \sum_{i=1}^n b_i(x,t)\,(u-\bar{u})_{x_i}\,(u-\bar{u}) \, dxdt.\end{aligned}$$

Using a similar method as in the *a priori* estimates of Theorem 2.1, and rearranging terms, we have:

$$\begin{aligned}\frac{1}{2}\int_{\Omega\times\{s\}}(u-\bar{u})^2\,dx \;+\; & \int_{\Omega\times(0,s)}\sum_{i,j=1}^{n}a_{ij}(x,t)\,(u-\bar{u})_{x_i}\,(u-\bar{u})_{x_j}\;dxdt \\ & +\int_{\partial\Omega\times(0,s)}q(u-\bar{u})^2\,dsdt \\ = & \int_{\Omega\times(0,s)}f(u-\bar{u})(u-\bar{u})\,dxdt-\int_{\Omega\times(0,s)}h(u-\bar{u})^2\,dxdt \\ & +\int_{\Omega\times(0,s)}\sum_{i=1}^{n}b_i(x,t)\,(u-\bar{u})_{x_i}\,(u-\bar{u})\,dxdt.\end{aligned}$$

By assumption (1), we have:

$$\begin{aligned}&\frac{1}{2}\int_{\Omega\times\{s\}}(u-\bar{u})^2\;dx+\theta\int_{\Omega\times(0,s)}\sum_{i=1}^{n}(u-\bar{u})_{x_i}^2\;dxdt+\int_{\partial\Omega\times(0,s)}q(u-\bar{u})^2\,dsdt \\ &\leq\int_{\Omega\times(0,s)}f(u-\bar{u})(u-\bar{u})\,dxdt+\int_{\Omega\times(0,s)}\sum_{i=1}^{n}b_i(x,t)\,(u-\bar{u})_{x_i}\,(u-\bar{u})\,dxdt.\end{aligned}$$

Using Cauchy's inequality, we have:

$$\begin{aligned}&\frac{1}{2}\int_{\Omega\times\{s\}}(u-\bar{u})^2\;dx+\theta\int_{\Omega\times(0,s)}\sum_{i=1}^{n}(u-\bar{u})_{x_i}^2\;dxdt+\int_{\partial\Omega\times(0,s)}q(u-\bar{u})^2\,dsdt \\ \leq&\int_{\Omega\times(0,s)}f(u-\bar{u})(u-\bar{u})\,dxdt+C_{\theta,b}\int_{\Omega\times(0,s)}(u-\bar{u})^2\;dxdt+\frac{\theta}{2}\int_{\Omega\times(0,s)}\sum_{i=1}^{n}(u-\bar{u})_{x_i}^2\;dxdt.\end{aligned}$$

Using assumptions (4) and (5), rearranging terms and multiplying the entire equation by a value of 2, gives:

$$\begin{aligned}&\int_{\Omega\times\{s\}}(u-\bar{u})^2\;dx+\theta\int_{\Omega\times(0,s)}\sum_{i=1}^{n}(u-\bar{u})_{x_i}^2\;dxdt+2\int_{\partial\Omega\times(0,s)}q(u-\bar{u})^2\,dsdt \\ &\qquad\leq\int_{\Omega\times(0,s)}2\left(C_g+C_{\theta,b}\right)(u-\bar{u})^2\,dxdt.\end{aligned}$$

In Gronwall's Inequality, let $\xi(s) = \int_{\Omega\times\{s\}} (u-\bar{u})^2 (x,s)\, dx$ and we obtain:

$$\xi(s) \leq G_1 \int_0^s \xi(\tau) d\tau$$

where $G_1 = 2(C_g + C_{\theta,b})$. Then

$$\xi(s) \leq G_1 e^{G_1 s} ||u_0 - u_0||^2_{L^2(\Omega)} = 0.$$

Taking the maximum over time, we obtain:

$$\max_{0\leq t\leq T} ||(u-\bar{u})(\cdot,t)||_{L^2(\Omega)} \leq 0, \tag{2.21}$$

which implies $u(x,t) = \bar{u}(x,t)$.

□

Now, having existence, uniqueness, and estimates for our state solution, we will now prove the existence of an optimal control for our problem.

Theorem 2.4. *There exists an optimal control, $h^* \in \mathcal{H}$, satisfying*

$$J(h^*) = \sup_{h\in\mathcal{H}} J(h).$$

Proof. Note, from estimates (2.6)-(2.7), $\sup_{h\in\mathcal{H}} J(h)$ is finite. We can choose a maximizing sequence, $\{h^n\}$ in $\mathcal{H}$ such that

$$\lim_{n\to\infty} J(h^n) = \sup_{h\in\mathcal{H}} J(h).$$

By the *a priori* estimates (2.6)-(2.8), there also exists functions $h^* \in \mathcal{H}$ and $u^* \in V$ such that, on a subsequence:

$$h^n \rightharpoonup h^* \quad \text{weakly in} \quad L^2(Q) \tag{2.22}$$

$$u^n \rightharpoonup u^* \quad \text{weakly in} \quad V = L^2((0,T); H^1(\Omega)) \tag{2.23}$$

$$u^n \rightharpoonup u^* \quad \text{weakly in} \quad L^2((0,T), L^2(\partial\Omega)) \tag{2.24}$$

$$u_t^n \rightharpoonup u_t^* \quad \text{weakly in} \quad V^* = L^2((0,T); H^1(\Omega)^*). \tag{2.25}$$

By a result of Simon [58]:

$$u^n \to u^* \quad \text{strongly in} \quad L^2(Q). \tag{2.26}$$

We now need to show that $u^* = u(h^*)$, such that,

$$u_t^* = f(u^*) - h^*(x,t)u^* + \sum_{i,j=1}^{n} (a_{ij}(x,t)u_{x_i}^*)_{x_j} + \sum_{i=1}^{n} b_i(x,t)u_{x_i}^*. \tag{2.27}$$

We will use the fact that we have L^∞ bounds on the controls and corresponding states. We have the PDE (2.1) for the subsequence, u^n:

$$u_t^n = f(u^n) - h^n(x,t)u^n + \sum_{i,j=1}^{n} (a_{ij}(x,t)u_{x_i}^n)_{x_j} + \sum_{i=1}^{n} b_i(x,t)u_{x_i}^n. \tag{2.28}$$

We will show that each term in the PDE for u^n and h^n converges to the corresponding term with u^* and h^*.

1. By assumption, the diffusion coefficients, $a_{ij}(x,t)$, are bounded and since $\phi \in V$, its first spatial derivatives exist and are in $L^2(Q)$. From *a priori* estimates above, $u_{x_i}^n \rightharpoonup u_{x_i}^*$ weakly in $L^2(Q)$, giving

$$-\int_Q \sum_{i,j=1}^{n} a_{ij}(x,t)(u_{x_i}^n - u_{x_i}^*)\phi_{x_j}\, dxdt \to 0.$$

2. Similarly, with assumptions on the boundedness of the advection coefficients, $b_i(x,t)$, and $\phi \in V$, we have
$$\int_Q \sum_{i=1}^{n} b_i(x,t)(u^n_{x_i} - u^*_{x_i})\phi \, dxdt \to 0.$$

3. By (2.26), we know u^n converges pointwise a.e. Since f is continuous, we have $f(u^n) \to f(u^*)$ pointwise. Thus,
$$\int_Q (f(u^n) - f(u^*))\phi \, dxdt \to 0.$$

4. Using the weak convergence, (2.24), with $q\phi \in L^2(\partial\Omega \times (0,T))$,
$$\left| \int_{\partial\Omega\times(0,T)} q(u^n - u^*)\phi \, dsdt \right| \to 0.$$

5. By assumptions, we know the h^n sequence and u^* are bounded in L^∞. By adding and subtracting terms, we have the following:
$$\begin{aligned} \left| \int_Q (h^n u^n \phi - h^* u^* \phi) \, dxdt \right| &= \left| \int_Q (h^n u^n \phi + h^n u^* \phi - h^n u^* \phi - h^* u^* \phi \, dxdt \right| \\ &\leq \left| \int_Q (h^n (u^n - u^*)\phi \, dxdt \right| + \left| \int_Q (h^n - h^*) u^* \phi \, dxdt \right| \\ &\leq \int_Q |h^n||u^n - u^*||\phi| \, dxdt + \left| \int_Q (h^n - h^*) u^* \phi \, dxdt \right| \to 0. \end{aligned} \tag{2.29}$$

For the first term in (2.29), the convergence (2.26) and Cauchy's Inequality give
$$\int_Q |h^n||u^n - u^*||\phi| \, dxdt \leq C \left(\int_Q |u^n - u^*|^2 \, dxdt \right)^{1/2} \left(\int_Q \phi^2 \, dxdt \right)^{1/2} \to 0.$$

For the second term, since u^* is bounded in L^∞ by results above and $\phi \in V \subset L^2(Q)$, the product $u^*\phi \in L^2(Q)$. The weak convergence of $\{h^n\}$ gives
$$\left| \int_Q (h^n - h^*) u^* \phi \, dxdt \right| \to 0.$$

Using the above results, we conclude that

$$u^* = u(h^*).$$

Now, looking at the objective functional (2.4), by our choice of maximizing sequence, we have:

$$\sup_h J(h) = \lim_{n\to\infty} J(h^n) = \lim_{n\to\infty} \int_0^T \int_\Omega e^{-\mu t} h^n u^n \, dxdt.$$

From convergences (2.22) and (2.26), we have

$$\lim_{n\to\infty} \int_0^T \int_\Omega e^{-\mu t} h^n u^n \, dxdt = \int_0^T \int_\Omega e^{-\mu t} h^* u^* \, dxdt = J(h^*),$$

and hence h^* is an optimal control. □

2.4 Derivation of the Optimality System

We want to derive the optimality system which consists of the state system coupled with the adjoint system and an optimal control characterization. We will need to differentiate the map $h \to J(h)$ to obtain our control characterization. Since u is involved in $J(h)$, we first differentiate the map $h \to u$.

Theorem 2.5. *Let h^* be an optimal control with corresponding state, u^*, and $h^\epsilon = h^* + \epsilon l$ be another control, where $\epsilon > 0$ and $l \in L^\infty(Q)$ is a variation function. The mapping $h \to u(h) \in V$ is weakly differentiable in the directional derivative sense:*
$\exists\, \psi \in V$ and $\psi_t \in V^*$ such that

$$\lim_{\epsilon\to 0^+} \frac{u(h^* + \epsilon l) - u(h^*)}{\epsilon} = \psi(x,t)$$

weakly in V for any $h \in \mathcal{H}$. Then the sensitivity function ψ corresponding to the control satisfies:

$$\psi_t = f'(u^*)\psi - h^*\psi + \sum_{i,j=1}^{n}(a_{ij}(x,t)\psi_{x_i})_{x_j} + \sum_{i=1}^{n} b_i(x,t)\psi_{x_i} - lu^* \qquad \Omega \times (0,T) \tag{2.30}$$

$$\frac{\partial \psi}{\partial \nu} + q\psi = 0 \qquad \partial\Omega \times (0,T) \tag{2.31}$$

$$\psi(x,0) = 0 \qquad \Omega \times \{t = 0\}. \tag{2.32}$$

Proof. Let $u^\epsilon = u(h^\epsilon)$ where $h^\epsilon = h^* + \epsilon l$ and $u^* = u(h^*)$ where h^* is an optimal control, with the corresponding PDEs

$$u_t^\epsilon = f(u^\epsilon) - (h^* + \epsilon l)u^\epsilon + \sum_{i,j=1}^{n}(a_{ij}(x,t)u_{x_i}^\epsilon)_{x_j} + \sum_{i=1}^{n} b_i(x,t)u_{x_i}^\epsilon \tag{2.33}$$

$$u_t^* = f(u^*) - h^*u^* + \sum_{i,j=1}^{n}(a_{ij}(x,t)u_{x_i}^*)_{x_j} + \sum_{i=1}^{n} b_i(x,t)u_{x_i}^*. \tag{2.34}$$

Subtracting equations (2.33)-(2.34) and dividing by ϵ, we get:

$$\frac{u_t^\epsilon - u_t^*}{\epsilon} = \frac{f(u^\epsilon) - f(u^*)}{\epsilon} - h\left(\frac{u^\epsilon - u^*}{\epsilon}\right) + \sum_{i,j=1}^{n}\left(a_{ij}(x,t)\left(\frac{u_{x_i}^\epsilon - u_{x_i}^*}{\epsilon}\right)\right)_{x_j} + \sum_{i=1}^{n} b_i(x,t)\left(\frac{u_{x_i}^\epsilon - u_{x_i}^*}{\epsilon}\right) - \frac{\epsilon l u^\epsilon}{\epsilon}.$$

By the techniques of Theorem 2.1 applied to the difference quotient in Theorem 2.5, we have boundedness of the difference quotients, the existence of ψ, and the corresponding convergence of difference quotients. For the nonlinear term, we see that, as $\epsilon \to 0$,

$$\frac{f(u^\epsilon) - f(u^*)}{\epsilon} = \frac{f(u^\epsilon) - f(u^*)}{u^\epsilon - u^*}\frac{u^\epsilon - u^*}{\epsilon} \to f'(u^*)\psi$$

using the result that $u^\epsilon \to u^*$ in $L^2(Q)$. Thus, with the convergence of each of the above difference quotients, the sensitivity ψ satisfies in the weak sense:

$$\psi_t = f'(u^*)\psi - h^*\psi + \sum_{i,j=1}^{n}(a_{ij}(x,t)\psi_{x_i})_{x_j} + \sum_{i=1}^{n} b_i(x,t)\psi_{x_i} - lu^* \qquad \Omega \times (0,T)$$

$$a\frac{\partial \psi}{\partial \eta} + q\psi = 0 \qquad \partial\Omega \times (0,T)$$

$$\psi(x,0) = 0 \qquad \Omega \times \{t=0\}.$$

The sensitivity PDE has the same initial and boundary conditions as the original PDE. □

Next, we use our adjoint function to characterize our optimal control. We rewrite the sensitivity PDE (2.30) as:

$$L\psi = -lu^*,$$

where L is the operator:

$$L\psi = \psi_t - f'(u^*)\psi - \sum_{i,j=1}^{n}(a_{ij}(x,t)\psi_{x_i})_{x_j} - \sum_{i=1}^{n} b_i(x,t)\psi_{x_i} + h^*\psi.$$

The adjoint operator L^* is related to the operator L by the following L^2 operator duality:

$$< \lambda, L\psi > = < L^*\lambda, \psi > .$$

To use $L\psi$ to get an expression for $L^*\lambda$, the adjoint operator, formally we write

$$\int_0^T \int_\Omega e^{-\mu t} h^*\psi \, dxdt = \int_0^T \int_\Omega e^{-\mu t} L^*\lambda\psi \, dxdt = \int_0^T \int_\Omega e^{-\mu t}\lambda L\psi \, dxdt.$$

We introduce the transversality condition for the adjoint function:

$$\lambda(x,T) = 0 \quad \text{on} \quad \Omega \times \{t=T\}. \tag{2.35}$$

Formally, we consider

$$\begin{aligned}\int_Q e^{-\mu t}\lambda L\psi \, dxdt &= \int_Q e^{-\mu t}\lambda\Bigg(\psi_t - f'(u^*)\psi - \sum_{i,j=1}^{n}(a_{ij}(x,t)\psi_{x_i})_{x_j} \\ &\quad - \sum_{i=1}^{n} b_i(x,t)\psi_{x_i} + h^*\psi\Bigg)\, dxdt \\ &= \int_Q e^{-\mu t}\lambda\psi_t \, dxdt - \int_Q e^{-\mu t} f'(u^*)\psi\lambda \, dxdt \\ &\quad - \int_Q e^{-\mu t}\sum_{i,j=1}^{n}(a_{ij}(x,t)\psi_{x_i})_{x_j}\lambda \, dxdt - \int_Q e^{-\mu t}\sum_{i=1}^{n} b_i(x,t)\psi_{x_i}\lambda \, dxdt \\ &\quad + \int_Q e^{-\mu t} h\psi\lambda \, dxdt.\end{aligned} \tag{2.36}$$

To find the weak form, we use integration by parts on several terms in (2.36). Throwing a time derivative gives:

$$\begin{aligned}\int_Q e^{-\mu t}\lambda\psi_t \, dxdt &= -\int_Q e^{-\mu t}\psi\lambda_t \, dxdt + \int_{\Omega\times T} e^{-\mu t}\lambda\psi \, dx - \int_{\Omega\times 0} e^{-\mu t}\lambda\psi \, dx \\ &\quad + \int_Q \mu e^{-\mu t}\lambda\psi \, dxdt.\end{aligned}$$

By the initial conditions on the sensitivity (2.32) and transversality conditions on the adjoint (2.35), the terms at the boundary drop out and we are left with:

$$\int_Q e^{-\mu t}\lambda\psi_t \, dxdt = -\int_Q e^{-\mu t}\psi\lambda_t \, dxdt + \int_Q \mu e^{-\mu t}\lambda\psi \, dxdt.$$

Integration by parts on the diffusion term gives:

$$\begin{aligned}-\int_Q e^{-\mu t}\sum_{i,j=1}^{n}(a_{ij}(x,t)\psi_{x_i})_{x_j}\lambda \, dxdt &= \int_Q e^{-\mu t}\sum_{i,j=1}^{n} a_{ij}(x,t)\psi_{x_i}\lambda_{x_j} dxdt \\ &\quad - \int_{\partial\Omega\times(0,T)} e^{-\mu t}\sum_{i=1}^{n}\psi_{x_i}\nu_i\lambda \, dsdt.\end{aligned}$$

Throwing a second derivative gives:

$$= -\int_Q e^{-\mu t} \sum_{i,j=1}^{n} \left(a_{ij}(x,t)\lambda_{x_j}\right)_{x_i} \psi \; dxdt + \int_{\partial\Omega\times(0,T)} e^{-\mu t} \sum_{j=1}^{n} \lambda_{x_j}\nu_j\psi \; dsdt$$
$$- \int_{\partial\Omega\times(0,T)} e^{-\mu t} \sum_{i=1}^{n} \psi_{x_i}\nu_i\lambda \; dsdt$$

where $\nu_i = \sum_{j=1}^{n} a_{ij}\eta_j$, is the conormal derivative.

Throwing derivatives in the advection terms gives:

$$-\int_Q e^{-\mu t} \sum_{i=1}^{n} b_i(x,t)\psi_{x_i}\lambda dxdt = \int_Q e^{-\mu t} \sum_{i=1}^{n} (b_i(x,t)\lambda)_{x_i}\psi \; dxdt$$
$$- \int_{\partial\Omega\times(0,T)} e^{-\mu t} \sum_{i=1}^{n} b_i(x,t)\psi\lambda\eta_i \; dsdt.$$

Substituting these into (2.36) yields

$$\begin{aligned}
\int_Q e^{-\mu t}\lambda L\psi dxdt \;\; = \;\; & -\int_Q e^{-\mu t}\psi\lambda_t dxdt + \int_Q \mu e^{-\mu t}\lambda\psi dxdt - \int_Q e^{-\mu t} f'(u^*)\psi\lambda \; dxdt \\
& + \int_Q e^{-\mu t} h\psi\lambda dxdt - \int_Q e^{-\mu t} \sum_{i,j=1}^{n} \left(a_{ij}(x,t)\lambda_{x_j}\right)_{x_i} \psi \; dxdt \\
& + \int_Q e^{-\mu t} \sum_{i=1}^{n} (b_i(x,t)\lambda)_{x_i}\psi \; dxdt + \int_{\partial\Omega\times(0,T)} e^{-\mu t} \sum_{j=1}^{n} \nu_j\lambda_{x_j}\psi \; dsdt \\
& - \int_{\partial\Omega\times(0,T)} e^{-\mu t} \sum_{i=1}^{n} \nu_i\psi_{x_i}\lambda \; dsdt - \int_{\partial\Omega\times(0,T)} e^{-\mu t} \sum_{i=1}^{n} b_i(x,t)\psi\lambda\eta_i \; dsdt.
\end{aligned}$$

After combining terms, we formally have:

$$\begin{aligned}\int_Q e^{-\mu t}\lambda L\psi dxdt &= \int_Q e^{-\mu t}\psi\Bigg[-\lambda_t+\mu\lambda-f'(u^*)\lambda+h\lambda \\ &\quad -\sum_{i,j=1}^{n}\left(a_{ij}(x,t)\lambda_{x_j}\right)_{x_i}+\sum_{i=1}^{n}(b_i(x,t)\lambda)_{x_i}\Bigg]\,dxdt \\ &+ \int_{\partial\Omega\times(0,T)} e^{-\mu t}\left[\sum_{j=1}^{n}\nu_j\lambda_{x_j}\psi-\sum_{i=1}^{n}\nu_i\psi_{x_i}\lambda-\sum_{i=1}^{n}b_i(x,t)\psi\eta_i\lambda\right]\,dsdt.\end{aligned}$$

We choose the following boundary conditions for ψ and λ:

$$\begin{aligned}\sum_{j=1}^{n}\nu_j\lambda_{x_j}+q\lambda-\sum_{i=1}^{n}b_i(x,t)\eta_i\lambda=0 \qquad & \partial\Omega\times(0,T) \\ \sum_{i=1}^{n}\nu_i\psi_{x_i}+q\psi=0 \qquad & \partial\Omega\times(0,T),\end{aligned}$$

where $\sum_{j=1}^{n}a_{ij}\eta_j=\nu_i$, is the conormal derivative. Doing so, the integrals on the boundary drop out:

$$\begin{aligned}&\int_{\partial\Omega\times(0,T)} e^{-\mu t}\left[\sum_{j=1}^{n}\nu_j\lambda_{x_j}\psi-\sum_{i=1}^{n}\nu_i\psi_{x_i}\lambda-\sum_{i=1}^{n}b_i(x,t)\psi\lambda\eta_i\right]\,dsdt \\ &\quad=\int_{\partial\Omega\times(0,T)} e^{-\mu t}\left[\psi\left(-q\lambda+\sum_{i=1}^{n}b_i(x,t)\lambda\eta_i\right)+\lambda\left(q\psi\right)-\sum_{i=1}^{n}b_i(x,t)\psi\lambda\eta_i\right]dsdt=0.\end{aligned}$$

Equation (2.36) formally becomes:

$$\begin{aligned}\int_Q e^{-\mu t}\lambda L\psi \; dxdt &= \int_Q e^{-\mu t}\lambda \left[\psi_t - f(u^*)\psi - \sum_{i,j=1}^{n}(a_{ij}(x,t)\psi_{x_i})_{x_j} - \sum_{i=1}^{n} b_i(x,t)\psi_{x_i} + h^*\psi\right] \; dxdt \\ &= \int_Q e^{-\mu t}\psi \left[-\lambda_t + \mu\lambda - f'(u^*)\lambda + h\lambda - \sum_{i,j=1}^{n}\left(a_{ij}(x,t)\lambda_{x_j}\right)_{x_i} + \sum_{i=1}^{n}(b_i(x,t)\lambda)_{x_i}\right] \; dxdt \\ &= \int_Q e^{-\mu t}\left(L^*\lambda + \mu\lambda\right)\psi \;\; dxdt.\end{aligned}$$

The adjoint operator L^* and the adjoint PDE, with initial and boundary conditions, are:

$$L^*\lambda = -\lambda_t - f'(u^*)\lambda + h\lambda - \sum_{i,j=1}^{n}\left(a_{ij}(x,t)\lambda_{x_j}\right)_{x_i} + \sum_{i=1}^{n}(b_i(x,t)\lambda)_{x_i}$$

$$\begin{aligned} L^*\lambda + \mu\lambda &= h^* && \Omega \times (0,T) \\ \frac{\partial\lambda}{\partial\nu} + q\lambda - \sum_{i=1} b_i(x,t)\eta_i\lambda &= 0 && \partial\Omega \times (0,T) \\ \lambda &= 0 && \Omega \times \{t = T\}\end{aligned}$$

where the non-homogeneous term h^* in the adjoint PDE comes from:

$$\frac{\partial(\text{integrand of } J)}{\partial(\text{state})} = \frac{\partial(hu)}{\partial u} = h^*.$$

Using the sensitivity, ψ, as the test function, have the weak form of the adjoint:

Definition 2.5.1. *The function $\lambda \in V$ with $\lambda_t \in V^*$ is a weak solution to our problem (2.38)-(2.40) if:*

$$\int_Q -\lambda_t \phi \, dxdt + \int_Q \mu\lambda\phi \, dxdt - \int_Q (f(u^*) - h^*u)\lambda\phi \, dxdt + \int_Q \sum_{i,j=1}^{n} a_{ij}(x,t)\lambda_{x_j}\phi_{x_i} \, dxdt$$
$$- \int_Q \sum_{i=1}^{n} b_i(x,t)\lambda\phi_{x_i} \, dxdt + \int_{\partial\Omega\times(0,T)} q\lambda\phi \, dsdt = \int_Q h^*\phi \, dxdt \tag{2.37}$$

for all $\phi \in V$ and with $\lambda(x,T) = 0$ for $x \in \Omega$.

Since the adjoint PDE problem is linear in λ, by [22], an adjoint solution exists.

Theorem 2.6. *Given an optimal control h^* and the corresponding solution, u^*, there exists weak solution $\lambda \in V$ satisfying the adjoint system:*

$$L^*\lambda = -\lambda_t - f'(u^*)\lambda + h\lambda - \sum_{i,j=1}^{n} \left(a_{ij}(x,t)\lambda_{x_j}\right)_{x_i} + \sum_{i=1}^{n} (b_i(x,t)\lambda)_{x_i}$$

$$L^*\lambda + \mu\lambda = h^* \qquad \Omega \times (0,T) \tag{2.38}$$

$$\frac{\partial\lambda}{\partial\nu} + q\lambda - \sum_{i=1} b_i(x,t)\eta_i\lambda = 0 \qquad \partial\Omega \times (0,T) \tag{2.39}$$

$$\lambda = 0 \qquad \Omega \times \{t = T\}. \tag{2.40}$$

Furthermore, we have the optimality conditions:

$$h^*(x,t) = \begin{cases} h_{max} & : \lambda(x,t) < 1 \\ h_{singular} & : \lambda(x,t) = 1 \\ 0 & : \lambda(x,t) > 1, \end{cases} \tag{2.41}$$

where $h_{singular}$ can be found from the u^* PDE.

Proof. We will find the control characterization by differentiating the map, $h \to J(h)$, and using the sensitivity and the adjoint functions. If h^* is optimal, then the difference quotient will be non-positive since $J(h^*)$ would be the maximum value. So, using the sensitivities we have:

$$\begin{aligned} 0 &\geq \lim_{\epsilon \to 0^+} \frac{J(h^* + \epsilon l) - J(h^*)}{\epsilon} \\ &= \lim_{\epsilon \to 0^+} \int_Q e^{-\mu t} \frac{1}{\epsilon} \left[(h^* + \epsilon l) u^\epsilon - h^* u^* \right] \; dxdt \\ &= \lim_{\epsilon \to 0^+} \int_Q e^{-\mu t} \left[h^* \left(\frac{u^\epsilon - u^*}{\epsilon} \right) + l u^\epsilon \right] \; dxdt \\ &= \int_Q e^{-\mu t} \left[h^* \psi + l u^* \right] \; dxdt. \end{aligned}$$

Using the weak formulations for the adjoint and the sensitivity functions, we obtain:

$$\begin{aligned} 0 \geq & \int_Q e^{-\mu t} \Bigg[\left(-\lambda_t + \mu\lambda - f'(u^*)\lambda + h^*\lambda \right) \psi + \sum_{i,j=1}^{n} a_{ij}(x,t) \lambda_{x_j} \psi_{x_i} \\ & - \sum_{i=1}^{n} b_i(x,t) \lambda \psi_{x_i} + l u^* \Bigg] \; dxdt + \int_{\partial\Omega \times (0,T)} e^{-\mu t} q \lambda \psi \; dsdt \\ = & \int_Q e^{-\mu t} \Bigg[\lambda \left(\psi_t - f'(u^*)\psi + h^* \psi \right) + \sum_{i,j=1}^{n} a_{ij}(x,t) \lambda_{x_j} \psi_{x_i} \\ & - \sum_{i=1}^{n} b_i(x,t) \lambda \psi_{x_i} + l u^* \Bigg] \; dxdt + \int_{\partial\Omega \times (0,T)} e^{-\mu t} q \lambda \psi \; dsdt \\ = & \int_Q e^{-\mu t} [-\lambda l u^* + l u^*] \; dxdt \\ = & \int_Q e^{-\mu t} \; [l u^* (1 - \lambda)] \; dxdt. \end{aligned}$$

Our problem is linear in the control, h, and the switching function is $u^*(1 - \lambda)$. Since $u^* \geq 0$ in Q, we investigate the sign of $(1 - \lambda)$. There are three cases:

1. On the set $\{(x,t)|h^*(x,t) = h_{max}\}$, any variation, with support on this set, satisfies $l \leq 0$. Then
$$0 \geq \int_Q e^{-\mu t} \ \ l(u^*(1-\lambda)) \ \ dxdt$$
implies $\lambda \leq 1$ on this set.

2. On the set $\{(x,t)|h^*(x,t) = 0\}$, any variation, with support on this set, satisfies $l \geq 0$. Then
$$0 \geq \int_Q e^{-\mu t} \ \ l(u^*(1-\lambda)) \ \ dxdt$$
implies $\lambda \geq 1$ on this set.

3. On the set $\{(x,t)|0 < h^*(x,t) < h_{max}\}$, any variation function, l, with support on this set, can have arbitrary sign. The inequality (2.42) implies $(1-\lambda) = 0$ on this set. When $\lambda = 1$ on a set of positive measure, then $\lambda_t = 0$ and $\lambda_{x_i} = 0$ for $i = 1, \ldots, n$. Thus our adjoint PDE becomes:
$$-f'(u^*) + h + \mu + \sum_{i=1}^{n} (b_i(x,t))_{x_i} = h.$$
Using a similar approach as [31], we solve for u^*:
$$u^*(x,t) = (f')^{-1}(\mu + \sum_{i=1}^{n} (b_i(x,t))_{x_i}).$$
We then can solve the state PDE for h^* to find the singular case, $h_{singular}$. We need $(\mu + \sum_{i=1}^{n} (b_i(x,t))_{x_i})$ to be in the range of (f'). If not, then the singular case would not occur. If this set has measure 0, then we do not need to consider this case. Thus, these three conditions give us our optimality conditions:
$$h^*(x,t) = \begin{cases} h_{max} & : \lambda(x,t) < 1 \\ h_{singular} & : \lambda(x,t) = 1 \\ 0 & : \lambda(x,t) > 1 \end{cases} \tag{2.42}$$

□

Remark 2.6.1. *When* $\sum_{i=1}^{n}(b_i(x,t))_{x_i} = C$, *where* C *is a constant, then we have the expression for* $h_{singular}$ *at* $\lambda = 1$*:*

$$0 = f(u) - hu = u(g(u) - h)$$

which can be solved for h^**:*

$$h^* = g((f')^{-1}(\mu + C)).$$

Numerical simulations are run to determine approximate solutions to the optimality system (2.1)-(2.3),(2.38)-(2.40),(2.42). Results are shown in the next section.

2.5 Numerical Simulations

For our illustrative examples, we consider the model for fish stock density on a one-dimensional spatial domain of length, L, with Robin boundary conditions,

$$u_t = (a(x,t)u_x)_x + b(x,t)u_x + f(u) - h(x,t)u, \tag{2.43}$$

$$\frac{\partial u}{\partial \nu}(x,t) + qu(x,t) = 0, \tag{2.44}$$

where the diffusion and advection coefficients, $a(x,t)$ and $b(x,t)$, respectively, are positive and can be heterogeneous functions in space and time. We assume the logistic growth function, $f(u) = u(1-u)$, where u is the stock density in proportion to the carrying capacity, K.

The corresponding adjoint equation and optimal control characterization are

$$-\lambda_t - (1 - 2u^*)\,\lambda + h\lambda - (a(x,t)\lambda_x)_x + (b(x,t)\lambda)_x + \mu\lambda = h^* \tag{2.45}$$

$$\frac{\partial \lambda}{\partial \nu} + q\lambda - b(x,t)\eta\lambda = 0 \tag{2.46}$$

and

$$h^*(x,t) = \begin{cases} h_{max} & : \lambda(x,t) < 1 \\ h_{singular} & : \lambda(x,t) = 1 \\ 0 & : \lambda(x,t) > 1, \end{cases} \tag{2.47}$$

where h^* is the optimal harvest, u^* is the corresponding optimal state.

The forward-backward iterative technique [39] was used to solve the optimality system, which consists of 2.43-2.44, 2.45-2.46, and 2.47. To solve the PDEs, we use an explicit finite difference method with appropriate unwinding schemes for first order time derivatives. An Euler method is used for the time derivative while a first order upwind scheme is used for first spatial derivatives. See Appendix A and the introductory chapter for more details.

We chose an initial condition (IC) for our fish stock that satisfied both Robin and Dirichlet boundary conditions. The function was chosen so that the stock of fish would have a bell-shaped curve where most of the stock is concentrated on the middle of the domain:

$$u(x,0) = \frac{1}{24}x^2(x-L)^2. \tag{2.48}$$

Parameter values for simulations are listed in Table 2.1. We consider a spatial domain in terms of kilometers and time in terms of years. Our time scale was chosen such that the population would reach the steady state approximately halfway through the simulation. We set our diffusion coefficient and varied the value of the advection coefficient. The values for our advection coefficient will be chosen in the interval $[0,1]$. In our numerical simulations, the singular control case never occurred. There was also no evidence of non-uniqueness in the optimal control.

An illustration of the stock density at the initial time with the IC, (2.48), is given in Figure 2.1, which we will use to compare results with Dirichlet and Robin boundary conditions. When comparing scenarios with Robin boundary conditions, we will use the steady states for the model, with varying levels of exploited initial stock densities. Those steady states were

Table 2.1: Parameter Description, Values, and Units

Parameters	Value	Description	Units
L	4	habitat length	kilometers (km)
T	4	final time	years (yrs)
μ	0.2	discount term	1/yrs
q	1	boundary coefficient	1/km
$a(x,t)$	1	diffusion coefficient	km^2/yrs
$b(x,t)$	varied	advection coefficient	km/yrs

found using different levels of constant harvest on the system. They are visually represented in Figure 2.2.

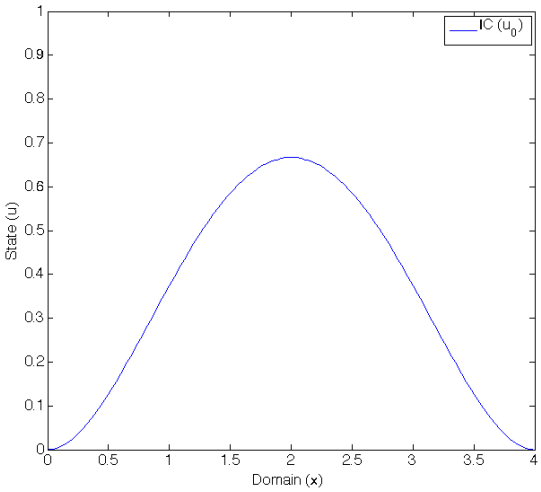

Figure 2.1: Initial Stock Density used in Dirichlet and Robin Boundary Condition Comparisons

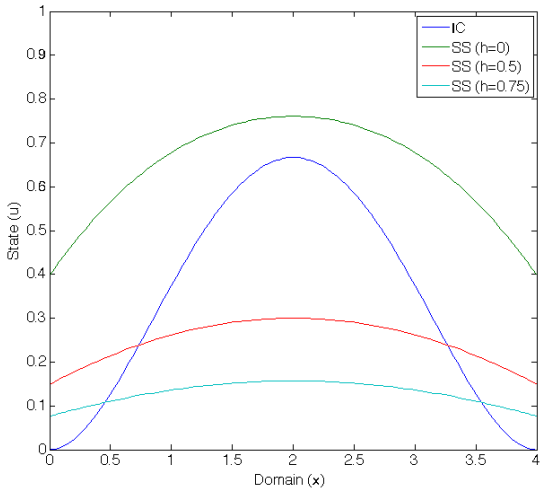

Figure 2.2: Steady States For Varying Levels of Constant Harvest

2.5.1 Comparison of Boundary Conditions

Given the initial condition, (2.48), we simulated the model without harvest and without advection to investigate the dynamics of the fish stock. Robin boundary conditions allow for the flux across the boundary to be proportional to the stock at the boundary. Dirichlet boundary conditions are lethal to the fish stock at the boundary while Neumann boundary conditions represent a no-flux boundary where the stock cannot leave the boundary. The three cases are shown in the Figure 2.3.

We compare results with Robin boundary conditions with previous work with Dirichlet boundary conditions [31], using the IC (2.48). We first compare results without advection ($b(x,t) = 0$). The results are shown in Figure 2.4.

With Robin boundary conditions, fish stock diffusing to the boundary has less threat of dying as in the Dirichlet boundary case with its lethal boundary. We see in Figure 2.4a that a reserve exists in the Dirichlet boundary case but is smaller due to the higher chance of the stock reaching the boundary, dying, and no longer being of any value to the stockholder. Due to the conditions of the habitat at the Dirichlet boundary, the projected yield value of

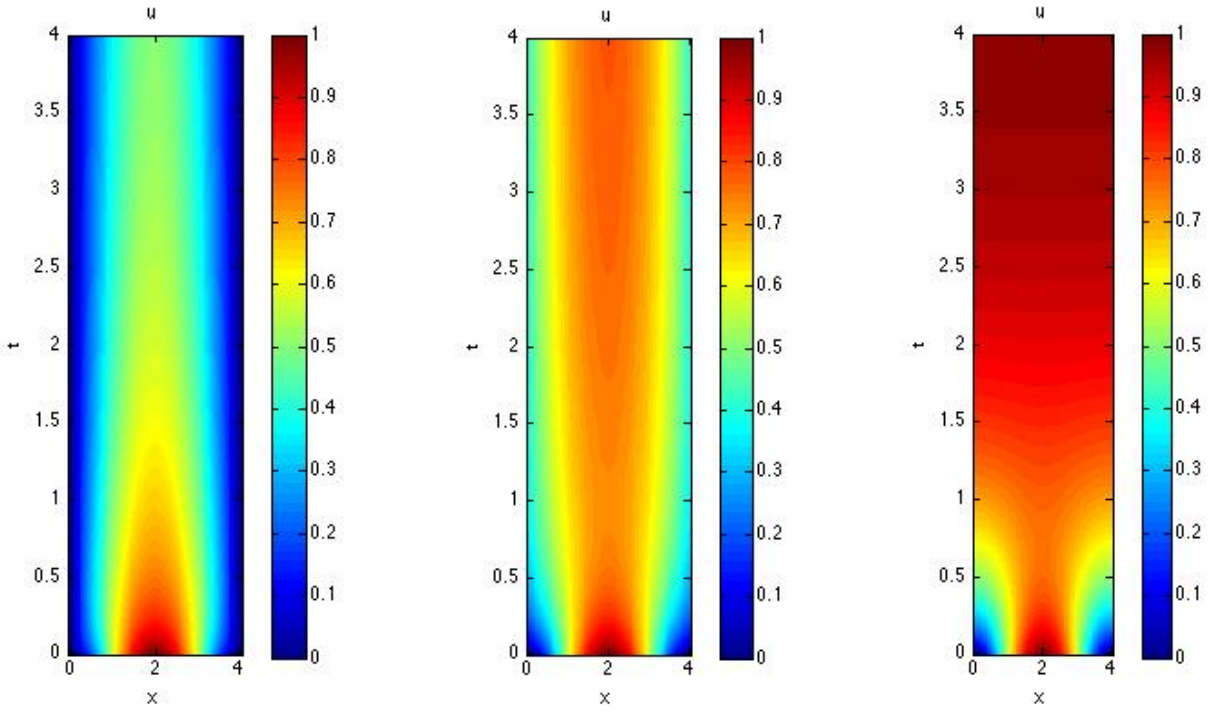

(a) Dirichlet **(b)** Robin **(c)** Neumann

Figure 2.3: Comparison of Fish Stock Dynamics with Three Different Boundary Conditions

the stock is higher, thus the stock is harvested at maximum strength in a larger amount of the habitat than in the Robin boundary case.

In the Robin boundary condition case, Figure 2.4b, more of the habitat is kept as a reserve, and for longer time, than in the Dirichlet boundary case since there is less threat of losing stock at the boundary. There are also more fish present in the habitat longer in time as seen in the states in Figure 2.4. When comparing the objective functional values for both cases, found in Table 2.2, notice that, even with the larger reserve, the value of the objective functional in the Robin boundary condition case is higher. As expected, the objective functional values for the optimal strategy are higher than cases where the domain is harvested at the maximum level for the entire time.

Table 2.2: Objective Functional Values for Dirichlet and Robin Boundary Condition Cases without Advection

Boundary Condition	Optimal Objective Functional Value	Max Harvest for All Time
Dirichlet	1.3624	1.3551
Robin	1.9770	1.9143

We now investigate scenarios with advection to compare results between Robin and Dirichlet boundary conditions. Advection acts by pulling the stock in a certain direction and represents currents in the environment. We investigate constant advection throughout space and time, as well as several heterogeneous advection terms. First, in Figure 2.5, we illustrate a constant advection coefficient, $(b(x,t) = 0.5)$. We then compare results with heterogeneous advection function coefficients varying in space. Two advection function coefficients, $(b(x) = \sin\left(\frac{\pi x}{4}\right))$ and $(b(x) = e^{-0.5x})$, are illustrated in Figure 2.6. Lastly, we investigate one scenario where the advection function varies in space and time. The spatial domain tries to account for regions of high and low currents that shift over time. We consider the function, $(b(x,t) = \frac{1}{2}\left(\sin(\pi x + t) + 1\right))$, illustrated in Figure 2.9.

With a constant advection, seen in Figure 2.5, the location of the reserve shifts in the opposite direction of where advection pulls the stock in both cases. This is because the location farthest from where the stock is moving has the least biomass value. Stock in this

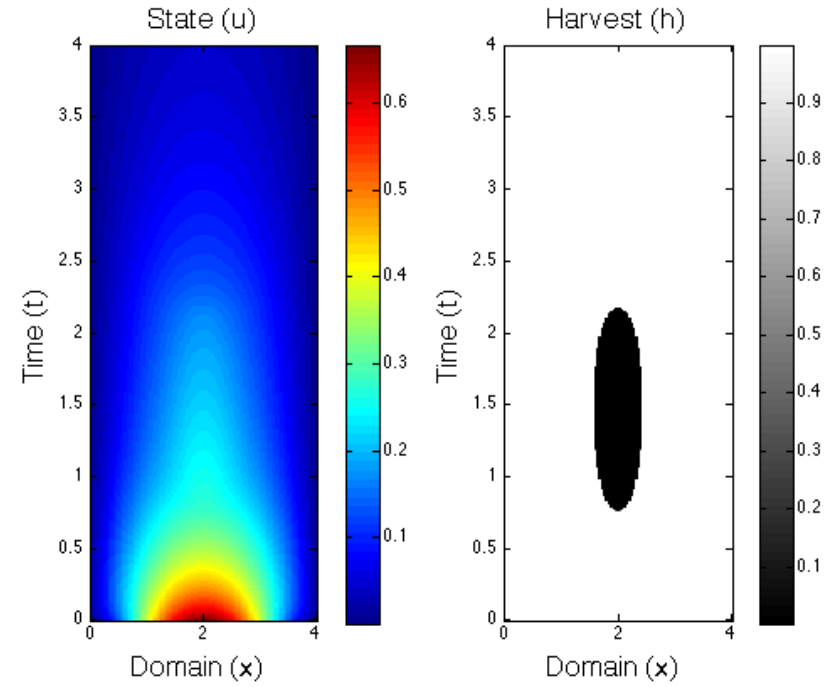

(a) Dirichlet

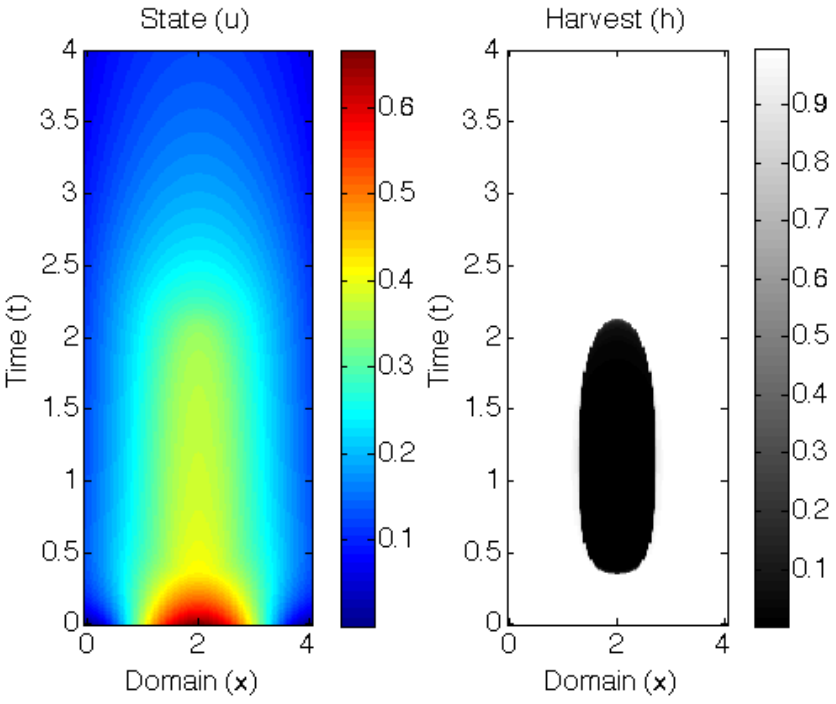

(b) Robin

Figure 2.4: Comparison of Stock Dynamics and Optimal Harvesting Strategies for Dirichlet and Robin Boundary Conditions without Advection, $b(x,t) = 0$

area has less of a chance of being lost at the boundary. In the Dirichlet boundary case, Figure 2.5a, since stock is being strongly pulled towards a lethal boundary, the reserve is shifted in the opposite direction and the reserve is smaller than in the cases without advection. This is due to advection raising the risk of stock dying on one side of the boundary. In the Robin boundary case, Figure 2.12a, since the boundary is not necessary lethal, it is not as valuable to harvest at maximum strength in as large of an area as the Dirichlet boundary case. A larger reserve exists and opens sooner because there is a smaller chance that stock in that area of the habitat will be lost.

Results on how advection function coefficients affect the harvest strategy are found in Figures 2.7 and 2.8. Tables 2.3 and 2.4 compare the objective functional values for the Dirichlet and Robin boundary condition cases. Despite larger reserves forming, the objective functional values for the Robin boundary condition cases are always higher than the Dirichlet boundary cases.

In the cases where the advection coefficient is heterogeneous across the spatial domain, we see similar results as in the constant advection cases. The reserve is still shifted in the direction opposite from where the stock is being pulled, however, the shape and length of the reserves vary, especially seen in Figure 2.7. In this case, there is a strong advection term in the center of the habitat, where the fish stock is initially concentrated. The reserve begins much earlier and is shifted further than other cases. Since advection is strong in the center of the domain, there is a larger risk of stock being pulled to the boundary and lost so it becomes more profitable to harvest. Again, we see the reserve opening earlier and persisting longer in the Robin boundary case because the stock is less valuable to harvest since there is less chance of being pulled to the boundary and lost.

In Figure 2.8, the result is more similar to the constant advection case from Figure 2.5. In this case, the advection is strongest on one side of the habitat. The reserve in the Robin boundary case is wider, opens earlier, and shifted more than in Dirichlet boundary case. This is due to areas where advection is highest being the most valuable to harvest because of the chance for stock to be lost at the boundary. The stock in other parts of the domain, where

the current is less strong, is less valuable to harvest, which is a reason why the reserve forms here and is larger. Another thing to note is that the reserve does not hit either edge of the habitat in any of the cases. Although the advection is strongly pulling the stock to one side of the habitat, there is still diffusion distributing the stock across the domain and there is still stock moving to both ends of the habitat. Thus, it is advantageous to harvest in all areas closest to the boundary.

Figure 2.10 illustrates when the advection coefficient changes in both space and time. Notice, for both cases, the similar shift in the direction the reserve forms that is dependent on the direction the current moves. Again, as previously seen, a larger reserve is formed in the Robin boundary condition case than in Dirichlet boundary case. When comparing the harvesting strategies with the advection function, $b(x,t)$, seen in Figure 2.9, it is interesting to note where the reserve forms. The reserve in both cases forms next to an area of the domain with the highest advection values, always on the side opposite of where stock is being pulled.

Table 2.3: Objective Functional Values for Dirichlet and Robin Boundary Condition Cases with Varying Advection Coefficients

Boundary Condition	$[b(x) = 0.5]\ J(h)$	$[b(x) = \sin\left(\frac{\pi x}{4}\right)]\ J(h)$	$[b(x) = e^{-0.5x}]\ J(h)$
Dirichlet	1.3148	1.2587	1.4756
Robin	1.9337	1.9855	2.1501

Table 2.4: Objective Functional Values for Dirichlet and Robin Boundary Condition Cases with Advection Coefficient Varying in Space and Time

Boundary Condition	$[b(x,t) = \frac{1}{2}(\sin(\pi x + t) + 1)]\ J(h)$
Dirichlet	1.3468
Robin	2.0034

2.5.2 Comparison of Varying Scenarios with Robin Boundary Conditions

As we saw in the previous subsection, there is a definite difference when the domain incorporates Dirichlet or Robin boundary conditions. Although reserves were always part of the optimal harvesting strategy, the size, shape, and timing are affected by both the boundary conditions and varying advection function coefficients. In this section, we will investigate more closely the domain with Robin boundary conditions and how different scenarios affect the optimal harvesting strategies. We begin with results for constant advection coefficients, $b(x)$, with varying constant values on the interval $[0, 1]$. The optimal harvesting result for this case is found in Figure 2.11. We then compare the optimal harvesting results with advection coefficients that are heterogenous in space or time, bounded on the interval $[0, 1]$. In these scenarios, we use the steady state of unexploited fish stock without harvest as our initial condition (see Figure 2.2). The results are shown in Figure 2.12.

In Figure 2.11, as the constant advection coefficient increases, we see an increase in the shift of the reserve in the opposite direction of the pull. We also see in Figure 2.11d that once the advection coefficient is strong enough, the reserve will move to the boundary on one side. It becomes more advantageous to not harvest fish on one side of the habitat, despite the effects of diffusion, due to the stronger pull of advection in the opposite direction.

In the cases with a heterogenous advection coefficient, Figure 2.12, there is more variation in the shape of the reserve. In Figure 2.12c, when advection is strongest in the center of the domain, the reserve opens much earlier and lasts longer than previous cases. The location of strong currents in a domain affects harvest strategies. Stronger currents through the center of a domain affect a larger portion of the stock than if only concentrated on one side of the domain or constant throughout, thus altering where and when reserves develop and their size.

When the advection function varies in time, seen in Figure 2.12d, a reserve forms to the right of the areas with the highest advection. As advection changes in time, the reserve follows, forming on a diagonal. An understanding of ocean currents within a fishery, as

well as their variation in time, appears necessary in determining where reserves should be implemented.

2.5.3 Optimal Harvesting Strategy Results for an Initially Unexploited and Exploited Stock

In previous results, simulations were run using the steady state of an unexploited fish stock. Due to current fishing practices, many stocks are either exploited or overexploited. In this subsection, we investigate optimal harvesting strategies with different levels of fish stock at the initial time. We compare results when maximizing yield of fish stock when the stock is initially unexploited, exploited, or overexploited. Figure 2.2 shows the steady states considered, with varying harvest values. Figure 2.13 shows varying results with different levels of stock at the initial time.

With an initially overexploited fish stock, there is a need for an initial reserve to exist to rebuild the stock. Once the stock recovers, the reserve decreases in size, eventually closing, and maximum harvest persists for the remaining time. This makes sense in cases when trying to maximize yield. It is important for stock to grow before depleting the stock again. The practicality of its implementation is debatable since, depending on the level of overexploitation, large portions of the habitat would be closed to fishing. The effect on the fishing industry would be drastic in the short term.

2.5.4 Approximations of Optimal Harvesting Strategy Results

In the implementation of a harvesting strategy, there is debate on the feasibility of adjusting the effort through space and time. In this section, we compare the optimal harvesting strategy results from the previous sections with an approximation of the harvesting strategy that is either constant in space or in both space and time. When implementing a harvesting strategy, how realistic it is to adjust the harvesting effort through space and time is debatable. We

compare the objective functional values for both to determine how close the approximation is to the optimal result.

In the previous section, we found the optimal harvesting strategies for Robin boundary conditions given certain scenarios. We investigate the scenario without advection and then two with advection coefficients. The results for the case without advection are found in Figure 2.14 and Table 2.5. We investigate the constant advection coefficient of ($b(x) = 0.75$) and the heterogeneous advection coefficient, ($b(x) = \sin\left(\frac{\pi x}{4}\right)$). The results are shown in Figures 2.15 and 2.16, and Tables 2.6 and 2.7, respectively.

In each of the cases, harvest approximations can be found that are close to the optimal harvest strategies found through the simulations. In all the cases, as seen by the objective functional values in Tables 2.5, 2.6, and 2.7, the approximations are obviously less than the optimal but there is evidence to believe that if you approximated the harvest, the resulting objective functional would be very close. The largest difference between the approximate and actual optimal objective functional values is less than 0.5%. The approximations may be more realistic in regards to actual implementation of reserves because it is easier to form reserves that are constant in space and open/close in time.

Another option to consider is when the harvest does not vary in time. In Figures 2.17-2.18, with Table 2.8, we compare the results with the optimal harvesting strategy in the dynamic harvest case with no advection. We also include the objective functional values for the case with maximum harvest on the entire domain in Table 2.8 for comparison. When the domain is harvested at the maximum for the entire time, we see suboptimal results as expected, with an objective functional value lower than in the optimal harvest case (approx. 1% lower). When considering a harvest not varying in time, the objective functional value is still lower than in the optimal case, seen in Table 2.8. In this approximate case, there are higher stock levels at the final time, seen in Figure 2.18. However, when trying to maximize yield only, it is not as close to optimal as other approximations (approx. 5% lower). This points to evidence that time managed reserves are important when considering reserves. More work needs to be done in this area, such as investigating harvest dependent only on space or time

and determining the optimal harvesting strategies associated with them, rather than just using these approximations of the optimal.

Table 2.5: Objective Functional Values for the Optimal Harvest Strategy and an Approximation to that Harvesting Strategy, without Advection, $b(x,t) = 0$

Harvest	Objective Functional Value
Optimal Harvest	2.8522
Harvest Approximation	2.8504

2.6 Conclusions

A more realistic boundary condition produces different harvesting results than previous results with Dirichlet boundary conditions. When considering open ocean fisheries, the implementation of a non-lethal boundary, using Robin boundary conditions, produced results with larger yield values as well as reserve sizes. Our work highlights the importance of appropriate boundary conditions, corresponding to specific fishing scenarios, in finding harvest management strategies.

We further investigated how the interplay between Robin boundary conditions and advection within the domain affected harvesting strategies. Similar to previous work of Joshi *et al.* [31], a reserve opens and is shifted in the opposite direction from that towards which the stock is being pulled. However, the reserves are larger than in previous work. When we investigated advection functions that varied in space or time, there was even more disparity among the size and shape of reserves. When the advection shifted in time, a reserve forms that followed a similar directional pattern as the advection.

Table 2.6: Objective Functional Values for the Optimal Harvest Strategy and an Approximation to that Harvesting Strategy, with Constant Advection, $b(x,t) = 0.75$

Harvest	Objective Functional Value
Optimal Harvest	2.7414
Harvest Approximation	2.7399

Table 2.7: Objective Functional Values for the Optimal Harvest Strategy and an Approximation to that Harvesting Strategy, with Advection Function Coefficient, $b(x) = \sin\left(\frac{\pi x}{4}\right)$

Harvest	Objective Functional Value
Optimal Harvest	2.8400
Harvest Approximation	2.8387

Table 2.8: Objective Functional Values for the Optimal Harvest Strategy, an Approximation to that Harvesting Strategy, and Maximum Harvest on Entire Domain, and Not Varying in Time and without Advection

Harvest	Objective Functional Value
Optimal Harvest	2.8522
Harvest Approximation	2.7259
Maximum Harvest	2.8310

We also compared harvesting strategies for scenarios when the stock size is initially unexploited, exploited, and overexploited. We saw that when the stock is initially overexploited, reserves are opened immediately and cover most of the domain. Once the stock has time to recover, the reserve closes and the domain is harvested at maximum levels the rest of the time.

When considering the implementation of these reserves, we decided to approximate the optimal harvest strategies using reserves that, once open, do not vary in space. We saw that approximate reserves produced suboptimal objective values but the values were relatively close (less than 0.5% difference). In the case where we compared the optimal harvest strategy with an approximate harvest strategy with reserves not varying in time, there was a significant difference in objective values and the stock levels at the final time (objective values approximately 5% less). Using spatial boundaries that are constant in time (reserve is rectangular in space and time) and restricting the length of time to impose a reserve are realistic and can achieve near optimal results.

2.7 Future Work

We saw that currents varying through space and time affected harvesting strategies. There is evidence that a better understanding of ocean currents within a habitat and how they vary through time is important when determining the location and time of a reserve, as well as its size. With the added complexity to the domain, we believe harvesting strategies will also be affected.

There are several directions to take this work in the future. This work models a single population of fish in a heterogeneous spatial domain. The mathematical results are on a multidimensional domain, so completing simulations in 2 and 3 spatial dimensions would be an interesting extension. The effect of advection in these dimensions may be quite interesting. There is also interest in varying the time horizon to determine if the fraction of domain considered no-take reserve is constant as the final time varies.

There is also interest in looking at a multipopulation model, whether multiple species or an age-structured fishery model. An age-structured model would investigate the harvest strategies when dealing with both juvenile and adult classes of fish (or more refined age classes). One question to consider is which population brings in more yield. Multiple species models would investigate harvesting strategies with competition and investigate how harvesting of one species population affects the dynamics in the other species population. This is a relevant problem due to fishery by-catches, as well as overexploited fish stock being harvested with non-fully exploited stocks. Harvesting strategies that maximize yield under these scenarios is an important question.

Another question to consider is: What is the best strategy when trying to save juveniles and/or adults? In our results, the population at the final time is quite small. One way to save the stock is the addition of a salvage term, $\int_\Omega u(x,T)dx$, or $\int_\Omega u(x,t)\,dxdt$ to the objective functional. In most situations, there is a desire to keep the fish stock at a certain level and a salvage term allows for maximizing the yield while maintaining a certain level of the population at the final time, which will produce different results.

Another extension to investigate is how harvesting negatively affects the habitat. Ocean pollution from harvesting could negatively impact fish stock, reduce their food source and harm marine habitats. Moeller and Neubert [43] have recently done work on maximizing harvest at the population steady state while incorporating the negative effects of harvesting on the environment. An alternative objective of the problem could be to look at minimizing negative effects to the habitat due to fishing while still trying to maximize yield with spatial-temporal fish dynamics. Modeling these dynamic systems can help predict the impact of fishing regulations.

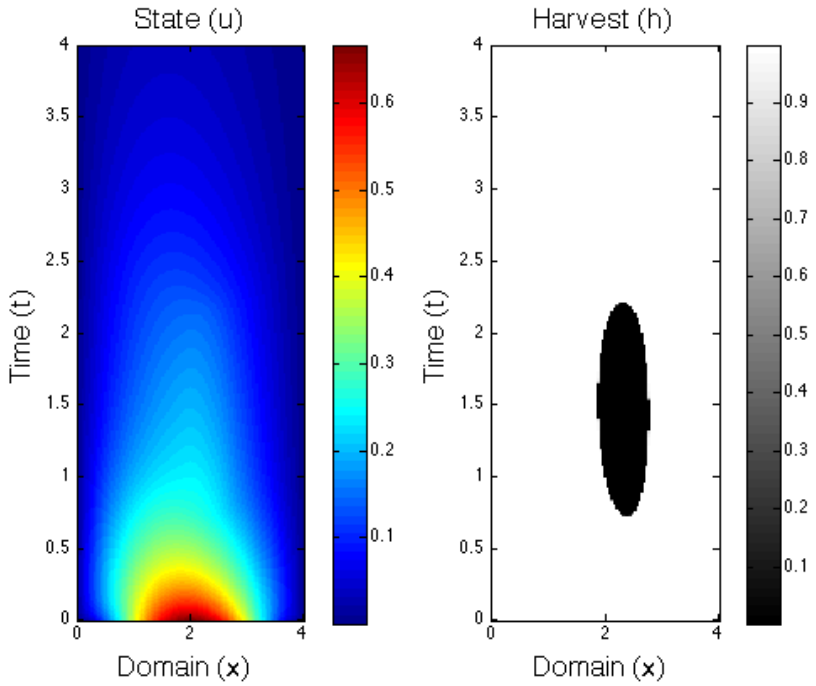

(a) Dirichlet

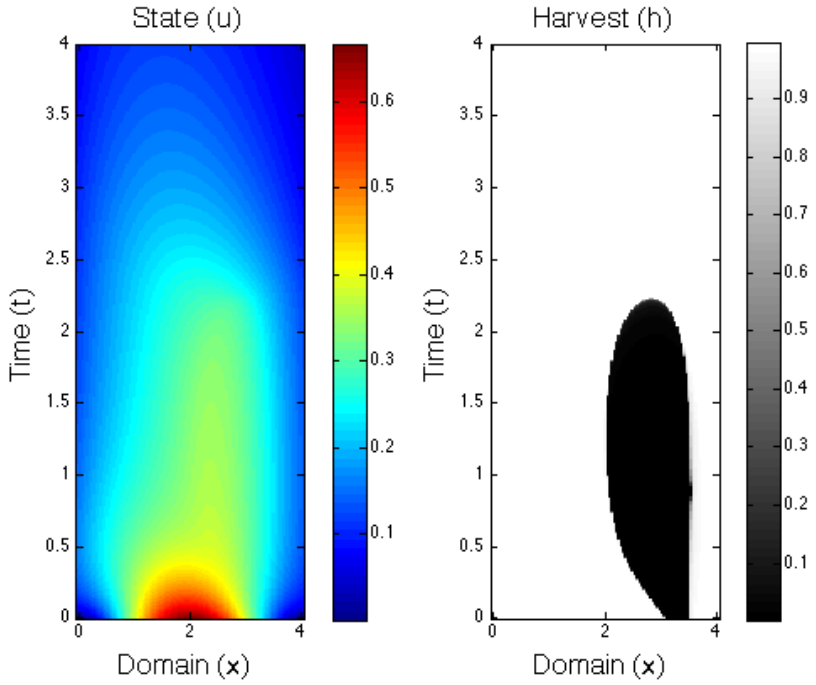

(b) Robin

Figure 2.5: Comparison of Stock Dynamics and Optimal Harvesting Strategies for Dirichlet and Robin Boundary Conditions with Constant Advection, $b(x,t) = 0.5$

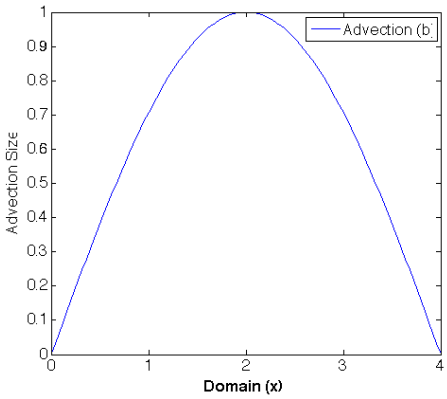

(a) Advection $b(x) = \sin\left(\frac{\pi x}{4}\right)$

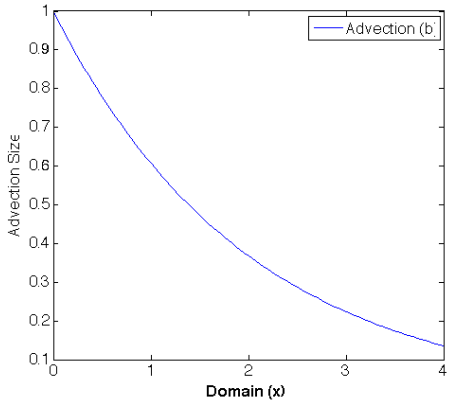

(b) Advection $b(x) = e^{-0.5x}$

Figure 2.6: Comparison of Function Advection Coefficients, $b(x, t)$, on the Domain

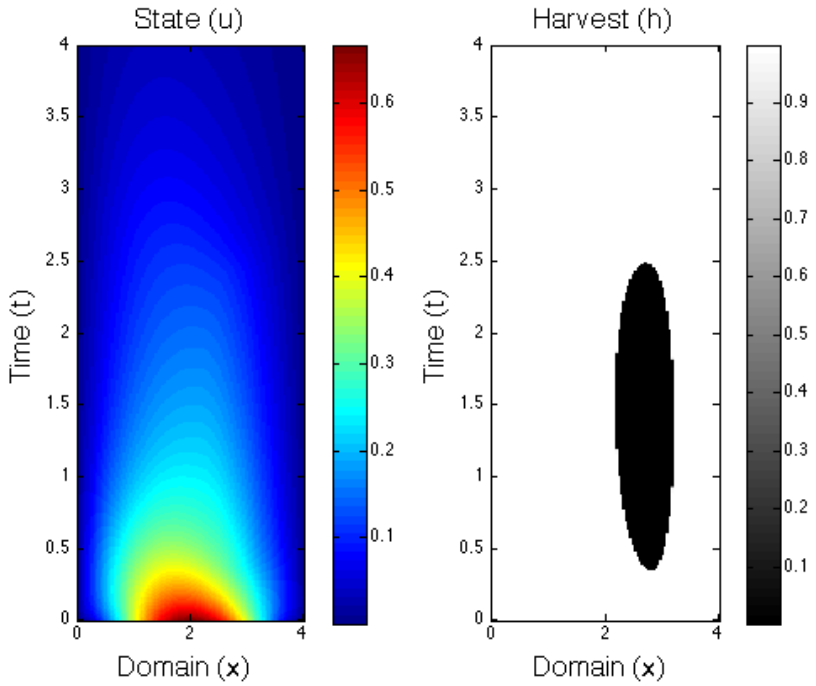

(a) Dirichlet

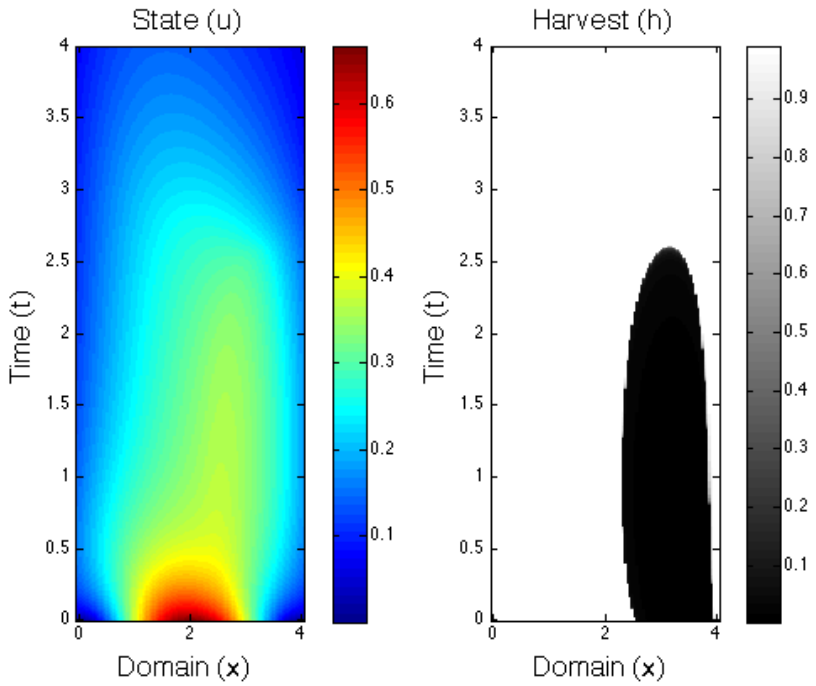

(b) Robin

Figure 2.7: Comparison of Stock Dynamics and Optimal Harvesting Strategies for Dirichlet and Robin Boundary Conditions with Advection, $b(x) = \sin\left(\frac{\pi x}{4}\right)$

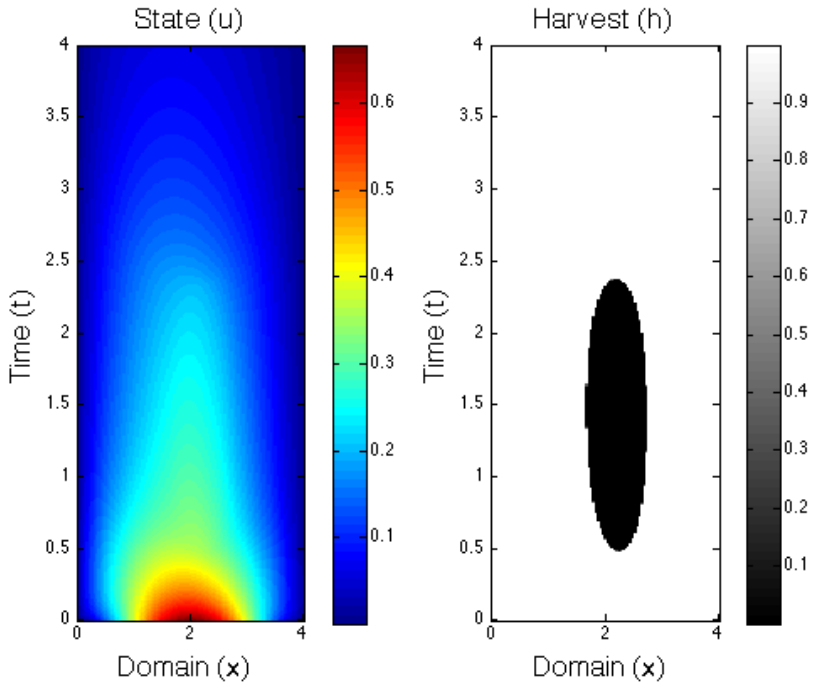

(a) Dirichlet

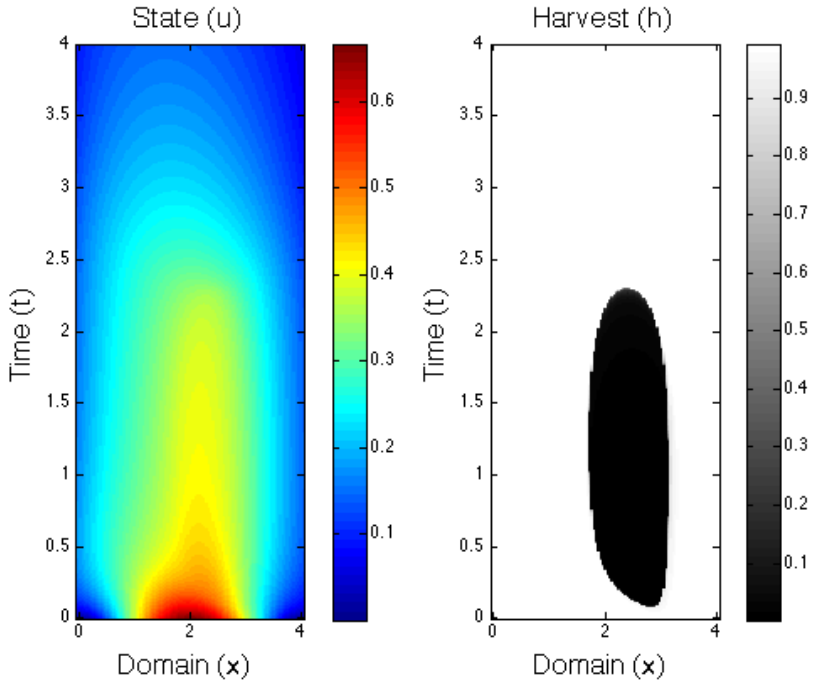

(b) Robin

Figure 2.8: Comparison of Stock Dynamics and Optimal Harvesting Strategies for Dirichlet and Robin Boundary Conditions with Advection, $b(x) = e^{-0.5x}$

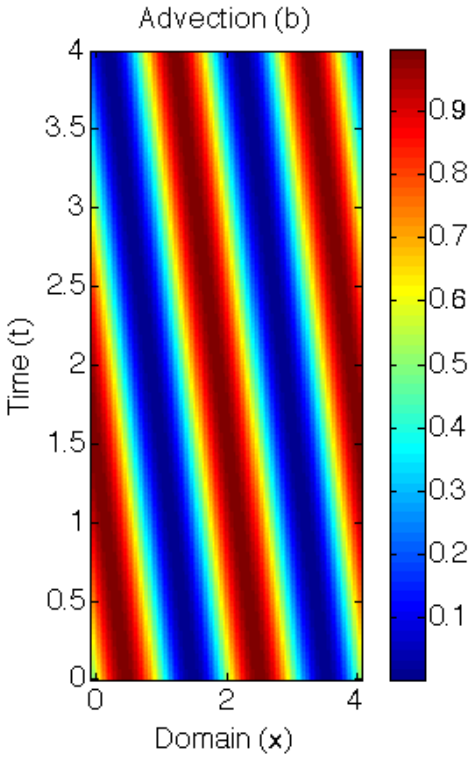

Figure 2.9: Function Advection Coefficient, $b(x,t)$, Varying in Space and Time on the Domain

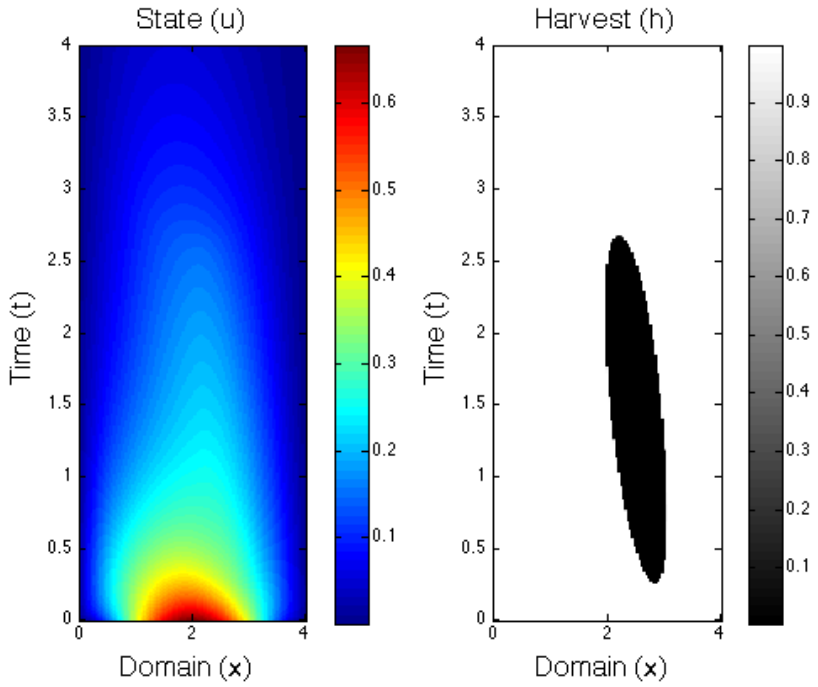

(a) Dirichlet

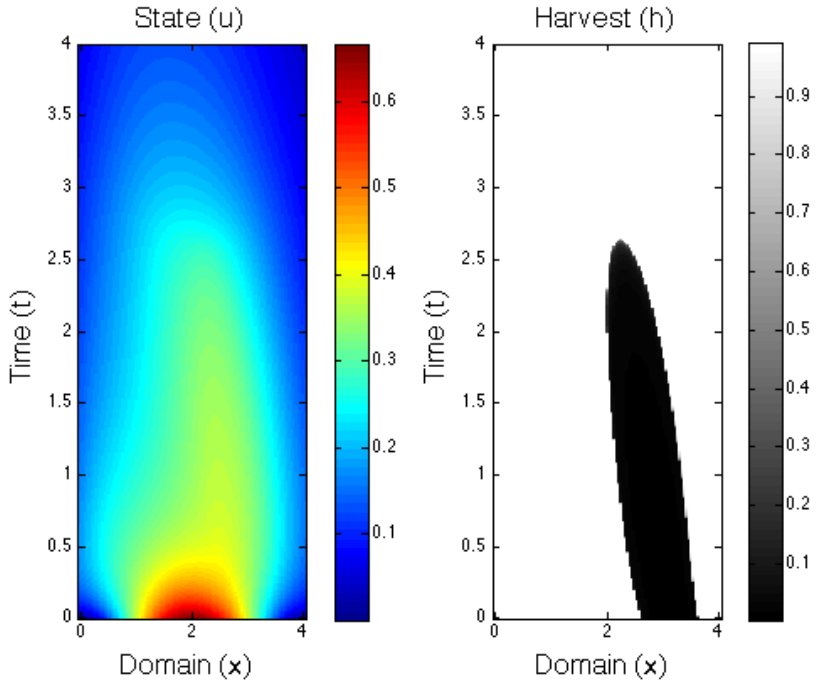

(b) Robin

Figure 2.10: Comparison of Stock Dynamics and Optimal Harvesting Strategies for Dirichlet and Robin Boundary Conditions with Advection, $b(x) = \frac{1}{2}\left(\sin(\pi x + t) + 1\right)$

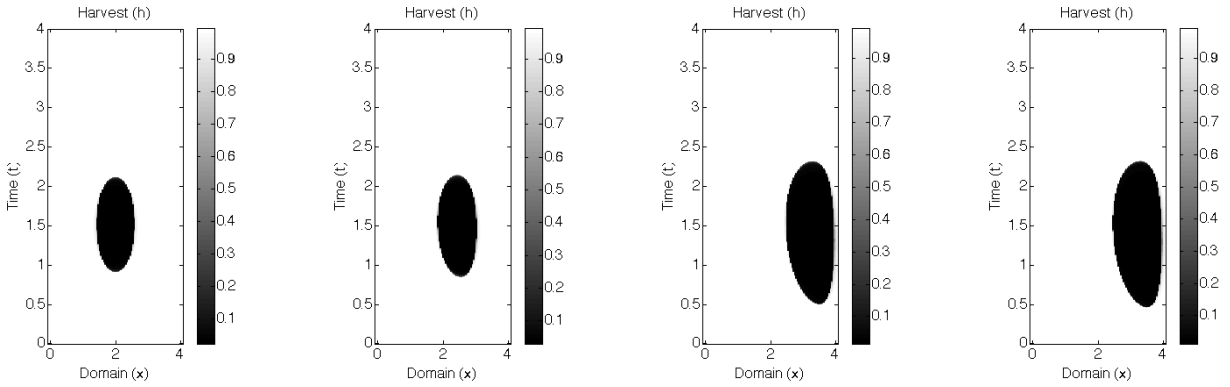

(a) $b = 0$ **(b)** $b = 0.25$ **(c)** $b = 0.5$ **(d)** $b = 0.75$

Figure 2.11: Comparison of Optimal Harvesting Strategies for Robin Boundary Conditions with Varying Constant Advection Coefficients

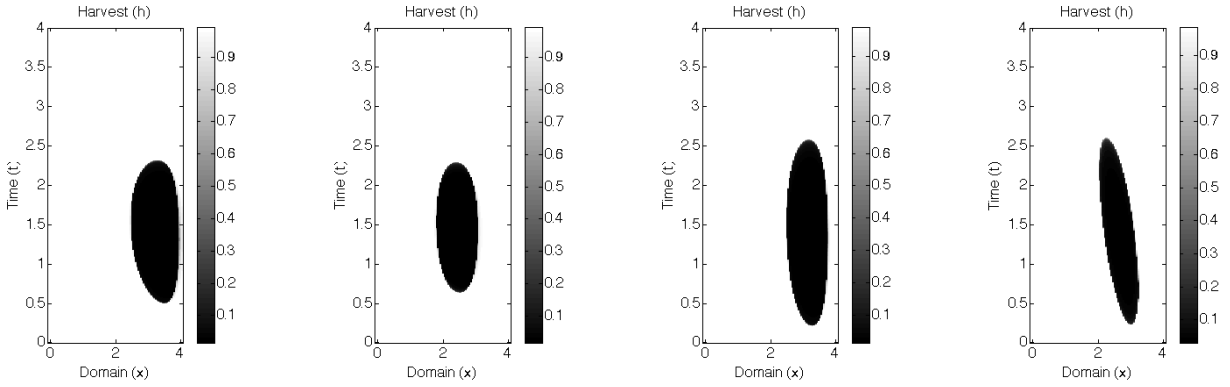

(a) $b(x) = 0.5$ **(b)** $b(x) = e^{-0.5x}$ **(c)** $b(x) = \sin\left(\frac{\pi x}{4}\right)$ **(d)** $b(x) = \frac{1}{2}\left(\sin(\pi x + t) + 1\right)$

Figure 2.12: Comparison of Optimal Harvesting Strategies for Robin Boundary Conditions with Varying Advection Function Coefficients

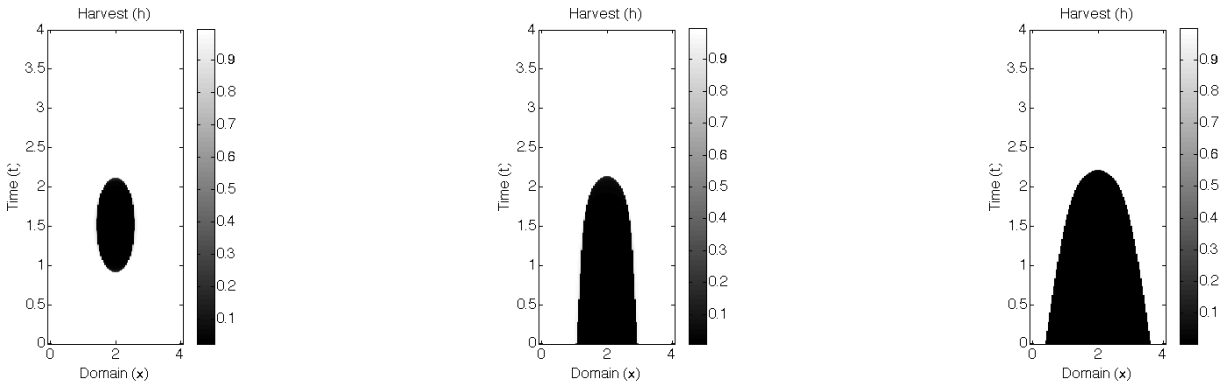

(a) SS $h(x,t) = 0$ **(b)** SS $h(x,t) = 0.5$ **(c)** SS $h(x,t) = 0.75$

Figure 2.13: Comparison of Optimal Harvesting Strategies for Robin Boundary Conditions with Various Exploited Initial Stock Densities

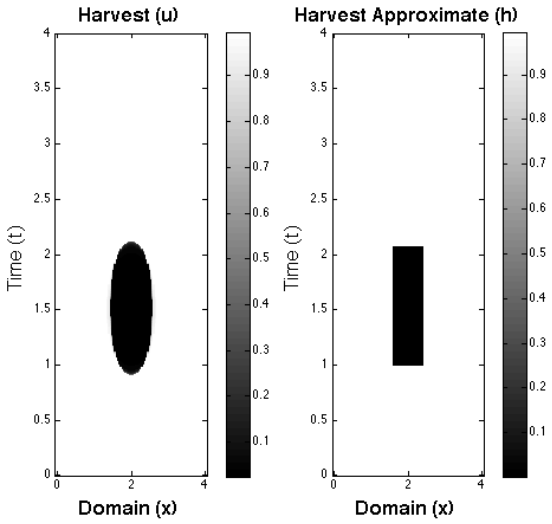

Figure 2.14: Comparison of Optimal Harvesting Strategy for Robin Boundary Conditions and an Approximation of that Harvesting Strategy, Without Advection

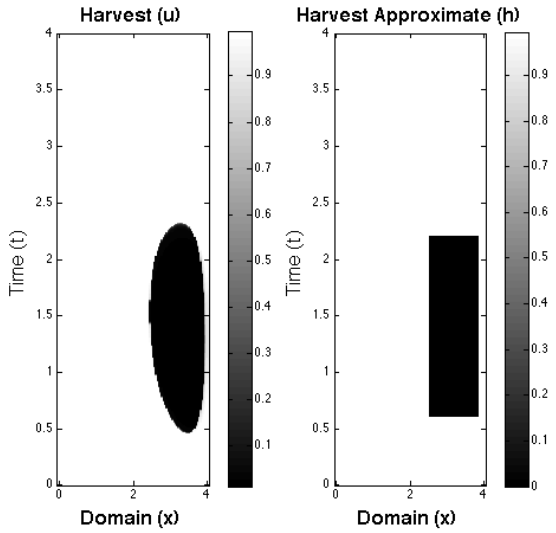

Figure 2.15: Comparison of Optimal Harvesting Strategy for Robin Boundary Conditions and an Approximation of that Harvesting Strategy, with Constant Advection, $b(x,t) = 0.75$

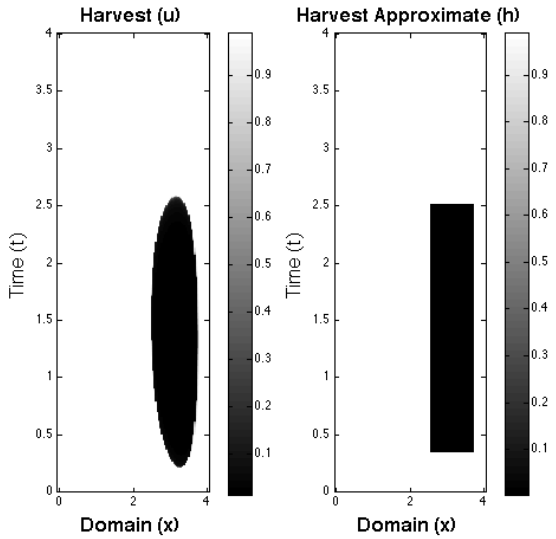

Figure 2.16: Comparison of Optimal Harvesting Strategy for Robin Boundary Conditions and an Approximation of that Harvesting Strategy, with Advection Function Coefficient, $b(x) = \sin\left(\frac{\pi x}{4}\right)$

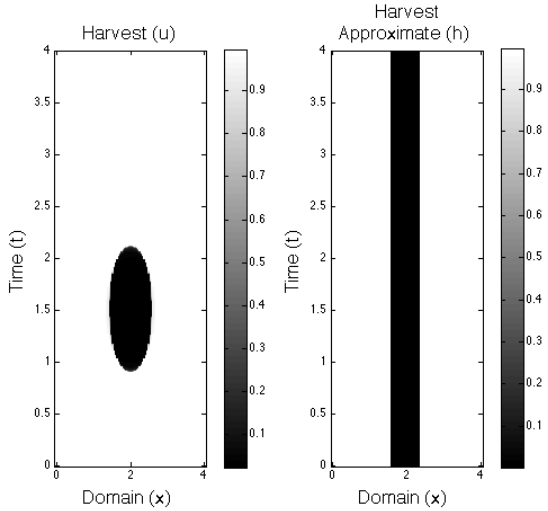

Figure 2.17: Comparison of Optimal Harvesting Strategy for Robin Boundary Conditions and an Approximation of that Harvesting Strategy, Not Varying in Time, without Advection

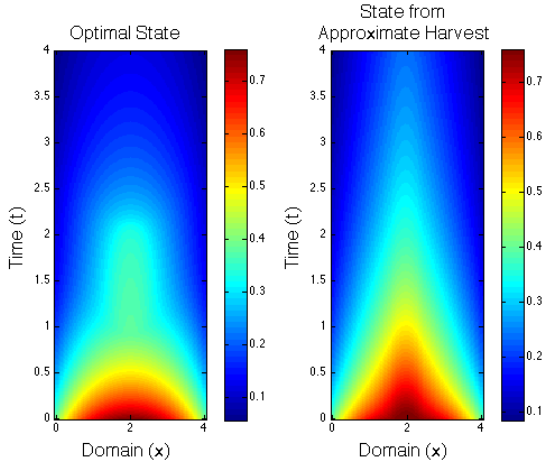

Figure 2.18: Comparison of the Corresponding State Solution for the Optimal Harvesting Strategy and the Approximation to that Harvesting Strategy, Not Varying in Time, without Advection

Chapter 3

The impact of spatial arrangements on intervention strategies in epidemic models

3.1 Introduction

Questions have arisen regarding the importance of spatial features for disease spread and how movement patterns affect management strategies. Recently, the spatial arrangements of departments in Haiti, as well as human and water movement, had an impact on the spread of a cholera outbreak [64, 51, 20]. There is a need to find intervention strategies that could help control the disease while also optimizing the use of available resourcesc In addition, this strategy needs to consider the patterns of mobility of the population. The situation in Haiti raised an interesting question: How do metapopulation spatial arrangements affect disease management strategy?

Cholera is a infectious disease caused by the infection of the intestine with the aquatic bacterium, *Vibrio cholerae*. In recent years, there have been several cholera epidemics throughout the world. The disease is also endemic in several areas of Asia and Africa. There are an estimated 3-5 million cholera cases and 100,000-120,000 deaths due to cholera every

year [49]. The disease causes rapid dehydration and electrolyte imbalances. Without prompt treatment, a person with cholera may die of dehydration within a few hours of infection [17].

Cholera is a waterborne disease with multiple modes of infection, both direct and indirect transmission. Waterborne diseases are characterized by the capability for the disease to persist outside human hosts and transmission through water is possible [49]. Cholera is transmitted directly from an aquatic reservoir to human hosts or through the ingestion of contaminated food or water. Infected individuals shed pathogen into the water and new infections arise both from indirect exposure to contaminated water as well as person-to-person transmission [59].

Previous work found evidence that the aquatic reservoir played an important role in the transmission of the disease [17, 7, 8, 64]. How the pathogen can spread to other communities could greatly affect disease dynamics. The movement of both humans and pathogen in aquatic reservoirs has been suggested to influence the spatial spread of the disease in Haiti. Bertuzzo *et al.* [7, 8], studied the role of river networks in the transportation and redistribution of *V. cholera* between communities. The model included local epidemic dynamics within a patch as well as the transportation of the bacteria between patches. They modeled bacteria movement both inward and outward of each node, or patch, with biased movement in the direction of water flow. They concluded that the role of waterways and river networks play an important role in the spread of the disease throughout a network of communities.

Later work of Bertuzzo *et al.* [9] studied the epidemic in Haiti using a gravity model, where the spread of the pathogen is a function of both distance between communities as well as community size. This is done to capture the transport mechanisms of the disease, namely, water contamination and human mobility. Rinaldo *et al.* [54] extended that work to model human and water movement separately and their effect on disease spread.

Tien and Earn [59] introduced a model using ordinary differential equations (ODEs) for multiple transmission pathways of a waterborne pathogen. They extended the traditional

Susceptible-Infected-Recovered compartmental model framework by adding a water compartment, tracking pathogen concentration in an aquatic reservoir. They introduced two modes of transmission, both direct transmission and indirect transmission. Their model allowed for infection through exposure to contaminated water as well as the classical person-to-person contact. Tuite *et al.* [64] applied a multiple transmission model to a recent outbreak in Haiti. They investigated the spread of cholera in Haiti due to water contamination and human mobility by a gravity model, where pathogen levelwas modeled as a function of both distance between communities as well as community size. Their model incorporated both fast and slow transmission but ignored water movement.

The use of multi-patch metapopulation models is another effective way to model the spread of a disease through a system of patches. There has been a large body of work in ecology using this modeling strategy [40, 27]. The use of metapopulations has become popular in infectious disease modeling. One illustration is from Castillo-Chavez and Yakubu [12], who built an epidemic model for the dispersal of susceptible and infected individuals among patches in order to answer questions about the role of population dynamics on disease dynamics. Arino and his collaborators have also done work on epidemic models with spatial dynamics. Arino and van den Driessche [4] introduced a multi-city epidemic model that incorporated travel between the cities using directed graphs. Later work investigated multi-species models within a patchy environment with movement [2]. For a survey of other epidemic metapopulation models, see [3, 5, 32].

There have been several extensions to the model of Tien and Earn [59] to include spatial dynamics. Eisenberg *et al.* [21] extended this model to incorporate a multi-patch structure with both water and human movement. They investigated the dependence of the basic reproduction number, $\mathcal{R}_0$, on connectivity and water movement. Tien *et al.* [60] similarly built a patch network model with water and human movement where disease invasibility was determined by the basic reproduction number on the domain. They use rooted spanning trees to average the basic reproduction number across the network in a manner that respects network structure [60]. Based on their results, they determined that control efforts should be

highest in communities with the greatest network risk, which is determined by the weighted contribution of a patch to the network basic reproduction number.

There are several intervention strategies to limit cholera outbreaks. Miller Neilan *et al.* [46] used optimal control theory to study the effect of three control efforts on cholera outbreaks in a system of ODEs: vaccination, sanitation, and the provision of clean water. Although improved water and sanitation infrastructure would be valuable in preventing the spread of the disease, in many developing countries, this is not a viable short-term option. One short-term intervention strategy is the use of vaccinations. Vaccinations are currently being used as an intervention strategy to control cholera, specifically in Haiti [33]. In work by Chao *et al.* [13], an individual-based stochastic model for cholera transmission was analyzed, comparing preemptive vaccination strategies to response strategies.

There are two oral vaccines that are being used in the prevention of cholera, Dukoral and Shanchol. These oral vaccines are easier to administer, more acceptable to recipients, and have reduced risk of transmitting blood-borne infections than those administered through injection [57]. Dukoral is a killed whole-cell vaccine and is administered to persons over 2 years of age. It requires a liquid buffer for intake, which requires clean water. This can be a dilemma in areas where clean water is unavailable. Shanchol is a killed whole-cell vaccine as well, which can be administered to persons over 1 year of age, and does not require a liquid buffer for intake. The costs of each of these vaccines differ. Dukoral is more costly, around \$5.25 per dose, while Shanocol is significantly cheaper at \$0.75 per dose. The protection provided by the vaccines also vary. Dukoral lasts about two years while Shanchol protects greater than three years in some cases [57, 48].

To study the use of vaccinations to manage this disease effectively, we use optimal control together with models that incorporate varying spatial arrangements. We investigate how the spatial arrangement of patches and corresponding connections can affect intervention strategies for disease outbreaks or endemic cases. We use an extension of a model for multiple transmission pathways of a waterborne pathogen, first developed by Tien and Earn [59]. We plan to investigate optimal intervention strategies for a cholera outbreak in a metapopulation

with movement among the patches. We sought answers to the question of where control efforts should be focused depending on spatial structure and path dynamics. We will start an investigation of certain spatial features and intervention strategies in epidemic models, motivated by the cholera outbreak in Haiti. We will then compare our optimal intervention strategies with the disease control strategies of Tien, Eisenberg, and their collaborators that were based on the network reproduction numbers and disease invasibility [60, 21].

We will investigate both population and water movement. Incorporating water movement along hydrological connections is one way to model the spread of pathogen in aquatic reservoirs. By including both water and population movement, we can decide how to apply control measures for a system of interconnected communities. We investigate the importance of spatial connectivity of communities since the pathogen in one aquatic reservoir could spread to surrounding susceptible communities through these shared water sources.

We first consider optimal vaccination in an endemic waterborne disease scenario, comparing a linear spatial arrangement of connected patches with a hub arrangement with connecting smaller patches. The use of data [64] will help to analyze the effectiveness of our model and we use data related to Haiti and its recent cholera outbreak. We will investigate how the disease spreads through the population with and without the application of intervention strategies. We apply a single control, vaccination, as an intervention strategy. We will determine how the optimal vaccination strategies depend on chosen spatial arrangements.

After a brief background on the model by Tien and Earn [59], we introduce and describe our metapopulation model, as well as the parameters, for our problem in Section 3.2. In Section 3.3, we explain the role of connectivity and the associated spatial arrangements we will consider. The model is analyzed by computing the basic reproduction number in Section 3.4. We formulate the optimal control problem and corresponding state system of equations in Section 3.5. We also prove the existence and uniqueness of the optimal control. In Section 3.6, we use numerical simulations to illustrate solutions to the problem for varying spatial arrangements and scenarios. The chapter ends with a conclusion section.

Table 3.1: Description of Compartments with Units for *Tien and Earn* Model

Variables	Description	Units
S	susceptible individual density	individuals km^{-2}
I	infected individual density	individuals km^{-2}
R	recovered/removed individual density	individuals km^{-2}
W	pathogen concentration in water reservoir	cells ml^{-3}

Table 3.2: Description of Parameters with Units for *Tien and Earn* Model

Parameters	Description	Units
μ	birth and death (non-disease related)	day^{-1}
b_I	person-person contact rate	km^2 individuals^{-1} day^{-1}
b_W	reservoir-person contact rate	ml^3 cells^{-1} day^{-1}
γ	duration of infectiousness of the disease	day^{-1}
α	person-reservoir contact rate ("shedding")	cells ml^{-3} day^{-1} km^2 individuals^{-1}
ξ	mean survival of pathogen in water	day^{-1}

3.1.1 Background

The model for multiple transmission pathways of a waterborne pathogen, first developed by Tien and Earn [59, 64], is a compartmental ODE model extending the classical SIR framework by adding a water compartment to track pathogen concentration in an aquatic reservoir. Their model, for a single population, is given by:

$$\frac{dS}{dt} = \mu N - b_W SW - b_I SI - \mu S \tag{3.1}$$

$$\frac{dI}{dt} = b_W SW + b_I SI - \gamma I - \mu I \tag{3.2}$$

$$\frac{dR}{dt} = \gamma I - \mu R \tag{3.3}$$

$$\frac{dW}{dt} = \alpha I - \xi W \tag{3.4}$$

with the total population: $N = S + I + R$. The compartment variables and the other parameters are defined in Tables 3.1 and 3.2.

The model allows for infection through exposure to contaminated water as well as the classical person-to-person contact. Susceptibles infected with cholera move to the infected class. There is a mean infectious period, $\frac{1}{\gamma}$, after which the infectious move to the recovered class. Those in the infected class contribute to the pathogen concentration at a shedding rate, α. The pathogen in the aquatic reservoir also has a natural decay rate, ξ. There is also a natural birth/death rate, μ, in which individuals enter the susceptible class and are removed proportionally in each compartment. They analyzed the nondimensional version of the system, eliminating the recovered/removed class. They also did not include deaths due to disease.

3.2 Description of Model

We will extend the model (3.1)-(3.4) to include spatial movement among patches in a metapopulation setting, with both person and water movement. We also include a death due to disease term. We investigate the cholera model with a scaled pathogen concentration in the water compartment. We consider a multi-patch system, with each patch having four ordinary differential equations. The model accounts for both direct person-to-person transmission and indirect transmission from reservoir to person. Infected individuals contribute the pathogen to the aquatic reservoir. The pathogen then infects individuals within that community or could be transported to surrounding communities, infecting their aquatic reservoirs, which could lead to further transmission of the disease.

The model incorporates both population movement as well as the hydrological links between communities that spread the disease. The dynamics for human movement and pathogen movement in water will be investigated. Both interconnections are modeled using connectivity matrices. Pathogen spreads both upstream and downstream with upstream movement at a lower rate than downstream (similar to work by Bertuzzo [7, 8, 10]).

Using connectivity matrices, we create metapopulations in which pathogen is spread through patches. We investigate various spatial arrangements of populations including linear

and hub arrangements. The idea of a hub allows the model to account for patches of larger populations with higher human connectivity to surrounding patches. Also, using a connectivity matrices, we are able to implement strong and weak connections among patches.

The pathogen levels contributed to the water compartment from the infected population is known to be highly variable, depending on the individual. Due to the high variability in the "shedding" rate, α, we scale the water compartment to eliminate the term from our model. Following a similar approach as in Tien and Earn [59], we make the following substitution into the system of equations (3.1)-(3.4) to scale the water compartment:

$$w = \frac{\xi}{\alpha} W \quad \text{and} \quad \beta_W = b_W \frac{\alpha}{\xi} \quad \text{and} \quad \beta_I = b_I.$$

We extend (3.1)-(3.4) as a metapopulation model with a scaled water compartment, and with disease-related mortality.

$$\frac{dS_i}{dt} = \mu_i N_i - \beta_I^i S_i I_i - \beta_W^i S_i w_i - \mu_i S_i + d_S \sum_{k=1}^{n} (M_{ik} S_k - M_{ki} S_i) \tag{3.5}$$

$$\frac{dI_i}{dt} = \beta_I^i S_i I_i + \beta_W^i S_i w_i - (\gamma_i + \mu_i + \delta_i) I_i + d_I \sum_{k=1}^{n} (M_{ik} I_k - M_{ki} I_i) \tag{3.6}$$

$$\frac{dR_i}{dt} = \gamma_i I_i - \mu_i R_i + d_R \sum_{k=1}^{n} (M_{ik} R_k - M_{ki} R_i) \tag{3.7}$$

$$\frac{dw_i}{dt} = \xi_i [I_i - w_i] + d_W \sum_{k=1}^{n} (H_{ik} w_k - H_{ki} w_i) \tag{3.8}$$

subject to initial conditions:

$$S_i(0) = S_{i_0}, I_i(0) = I_{i_0}, R_i(0) = R_{i_0}, w_i(0) = W_{i_0}. \tag{3.9}$$

We let $M_{i,j}$, $H_{i,j}$ be the connectivity of human and pathogen movement from Patch j to Patch i, respectively. We assume the travel rates of individuals and pathogen from patch i to patch j, are nonnegative, $M_{i,j} \geq 0$, $H_{i,j} \geq 0$, respectively, and we give specific structure

Table 3.3: Description of Compartments with Units for Metapopulation Model

Parameters	Description	Units
S_i	susceptible individual density	ind. km^{-2}
I_i	infected individual density	ind. km^{-2}
R_i	immune due to vaccination or recovery	ind. km^{-2}
N_i	total population density	ind. km^{-2}
W_i	scaled pathogen concentration in water reservoir	ind. km^{-2}

Table 3.4: Description of Parameters with Units for Metapopulation Model

Parameters	Description	Units
μ_i	birth and death (non-disease related)	day^{-1}
β_I^i	person-person contact rate	km^2 ind.$^{-1}$ day^{-1}
β_W^i	reservoir-person contact rate	km^2 ind.$^{-1}$ day^{-1}
γ_i	duration of infectiousness of the disease	day^{-1}
δ_i	death due to disease	day^{-1}
ξ_i	mean survival of pathogen in water	day^{-1}
d_S	diffusion coefficient (for all susceptibles)	day^{-1}
d_R	diffusion coefficient (for all recovered)	day^{-1}
d_I	diffusion coefficient (for infecteds)	day^{-1}
d_W	diffusion coefficient (for pathogen)	day^{-1}

later. The parameters μ and ξ are positive while the parameters γ and δ are nonnegative. We also assume the transmission rates, β_I and β_W, are nonnegative.

In order to appropriately model the pathogen movement in water through the system of patches, we incorporate a term that removes pathogen from the system. This term only removes a proportion of pathogen from the system. There is no import of pathogen, after the initial time, from outside the system.

Assume the patches of the system are located along a river and that the patches are positioned such that one patch is located at the uppermost part of the river and another at the farthest downstream. Just as pathogen moves among the patches through the hydrological connections, there is a proportion of the pathogen that leaves the system at the bottom of the river and a smaller proportion leaving at the top. The patches located in the positions at the top and bottom of the river will be referred to as the water source and terminal patches, respectively.

For simplicity, we will use the notation for the pathogen in water, W, when referring to the scaled water compartment, w, and now equation (3.8) becomes:

$$\frac{dW_i}{dt} = \xi_i[I_i - W_i] + d_W \sum_{k=1}^{n} (H_{ik}W_k - H_{ki}W_i) - \phi_i W_i \tag{3.10}$$

where the coefficient ϕ_i is defined as the following:

$$\phi_i = \begin{cases} \rho_u & \text{if Patch i is the water source patch} \\ \rho_d & \text{if Patch i is the water terminal patch} \\ 0 & \text{otherwise} \end{cases} \tag{3.11}$$

where ρ_u, ρ_d are the coefficients for pathogen moving outside the system in the upstream and downstream directions, respectively.

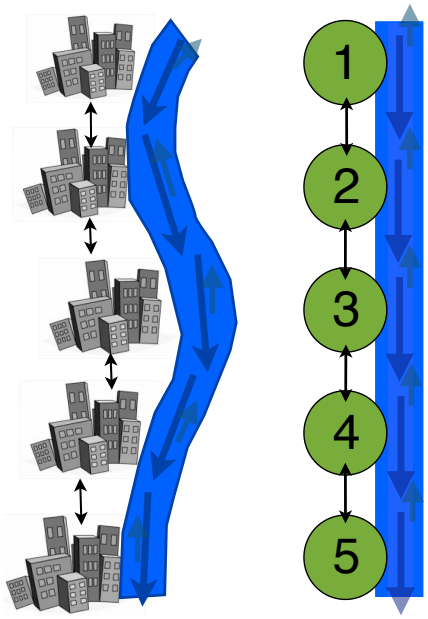

(a) Linear Spatial Arrangement

(b) Numbering of Linear Spatial Arrangement

Figure 3.1: Visual Description of a 5-Patch Linear Spatial Arrangement

3.3 Role of Connectivity and Metapopulations

We consider several spatial arrangements, each representing how interconnected populations interact along with their corresponding water sources. The arrangements are weighted directional graphs involving both water and population movement. We specifically investigate spatial arrangements by varying their connectivities, rates of movement, parameter values, and population sizes. The connectivity patterns of linear and hub arrangements can be visually represented in Figures 3.1 and 3.2.

3.3.1 Linear Spatial Arrangement

Our first scenario is a sequence of patches along a river. There is travel between nearest neighbors only.

The connectivity matrix for population movement in the n-patch linear spatial arrangement:

$$M = \begin{bmatrix} 0 & M_{12} & 0 & \dots & 0 \\ M_{21} & 0 & M_{23} & \ddots & \vdots \\ 0 & M_{32} & 0 & \ddots & 0 \\ \vdots & \ddots & \ddots & \ddots & M_{n-1,n} \\ 0 & \dots & 0 & M_{n,n-1} & 0 \end{bmatrix}.$$

We assume that individuals are bidirectional, moving both to and from a patch, at identical rates. As an example, $M_{j,i}$ is the coefficient for human movement to Patch j from Patch i and $M_{i,j}$ is the coefficient for human movement to Patch i from Patch j. In the linear spatial arrangements, we assume the coefficients are equal in both directions, $M_{i,j} = M_{j,i}$ for all i, j.

The connectivity for water movement in the n-patch linear spatial arrangement:

$$H = \begin{bmatrix} 0 & H_{12} & 0 & \dots & 0 \\ H_{21} & 0 & H_{23} & \ddots & \vdots \\ 0 & H_{32} & 0 & \ddots & 0 \\ \vdots & \ddots & \ddots & \ddots & H_{n-1,n} \\ 0 & \dots & 0 & H_{n,n-1} & 0 \end{bmatrix}.$$

We assume that pathogen moves in both the up and downstream direction, however due to the directional flow of the river, the movement rate downstream will be larger than upstream. This natural occurrence is incorporated into the model through the coefficients of the connectivity matrix. The coefficients for downstream movement will be larger than the those for upstream movement. Thus, $H_{i,j}$ (downstream) $> H_{j,i}$ (upstream) for $i > j$.

Similar to the connectivity matrix for population movement, $H_{j,i}$ is the coefficient for pathogen movement to Patch j from Patch i, which is a downstream movement. The value of this coefficient will be larger than the value of the coefficient, $H_{i,j}$, representing the movement

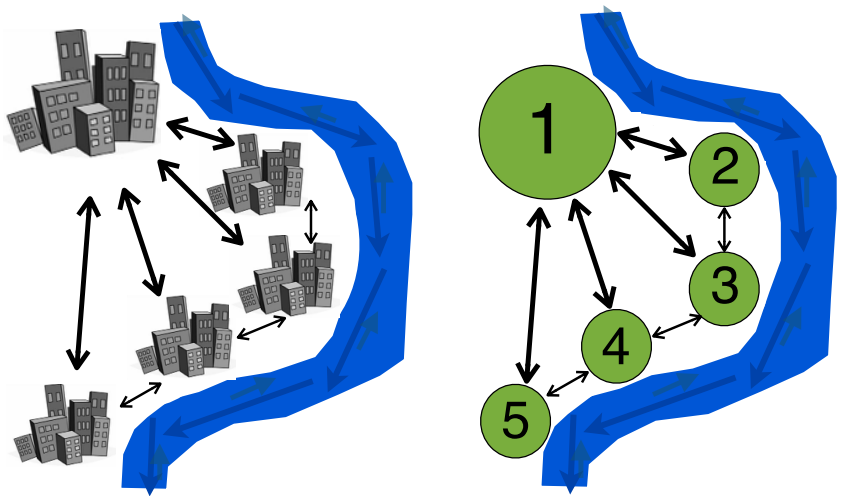

(a) Hub Arrangement

(b) Numbering of Hub Arrangement

Figure 3.2: Visual Description of a 5-Patch Hub Spatial Arrangement

of pathogen upstream to Patch i from Patch j. This relationship is determined based on the spatial arrangement considered.

3.3.2 Hub Spatial Arrangement

We compare the linear spatial arrangement with a scenario which incorporates a hub patch, representing a large, populous area with higher human movement to and from each of the other patches in the system. The movement coefficients to and from the hub will be larger than movement between all other patches. In the connectivity matrix below, assuming Patch 1 is the hub, the coefficients M_{1j} and M_{i1} for $i, j = 1, \ldots, n$, represent movement to and from the hub patch, with the following inequality conditions, $M_{1j} > M_{i,j}$ for all $i, j \neq 1$ and $M_{i,1} > M_{i,j}$ for all $j, i \neq 1$.

We still have the patches located along a linear river arrangement and assume movement of the population in non-hub patches is to the hub and its nearest neighbors. Just as in the linear spatial arrangement case, we assume up and downstream movement of pathogen in the water, with upstream at a smaller rate.

The connectivity matrix for population movement in an n-patch hub arrangement, with Patch 1 as hub:

$$M = \begin{bmatrix} 0 & M_{12} & M_{13} & \dots & \dots & M_{1,n} \\ M_{21} & 0 & M_{23} & 0 & \dots & 0 \\ M_{31} & M_{32} & \ddots & \ddots & \ddots & \vdots \\ \vdots & 0 & \ddots & \ddots & \ddots & 0 \\ \vdots & \vdots & \ddots & \ddots & \ddots & M_{n-1,n} \\ M_{n,1} & 0 & \dots & 0 & M_{n,n-1} & 0 \end{bmatrix}.$$

The connectivity for water movement in an n-patch hub arrangement is the same as in the linear spatial arrangement:

$$H = \begin{bmatrix} 0 & H_{12} & 0 & \dots & 0 \\ H_{21} & 0 & H_{23} & \ddots & \vdots \\ 0 & H_{32} & 0 & \ddots & 0 \\ \vdots & \ddots & \ddots & \ddots & H_{n-1,n} \\ 0 & \dots & 0 & H_{n,n-1} & 0 \end{bmatrix}.$$

3.4 Basic Reproduction Number

We begin by finding the basic reproduction number for our model. We use the next-generation approach, introduced by Dieckmann and Heesterback [18] and Watmough and van den Driessche [65]. We arrange our system of equations into the form $\bar{x}' = \mathcal{F} - \mathcal{V}$, with $\mathcal{F}$ containing new infected terms and $\mathcal{V}$ containing transition terms, with the order of components being $(I_i, \dots, W_i, \dots, S_i, \dots, R_i)$, for $i = 1, \dots, n$. The equations of our system that correspond to infected compartments are:

For $i = 1, \dots, n$

$$\begin{bmatrix} I_i \\ W_i \end{bmatrix}' = \begin{bmatrix} \beta_I^i S_i I_i + \beta_W^i S_i W_i \\ 0 \end{bmatrix} - \begin{bmatrix} (\gamma_i + \mu_i + \delta_i) I_i - d_I \sum_{k=1}^{n} [M_{ik} I_k - M_{ki} I_i] \\ -\xi_i (I_i - W_i) - d_W \sum_{k=1}^{n} [H_{ik} W_k - H_{ki} W_i] + \phi_i W_i \end{bmatrix}.$$

The unique disease-free equilibrium (DFE) is found by setting $I_i = W_i = 0$ for $i = 1, ..., n$. The DFE exists since removing the infected population and pathogen leaves a fully susceptible population that will remain disease-free,

$$DFE = (S_1, \ldots, S_n, I_1, \ldots, I_n, R_1, \ldots, R_n, W_1, \ldots, W_n) = (N_1, \ldots, N_n, 0, \ldots, 0).$$

By taking the Jacobian of the submatrix of the $\mathcal{F}$ matrix with respect to each of the infected and water compartments, and then evaluating at the DFE, we get the following $2n \times 2n$ matrix, F:

$$F = \begin{bmatrix} F_{11} & F_{12} \\ 0 & 0 \end{bmatrix}$$

where $F_{11} = diag(\beta_I^i N_i)$ and $F_{12} = diag(\beta_W^i N_i)$, $n \times n$ matrices. Similarly, taking the Jacobian of the submatrix of $\mathcal{V}$ with respect to the infected and water compartments, then evaluating at the DFE, we get the $2n \times 2n$ matrix, V:

$$V = \begin{bmatrix} V_{11} & 0 \\ -V_{21} & V_{22} \end{bmatrix}$$

where $V_{21} = diag(\xi_i)$, an $n \times n$ matrix,

$$V_{11} = \begin{bmatrix} A_1 & -d_I M_{12} & \ldots & -d_I M_{1n} \\ -d_I M_{21} & \ddots & \ddots & \vdots \\ \vdots & \ddots & \ddots & -d_I M_{n-1n} \\ -d_I M_{n1} & \ldots & -d_I M_{nn-1} & A_n \end{bmatrix},$$

$V_{22} =$

$$\begin{bmatrix} B_1 & -d_W H_{12} & \dots & -d_W H_{1n} \\ -d_W H_{21} & \ddots & \ddots & \vdots \\ \vdots & \ddots & \ddots & -d_W H_{n-1n} \\ -d_W H_{n1} & \dots & -d_W H_{nn-1} & B_n \end{bmatrix},$$

and

$$\begin{aligned} A_i &= (\gamma_i + \mu_i + \delta_i) + d_I \sum_{k=1}^{n} M_{ki} \\ B_i &= \xi_i + d_W \sum_{k=1}^{n} H_{ki} - \phi_i. \end{aligned}$$

We use an approach by Arino [3] which incorporates block matrices to compute the basic reproduction number. The matrices V_{11} and V_{22} are both non-positive on the off-diagonal and satisfy the definition of non-singular M-Matrices, meaning that they can be written in the form, $A = sI - B$, where $s > 0$ and $B \geq 0$, and $s > \rho(B)$, the spectral radius of B. Since both matrices, V_{11} and V_{22}, are nonsingular M-Matrices, they have positive inverses and are both irreducible [6]. We have

$$V^{-1} = \begin{bmatrix} V_{11}^{-1} & 0 \\ V_{22}^{-1} V_{21} V_{11}^{-1} & V_{22}^{-1} \end{bmatrix}.$$

We form the next generation matrix, FV^{-1}:

$$FV^{-1} = \begin{bmatrix} F_{11} V_{11}^{-1} + F_{12} V_{22}^{-1} V_{21} V_{11}^{-1} & F_{12} V_{22}^{-1} \\ 0 & 0 \end{bmatrix}.$$

The spectral radius for FV^{-1} is the same as the spectral radius of the matrix in the upper left block of FV^{-1},

$$\mathcal{R}_0 = \rho(FV^{-1}) = \rho(F_{11}V_{11}^{-1} + F_{12}V_{22}^{-1}V_{21}V_{11}^{-1}),$$

which is dependent on which spatial arrangement and the corresponding connectivity matrices, M and H. In the case of a single patch, $\mathcal{R}_0$ simplifies to the following:

$$\mathcal{R}_0 = \frac{(\beta_I + \beta_W)N_1}{\gamma + \mu + \delta}.$$

From [65], we obtain our stability result:

Theorem 3.1. *When $\mathcal{R}_0 < 1$, the disease-free equilibrium is locally asymptotically stable but if $\mathcal{R}_0 > 1$, the equilibrium will be unstable.*

3.5 Optimal Control Formulation and Analysis

3.5.1 Formulation

To investigate how the management of vaccination strategies depend on the spatial arrangement of patches, we include a vaccination term in the system (3.5)-(3.7),(3.10). The vaccination rates, $\mathrm{v}_i(t)$, represent the rate of vaccination effort transferring susceptibles directly to the recovered class within patch i. It is a combined coefficient, $\eta\sigma_i(t)$ where η represents the efficacy of the vaccination distribution and σ_i is the rate of vaccine distribution.

When including a vaccination term, with rate v_i in the patch i, our model takes the form:

$$\frac{dS_i}{dt} = \mu_i N_i - \beta_I^i S_i I_i - \beta_W^i S_i W_i - \mu_i S_i + d_S \sum_{k=1}^{n}(M_{ik}S_k - M_{ki}S_i) - \mathrm{v}_i(t)S_i \quad (3.12)$$

$$\frac{dI_i}{dt} = \beta_I^i S_i I_i + \beta_W^i S_i W_i - (\gamma_i + \mu_i + \delta_i)I_i + d_I \sum_{k=1}^{n}(M_{ik}I_k - M_{ki}I_i) \quad (3.13)$$

$$\frac{dR_i}{dt} = \gamma_i I_i - \mu_i R_i + d_R \sum_{k=1}^{n}(M_{ik}R_k - M_{ki}R_i) + \mathrm{v}_i(t)S_i \quad (3.14)$$

$$\frac{dW_i}{dt} = \xi_i[I_i - W_i] + d_W \sum_{k=1}^{n}(H_{ik}W_k - H_{ki}W_i) - \phi_i W_i \quad (3.15)$$

with initial conditions (3.9).

We seek to find an optimal vaccination strategy that minimizes the number of infected in the network while minimizing some nonlinear cost involved with the vaccination program. The cost involved with the vaccination strategy includes two terms. We have a nonlinear cost associated with vaccination which incorporates the cost of housing distribution centers, employing individuals to administer the vaccines, and other large costs for implementing a vaccination campaign. The linear part represents the total number of susceptibles vaccinated, including the cost of vaccination for each individual. See [25] for some justification for including such a nonlinearity in the cost with vaccination control. The objective functional is given by:

$$J(\mathbf{v}) = \int_0^T \sum_{i=1}^{n} A_i I_i + \sum_{i=1}^{n} B_i \mathrm{v}_i^2 + \sum_{i=1}^{n} C_i \mathrm{v}_i S_i \, d\mathrm{v} \quad (3.16)$$

over the control set:

$$V = \{\mathbf{v} = (\mathrm{v}_1, \ldots, \mathrm{v}_n) \mid \mathrm{v}_i : [0,T] \to \mathbb{R}, 0 \leq \mathrm{v}_i(t) \leq \mathrm{v}_{max}, \mathrm{v}_i \text{ Lebesgue measurable}\}.$$

The positive constants, A_i, B_i, C_i are constants to weight the relative importance of each of the terms in the objective functional. The optimal control problem is stated as:

Find $\mathrm{v}^* \in V$ such that

$$J(\mathbf{v}^*) = \inf_{\mathbf{v} \in V} J(\mathbf{v})$$

subject to state equations (3.12)-(3.15) and initial conditions (3.9).

3.5.2 Boundedness and Positivity of State Solutions

Now that we have formulated the optimal control problem, we need to prove that a nonnegative, bounded state solution exists to the problem.

Theorem 3.2. *Given a vector of controls,* $\mathbf{v} = (\mathrm{v}_1, \ldots, \mathrm{v}_n) \in V$*, there exists a nonnegative, bounded solution,* $\mathbf{x} = (S_1, I_1, R_1, W_1, \ldots, S_n, I_n, R_n, W_n)$*, to the initial value problem defined by (3.12)-(3.15) with initial conditions (3.9).*

Proof. To prove nonnegativity of solutions, we will use similar approach as in [60] to prove the system is positively invariant. By our assumptions on the model, we ensure that the solutions of the system, starting with nonnegative initial conditions, stays nonnegative for all $t > 0$, i.e. $S_i(t) \geq 0$,$I_i(t) \geq 0$,$R_i(t) \geq 0$,$W_i(t) \geq 0$, for $i = 1, \ldots, n$.

In proving the boundedness of the solutions, we follow a similar approach as [21] and use the following notation. Let $\bar{N} = \sum_{i=1}^{n} N_i$, where $N_i = S_i + I_i + R_i$. By adding the state equations for individuals, S_i, I_i, R_i, we have the following:

$$\frac{d\bar{N}}{dt} = -(\delta_1 I_1 + \ldots + \delta_n I_n).$$

Since $\delta_i I_i \geq 0$ for all $i = 1, \ldots, n$, we can conclude that:

$$\frac{d\bar{N}}{dt} \leq 0.$$

Thus, the population is bounded by the initial condition,

$$\bar{N}(t) \leq \bar{N}_0,$$

where $\bar{N}_0 = \bar{N}(0)$. We still need an upper bound on the compartment for pathogen in water. Again, we use the notation, $\bar{W} = \sum_{i=1}^{n} W_i$ and $\bar{\xi} = \max\{\xi_i | i = 1, \ldots, n\}$. By summing the water compartments, we have:

$$\frac{d\bar{W}}{dt} = \xi_1(I_1 - W_1) + \ldots + \xi_n(I_n - W_n).$$

The bounds on:

$$\frac{d\bar{W}}{dt} \leq \sum_{i=1}^{n} \xi_i I_i \leq \bar{\xi} \sum_{i=1}^{n} I_i \leq \bar{\xi}\bar{N} \leq \bar{\xi}\bar{N}_0,$$

gives the upper bound:

$$\bar{W}(t) \leq \bar{\xi}\bar{N}_0 T + \bar{W}_0,$$

where T is the final time and $\bar{W}_0 = \bar{W}(0)$.

Therefore the feasible region for our state system is:

$$\begin{aligned} \Gamma \quad &= \{(S_1, I_1, R_1, W_1, \ldots, S_n, I_n, R_n, W_n) \in \mathcal{R}_+^{4n} | \\ &\bar{N} = \sum_{i=1}^{n} (S_i + I_i + R_i) \leq \bar{N}_0, \;\; \bar{W} = \sum_{i=1}^{n} W_i \leq \bar{\xi}\bar{N}_0 T + \bar{W}_0\}. \end{aligned}$$

□

3.5.3 Existence of the Optimal Control

In order to use Pontryagin's Maximum Principle (PMP) [52], the existence of an optimal control must be proven.

Theorem 3.3. *There exists an optimal control vector,* $\mathbf{v}^* = (\mathrm{v}_1^*, \ldots, \mathrm{v}_n^*) \in V$ *with corresponding states* $\mathbf{x}^* = (S_1^*, I_1^*, R_1^*, W_1^*, \ldots, S_n^*, I_n^*, R_n^*, W_n^*)$*, that minimizes the objective functional* $J(\mathbf{v})$ *defined by (3.16).*

Proof. Since our controls are Lebesgue measurable in the set V and both the controls and states are positive,

$$0 \leq J(\mathbf{v}) \ \ \forall \mathbf{v} \in V.$$

Thus, the $\inf_{\mathbf{v}\in V} J(\mathbf{v})$ exists and is finite. There exists a minimizing sequence of controls, $\mathbf{v}^k = (\mathrm{v}_1^k, \ldots, \mathrm{v}_n^k)$, in V such that

$$\lim_{k\to\infty} J(\mathbf{v}^k) = \inf_{\mathbf{v}\in V} J(\mathbf{v}).$$

By [24], since $||\mathbf{v}^k||_{L^\infty} \leq C_1$, there exists $\mathbf{v}^* \in (L^2([0,T]))^n$ such that on a subsequence, for each i,

$$\mathbf{v}_i^k \rightharpoonup \mathbf{v}_i^* \text{ weakly in } L^2([0,T]) \text{ as } k \to \infty.$$

Given that the controls are uniformly bounded and by Theorem 3.2, the state sequence corresponding to the sequence of minimizing controls is also uniformly bounded, i.e., there exists C_2 such that, for $k = 1, \ldots$ and $i = 1, \ldots, n$,

$$|\mathbf{x}_i^k(t)| \leq C_2 \ \ \forall t \in [0,T].$$

By the structure of the system and the fact that the state sequence is uniformly bounded, we have uniformly bounded derivatives, for $k = 1, \ldots$ and $i = 1, \ldots, n$,

$$|(\mathbf{x}_i^k(t))'| \leq C_3 \ \ \forall t \in [0,T].$$

Given that the state sequence is uniformly Lipschitz, the state solution sequence $\{\mathbf{x}^k\}$ is equicontinuous. By the Ascoli-Azela Theorem, there exists $\mathbf{v}^* \in V$ and $\mathbf{x}^*$ such that

$$\mathbf{v}^k \rightharpoonup \mathbf{v}^* \text{ weakly in } L^2(0,T) \text{ and } \mathbf{x}^k \to \mathbf{x}^* \text{ uniformly on } [0,T].$$

This uniform convergence is needed to get convergence of terms like $\mathrm{v}_i S_i$ in our system. By passing the limit in the system of differential equations, we can show $\mathbf{x}^*$ is the state corresponding to the control $\mathbf{v}^*$. Using lower semicontinuity of L^2 norms with respect to L^2 weak convergence and the convergences above, we have

$$\begin{aligned}
\inf_{\mathbf{v}} J(\mathbf{v}) &= \lim_{k\to\infty} J(\mathbf{v}^k) \\
&= \int_0^T \sum_{i=1}^n \left(A_i I_i^* + \sum_{i=1}^n C_i \mathrm{v}_i^* S_i^* \right) d\mathbf{v} + \lim_{k\to\infty} \int_0^T \sum_{i=1}^n B_i (\mathrm{v}_i^k)^2 \, d\mathbf{v} \\
&\geq \int_0^T \sum_{i=1}^n \left(A_i I_i^* + \sum_{i=1}^n C_i \mathrm{v}_i^* S_i^* \right) d\mathbf{v} + \int_0^T \sum_{i=1}^n B_i (\mathrm{v}_i^*)^2 \, d\mathbf{v} \\
&= J(\mathbf{v}^*).
\end{aligned}$$

Thus, $\mathbf{v}^*$ is an optimal control. □

3.5.4 Optimality System

Having obtained the existence of an optimal control, we can now apply PMP, forming the Hamiltonian, H:

$$\begin{aligned} H &= \sum_{i=1}^{n} \left[A_i I_i + B_i \mathrm{v}_i^2 + C_i \mathrm{v}_i S_i \right] \\ &+ \sum_{i=1}^{n} \lambda_{S_i} \left[\mu_i N_i - \beta_I^i S_i I_i - \beta_W^i S_i w_i - \mu_i S_i + d_S \sum_{k=1}^{n} (M_{ik} S_k - M_{ki} S_i) - \mathrm{v}_i(t) S_i \right] \\ &+ \sum_{i=1}^{n} \lambda_{I_i} \left[\beta_I^i S_i I_i + \beta_W^i S_i w_i - (\gamma_i + \mu_i + \delta_i) I_i + d_I \sum_{k=1}^{n} (M_{ik} I_k - M_{ki} I_i) \right] \\ &+ \sum_{i=1}^{n} \lambda_{R_i} \left[\gamma_i I_i - \mu R_i + d_R \sum_{k=1}^{n} (M_{ik} R_k - M_{ki} R_i) + \mathrm{v}_i(t) S_i \right] \\ &+ \sum_{i=1}^{n} \lambda_{w_i} \left[\xi_i (I_i - w_i) + d_W \sum_{k=1}^{n} (H_{ik} w_k - H_{ki} w_i) - \phi_i w_i \right] \end{aligned} \tag{3.17}$$

where the adjoint variables (λ_j), corresponding to their respective states, attach the right hand side of the state equations to the objective functional. Since an optimal solution exists, we can obtain the necessary conditions for optimality using Pontryagin's Maximum Principle.

Theorem 3.4. *Given an optimal control vector* $\mathbf{v}^* \in V$*, and corresponding states* $\mathbf{x}^*$*, there exist adjoint functions satisfying*

$$\begin{aligned}
\frac{d\lambda_{S_i}}{dt} &= -\Bigg(C_i \mathrm{v}_i(t) + \lambda_{S_i}\left[-\beta_I^i I_i - \beta_W^i w_i - d_S \sum_{k=1}^{n} M_{ki} - \mathrm{v}_i(t)\right] \qquad (3.18)\\
&\quad +\lambda_{I_i}\left[\beta_I^i I_i + \beta_W^i w_i\right] + \lambda_{R_i}\mathrm{v}_i(t) + d_S \sum_{k=1}^{n}(\lambda_{S_k} M_{ki})\Bigg)\\
\frac{d\lambda_{I_i}}{dt} &= -\Bigg(A_i + \lambda_{S_i}\left(\mu_i - \beta_I^i S_i\right) + \lambda_{I_i}\left[\beta_I^i S_i - (\gamma_i + \mu_i + \delta_i) - d_I \sum_{k=1}^{n} M_{ki}\right] \qquad (3.19)\\
&\quad +\lambda_{R_i}\gamma_i + \lambda_{W_i}\xi_i + d_I \sum_{k=1}^{n}(\lambda_{I_k} M_{ki})\Bigg)\\
\frac{d\lambda_{R_i}}{dt} &= -\left(\lambda_{S_i}\mu_i - \lambda_{R_i}\left(\mu_i + d_R \sum_{k=1}^{n} M_{ki}\right) + d_R \sum_{k=1}^{n}(\lambda_{R_k} M_{ki})\right) \qquad (3.20)\\
\frac{d\lambda_{W_i}}{dt} &= -\Bigg(-\lambda_{S_i}\beta_W^i S_i + \lambda_{I_i}\beta_W^i S_i - \lambda_{W_i}\left(\xi_i + d_W \sum_{k=1}^{n} H_{ki} + \phi_i\right)\\
&\quad +d_W \sum_{k=1}^{n}(\lambda_{W_k} H_{ki})\Bigg) \qquad (3.21)
\end{aligned}$$

for $i = 1, \ldots, n$ *with the following transversality conditions at the final time,* T*,*

$$\lambda_{S_i}(T) = \lambda_{I_i}(T) = \lambda_{R_i}(T) = \lambda_{W_i}(T) = 0. \qquad (3.22)$$

This optimal control is characterized by

$$\mathrm{v}_i^* = max\left(min\left(\mathrm{v}_{max}, \frac{\lambda_{S_i} S_i - \lambda_{R_i} S_i - C_i S_i}{2B_i}\right), 0\right). \qquad (3.23)$$

Proof. The differential equations for the adjoint are standard results of Pontryagin's Maximum Principle [52]. The right hand sides of the differential equations are easily

computed by:

$$\begin{aligned}
\frac{d\lambda_{S_i}}{dt} &= -\frac{\partial H}{\partial S_i}, \\
\frac{d\lambda_{I_i}}{dt} &= -\frac{\partial H}{\partial I_i}, \\
\frac{d\lambda_{R_i}}{dt} &= -\frac{\partial H}{\partial R_i}, \\
\frac{d\lambda_{W_i}}{dt} &= -\frac{\partial H}{\partial W_i}.
\end{aligned}$$

The final time conditions are the transversality conditions. Because there is no salvage term in the objective functional, the final time conditions are zero. The adjoint differential equations are linear in the adjoint function, and thus a unique adjoint solution exists.

We consider three cases when characterizing the controls, $\mathbf{v}^* = (\mathrm{v}_1^*, \ldots, \mathrm{v}_n^*)$. We use that the fact that $\mathbf{v}^*$ minimizes H with respect to $\mathbf{v}$ at t, $\mathbf{x}(t)$, and $\lambda(t)$.

1. On the interior of the control set, $\{t \mid 0 < \mathrm{v}_i^*(t) < \mathrm{v}_{max}\}$, we have, for $i = 1, \ldots, n$,

$$0 = \frac{\partial H}{\partial \mathrm{v}_i} = 2B_i\mathrm{v}_i(t) + C_iS_i - \lambda_{S_i}S_i + \lambda_{R_i}S_i.$$

   Solving for the controls, we have

$$\mathrm{v}_i^*(t) = \frac{(\lambda_{S_i} - \lambda_{R_i} - C_i)S_i}{2B_i}.$$

2. On the set $\{t \mid \mathrm{v}_i^*(t) = 0\}$, we have

$$0 \leq \frac{\partial H}{\partial \mathrm{v}_i} = 2B_i\mathrm{v}_i^* + C_iS_i - \lambda_{S_i}S_i + \lambda_{R_i}S_i.$$

Since $2B_i > 0$, we have:

$$\frac{(\lambda_{S_i} - \lambda_{R_i} - C_i)S_i}{2B_i} \leq 0.$$

3. On the set $\{t \mid \mathrm{v}_i^*(t) = \mathrm{v}_{max}\}$, we have

$$0 \geq \frac{\partial H}{\partial \mathrm{v}_i} = 2B_i \mathrm{v}_{max}^* + C_i S_i - \lambda_{S_i} S_i + \lambda_{R_i} S_i.$$

Again, since $2B_i > 0$, we have:

$$\frac{(\lambda_{S_i} - \lambda_{R_i} - C_i)S_i}{2B_i} \geq \mathrm{v}_{max}^*.$$

Given the three cases above, we have a characterization for this optimal control:

$$\mathrm{v}_i^* = \max\left(\min\left(\mathrm{v}_{max}, \frac{(\lambda_{S_i} - \lambda_{R_i} - C_i)S_i}{2B_i}\right), 0\right).$$

Also note, $\frac{\partial^2 H}{\partial \mathrm{v}_i^2} = 2B_i > 0$ confirming that our optimal control minimizes the Hamiltonian.

□

The optimality system for our problem consists of the state equations (3.12)-(3.15), the adjoint equations (3.18)-(3.21), and the control characterization (3.23).

3.5.5 Uniqueness of the Optimality System

We now must prove that our optimal control is unique. We do this by proving the uniqueness of our optimality system, since the optimal control together with its states and adjoints solve the optimality system.

Theorem 3.5. *For t_1 sufficiently small, the optimal control is unique.*

Proof. Our state solutions are bounded by Theorem 3.2. Since our adjoint system is linear and both our controls and state solutions are bounded, we have a bounded adjoint system.

Suppose, for n patches,

$$(S_1, I_1, R_1, W_1, \ldots, S_n, I_n, R_n, W_n, \lambda_{S_1}, \lambda_{I_1}, \lambda_{R_1}, \lambda_{W_1}, \ldots, \lambda_{S_n}, , \lambda_{I_n}, \lambda_{R_n}, \lambda_{W_n})$$

and

$$(\hat{S}_1, \hat{I}_1, \hat{R}_1, \hat{W}_1, \ldots, \hat{S}_n, \hat{I}_n, \hat{R}_n, \hat{W}_n, \hat{\lambda}_{S_1}, \hat{\lambda}_{I_1}, \hat{\lambda}_{R_1}, \hat{\lambda}_{W_1}, \ldots, \hat{\lambda}_{S_n}, \hat{\lambda}_{I_n}, \hat{\lambda}_{R_n}, \hat{\lambda}_{W_n})$$

are two solutions with identical initial conditions. Let $\mathbf{v} = (\mathrm{v}_1, \ldots, \mathrm{v}_n)$ and $\hat{\mathbf{v}} = (\hat{\mathrm{v}}_1, \ldots, \hat{\mathrm{v}}_n)$ by the corresponding controls from the characterization. We use a similar approach as Fister [23] to prove uniqueness.

For $\delta > 0$ to be chosen below, let $S_i = e^{\delta t}x_i$, $I_i = e^{\delta t}y_i$, $R_i = e^{\delta t}z_i$, $W_i = e^{\delta t}w_i$, $\lambda_{S_i} = e^{-\delta t}p_i$, $\lambda_{I_i} = e^{-\delta t}a_i$, $\lambda_{R_i} = e^{-\delta t}b_i$, and $\lambda_{W_i} = e^{-\delta t}d_i$. Similarly, for $\hat{S}_i, \ldots, \hat{\lambda}_{W_i}$

We can substitute these change of variables into each of the differential equations for our states and adjoints. For example, in $\frac{dS_i}{dt}$:

$$e^{\delta t}x_i' + \delta e^{\delta t}x_i = \mu(y_i + z_i)e^{\delta t} - \beta_I x_i y_i e^{2\delta t} - \beta_W x_i w_i e^{2\delta t} + d_S \sum_{k=1}^{n}(M_{ik}x_k - M_{ki}x_i)e^{\delta t} - \mathrm{v}_i x_i e^{\delta t},$$

which can be rewritten as:

$$x_i' + \delta x_i = \mu(y_i + z_i) - \beta_I x_i y_i e^{\delta t} - \beta_W x_i w_i e^{\delta t} + d_S \sum_{k=1}^{n}(M_{ik}x_k - M_{ki}x_i) - \mathrm{v}_i x_i.$$

A similar approach could be used for each of the state differential equations. We also illustrate the change of variables for the adjoint equations. Using $\frac{d\lambda_{S_i}}{dt}$ as an example,

$$-[p_i' - \delta p_i] = C_i e^{\delta t}\mathrm{v}_i - e^{\delta t}(p_i - a_i)(\beta_I^i y_i + \beta_W^i w_i) - p_i d_S \sum_{k=1}^{n} M_{ki} + d_S \sum_{k=1}^{n} p_k M_{ki} - \mathrm{v}_i(p_i - b_i).$$

We then form the differences of equations for $S_i - \hat{S}_i$, $I_i - \hat{I}_i$,..., $\lambda_{R_i} - \hat{\lambda}_{R_i}$, $\lambda_{W_i} - \hat{\lambda}_{W_i}$. Again, for illustration, the difference of equations for $S_i - \hat{S}_i$ is

$$(x_i - \hat{x}_i)' + \delta(x_i - \hat{x}_i) = \mu(z_i - \hat{z}_i + y_i - \hat{y}_i) - \beta_I(x_i y_i - \hat{x}_i \hat{y}_i)e^{\delta t} - \beta_W(x_i w_i - \hat{x}_i \hat{w}_i)e^{\delta t}$$
$$+ d_S \sum_{k=1}^{n} (M_{ik}(x_k - \hat{x}_k) - M_{ki}(x_i - \hat{x}_i)) - (\mathrm{v}_i x_i - \hat{\mathrm{v}}_i \hat{x}_i).$$

We then multiply each of the differential equations by the appropriate difference, integrate from t_0 to t_1, and use initial conditions:

$$\begin{aligned}
\frac{1}{2}(x_i - \hat{x}_i)^2(t_1) \quad &+ \quad \delta \int_{t_0}^{t_1} (x_i - \hat{x}_i)^2 \, dt \\
&= \quad \mu_i \int_{t_0}^{t_1} [(z_i - \hat{z})_i + (y_i - \hat{y}_i)](x_i - \hat{x}_i) \, dt \\
&\quad -\beta_I \int_{t_0}^{t_1} e^{\delta t}(x_i y_i - \hat{x}_i \hat{y}_i)(x_i - \hat{x}_i) \, dt \\
&\quad -\beta_W \int_{t_0}^{t_1} e^{\delta t}(x_i w_i - \hat{x}_i \hat{w}_i)(x_i - \hat{x}_i) \, dt \\
&\quad + \int_{t_0}^{t_1} d_S \sum_{k=1}^{n} (M_{ik}(x_k - \hat{x}_k) - M_{ki}(x_i - \hat{x}_i))(x_i - \hat{x}_i) \, dt \\
&\quad - \int_{t_0}^{t_1} (\mathrm{v}_i x_i - \hat{\mathrm{v}}_i \hat{x}_i)(x_i - \hat{x}_i) \, dt.
\end{aligned}$$

A similar process could be done for the other state differential equations, for $i = 1, \ldots, n$, and for the adjoint differential equations (using the transversality conditions). Take note of the sign on the time derivative term gives the correct sign on the right hand side of the

equation. As an example,

$$\begin{aligned}
\frac{1}{2}(p_i-\hat{p}_i)^2(t_0) \;+\; & \delta\int_{t_0}^{t_1}(p_i-\hat{p}_i)^2\,dt \\
&= C_i\int_{t_0}^{t_1} e^{\delta t}(\mathrm{v}_i-\hat{\mathrm{v}}_i)(p_i-\hat{p}_i)\,dt \\
&-\int_{t_0}^{t_1} e^{\delta t}(\beta_I(p_iy_i-\hat{p}_i\hat{y}_i)+\beta_W(p_iw_i-\hat{p}_i\hat{w}_i)(p_i-\hat{p}_i)\,dt \\
&-\int_{t_0}^{t_1} d_S\sum_{k=1}^{n}(M_{ki}(p_i-\hat{p}_i)^2\,dt-\int_{t_0}^{t_1}(\mathrm{v}_ip_i-\hat{\mathrm{v}}_i\hat{p}_i)(p_i-\hat{p}_i)\,dt \\
&+\int_{t_0}^{t_1} e^{\delta t}[\beta_I(a_iy_i-\hat{a}_i\hat{y}_i)+\beta_W(a_iw_i-\hat{a}_i\hat{w}_i)](p_i-\hat{p}_i)\,dt \\
&+\int_{t_0}^{t_1}(b_i\mathrm{v}_i-\hat{b}_i\hat{\mathrm{v}}_i)(p_i-\hat{p}_i)\,dt \\
&+\int_{t_0}^{t_1} d_S\sum_{k=1}^{n}(M_{ki}(p_k-\hat{p}_k))(p_i-\hat{p}_i)\,dt.
\end{aligned}$$

We use the fact that we have two sets of controls, $\mathbf{v}=(v_1,\ldots,v_n)$ and $\hat{\mathbf{v}}=(\hat{v}_1,\ldots,\hat{v}_n)$, where

$$\mathrm{v}_i=\max\left(\min\left(\mathrm{v}_{max},\frac{(\lambda_{S_i}-\lambda_{R_i}-C_i)S_i}{2B_i}\right),0\right)$$

and

$$\hat{\mathrm{v}}_i=\max\left(\min\left(\mathrm{v}_{max},\frac{(\hat{\lambda}_{S_i}-\hat{\lambda}_{R_i}-C_i)\hat{S}_i}{2B_i}\right),0\right).$$

Forming the difference, taking absolute values, and using the change of variables we have:

$$\begin{aligned}
|\mathrm{v}_i-\hat{\mathrm{v}}_i| \;=\; & \left|\frac{(p_i-b_i-C_ie^{\delta t})x_i}{2B_i}-\frac{(\hat{p}_i-\hat{b}_i-C_ie^{\delta t})\hat{x}_i}{2B_i}\right| \\
&\le \frac{1}{2B_i}\left|(p_ix_i-\hat{p}_i\hat{x}_i)-(b_ix_i-\hat{b}_i\hat{x}_i)-C_ie^{\delta t}(x_i-\hat{x}_i)\right| \\
&\le \frac{1}{2B_i}\left(|p_ix_i-\hat{p}_i\hat{x}_i|+\left|b_ix_i-\hat{b}_i\hat{x}_i\right|+\left|C_ie^{\delta t}(x_i-\hat{x}_i)\right|\right).
\end{aligned}$$

Our state and adjoint solutions are bounded, as well as our coefficients. Using the bound on $|\mathrm{v}_i - \hat{\mathrm{v}}_i|$, as well as adding and subtracting terms, we have the following state inequalities, wherever the control v_i is found. For example,

$$\begin{aligned}
\delta \int_{t_0}^{t_1} (x_i - \hat{x}_i)^2 \, dt \;\leq\; & K_1 \int_{t_0}^{t_1} \left(|z_i - \hat{z}_i| + |y_i - \hat{y}_i|\right) |x_i - \hat{x}_i| \, dt \\
& + K_2 \int_{t_0}^{t_1} e^{\delta t} \left(|x_i y_i - \hat{x}_i \hat{y}_i| + |x_i w_i - \hat{x}_i \hat{w}_i|\right) |x_i - \hat{x}_i| \, dt \\
& + K_3 \int_{t_0}^{t_1} \sum_{k=1}^{n} (M_{ik} |x_k - \hat{x}_k|) |x_i - \hat{x}_i| \, dt + K_4 \int_{t_0}^{t_1} (x_i - \hat{x}_i)^2 \, dt \\
& + K_5 \int_{t_0}^{t_1} \left(|p_i x_i - \hat{p}_i \hat{x}_i| + \left|b_i x_i - \hat{b}_i \hat{x}_i\right|\right) |x_i - \hat{x}_i| \, dt \\
& + K_6 \int_{t_0}^{t_1} e^{\delta t} (x_i - \hat{x}_i)^2 \, dt
\end{aligned}$$

and similarly for an adjoint inequality:

$$\begin{aligned}
\delta \int_{t_0}^{t_1} (p_i - \hat{p}_i)^2 \, dt \;\leq\; & D_1 \int_{t_0}^{t_1} e^{\delta t} \left(|p_i x_i - \hat{p}_i \hat{x}_i| + \left|b_i x_i - \hat{b}_i \hat{x}_i\right|\right) |p_i - \hat{p}_i| \, dt \\
& + D_2 \int_{t_0}^{t_1} \left(|p_i x_i - \hat{p}_i \hat{x}_i| + \left|b_i x_i - \hat{b}_i \hat{x}_i\right|\right) |p_i - \hat{p}_i| \, dt \\
& + D_3 \int_{t_0}^{t_1} e^{\delta t} |x_i - \hat{x}_i| |p_i - \hat{p}_i| \, dt + D_4 \int_{t_0}^{t_1} |b_i - \hat{b}_i| |p_i - \hat{p}_i| \, dt \\
& + K_2 \int_{t_0}^{t_1} e^{\delta t} (|p_i y_i - \hat{p}_i \hat{y}_i| + |p_i w_i - \hat{p}_i \hat{w}_i|) |p_i - \hat{p}_i| \, dt \\
& + K_2 \int_{t_0}^{t_1} e^{\delta t} \left(|a_i y_i - \hat{a}_i \hat{y}_i| + |a_i w_i - \hat{a}_i \hat{w}_i|\right) |p_i - \hat{p}_i| \, dt \\
& + K_3 \int_{t_0}^{t_1} \sum_{k=1}^{n} (M_{ki} |p_k - \hat{p}_k|) |p_i - \hat{p}_i| \, dt + K_4 \int_{t_0}^{t_1} (p_i - \hat{p}_i)^2 \, dt,
\end{aligned}$$

where D_i, K_i depend on the values of $|\mu_i|$, $|\beta_I|$, $|\beta_W|$, $|C_i|$, $|B_i|$, $\sum_{k=1}^{n} |M_{ki}|$, and $\max_i\{|\hat{x}_i|, |\hat{p}_i|, |b_i|, |\hat{\mathrm{v}}_i|, |\mathrm{v}_i|\}$. We now use the Cauchy Inequality,

$$ab \leq \frac{a^2}{2} + \frac{b^2}{2}$$

with $a, b > 0$, to simplify the above inequalities. We also will add and subtract terms. For simplification purposes, we let $\bar{x}_i = |x_i - \bar{x}_i|$, $\bar{y}_i = |y_i - \bar{y}_i|$, and so on. Using the first state inequality as an example,

$$\begin{aligned} \delta \int_{t_0}^{t_1} \bar{x}_i^2 \;\; &\leq \;\; \hat{K}_1^i \int_{t_0}^{t_1} \left(\bar{x}_i^2 + \bar{z}_i^2 + \bar{y}_i^2 + \bar{p}_i^2 + \bar{b}_i^2 + \sum_{k \neq i} \bar{x}_k^2 \right) \\ &\quad + \hat{K}_2^i \int_{t_0}^{t_1} e^{\delta T} \left(\bar{y}_i^2 + \bar{w}_i^2 + \bar{x}_i^2 \right) \end{aligned}$$

where $\hat{K}_1^i$, $\hat{K}_2^i$ depend on the maximum of all the K_i values, the number of patches n, and the bounds on the states and adjoints.

A similar approach can be done for each of the inequalities. The collection of state and adjoint inequalities can then be added together and we can take the maximum of all the constants collected. We let $\mathbf{K}_1 = \max_i \hat{K}_1^i$ and $\mathbf{K}_2 = \max_i \hat{K}_2^i$. The result is the inequality:

$$\left(\delta - \mathbf{K}_1 - \mathbf{K}_2 e^{\delta T}\right) \int_{t_0}^{t_1} \sum_{i=1}^{n} \left(\bar{x}_i^2 + \ldots + \bar{w}_i^2 + \bar{p}_i^2 + \ldots + \bar{d}_i^2 \right) \, dt \leq 0.$$

We need to choose δ then T such that:

$$\left(\delta - \mathbf{K}_1 - \mathbf{K}_2 e^{\delta T}\right) \geq 0.$$

We choose δ such that:

$$\delta - \mathbf{K}_1 - \mathbf{K}_2 > 0.$$

We then choose T such that:

$$T < \frac{1}{\delta} \ln \left| \frac{\delta - \mathbf{K}_1}{\mathbf{K}_2} \right|.$$

This guarantees $\delta - \mathbf{K}_1 - \mathbf{K}_2 e^{\delta T} > 0$ and

$$\int_{t_0}^{t_1} \sum_{i=1}^{n} \left(\bar{x}_i^2 + \ldots + \bar{w}_i^2 + \bar{p}_i^2 + \ldots + \bar{d}_i^2 \right) \, dt = 0.$$

Thus, the two solutions to the optimality system are equal and thus there is a unique optimal control. □

3.6 Numerical Simulations

The stability and control analysis were completed for any finite number of patches. For numerical purposes, we consider five patches of varying connectivities. We will consider linear and hub arrangements. Initially, we assume identical patch dynamics. We later investigate the role of "hot spots", or patches with higher infectivity. We will also investigate the role that hub size plays on intervention strategies.

The forward-backward iterative technique [39] was used to solve the optimality system, which consists of 3.12-3.15, 3.18-3.21, and 3.23. To solve the ODE systems, we use a fourth-order Runge Kutta method. See the introductory chapter for more details.

3.6.1 Linear Spatial Arrangement

We first investigate disease dynamics within a system of identical patches with a linear spatial arrangement. We assume a series of patches in a straight line along a river. We assume both human and population movement to nearest neighbor only. We want to find optimal vaccination strategies when the disease begins in patches along the river arrangement. The parameter values chosen are found in Table 3.5. Parameter values were chosen from the work of Tuite *et al.* [64] based on the outbreak in Haiti. The model is subject to initial conditions that depend on which patch the outbreak occurs. The weight coefficients in J were chosen to be $A_i = 1$, $B_i = 300,000$, and $C_i = 3.25$. The quadratic terms are thought to be the

Table 3.5: Parameter Values for Numerical Simulations with Identical Patches

Parameters	Description	Value
μ_i	birth and death (non-disease related)	$1.00E-4$
β_I^i	person-person contact rate	$2.64E-5$
β_W^i	reservoir-person contact rate	$1.21E-4$
γ_i	duration of infectiousness of the disease	0.25
δ_i	death due to disease	$5.0E-4$
ξ_i	mean survival of pathogen in water	$7.56E-3$
d_S	diffusion coefficient (for all susceptibles)	$5.00E-3$
d_R	diffusion coefficient (for all recovered)	$5.00E-3$
d_I	diffusion coefficient (for infecteds)	$1.00E-3$
d_W	diffusion coefficient (for pathogen)	$3.00E-5$
ρ_d	coefficient for pathogen leaving network downstream	$3.00E-5$
ρ_u	coefficient for pathogen leaving network upstream	$3.00E-6$
v_{max}	max vaccination	0.015
T	final time (days)	200
A_i	cost to minimize infecteds	1
B_i	quadratic cost of vaccination	$300,000$
C_i	linear cost of susceptibles vaccinated	3.25

distribution costs of the vaccination while the linear terms are the per-person cost of vaccine and its administration.

We begin with the five-patch spatial arrangement illustrated in Figure 3.1. Since movement is only to nearest neighbor, the connectivity matrices for both human and pathogen movement are identical. The connectivity matrix for population movement in the five-patch linear spatial arrangement is

$$M = \begin{bmatrix} 0 & M_{12} & 0 & 0 & 0 \\ M_{21} & 0 & M_{23} & 0 & 0 \\ 0 & M_{32} & 0 & M_{34} & 0 \\ 0 & 0 & M_{43} & 0 & M_{45} \\ 0 & 0 & 0 & M_{54} & 0 \end{bmatrix}.$$

We assume the values of the non-zero M_{ij} are identical and equal to one. The connectivity for water movement in the linear spatial arrangement is

Table 3.6: Initial Conditions for Model with Linear Spatial Arrangement and Outbreak in Patch i

Class	Patch i	Patches $j \neq i$
S	9,700	10,000
I	300	0
R	0	0
W	300	0

$$H = \begin{bmatrix} 0 & H_{12} & 0 & 0 & 0 \\ H_{21} & 0 & H_{23} & 0 & 0 \\ 0 & H_{32} & 0 & H_{34} & 0 \\ 0 & 0 & H_{43} & 0 & H_{45} \\ 0 & 0 & 0 & H_{54} & 0 \end{bmatrix}.$$

The value for the non-zero downstream connectivity movements, H_{ij} where $i > j$, is equal to one while for the non-zero upstream connectivity movements, H_{ij} for $j > i$, is equal to 0.1, or one-tenth the rate of the downstream movement. This is due to a stronger movement of pathogen downstream than upstream, which is consistent with the direction of river flow.

We first compare population dynamics and vaccination strategies for the arrangements for outbreaks occurring in each patch along the river system. For all simulations, we begin an outbreak with 300 infected individuals. This was chosen to simulate an epidemic, where a significant number of infected would need to be present in a community before a large scale intervention strategy would be implemented. The initial conditions for individuals and water in the system, assuming an outbreak begins in Patch i, are shown in Table 3.6.

Without vaccination, the dynamics of the infected population for an outbreak occurring in each of the five patches is given in Figure 3.3. Notice the patterns that form as the disease travels to nearest neighbor throughout the metapopulation. We also see the disease spreading to patches downstream at a faster rate than those upstream.

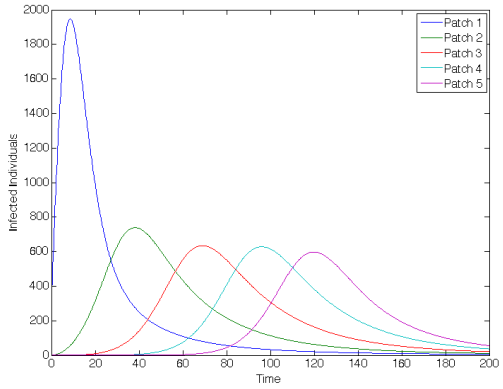

(a) Outbreak in Patch 1

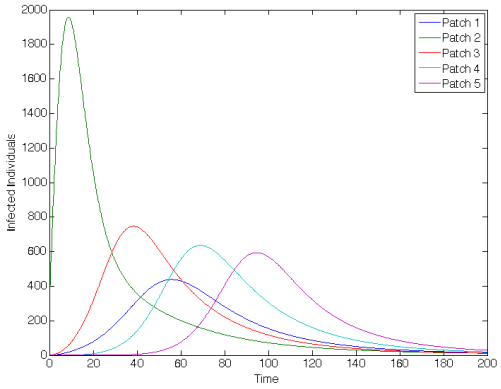

(b) Outbreak in Patch 2

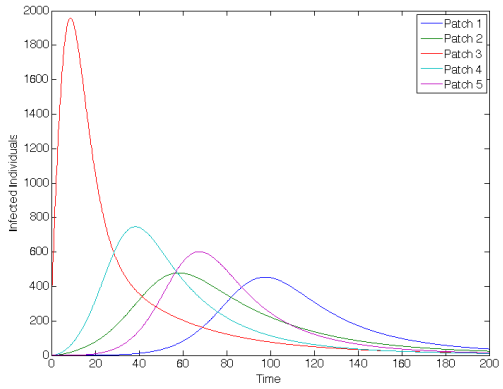

(c) Outbreak in Patch 3

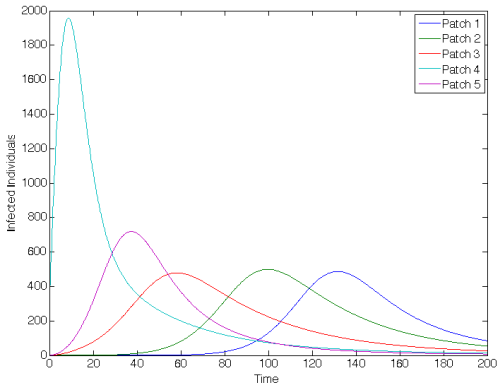

(d) Outbreak in Patch 4

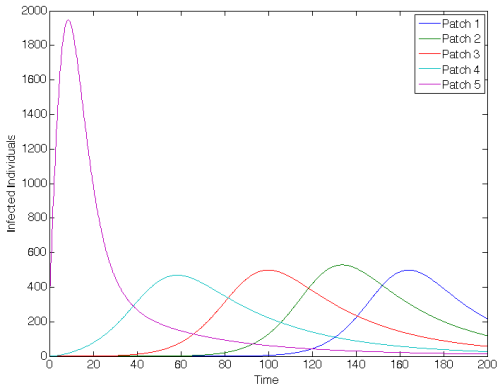

(e) Outbreak in Patch 5

Figure 3.3: Linear Arrangement: Infected population dynamics when outbreak occurs in each of the five patches (without vaccination)

Table 3.7: Linear Arrangement: Objective functional values for each scenario

Outbreak Patch		J(**v**) (w Vaccine)
1		161,080
2		175,200
3		170,470
4		152,540
5		114,390

Table 3.8: Linear Arrangement: Total number of infected individuals in metapopulation, with and without vaccine

	Total Infecteds (w/o Vaccine)	Total Infecteds (with Vaccine)
Outbreak 1	194,986	79,802
Outbreak 2	196,379	93,493
Outbreak 3	195,205	92,928
Outbreak 4	191,206	84,338
Outbreak 5	181,049	56,780

Due to each patch having identical dynamics within the patch, the basic reproduction number for each patch and for the entire metapopulation are the same,

$$\mathbf{R}_0 = R_0^i = 5.8819,$$

where $\mathbf{R}_0$ is the basic reproduction of the network and R_0^i is the basic reproduction of Patch i for $i = 1, ...5$.

The optimal vaccination results for several outbreak cases are illustrated. For each scenario, the objective functional values, the total infected with and without vaccination, and the total vaccinated in each patch and metapopulation are listed in Tables 3.7, 3.8, and 3.9, respectively. For the remainder of the chapter, we refer to vaccination effort as the control level and vaccination rate as the number of individuals vaccinated per time.

We now consider specific linear arrangement scenarios to illustrate how the optimal intervention strategies depend on where outbreaks occur. We report the control effort applied to each patch, the total number of susceptible individuals vaccinated in each patch at each time, and how the control strategy affected the infected population. We compare when the

Table 3.9: Linear Arrangement: Total individuals vaccinated in each patch for each scenario

		Patch 1	Patch 2	Patch 3	Patch 4	Patch 5	Total Vaccinated
Outbreak 1		1,180	4,522	6,319	6,122	3,448	21,591
Outbreak 2		4,612	1,308	4,502	6,258	4,975	21,655
Outbreak 3		4,193	5,295	1,328	4,345	5,473	20,634
Outbreak 4		2,785	5,245	5,372	1,306	3,751	18,459
Outbreak 5		1,469	3,177	4,715	5,226	1,238	15,825

outbreak occurs in three distinct areas of the metapopulation, at the uppermost, lowest, and central patches, Patches 1,3, and 5, respectively.

We first investigate when the outbreak occurs at the top of the river, in Patch 1. Results for this case are shown in Figures 3.4-3.5. When an outbreak occurs in the middle of the river, in Patch 3, results are shown in Figures 3.7, 3.8, and B.1. Lastly, with an outbreak at the bottom of the river, in Patch 5, results are shown in Figures 3.9, 3.10, and B.2.

For linear arrangement scenarios, where pathogen, as well as people, movement are following the same connectivity, we can draw several conclusions. It is evident that the control strategies do change depending on where outbreaks occur. Effort is always more focused on patches neighboring the outbreak patch, whether direct neighbor or one-removed neighbor, depending on the location of the outbreak. If an outbreak is upstream, the effort is higher in the one-removed downstream neighbor while in an outbreak downstream, the effort is highest in nearest upstream neighbor.

When outbreaks occur at the upper and lowermost patches of the metapopulation, the vaccination strategy has the greatest effect in lowering the number of infected individuals. However, more vaccinations are administered when outbreaks occur in upstream patches rather than those at the bottom. The role of pathogen movement in water is important because the difference in rates of movement upstream and downstream. These rates are the reason effort is focused on multiple patches downstream when outbreak occurs upstream versus being focused on nearest upstream patches with outbreaks occurring downstream.

When an outbreak occurs in upstream patches, patches below the outbreak receive the highest effort. Due to the movement of the pathogen, more vaccinations are given in

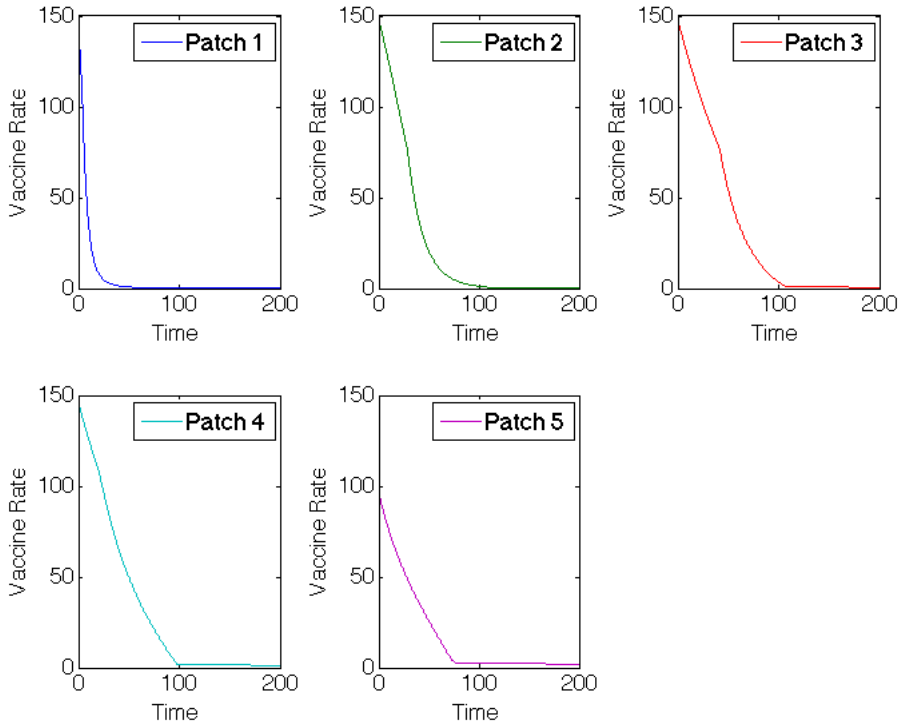

Figure 3.4: Linear Arrangement: Vaccination rates of patches with outbreak in Patch 1

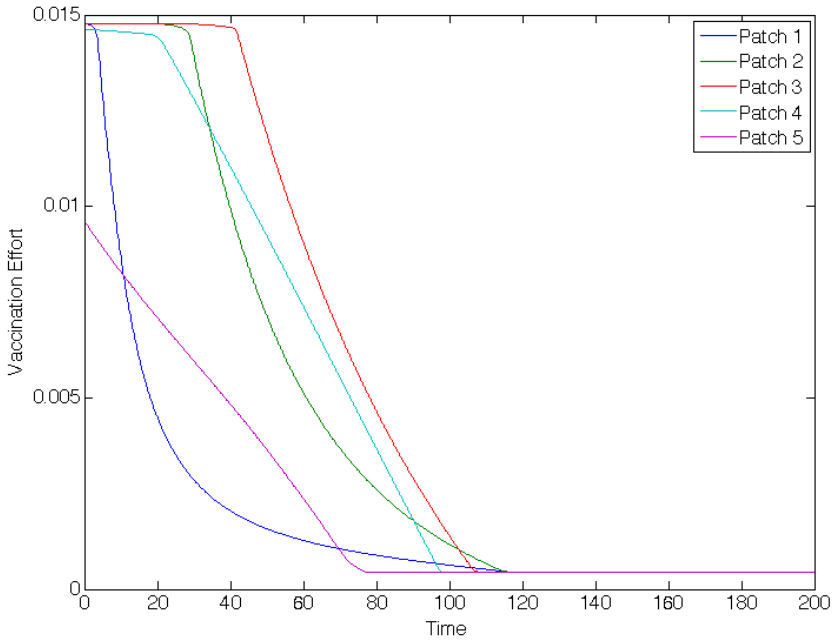

(a) Vaccination

Figure 3.5: Linear Arrangement: Vaccination effort of patches with outbreak in Patch 1

patches located two downstream from where the outbreak occurs rather than on the nearest downstream neighbor. This is due to the outbreak spreading too quickly to prevent the outbreak affecting the patch directly downstream so more effort is spent on the one below that to prevent the spread farther downstream.

Similarly when the outbreak begins in the center of the arrangement. Again, the highest number of vaccinations are given two patches downstream of the outbreak. An important difference is the high number of vaccinations administered in the nearest upstream neighbor of the outbreak patch. The ability to prevent the disease from reaching patches upstream of the outbreak is more manageable due to the lower rate of pathogen movement upstream.

When the outbreak occurs in the bottom half of the arrangement, the strategy shifts to protect the patches immediately upstream. This is a result of more susceptible patches upstream of the outbreak and the slower rate of pathogen movement upstream than downstream. Unlike the other scenarios where the outbreak spread too quick to protect the

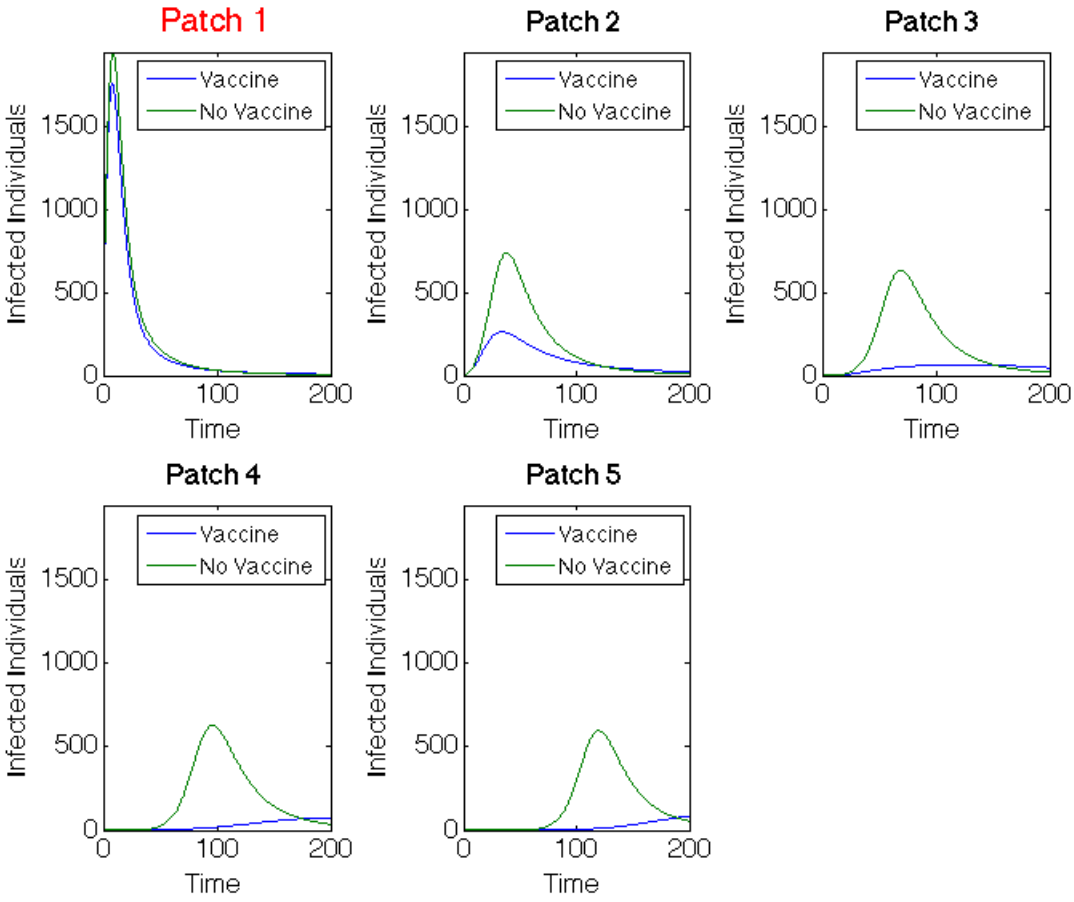

Figure 3.6: Linear Arrangement: Infected population dynamics comparison with and without vaccination with outbreak in Patch 1

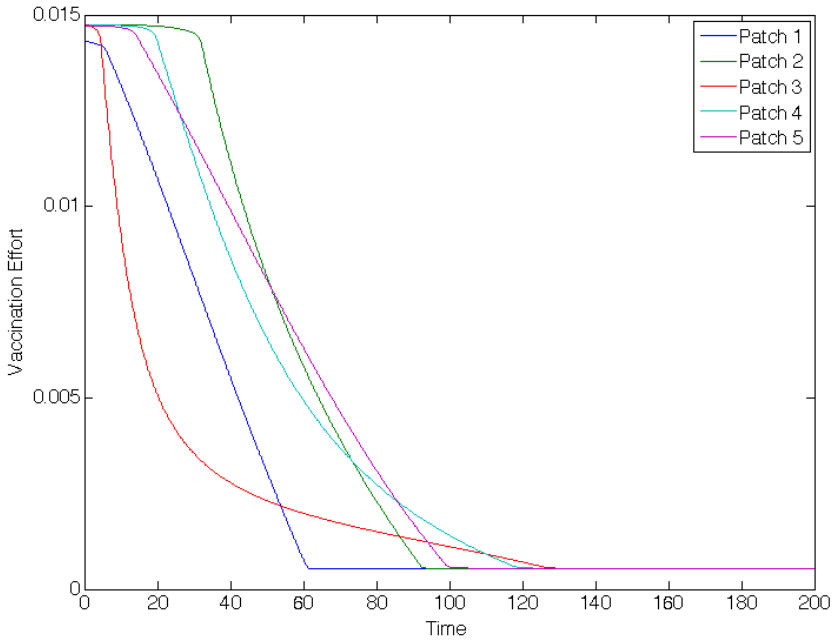

(a) Vaccination

Figure 3.7: Linear Arrangement: Vaccination effort of patches with outbreak in Patch 3

nearest downstream neighbor, the ability to prevent upstream spread is more manageable so more effort is spent immediately upstream.

In all the scenarios, vaccine effort is applied for the longest time in the outbreak patch. After an initial high effort in the outbreak patch, it then persists at low levels for a longer time than outlying patches. Also, in all cases, we saw significant decreases in the number of infecteds in all patches outside of the outbreak patch. This is due to the difficulty of controlling a patch by vaccination that is already invaded by the disease. It is evident that outbreaks occurring in a central location, compared to at the top and bottom of the patch network, are more complicated to control effectively.

3.6.2 Hub Spatial Arrangements

We now introduce patches known as hubs. A hub is a patch with a higher population than the surrounding patches with more connectivity between itself and each surrounding patch.

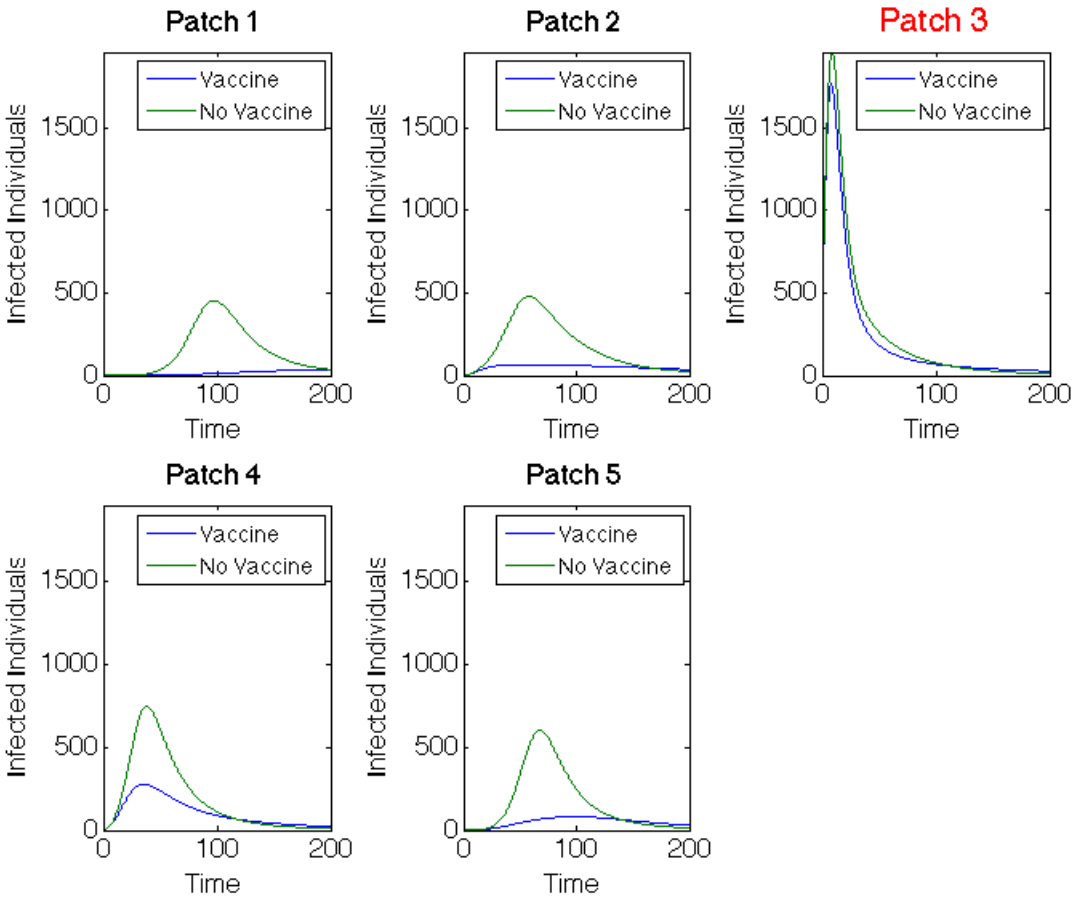

Figure 3.8: Linear Arrangement: Infected population dynamics comparison with and without vaccination with outbreak in Patch 3

Hubs have connectivity to every other patch in the metapopulation with higher movement coefficients. The surrounding patches continue to have nearest neighbor connectivity similar to the linear arrangements. The water connectivity of the patches remains the same as in the model with a linear arrangement. We consider a five-patch hub spatial arrangement illustrated in Figure 3.2, although we vary the location of the hub patch. We first assume Patch 1 is the hub but we investigate other options later. The connectivity matrix for population movement in the five-patch hub arrangement:

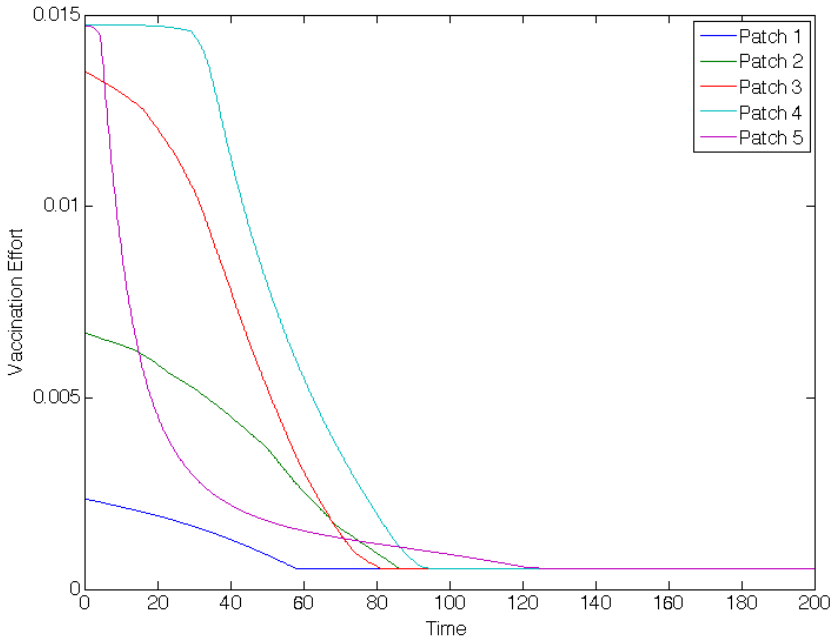

(a) Vaccination

Figure 3.9: Linear Arrangement: Vaccination effort of patches with outbreak in Patch 5

$$M = \begin{bmatrix} 0 & M_{12} & M_{13} & M_{14} & M_{15} \\ M_{21} & 0 & M_{23} & 0 & 0 \\ M_{31} & M_{32} & 0 & M_{34} & 0 \\ M_{41} & 0 & M_{43} & 0 & M_{45} \\ M_{51} & 0 & 0 & M_{54} & 0 \end{bmatrix},$$

where the connectivities to the hub are 25% greater than other connectivities. For example, assuming Patch 1 is the hub, $M_{1,j}, M_{k,1} = 1.25$ for $j, k \neq 1$, while the other non-zero $M_{i,j}$ coefficients are equal to one.

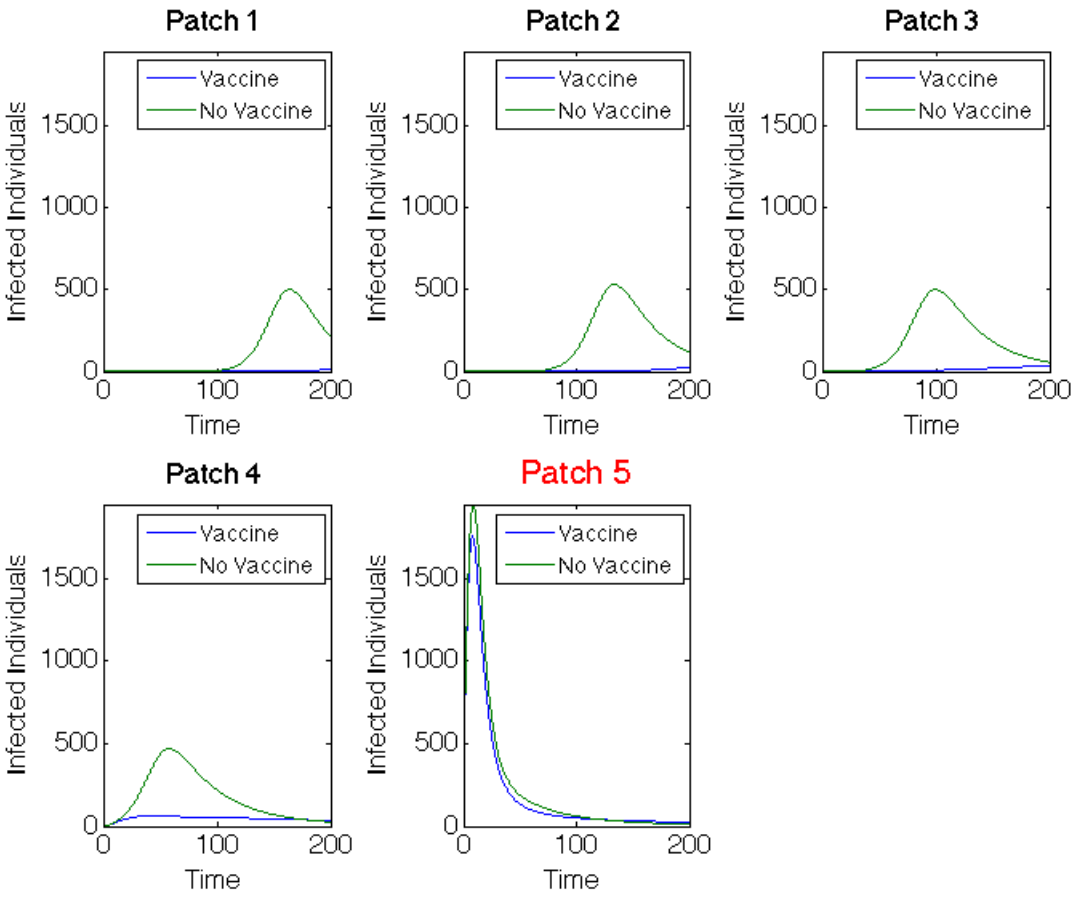

Figure 3.10: Linear Arrangement: Infected population dynamics comparison with and without vaccination with outbreak in Patch 5

The connectivity for water movement is the same as the linear arrangement:

$$H = \begin{bmatrix} 0 & H_{12} & 0 & 0 & 0 \\ H_{21} & 0 & H_{23} & 0 & 0 \\ 0 & H_{32} & 0 & H_{34} & 0 \\ 0 & 0 & H_{43} & 0 & H_{45} \\ 0 & 0 & 0 & H_{54} & 0 \end{bmatrix}.$$

The value for the non-zero downstream connectivity movements, $H_{i,j}$ where $i > j$, is equal to one while the non-zero upstream connectivity movements, $H_{i,j}$ for $j > i$, is equal to 0.1,

Table 3.10: Initial Conditions for Model with Hub Spatial Arrangement with Outbreak Outside Hub

Class	Hub Patch	Patch i	Patch $j \neq i$
S	30,000	4,700	5,000
I	0	300	0
R	0	0	0
W	0	300	0

Table 3.11: Initial Conditions for Model with Hub Spatial Arrangement with Outbreak in Hub

Class	Hub Patch i	Patch $j \neq i$
S	29,700	5,000
I	300	0
R	0	0
W	300	0

or one-tenth the rate of the downstream movement. This is due to a stronger movement of pathogen downstream than upstream, which is consistent with the direction of river currents.

We consider scenarios when an outbreak occurs in the hub as well as when in surrounding patches. We compare results with alternative hub patches in the metapopulation. Again, using patches at the uppermost, lowest, and centralized locations of the metapopulation, we investigate three systems with a hub in Patches 1, 3, or 5, respectively. In cases where the outbreak begins in Patch i, outside of the hub, the initial conditions are found in Table 3.10. When Patch i is a hub, the initial conditions are in Table 3.11.

We assume that all patches outside the hub are identical. The hub has a higher initial population and population movement rates entering and leaving the patch. Without vaccination, the dynamics of the infected population with outbreaks occurring in each of the five patches is given in Figure 3.11. Results with Patches 3 or 5 as hubs can be found in the Appendix B at the end of this dissertation.

The basic reproduction number of the network and for each patch with Patch 1 as the hub are recorded in Table 3.12. The reproduction number is independent of where the outbreak begins.

Table 3.12: Hub Patch 1 Arrangement: Basic reproduction number of network and for each patch

Network $\mathbf{R}_0$		Patch 1 (Hub)	Patch 2	Patch 3	Patch 4	Patch 5
13.3669		17.6457	2.9409	2.9409	2.9409	2.9409

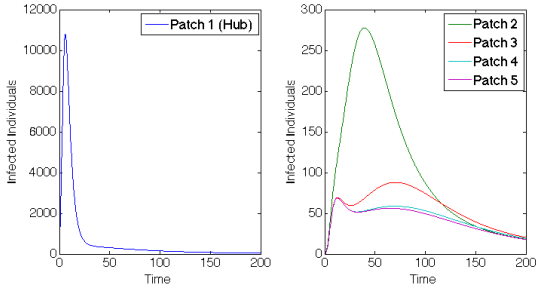

(a) Outbreak in Patch 1

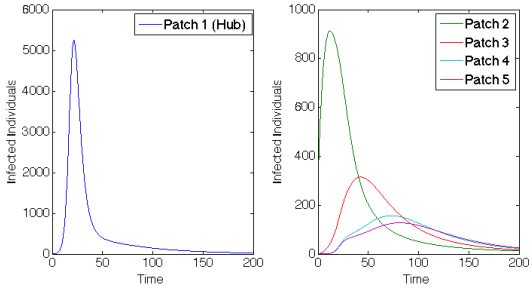

(b) Outbreak in Patch 2

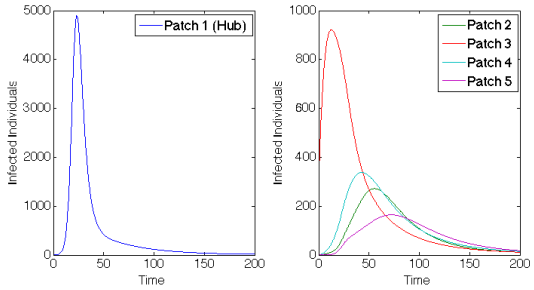

(c) Outbreak in Patch 3

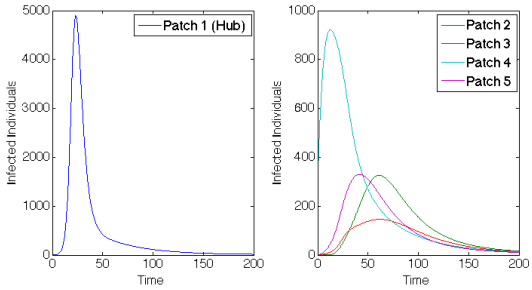

(d) Outbreak in Patch 4

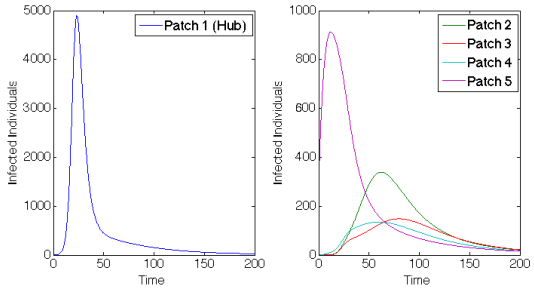

(e) Outbreak in Patch 5

Figure 3.11: Hub Patch 1 Arrangement: Infected population dynamics when outbreak occurs in each of the five patches (without vaccination), where plot on left is the hub only, plot on right is surrounding patches

Table 3.13: Hub Patch 1 Arrangement: Objective functional values for each scenario

Outbreak Patch		J(**v**) (w Vaccine)
1		187,660
2		183,380
3		187,890
4		187,860
5		181,720

Table 3.14: Hub Patch 1 Arrangement: Total number of infected individuals in metapopulation, with and without vaccine

		Total Infecteds (w/o Vaccine)	Total Infecteds (with Vaccine)
Outbreak 1		190,170	156,984
Outbreak 2		193,592	122,813
Outbreak 3		196,879	123,543
Outbreak 4		197,245	123,247
Outbreak 5		194,052	115,372

The optimal vaccination results for several outbreak cases are illustrated. We assume Patch 1, the uppermost patch of the system, is the hub. For each scenario, the objective functional values, the total infected with and without vaccination, and the total vaccinated in each patch and metapopulation are listed in Tables 3.13, 3.14, and 3.15. Results for when the outbreak occurs in the hub patch are shown in Figure 3.13. Results for when the outbreak occurs outside the hub, in Patches 3 or 5, are shown in Figures 3.16 and B.4. Figure B.4 is found in Appendix B at the end of the dissertation.

Table 3.15: Hub Patch 1 Arrangement: Total individuals vaccinated in each patch for each scenario

		Patch 1	Patch 2	Patch 3	Patch 4	Patch 5	Total Vaccinated
Outbreak 1 (Hub)		1,961	1,630	1,838	1,548	1,298	8,275
Outbreak 2		7,634	723	2,793	2,984	2,359	16,492
Outbreak 3		8,226	2,825	811	2,816	2,821	17,498
Outbreak 4		8,237	3,187	2,837	815	2,506	17,581
Outbreak 5		8,334	3,391	2,835	2,745	767	18,073

We draw several conclusions from hub arrangements. First, notice the basic reproduction number of the hub is much higher than in surrounding patches. The network $\mathbf{R}_0$ more than doubles from the linear spatial arrangement. The location of the hub also matters as we notice the highest network $\mathbf{R}_0$ value in hubs located farthest downstream (see Table B.5). However, we do not see the lowest network $\mathbf{R}_0$ value at the top of the network, differing from the results of Tien *et al.* [60], where they concluded that the network reproduction number would increase as it moves down a linear water network. One reason for the difference is that they investigated water movement only while we now include a more complicated movement structure, also allowing hubs and population movement among the patches.

The vaccination strategy in the hub does depend on where an outbreak occurs. Wherever the hub is located in the metapopulation, an outbreak occurring in the hub is always hardest to contain, as it is difficult to prevent the disease from spreading to the surrounding patches through the hub. Although the total number of infecteds in this scenario, without vaccination, is smallest when outbreak is in the hub, the total number vaccinated is also smallest and has the least impact on decreasing the total number of infecteds.

When an outbreak occurs outside of the hub, a much different strategy is implemented. First, the maximum vaccination effort is sustained longer in the hub. Also, the vaccination strategy drastically decreases the number of infecteds in the hub, however there is only a slight decrease within the outbreak patch. This is similar to the linear spatial arrangement cases. This points to the fact that it is usually too late to contain the outbreak once it has already invaded a patch and more effort should be focused on surrounding patches. Lastly, note that vaccination effort does continue in the outbreak patch for the longest time at a lower level. Although the effort does little to decrease the number of infecteds in the outbreak patch, to help minimize the number of infecteds in the metapopulation, low levels of vaccination continue to be administered in the patch.

In every non-hub outbreak scenario, the number of vaccinations in the hub is significantly higher than in the surrounding patches. Due to the high connectivities with the hub, in whichever patch the outbreak occurs, the disease spreads to the hub quickly and then to the

surrounding patches. The strategy suggests using high levels of effort to prevent, or lessen, the spread in the hub in order to limit its spread to the other patches. By limiting the number of infecteds in the hub, it will ultimately help limit the outbreak in other patches.

Outside the hub and outbreak patches, the number of vaccinations is almost uniform among the other patches and the effort spent in these patches follows similar patterns as in the linear arrangement cases. An outbreak in the upper patches of the water arrangement, after the hub, results in more vaccinations in patches two downstream from the outbreak. An outbreak in the center of the metapopulation again results in high effort downstream but now more effort spent immediately upstream from the outbreak.

An interesting result occurs with an outbreak in the lower portion of the metapopulation. Unlike the linear arrangement cases, the highest number of vaccinations, apart from the hub, does not necessarily occur in patches immediately upstream of the outbreak. Depending on the location of the hub, the second highest number of vaccinations occur either directly downstream the hub, directly above the hub, or above the outbreak. Since any outbreak will almost immediately invade the hub and then progress downstream the network, protecting patches immediately downstream the hub would be important. This is especially true when you take into account the higher movement of pathogen downstream rather than upstream the water arrangement.

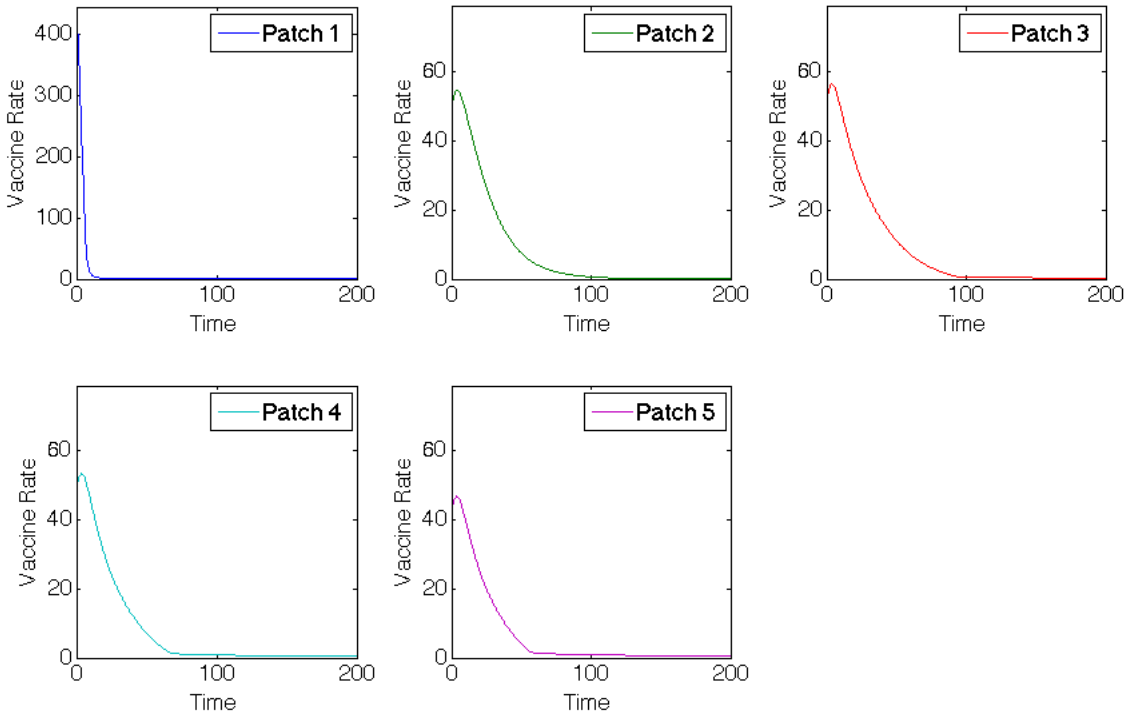

Figure 3.12: Hub Patch 1 Arrangement: Vaccination rates of patches with outbreak in hub, Patch 1

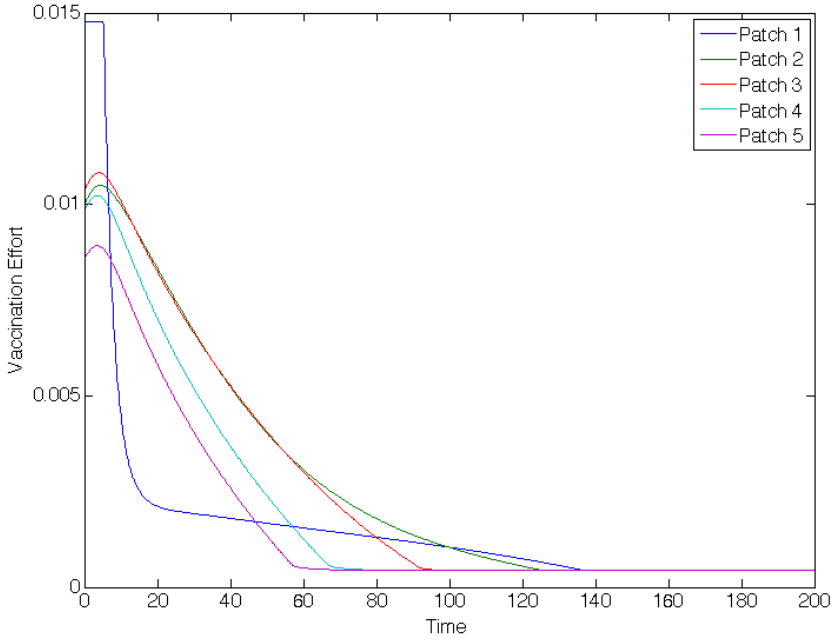

(a) Vaccination

Figure 3.13: Hub Patch 1 Arrangement: Vaccination effort of patches with outbreak in hub, Patch 1

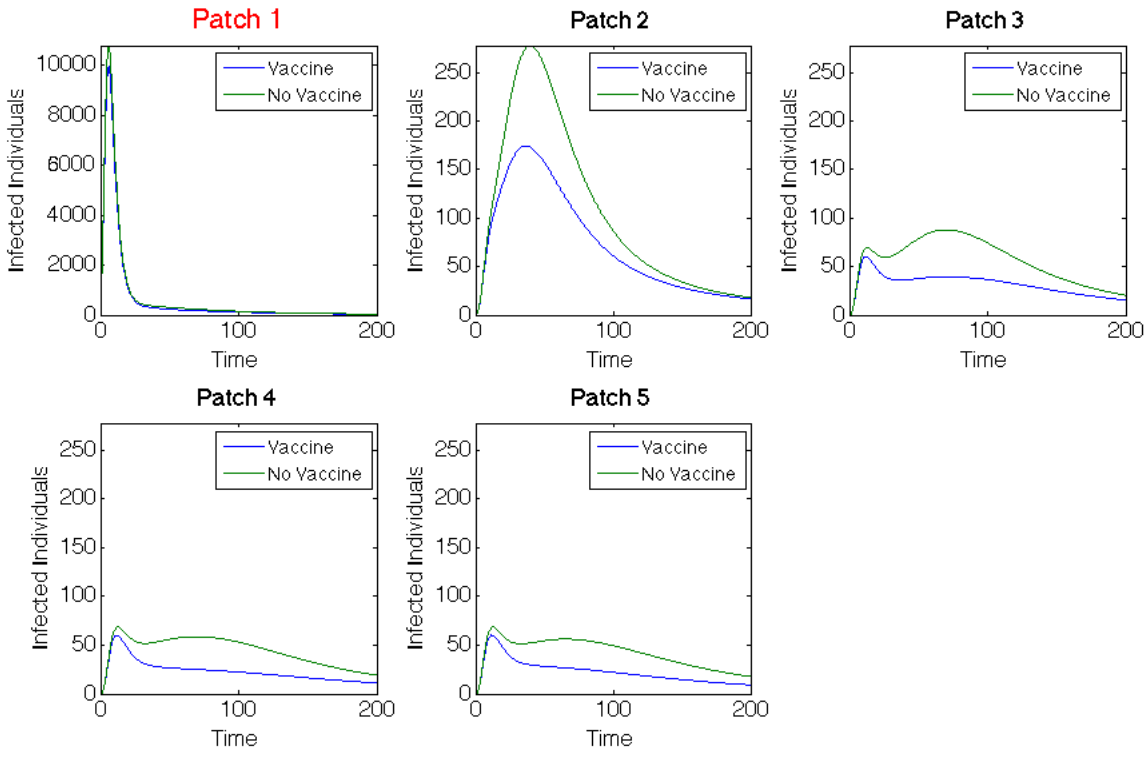

Figure 3.14: Hub Patch 1 Arrangement: Infected population dynamics comparison with and without vaccination with outbreak in hub, Patch 1

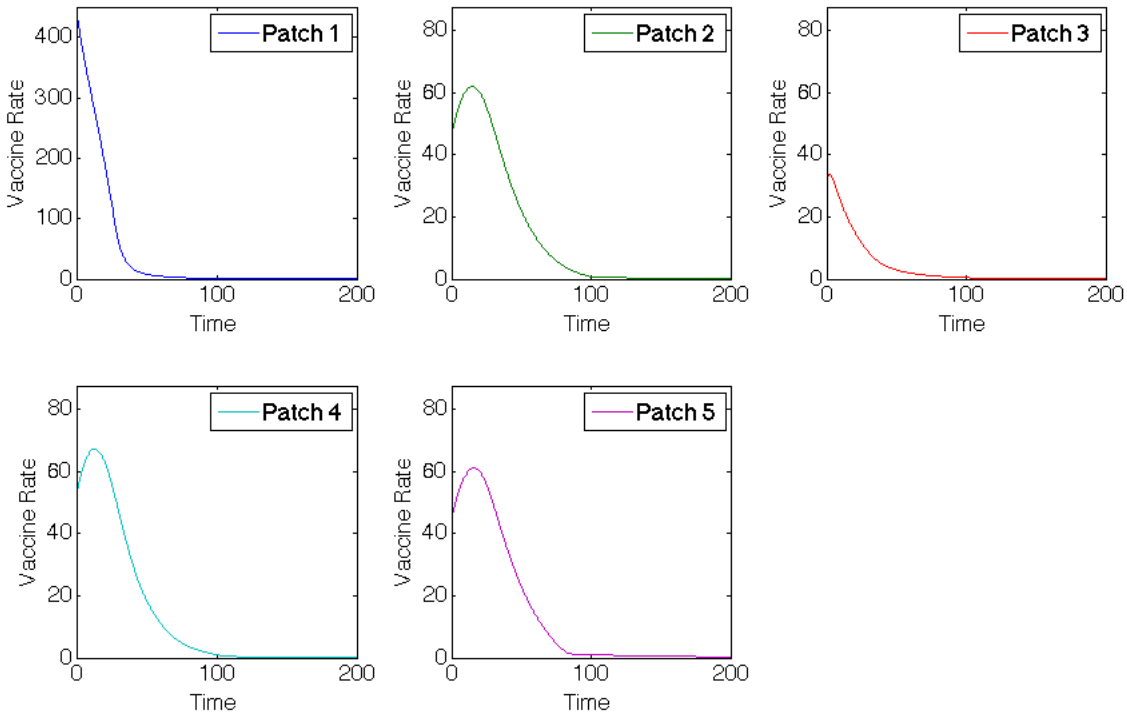

Figure 3.15: Hub Patch 1 Arrangement: Vaccination rates of patches with outbreak in Patch 3

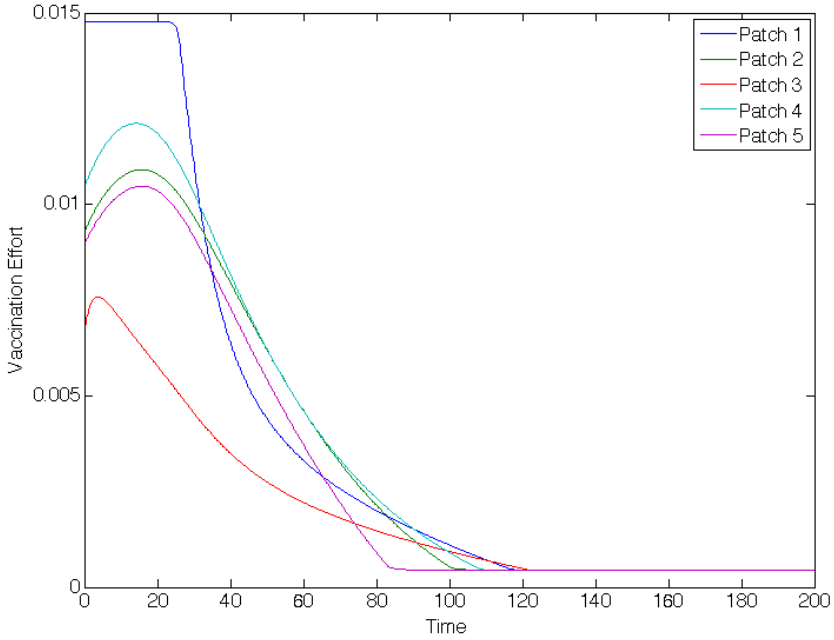

(a) Vaccination

Figure 3.16: Hub Patch 1 Arrangement: Vaccination effort of patches with outbreak in Patch 3

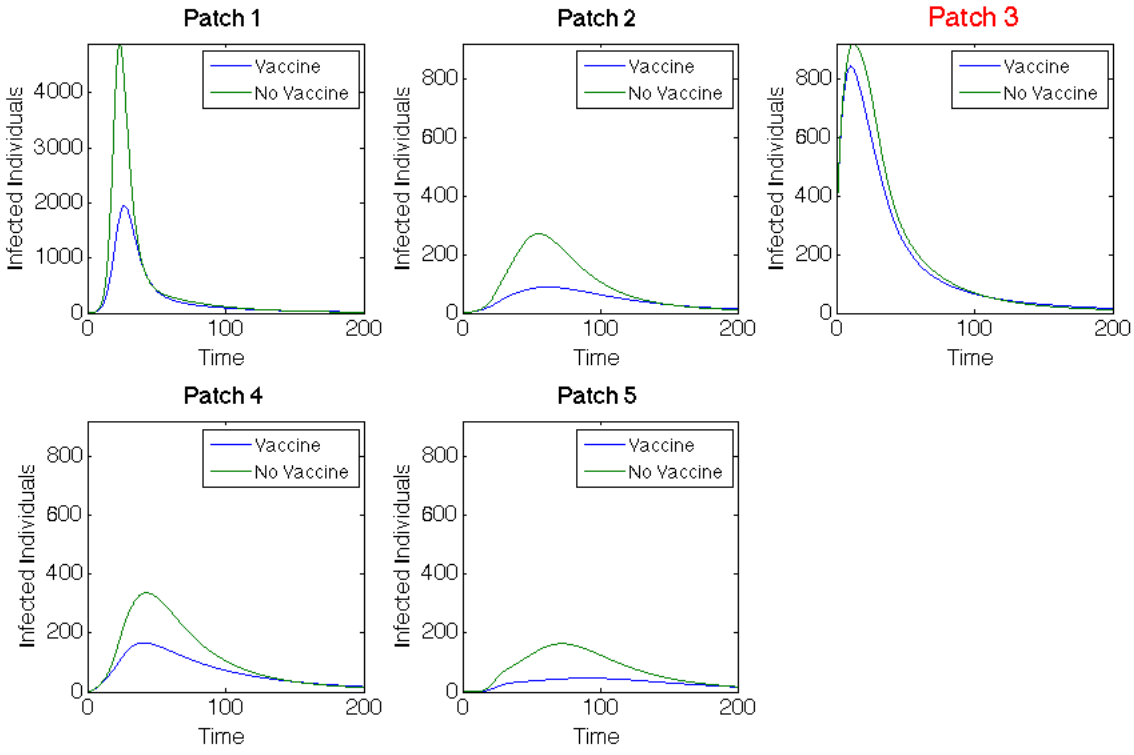

Figure 3.17: Hub Patch 1 Arrangement: Infected population dynamics comparison with and without vaccination with outbreak in Patch 3

Table 3.16: Comparison of Basic Reproduction Numbers for Varying Hub Sizes and Location

Hub Size	Hub Patch 1	Hub Patch 3	Hub Patch 5
40,000	17.8713	17.6877	22.6644
60,000	26.7339	26.3883	33.9123
80,000	35.6143	35.1237	45.1757

Table 3.17: Hub Patch 1: Objective functional values for metapopulations of each hub size

Outbreak Patch		J(**v**) (Hub 40, 000)	J(**v**) (Hub 60, 000)	J(**v**) (Hub 80, 000)
1		396,521	397,598	397,273
2		392,770	394,081	394,362
3		393,558	395,169	396,098
4		393,602	395,548	397,083
5		392,701	394,359	395,794

3.6.3 Hub Size Comparisons

The size of hubs and their proportion to the outlying patches is investigated in this section. We now consider a metapopulation with a larger population, $N = 100,000$ individuals. We compare three sizes of hubs and the optimal vaccination strategy associated with both. The sizes we consider are hubs of $40,000$, $60,000$, and $80,000$ individuals. We investigate how the population size of the hub in relation to the population size of the other patches might affect the vaccination strategy.

The basic reproduction numbers for each arrangement with hubs in Patches 1, 3, or 5, respectively, are given in Table 3.16. The objective functional values for each outbreak scenario, with Patch 1 as a hub and population sizes of $40,000$, $60,000$, and $80,000$ individuals is given in Table 3.17. The total infected, with and without vaccination, for each of the arrangements is given in Tables 3.18-3.20. The total vaccinated in each patch of the metapopulation is given in Tables 3.21-3.23.

We compare the results when the total population is $N = 100,000$ individuals with hubs varying in population size. We compare the optimal harvesting strategies when the hub contains $40,000$, $60,000$, and $80,000$ individuals as well as the vaccination effort in each

Table 3.18: Hub Patch 1 (with 40,000 Individuals): Total infected individuals in metapopulation, with and without vaccine

40,000	Total Infecteds (w/o Vaccine)	Total Infecteds (with Vaccine)
Outbreak 1	404,375	326,704
Outbreak 2	404,361	296,307
Outbreak 3	404,433	304,639
Outbreak 4	404,434	305,876
Outbreak 5	404,298	295,892

Table 3.19: Hub Patch 1 (with 60,000 Individuals): Total infected individuals in metapopulation, with and without vaccine

60,000	Total Infecteds (w/o Vaccine)	Total Infecteds (with Vaccine)
Outbreak 1	403,437	335,408
Outbreak 2	403,935	311,332
Outbreak 3	404,198	316,378
Outbreak 4	404,262	318,370
Outbreak 5	404,019	310,577

Table 3.20: Hub Patch 1 (with 80,000 Individuals): Total infected individuals in metapopulation, with and without vaccine

80,000	Total Infecteds (w/o Vaccine)	Total Infecteds (with Vaccine)
Outbreak 1	399,687	364,447
Outbreak 2	401,828	335,238
Outbreak 3	403,035	338,125
Outbreak 4	403,590	339,789
Outbreak 5	402,806	335,878

Table 3.21: Hub Patch 1 (with 40,000 Individuals): Total number of vaccinated in each patch

		Patch 1	Patch 2	Patch 3	Patch 4	Patch 5	Total Vaccinated
Outbreak 1		2,064	3,791	4,399	4,538	4,619	19,412
Outbreak 2		6,862	1,364	4,304	7,062	7,403	26,995
Outbreak 3		7,090	5,326	1,317	4,293	6,987	25,012
Outbreak 4		7,085	6,513	5,383	1,307	4,416	24,705
Outbreak 5		6,426	6,455	7,331	5,562	1,343	27,117

Table 3.22: Hub Patch 1 (with 60,000 Individuals): Total number of vaccinated in each patch

		Patch 1	Patch 2	Patch 3	Patch 4	Patch 5	Total Vaccinated
Outbreak 1		2,270	2,701	3,833	4,019	3,917	16,739
Outbreak 2		7,208	1,077	4,009	5,268	5,302	22,865
Outbreak 3		7,534	4,019	1,112	4,041	5,211	21,917
Outbreak 4		7,531	4,257	4,779	1,116	3,827	21,509
Outbreak 5		7,542	4,316	5,341	4,892	1,119	23,210

Table 3.23: Hub Patch 1 (with 80,000 Individuals): Total number of vaccinated in each patch

		Patch 1	Patch 2	Patch 3	Patch 4	Patch 5	Total Vaccinated
Outbreak 1		2,425	1,233	1,828	1,782	1,599	8,868
Outbreak 2		7,521	665	2,457	2,956	2,801	16,398
Outbreak 3		7,917	2,124	752	2,538	2,863	16,194
Outbreak 4		7,914	2,241	2,747	762	2,353	16,017
Outbreak 5		7,921	2,273	2,997	2,769	723	16,683

patch of the metapopulation for each hub size. We illustrate results for when the outbreak begins in Patches 1, 3, or 5 in Figures 3.21, 3.22 and B.29. The comparisons between the infected populations, with and without vaccine, for the hub sizes, are given in Figures 3.18, 3.19, and 3.20. The individual vaccination rates for each patch with hubs of the three sizes are given in Figures B.26-B.28, which can be found in Appendix B.

The size of hubs in relation to the surrounding patches does play a role in the vaccination strategy. Unlike previous results, there are cases where the hub patch does not necessarily have the highest number of vaccinations in the metapopulation. When the hub and surrounding patch population sizes are similar, there are higher numbers of vaccinations administered to surrounding patches than in cases where the hubs are very large in comparison. For example, in the case with a hub of 40,000 individuals, the most vaccinated patch is either the farthest downstream patch, the hub, or in the center, depending on where outbreak begins. As the hub size increases, we see similar results as in subsection 3.6.2, where the hub always had the highest number of vaccinations.

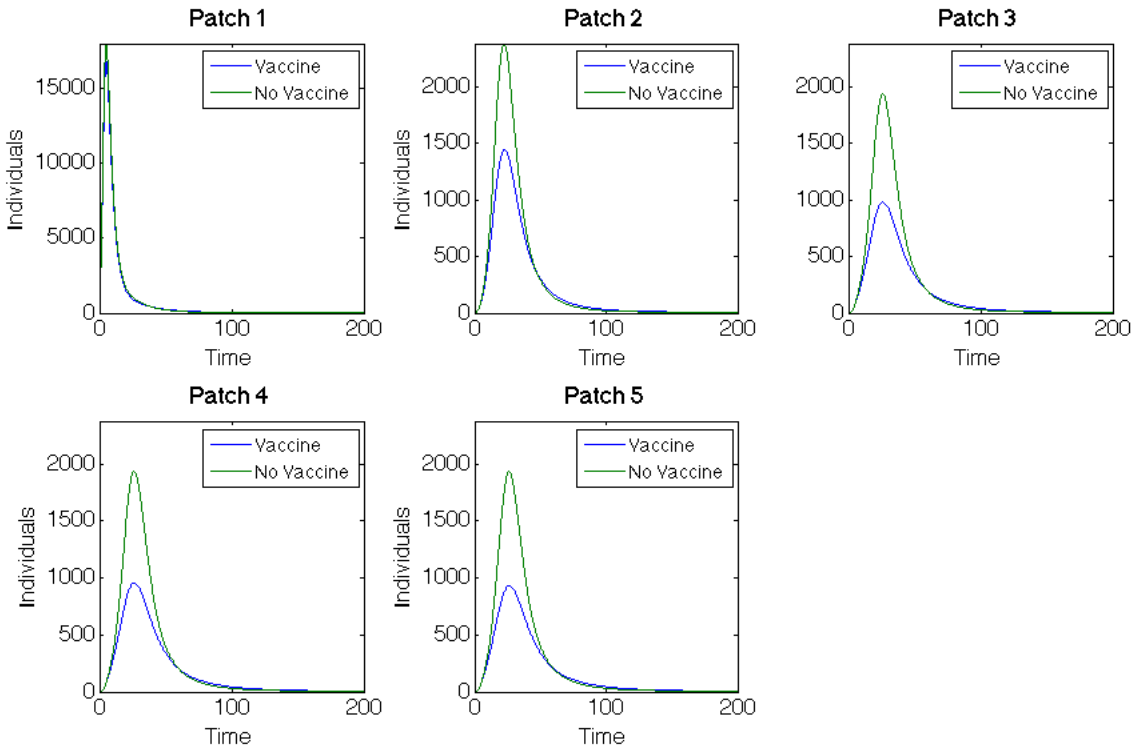

Figure 3.18: Hub Patch 1 Arrangement (with $40,000$ Individuals): Infected population dynamics comparison when outbreak occurs in hub, Patch 1

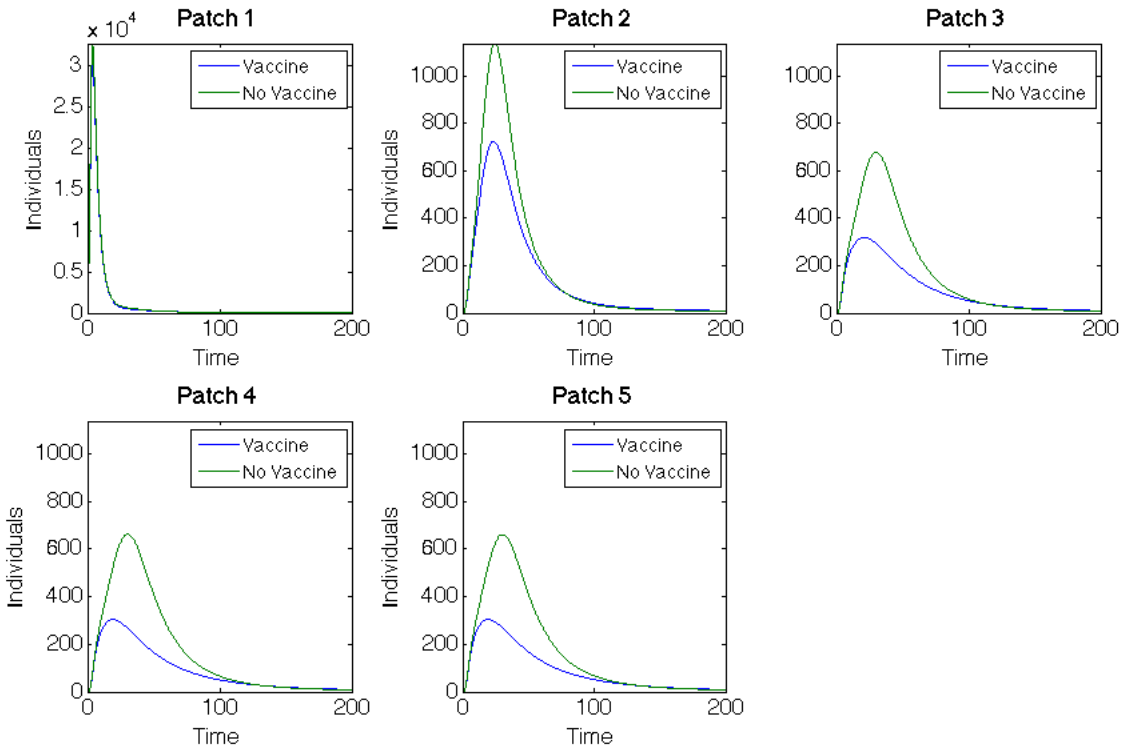

Figure 3.19: Hub Patch 1 Arrangement (with 60,000 Individuals): Infected population dynamics comparison when outbreak occurs in hub, Patch 1

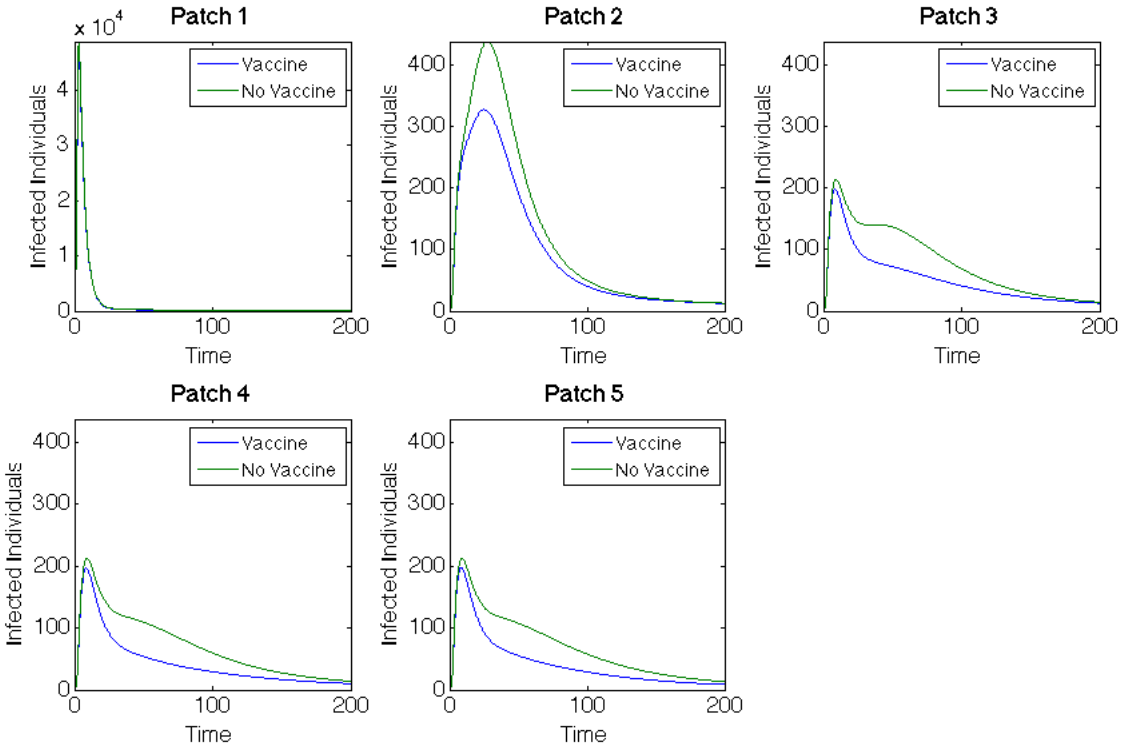

Figure 3.20: Hub Patch 1 Arrangement (with 80,000 Individuals): Infected population dynamics comparison when outbreak occurs in hub, Patch 1

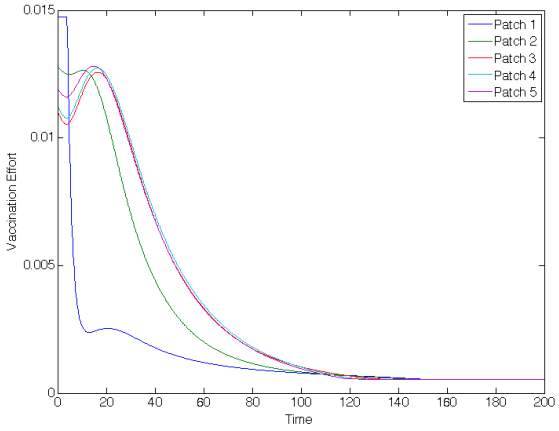

(a) Hub Patch 1 - Hub 40,000 - Vaccine

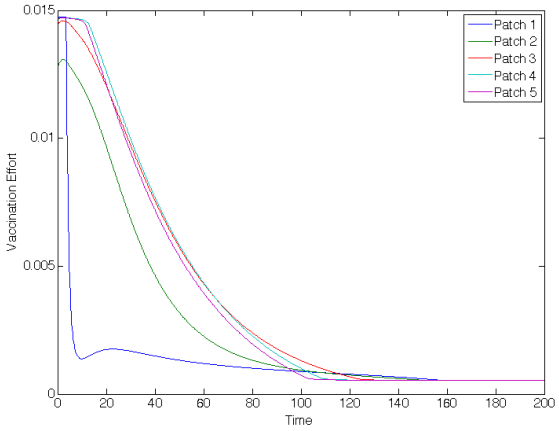

(b) Hub Patch 1 - Hub 60,000 - Vaccine

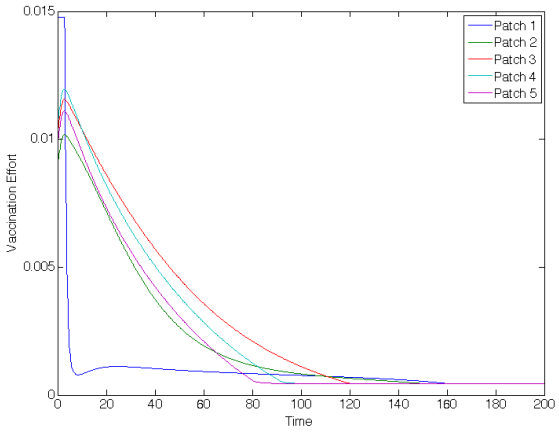

(c) Hub Patch 1 - Hub 80,000 - Vaccine

Figure 3.21: Hub Patch 1 Arrangement: Comparison of vaccination effort of metapopulation with varying hub sizes with outbreak in hub, Patch 1

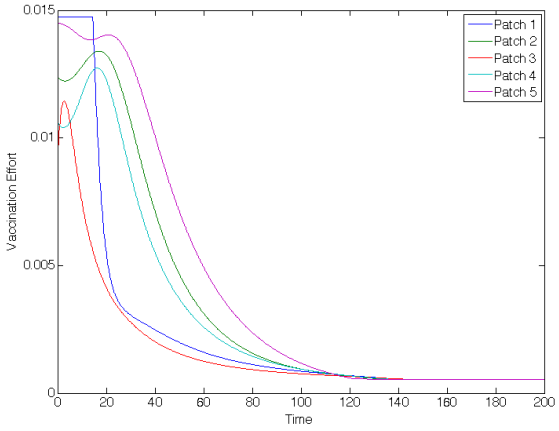

(a) Hub Patch 1 - Hub 40,000 - Vaccine

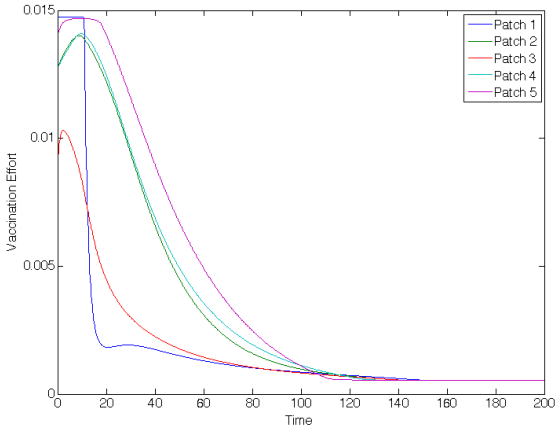

(b) Hub Patch 1 - Hub 60,000 - Vaccine

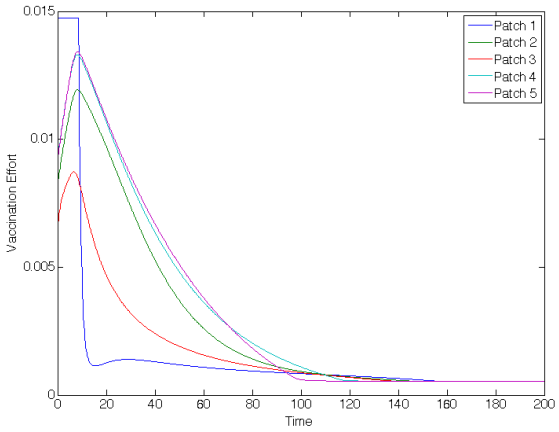

(c) Hub Patch 1 - Hub 80,000 - Vaccine

Figure 3.22: Hub Patch 1 Arrangement: Comparison of vaccination effort of metapopulation with varying hub sizes with outbreak in Patch 3

In all cases, there is always an emphasis on vaccinating the hub due to its high connectivity. However the effort to protect surrounding patches increases as their population sizes increase in comparison with the hub. This also depends upon where the outbreak occurs. One clear example of this occurs when the outbreak begins in Patch 5, with a hub of $40,000$ individuals in Patch 1. The number of vaccinations is higher in patches centrally located in the metapopulation rather than in the hub. The population size of the hub does not dominate over the importance of the surrounding patches so effort is more evenly spread throughout the metapopulation. However, it is evident that as the hub size increases and outlying patch population sizes decrease, effort in surrounding patches also decreases.

Similar to previous results, it always is hardest to contain an outbreak beginning in the hub. The total infecteds in each patch does decrease as a result of the vaccination, with the largest decrease in the total number occurring in cases with hub size $40,000$ individuals. However, the total number of infected individuals in the metapopulation, after vaccination, is always highest when the outbreak begins in hub. As the size of a hub increases, the outbreak becomes harder to contain. This is an important result when developing a vaccination program in areas with large cities in relation to their surrounding communities.

3.6.4 Linear Spatial Arrangement with a Hot Spot

Motivated by the work of Tien, Eisenberg, and their collaborators [60, 21], we consider scenarios where, although population sizes are similar, certain regions may possess a higher risk of infectivity. Two potential reasons could be worse sanitation or lower availability of clean water. Areas that have a higher risk of infectivity will be referred to as "hot spots." The idea of a hot spot with accompanying scenarios and $\mathbf{R}_0$, is discussed in [60]. We investigate hot spots in the linear arrangement with the same patch connectivity as previously considered to determine their effect on the optimal vaccination strategies.

The parameter values chosen for the hot spot patch are described in Table 3.24. We investigate when a hot spot is located at the uppermost patch, Patch 1, and compare with scenarios when the hot spot is in middle, Patch 3. Additionally, we include several results

Table 3.24: Parameter Values for Infectivity in Hot Spot and Surrounding Patches

Parameter	Description	Value in Hot Spot	Value Elsewhere
β_I	person-person contact rate	3.96E^{-5}	2.64E^{-5}
β_W	reservoir-person contact rate	1.82E^{-4}	1.21E^{-4}

Table 3.25: Hot Spot Patch 1: Basic reproduction number for network and for each patch

Network $\mathbf{R}_0$	Patch 1 (HS)	Patch 2	Patch 3	Patch 4	Patch 5
6.8677	8.8428	5.8819	5.8819	5.8819	5.8819

for when the hot spot is located in Patch 5 farthest downstream. We use the same initial conditions as in the previous linear arrangement simulations.

The basic reproduction numbers of the network and for each patch with Patches 1, 3, or 5 as the hot spot for infection are recorded in Tables 3.25, 3.29, and B.9, respectively. The objective functional values for the cases are recorded in Tables 3.26, 3.30, and B.10. The total number infected for each scenario is given in Tables 3.27, 3.31, and B.11, and the total vaccinated is given in Tables 3.28, 3.32, and B.12. The tables for the spatial arrangement with Patch 5 as the hot spot can be found in Appendix B.

We illustrate the optimal vaccination strategies for hot spot scenarios when the outbreak begins in Patches 1, 3, or 5. We compare when the hot spot is upstream in Patch 1, in the center, in Patch 3, and when it is downstream in Patch 5. Results for the for the outbreak occurring in the hot spot (Patch 1) of a linear arrangement are shown in Figures 3.24, 3.25, and 3.26. Results for when the outbreak begins in Patch 3, outside the hot spot patch,

Table 3.26: Hot Spot Patch 1: Objective functional values for each scenario

Outbreak Patch		J($\mathbf{v}$) (w Vaccine)
1		161,751
2		179,901
3		179,439
4		156,052
5		125,560

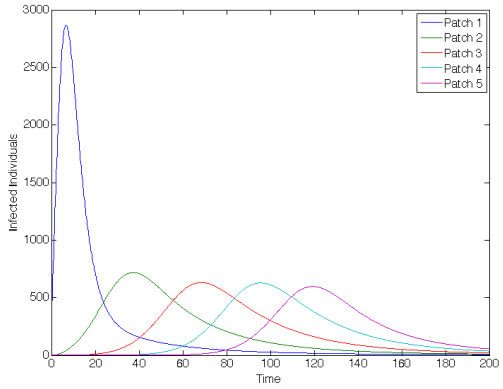

(a) Outbreak in Patch 1

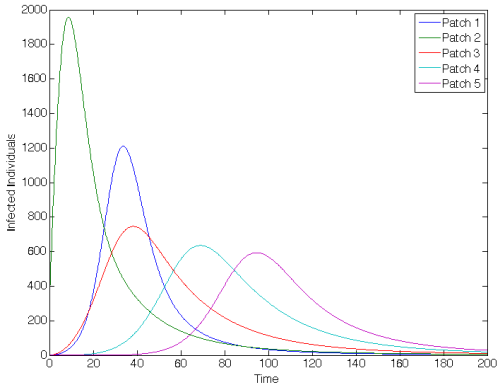

(b) Outbreak in Patch 2

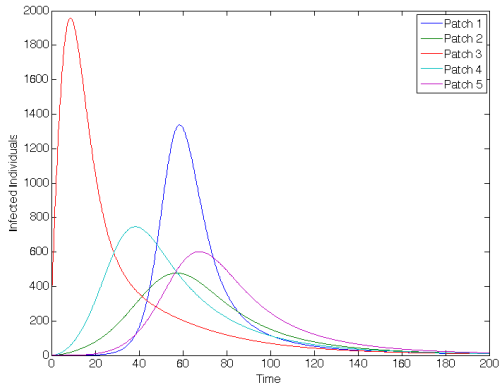

(c) Outbreak in Patch 3

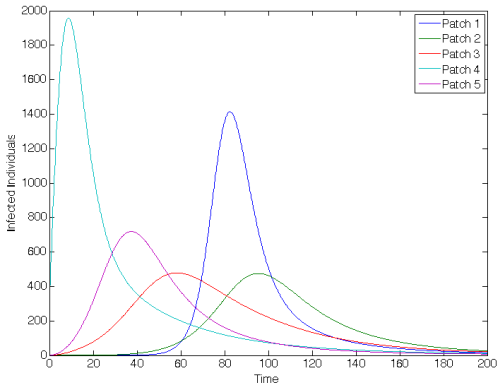

(d) Outbreak in Patch 4

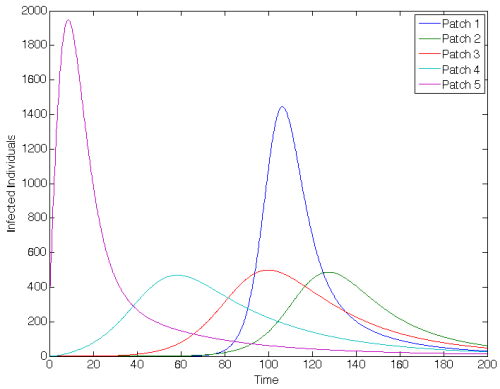

(e) Outbreak in Patch 5

Figure 3.23: Hot Spot Patch 1 Arrangement: Infected Dynamics (without vaccination) of the system with outbreak in each of the patches

Table 3.27: Hot Spot Patch 1: Total number of infected individuals in metapopulation, with and without vaccine

	Total Infecteds (w/o Vaccine)	Total Infecteds (with Vaccine)
Outbreak 1	195,255	82,833
Outbreak 2	198,104	103,555
Outbreak 3	198,803	92,921
Outbreak 4	197,085	81,635
Outbreak 5	192,327	57,455

Table 3.28: Hot Spot Patch 1: Total individuals vaccinated in each patch for each scenario

		Patch 1	Patch 2	Patch 3	Patch 4	Patch 5	Total Vaccinated
Outbreak 1 (HS)		698	4,382	6,309	6,152	3,459	20,999
Outbreak 2		3,393	1,193	4,487	6,253	4,974	20,300
Outbreak 3		6,526	5,064	1,302	4,338	5,469	22,700
Outbreak 4		5,434	4,288	5,178	1,294	3,745	19,939
Outbreak 5		4,928	2,722	4,612	5,269	1,236	18,767

are shown in Figures 3.27-3.29. Results for when the outbreak occurs in Patch 5, Figures B.30-B.32, are found in Appendix B.

Results for the outbreak occurring in the hot spot (Patch 3) of a linear arrangement are shown in Figures 3.34-3.36 and results for when the outbreak occurs outside the hub patch are shown in Figures 3.31-B.35. Results for when the outbreak occurs in Patch 5 are found in Appendix B.

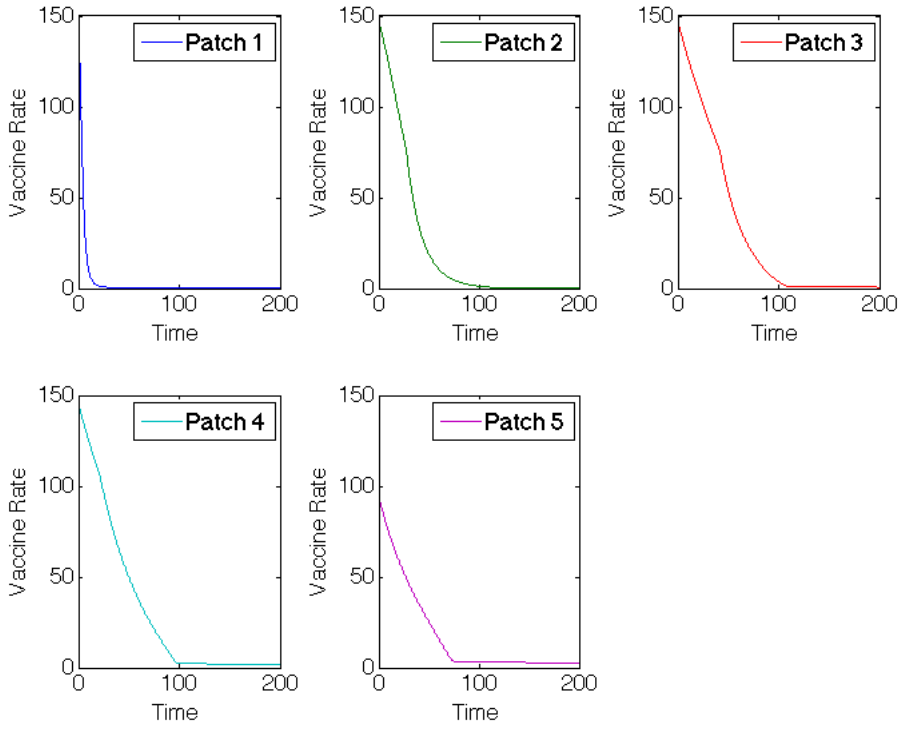

Figure 3.24: Hot Spot Patch 1 Arrangement: Vaccination rates for patches in linear arrangement with outbreak in Patch 1

Table 3.29: Hot Spot Patch 3: Basic reproduction number for network and for each patch

Network $\mathbf{R}_0$	Patch 1	Patch 2	Patch 3 (HS)	Patch 4	Patch 5
6.8250	5.8819	5.8819	8.8428	5.8819	5.8819

Previous results of Tien *et al.* [60] stated that the farther downstream a hot spot is located, the higher the network $\mathbf{R}_0$. They concluded that the greatest inflow to a patch was more of a factor than the greatest outflow. Our results did confirm the network reproduction number was highest when the hot spot was located at the bottom of the river network, however, the patch furthest upstream did not have the lowest. A potential reason for this result could be the addition of movement by infected individuals not addressed in [60]. Another factor could be that our model incorporated pathogen leaving the system both at the upper and lowermost patches in the water arrangement. This eliminates the water compartment in the

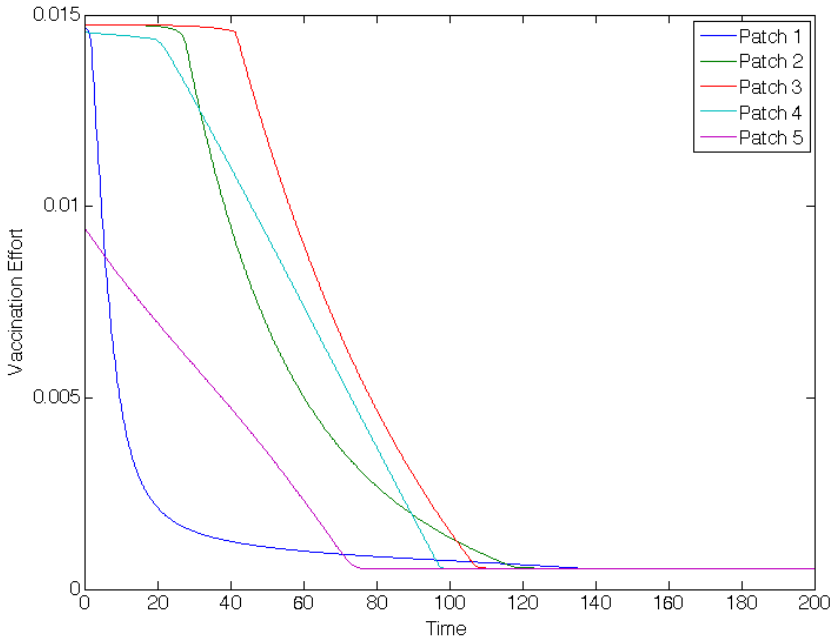

(a) Vaccination

Figure 3.25: Hot Spot Patch 1 Arrangement: Vaccination effort for linear arrangement with outbreak in Patch 1

Table 3.30: Hot Spot Patch 3: Objective functional values for each scenario

Outbreak Patch		J(**v**) (w Vaccine)
1		170,255
2		179,248
3		172,257
4		163,731
5		134,654

Table 3.31: Hot Spot Patch 3: Total number of infected individuals in metapopulation, with and without vaccine

	Total Infecteds (w/o Vaccine)	Total Infecteds (with Vaccine)
Outbreak 1	197,120	87,708
Outbreak 2	197,106	103,234
Outbreak 3	195,595	98,021
Outbreak 4	193,700	95,565
Outbreak 5	189,167	61,441

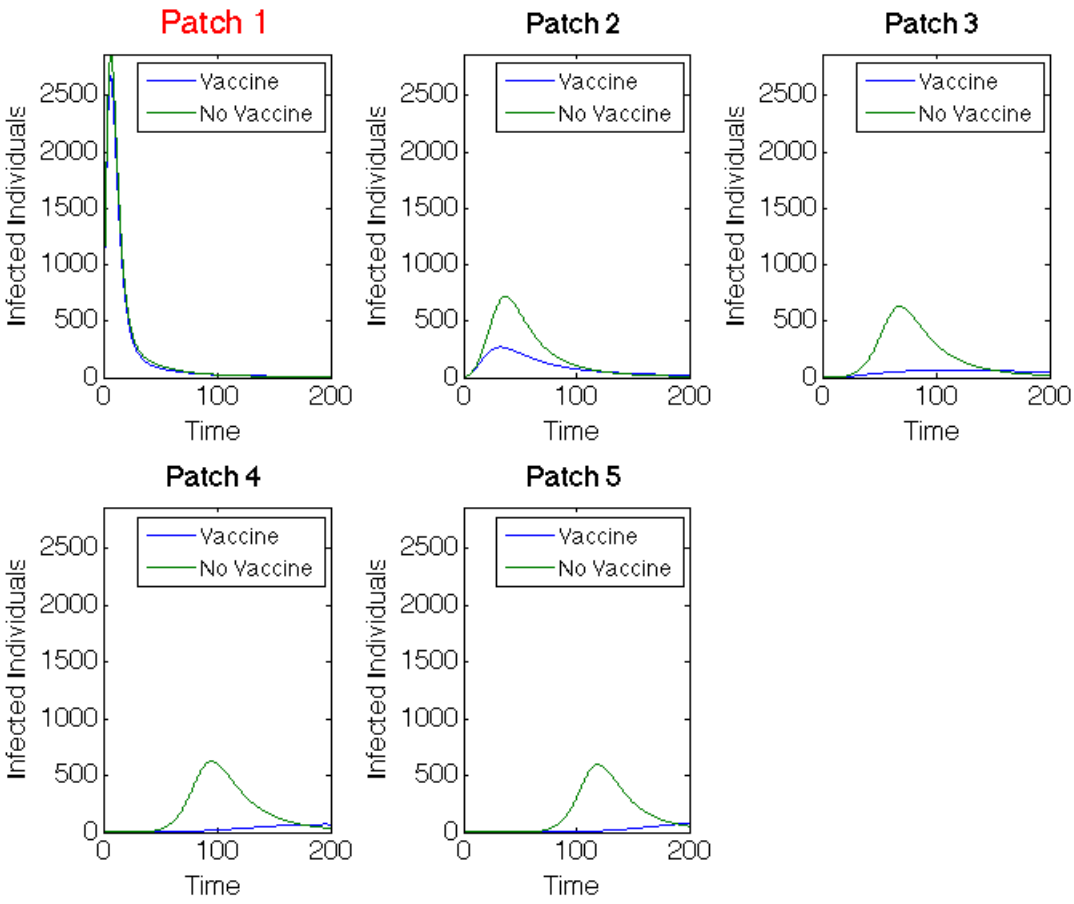

Figure 3.26: Hot Spot Patch 1 Arrangement: Infected population dynamics comparison with and without vaccination with outbreak in Patch 1

Table 3.32: Hot Spot Patch 3: Total individuals vaccinated in each patch for each scenario

		Patch 1	Patch 2	Patch 3	Patch 4	Patch 5	Total Vaccinated
Outbreak 1		1,096	4,351	6,140	6,451	3,797	21,835
Outbreak 2		4,585	1,226	3,231	6,009	5,142	20,193
Outbreak 3 (HS)		4,230	5,138	771	4,180	5,452	19,771
Outbreak 4		3,215	5,664	4,572	1,164	3,700	18,315
Outbreak 5		945	4,389	7,566	5,214	1,212	19,325

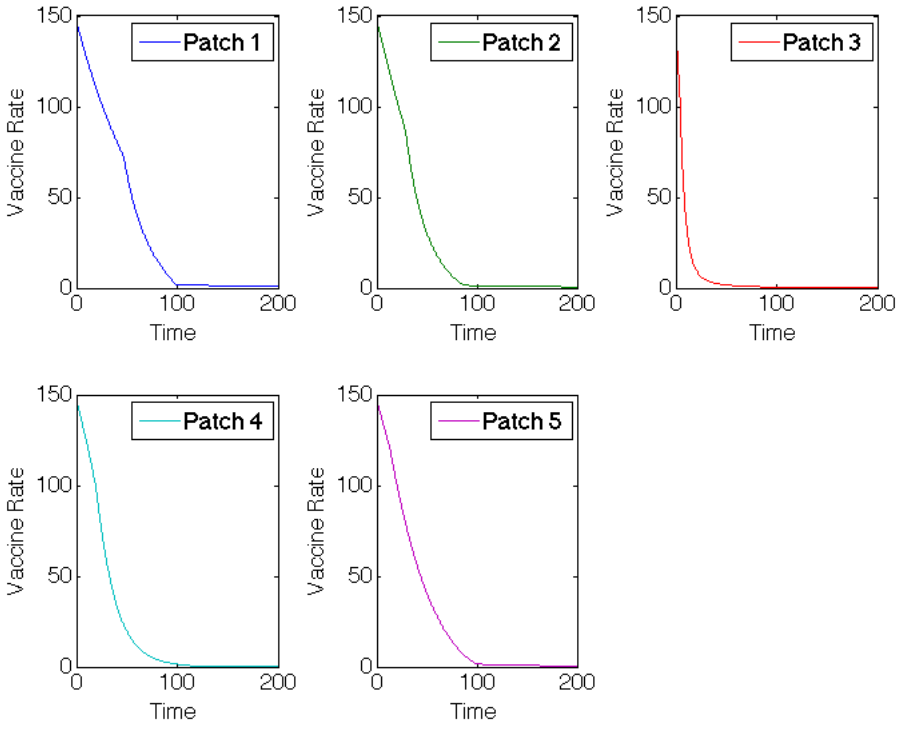

Figure 3.27: Hot Spot Patch 1 Arrangement: Vaccination rates for patches in linear arrangement with outbreak in Patch 3

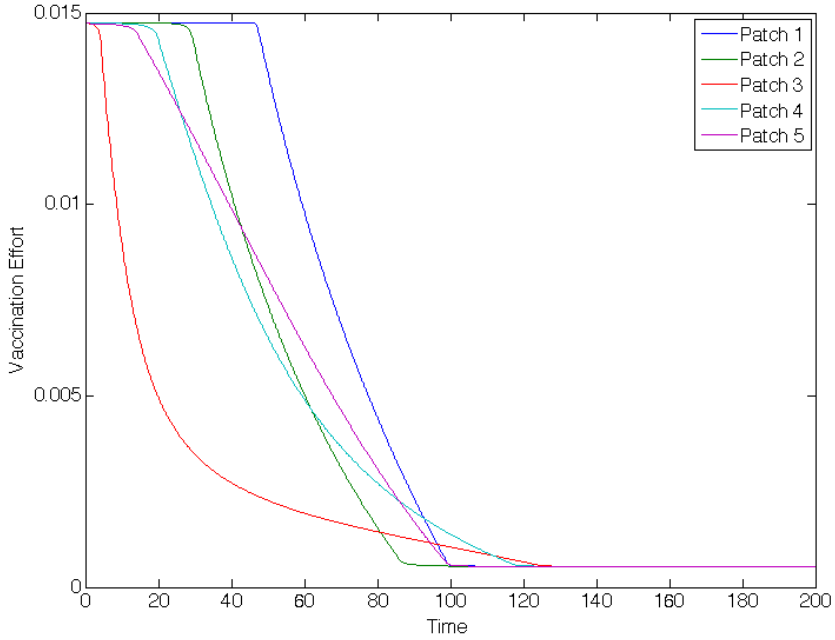

(a) Vaccination

Figure 3.28: Hot Spot Patch 1 Arrangement: Vaccination effort for linear arrangement with outbreak in Patch 3

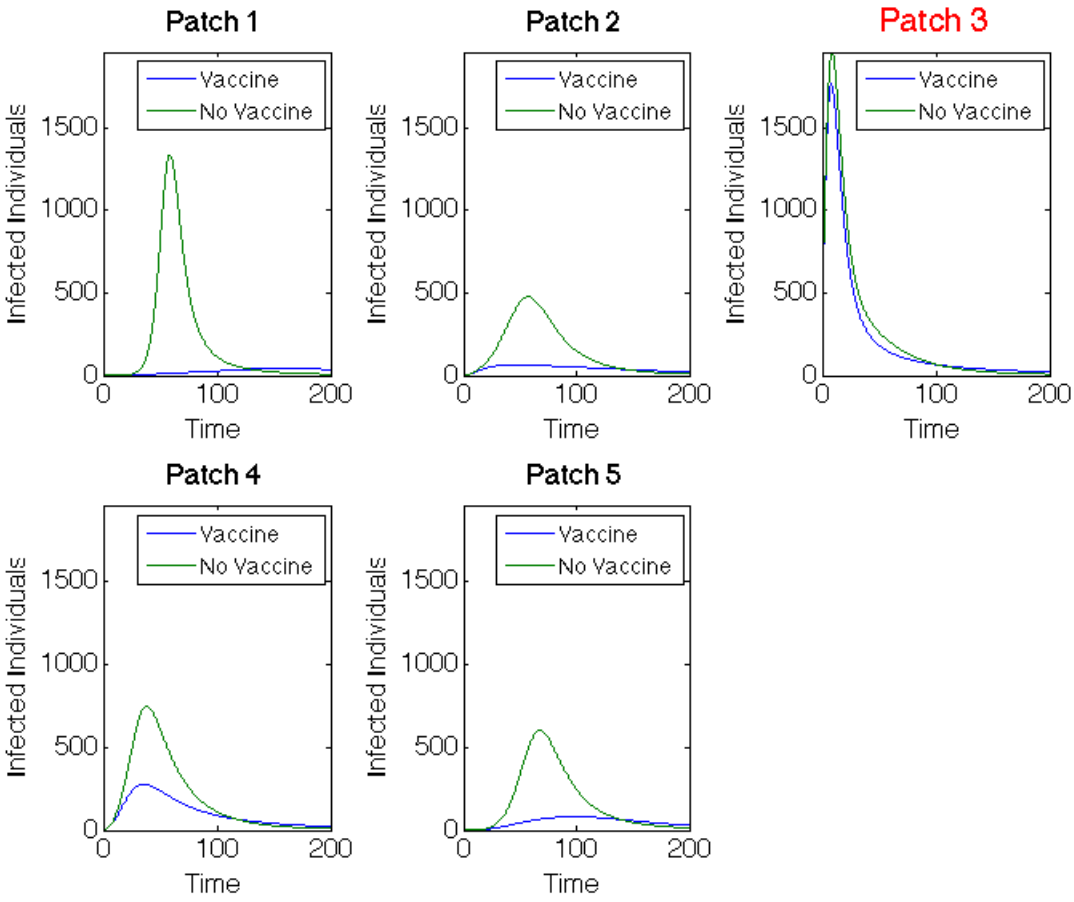

Figure 3.29: Hot Spot Patch 1 Arrangement: Infected population dynamics comparison with and without vaccination with outbreak in Patch 3

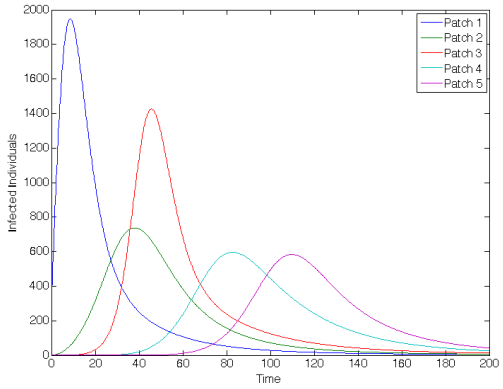

(a) Outbreak in Patch 1

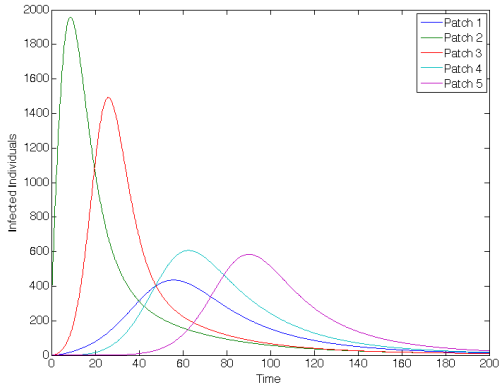

(b) Outbreak in Patch 2

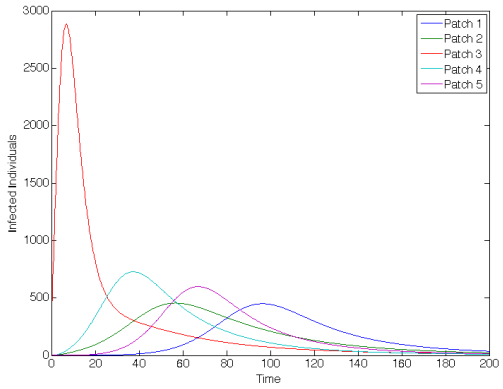

(c) Outbreak in Patch 3

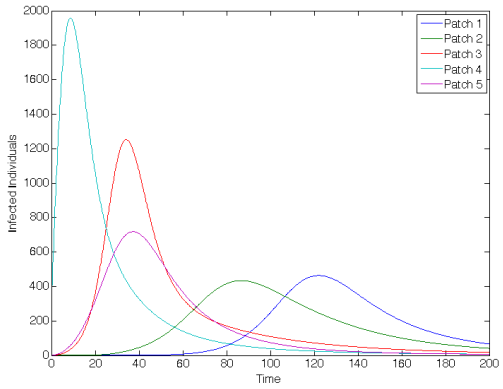

(d) Outbreak in Patch 4

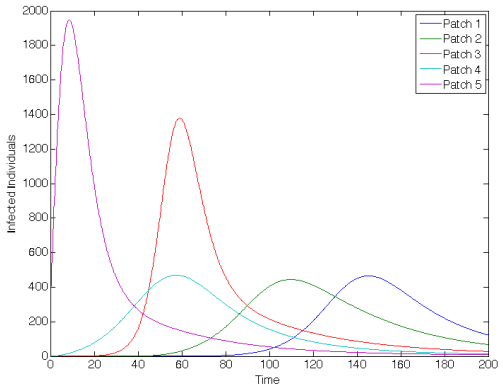

(e) Outbreak in Patch 5

Figure 3.30: Hot Spot Patch 3: Infected Dynamics (without vaccination) of the system with outbreak in each of the patches

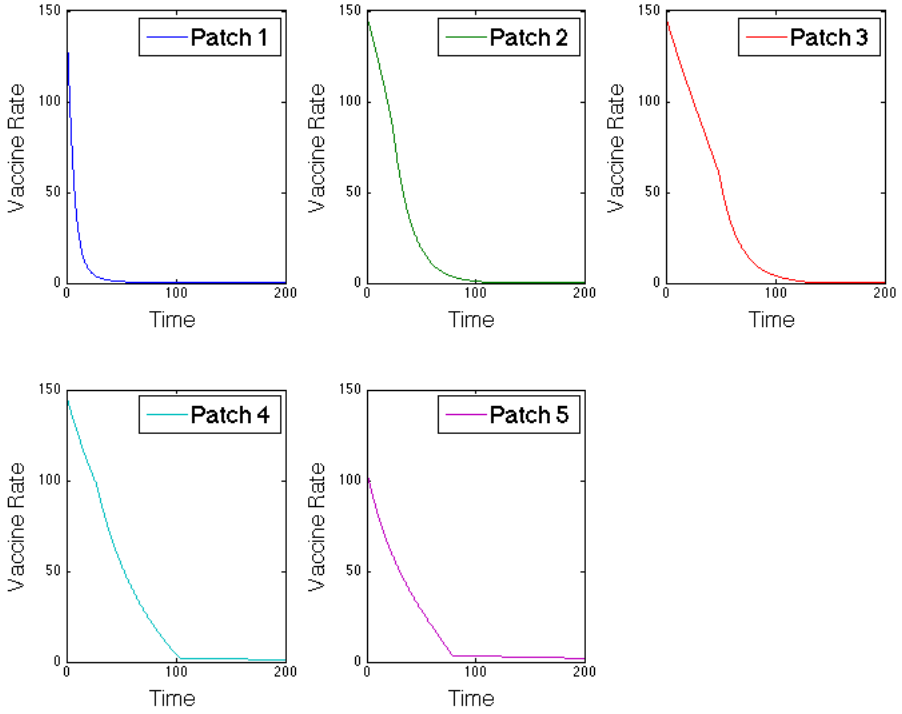

Figure 3.31: Hot Spot Patch 3 Arrangement: Vaccination rates for patches in linear arrangement with outbreak in Patch 1

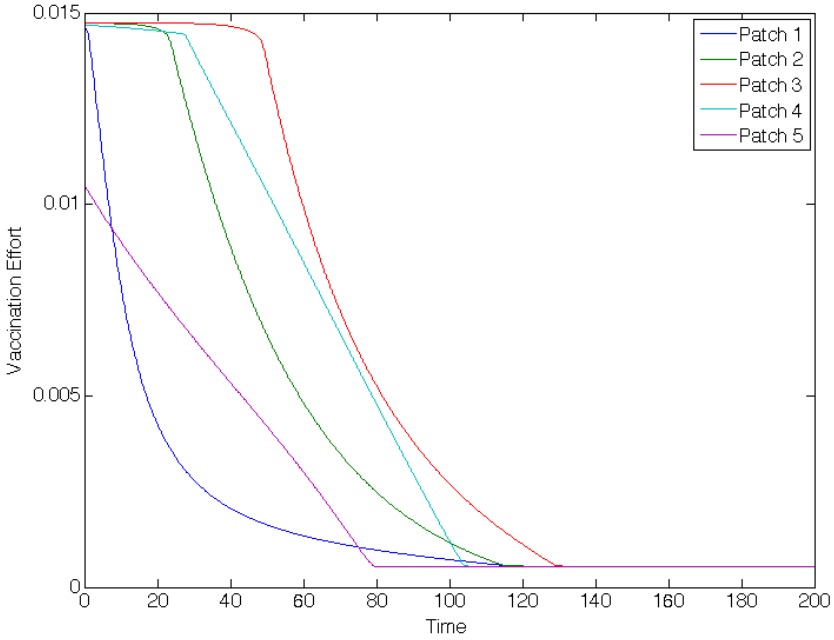

(a) Vaccination

Figure 3.32: Hot Spot Patch 3 Arrangement: Vaccination effort for linear arrangement with outbreak in Patch 1

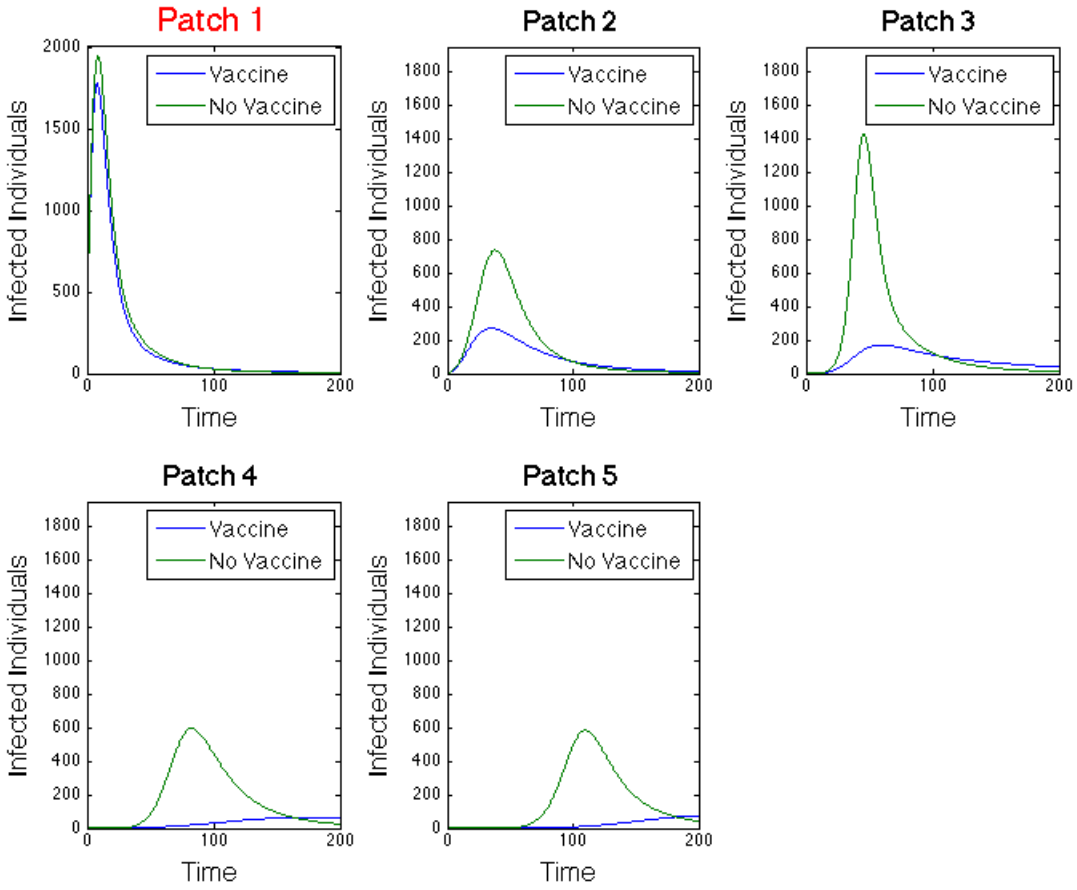

Figure 3.33: Hot Spot Patch 3 Arrangement: Infected population dynamics comparison with and without vaccination with outbreak in Patch 1

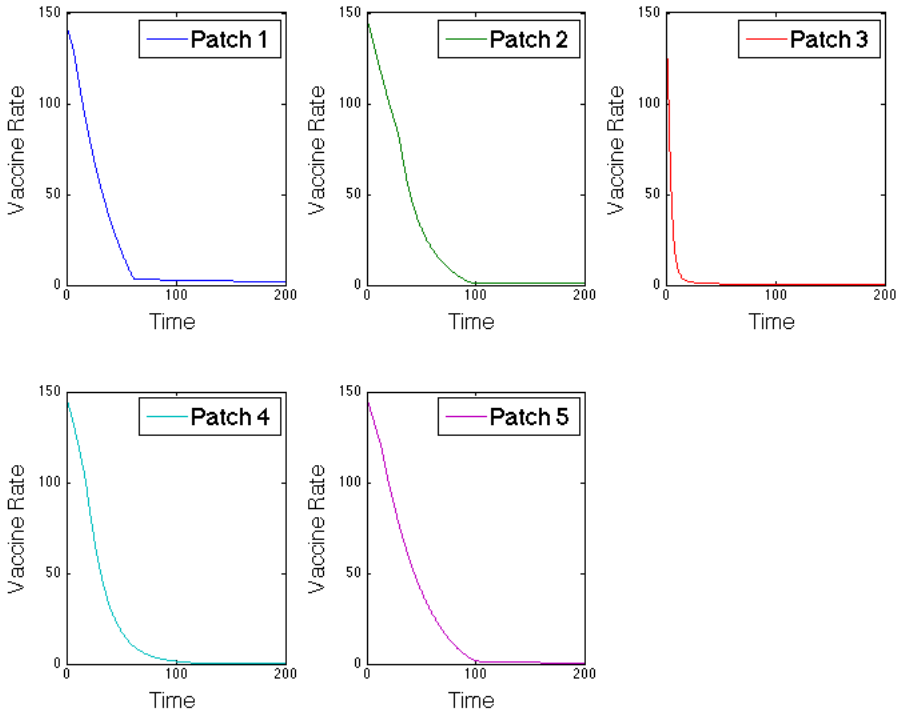

Figure 3.34: Hot Spot Patch 3 Arrangement: Vaccination rates for patches in linear arrangement with outbreak in Patch 3

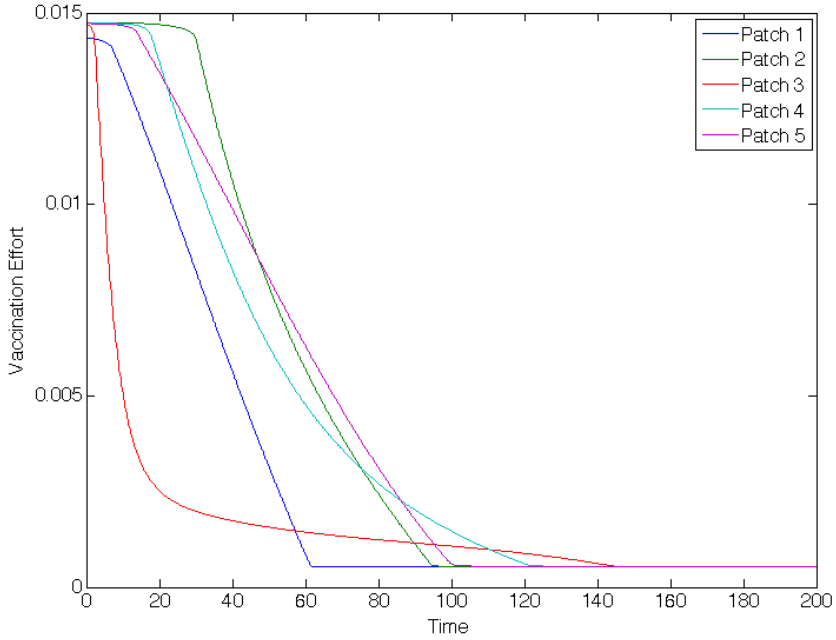

(a) Vaccination

Figure 3.35: Hot Spot Patch 3 Arrangement: Vaccination effort for linear arrangement with outbreak in Patch 3

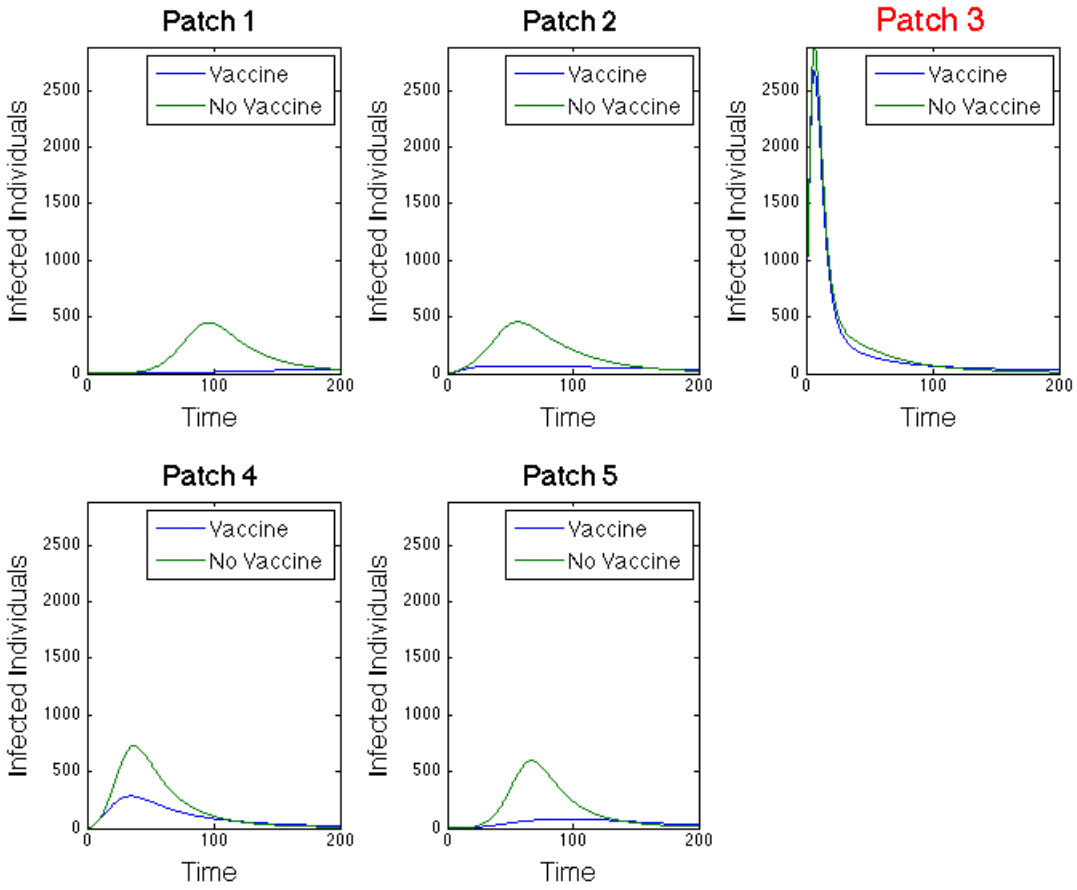

Figure 3.36: Hot Spot Patch 3 Arrangement: Infected population dynamics comparison with and without vaccination with outbreak in Patch 3

upper and lowermost patches from differing much from other patches in the linear spatial arrangement, in terms of pathogen in the aquatic reservoir. Unlike [60], the best case for a hot spot, based on network $\mathbf{R}_0$ values, would be in the center or upstream of the spatial arrangement, but not necessarily at the top.

As seen in our results, disease control efforts are not always highest in patches considered to have the highest network risk. Although hot spots have higher R_0 values, depending on where they are located and where an outbreak begins, the control effort for each patch varies, with the hot spot not always receiving the most vaccinations.

When the hot spot is located at the top of the network, Figures 3.24-3.29, we see similar results to the previous linear arrangement scenarios. Both population and pathogen only move to nearest neighbor so if the outbreak occurs in this hot spot, the effort is focused on protecting all downstream patches, seen in Figures 3.24-3.26.

When the outbreak occurs elsewhere in the metapopulation, we see similar effort levels in the outbreak patch as in previous scenarios but higher levels in the hot spot and for longer time, seen in Figures 3.27-3.29 and Figures B.30-B.32 in Appendix B. This is comparable to the hub arrangements when the outbreak occurred outside the hub. There is high effort in nearest neighbor patches but the hot spot is the priority with its high potential for invasion. When there is no direct connection between the hot spot and outbreak patch, increasing the effort in the hot spot almost eradicates the outbreak from this patch.

Another interesting result is in the number of vaccinations per patch. In comparing Table 3.28, the most vaccinations do not always occur in the hot spot patch. The most vaccinations are given to the hot spot only for outbreaks beginning close to the patch. When the outbreak occurs in the hot spot, more vaccinations are given in patches downstream of outbreak and for outbreaks beginning farther downstream, less vaccinations are spent in the hot spot and more are given to patches immediately upstream.

When the hot spot is centrally located in the metapopulation, there are additional differences in the vaccination strategy. From Table 3.32 and Figure 3.32, we see that when the outbreak begins upstream, effort is focused on patches downstream but not necessarily

nearest neighbor. There are more vaccinations administered in the patch below the hot spot. With an outbreak in the hot spot, seen in Figures 3.34-3.36, effort is spent longer on nearest upstream neighbor rather than downstream patches. The most vaccinations are administered in the farthest downstream patch as well as nearest upstream neighbor, seen in Table 3.32. This is similar to the previous linear arrangements. When the outbreak begins below the hot spot, the most vaccinations are administered in patches immediately upstream of the outbreak, whether a hot spot or not.

In comparing results of the linear arrangements, with and without hot spots, Tables 3.28 and 3.9 reveal the vaccination strategies differ most when a hot spot is located in upstream patches and an outbreak occurs downstream. With the addition of a hot spot, there is a large increase of vaccinations in the patch designated as a hot spot compared to the strictly linear arrangement case. This is similar to when the hot spot is centrally located, comparing Tables 3.32 and 3.9. There is a significant decrease in the number of vaccinations in the uppermost patch and a large increase of vaccinations at the hot spot.

3.7 Conclusions

After developing and analyzing an optimal control problem for a waterborne disease metapopulation model, we used numerical simulations to approximate solutions. We considered multiple scenarios and found the optimal vaccination strategies. We investigated a linear spatial arrangement with strictly nearest neighbor movement among the patches, hub spatial arrangements where one patch in the metapopulation had a larger population, higher connectivity among the patches, and higher movement rates, and linear spatial arrangements with patches of higher infectivity known as "hot spots." We sought answers to the question of where control efforts should be focused depending on metapopulation structure and path dynamics.

Vaccination strategies for the linear spatial arrangements were dependent on where the outbreak occurs. Vaccinations when outbreaks began at the top and bottom of the

arrangement had greater effect in lowering the number of infecteds in the metapopulation than when the outbreak was centrally located. The movement of the pathogen in the aquatic reservoir had a significant impact as well. When the outbreak occurred upstream, it was more important to protect patches farther downstream, whereas when the outbreak was downstream, the strategy shifts to protecting patches immediately upstream.

With the added connectivity of the hub spatial arrangements, the vaccination strategy and its impact is affected. The added connectivity of the hub makes the outbreak much harder to contain because it travels to every patch in the metapopulation shortly after it begins. When the outbreak occurs within a hub, vaccination effort is spent evenly among surrounding patches but its affect in preventing the disease is minimal. However, when the outbreak occurs outside the hub, there is a large effort spent protecting the hub due to its potential to spread the outbreak to all patches of the metapopulation.

We also compared sizes of hubs in relation to the outlying patches. The larger the hub, compared to the surrounding patches, the more vaccination effort is focused on the hub. When the hub and surrounding patches are more even in population size, effort is more evenly spread to the outlying patches. This is important to consider when investigating regions with large cities and how population sizes of the region matter when developing intervention strategies.

We compared our results with those of Tien, Eisenberg, and their collaborators [60, 21], by considering a linear spatial arrangement that includes "hot spot" patches. There were several differences between our results as well as differences from the identical patch linear arrangement scenarios. Wherever a hot spot is located in the arrangement, the vaccination strategy changes most when the outbreak begins in downstream patches of the metapopulation. There is a large increase in vaccinations in the hot spot patch compared to scenarios when the outbreak is in, or near, the hot spot. There is evidence that an increase in vaccination effort to the hot spot is only appropriate if an outbreak occurs far enough away from the patch, specifically when farther downstream. Otherwise, a similar vaccination strategy to the identical linear arrangement is appropriate.

Our work shows convincingly that spatial arrangements and heterogeneity in features (like hot spots, sizes, and connectivity) are important to management strategies. These features can have a significant impact on intervention decisions. These optimal control tools, applied to the varying scenarios, can give guiding "rule of thumb" strategies for the management of disease epidemics when concerned about spatial features of a landscape.

Guiding Strategies for Spatial Arrangement Scenarios

- It is too hard to contain a patch once invaded with the disease so the least effort is always in outbreak patch.
- Due to the directional flow of rivers affecting pathogen movement, more vaccinations are needed when outbreaks occur upstream rather than downstream.
- With more populations downstream, vaccine effort should be focused on (not necessarily nearest) patches downstream of outbreak.
- If the outbreak is centrally located, the optimal strategy is to contain outbreak with vaccines in patches above and below outbreak with higher effort downstream.
- With more populations upstream, vaccine effort focused immediately upstream since the pathogen has a harder time traveling upstream.
- With outbreaks in surrounding patches, the focus of vaccinations should be in the hub.
- Outbreaks are hardest to contain when starting in a hub, which implies that preemptive prevention of disease invasions in hubs is highly important.
- With a hub upstream, regardless of where outbreak occurs, it is important to vaccinate the patch immediately downstream of the hub to prevent the spread in the patch network.
- Depending on the size of hub, effort spent in the hub compared to the surrounding patches will change. The larger the hub patch, the higher the vaccination will be in that patch.

- Even if an area of higher risk of invasion ("hot spot"), if these areas are not located in close proximity to the outbreak location, it is more important to contain outbreak in surrounding patches than the hot spot itself.

3.8 Future Work

Many of the simulations investigated identical patches within a metapopulation. There is now a need to investigate a more heterogenous set of patches in the metapopulation (varying contact rates, recovery rates, movements, etc.) and investigate outbreak scenarios. We also want to compare our results with an actual spatial arrangement of communities, such as the departments of Haiti.

The spatial arrangement project for cholera has branched out to current work on a multi-dose vaccine model for the disease to depict a more accurate vaccine program. I am interested in investigating waning immunity in response to dose intakes. I have been developing this model which includes an exponential waning immunity term, as well as an extension using a gamma chain distribution, to investigate the effect of immunity on disease dynamics, the role of waning immunity from the disease and vaccination, and to find an optimal intervention strategy for its implementation.

In addition, further investigation should include the restriction to a limited number of vaccinations. There is currently interest in the creation of a vaccine stockpile so results with a finite number of vaccinations available would be significant. This work could also be applied to other diseases as well as alternative intervention strategies besides, or in addition to, vaccination.

Bibliography

[1] S. Anita, V. Arnautu, and V. Capasso. *Introduction to Optimal Control Problems in Life Sciences and Economics*. Springer, New York, 2011. 5

[2] J. Arino, J.R. Davis, D. Hartley, R. Jordan, J.M. Miller, and P. van den Driessche. A multi-species epidemic model with spatial dynamics. *Mathematical Medicine and Biology*, 22(2):129–142, 2005. 73

[3] J. Arino and P. van den Driessche. Disease spread in metapopulations. *American Mathematical Society*, Fields Institute Communications, Mathematics Subject Classification. 92D30, 34D23, 2000. 73, 86

[4] J. Arino and P. van den Driessche. A multi-city epidemic model. *Mathematical Population Studies*, 10(3):175–193, 2003. 73

[5] J. Arino and P. van den Driessche. Metapopulation epidemic models, a survey. *Fields Institute Communications*, 46:1–13, 2006. 73

[6] A. Berman and R.J. Plemmons. *Nonnegative Matrices in the Mathematical Sciences*. SIAM (republication of 1979 work published by Academic Press), Philadelphia, reprint edition, 1994. 86

[7] E. Bertuzzo, S. Azaele, A. Maritan, M. Gatto, I. Rodriguez-Iturbe, and A. Rinaldo. On a space-time evolution of a cholera epidemic. *Water Resources Research*, 44(W01424):doi:10.1029/2007WR006211., 2008. 72, 77

[8] E. Bertuzzo, R. Casagrandi, M. Gatto, I. Rodriguez-Iturbe, and Rinaldo A. On spatially explicit models of cholera epidemics. *J. R. Soc. Interface*, 7(43):321–333, 2009. 72, 77

[9] E. Bertuzzo, L. Mari, L. Righetto, M. Gatto, R. Casagrandi, M. Blokesch, I. RodriguezIturbe, and A. Rinaldo. Prediction of the spatial evolution and effects of control measures for the unfolding haiti cholera outbreak. *Geophysical Research Letters*, 38(L06403):doi:10.1029/2011GL046823, 2011. 72

[10] E. Bertuzzo, L. Mari, L. Righetto, M. Gatto, R. Casagrandi, I. Rodriguez-Iturbe, and A. Rinaldo. Hydroclimatology of dual-peak annual cholera incidence: Insights from a spatially explicit model. *Geophysical Research Letters*, 39(L05403), 2012. 77

[11] G.M. Brown and J. Roughgarden. A metapopulation model with private property and a common pool. *Ecol. Econ.*, 30:293–299, 1997. 11

[12] C. Castillo-Chavez and A-A. Yakubu. Intraspecific competition, dispersal and disease dynamics in discrete-time patchy ennvironments. In S. Castillo-Chavez, C. with Blower, P. van den Driessche, D. Kirschner, and Yakubu A-A, editors, *Mathematical approaches for emerging and reemerging infectious diseases: An introduction*, volume 125 of *IMA Volumes in Mathematics and Applications*, pages 165–181. Institute for Mathematics and its Applications, 2002. 73

[13] D. Chao, M. E. Halloran, and I. Longini. Vaccination strategies for epidemic cholera in haiti with implications for the developing world. *PNAS*, 108(17):7081–7085, 2011. 74

[14] C. W. Clark. *The Worldwide Crisis in Fisheries*. Cambridge University Press, New York, 2006. 10

[15] C.W. Clark. *Bioeconomic Modelling and Fisheries Management*. Wiley, New York, 1985. 10

[16] C.W. Clark. *Mathematical bioeconomics: The optimal management of renewable resources*. Wiley, New York, 2nd edition, 1990. 10

[17] C. T. Codeco. Endemic and epidemic dynamics of cholera: the role of the aquatic reservoir. *BMC Infectious Diseases*, 1(1), February 2001. 72

[18] O. Dieckmann and J.A.P. Heesterback. *Mathematical Epidemiology of Infectious Diseases: Model Building, Analysis, and Interpretation*. Wiley, England, 2000. 84

[19] W. Ding and S. Lenhart. Optimal harvesting of a spatially explicit fishery model. *Natural Resource Modeling*, 22(2), 2009. 11, 12

[20] S. F. Dowell and C. R. Braden. Implications of the introduction of cholera to haiti. *Emerging Infectious Diseases*, 17(7), 2011. 71

[21] M. Eisenberg, Z. Shuai, J. Tien, and P. van den Driessche. A cholera model in a patchy environment with water and human movement. *Mathematical Biosciences*, 246(1):105–112, 2013. 73, 75, 89, 134, 153

[22] L. Evans. *Partial Differential Equations*. American Mathematical Society, 2nd edition, 2010. 16, 22, 25, 29, 42

[23] R. Fister. Optimal control of harvesting in a predator-prey parabolic system. *Houston Journal of Mathematics*, 23(2), 1997. 97

[24] A. Friedman. *Foundations in Modern Analysis*. Dover Publications, New York, reprint originally published new york: holt, rinehart, and winston [1970] edition, 1982. 91

[25] H. Gaff and E. Schaefer. Optimal control applied to vaccination and treatment strategies for various epidemiological models. *Math. Biosci. Eng.*, 6(3):469–492.1551–0018, 2009. 88

[26] W. Hackbusch. A numerical method for solving parabolic equations with opposite orientations. *Computing*, 20(3):229–240, 1978. 7

[27] I.A. Haski and M.E. Gilpin. *Metapopulation Biology: Ecology, Genetics, and Evolution*. Academic Press, 1997. 73

[28] G.E. Herrera and S. Lenhart. *Spatial Ecology*, chapter Spatial optimal control of renewable resource stocks, pages 343–357. Mathematical and Computational Biology Series. Chapman & Hall, CRC, 2010. 10

[29] R. Hilborn. *Overfishing: What Everyone Needs to Know*. Oxford University Press, Oxford, 2012. 2, 9, 10

[30] A. Iserles. *A First Course in the Numerical Analysis of Differential Equations*. Cambridge University Press, New York, 2008. 7, 166

[31] H Joshi, G. Herrera, S. Lenhart, and M. Neubert. Optimal dynamic harvest of a mobile renewable resource. *Natural Resource Modeling*, 10(40), 2008. 2, 9, 12, 44, 48, 57

[32] M. J. Keeling and P. Rohani. *Modeling Infectious Diseases in Humans and Animals*. Princeton University Press, Princeton, New Jersey, 2008. 73

[33] R. Knox. Vaccination against cholera finally begins in haiti, April 2013. 74

[34] W. Krabs and S. W. Pickl. *Modelling, Analysis, and Optimization of Biosystems*. Springer, New York, 2010. 5

[35] N.V. Krylov. *Nonliner Elliptic and Parabolic Equations of the Second Order*. D. Reidel Publishing Company, Dordrecht, Holland, 1985. 26

[36] P. De Leenheer. Optimal placement of marine protected areas: a trade-off between fisheries goals and conservation efforts. *IEEE Transactions on Automatic Control*, 59(6), 2014. 11

[37] S. Lenhart, M. Liang, and V. Protopopescu. Optimal control of boundary habitat hostility for interacting species. *Mathematical Methods in the Applied Sciences*, 22:1061–1077, 1999. 12

[38] S. Lenhart and D.G. Wilson. Optimal control of a heat transfer problem with convective boundary condition. *Journal of Optimization Theory and Applications*, 79(3), 1993. 12

[39] S. Lenhart and J.T. Workman. *Optimal Control Applied to Biological Models*. Chapman & Hall, London, 2007. 4, 7, 46, 102

[40] S.A. Levin, T.M. Powell, and J.H. Steele, editors. *Patch Dynamics*, volume 96 of *Lecture Notes in Biomathematics*. Springer-Verlag, 1993. 73

[41] X. Li and J. Yong. *Optimal control theory for infinite dimensional systems*. Birkhäuser, Boston, 1994. 5

[42] G. M. Lieberman. *Second Order Parabolic Differential Equations*. World Scientific Publishing Company, 1996. 25

[43] H. Moeller and M. Neubert. Habitat damage, marine reserves, and the value of spatial management. *Ecological Applications*, 13(5):959–971, 2013. 60

[44] J. D. Murray. *Mathematical Biology I: An Introduction*. Springer, New York, 2001. 1

[45] J. D. Murray. *Mathematical Biology II: Spatial Models and Biomedical Applications*. Springer, New York, 2003. 1

[46] R. Miller Neilan, E. Schaefer, H. Gaff, K. R. Fister, and S. Lenhart. Modeling optimal intervention strategies for cholera. *Bulletin of Mathematical Biology*, 72:2004–2018, March 2010. 3, 74

[47] M. Neubert. Marine reserves and optimal harvesting. *Ecology Letters*, 6:843–849, 2003. 9, 11, 12

[48] World Health Organization. Oral cholera vaccines in mass immunization campaigns: Guidance for planning and use, 2010. 74

[49] "World Health Organization". Cholera fact sheet, no. 107, February 2014. 72

[50] S. Pedley and K. Pond. Emerging issues in water and infectious disease. *World Health Organization*, 2003. 3

[51] R. Piarroux, R. Barrais, B. Faucher, R. Haus, M. Piarroux, J. Gaudart, R. Magloire, and D. Raoult. Understanding the cholera epidemic, haiti. *Emerging Infectious Diseases*, 17(7), 2011. 71

[52] L.S. Pontryagin, V.G. Boltyanskii, R.V. Gamkrelize, and E.F. Mishchenoko. *The Mathematical Theory of Optimal Processes*. Wiley, New York, 1962. 5, 90, 94

[53] M. Protter and H. Weinberger. *Maximum Principles in Differential Equations*. Prentice-Hall, Inc., New Jersey, 1967. 23

[54] A. Rinaldo, E. Bertuzzo, L. Mari, L. Righetto, M. Blokesch, M. Gatto, R. Casagrandi, M. Murray, S. M. Vesenbeckh, and I. Rodriquez-Iturbe. Reassessment of the 2010–2011 haiti cholera outbreak and rainfall-driven multiseason projections. *Proceedings of the National Academy of Sciences of the United States of America*, 109(17), 2012. 72

[55] J.N. Sanchirico and J.E. Wilen. A bioeconomic model of marine reserve creation. *J. Environ. Econ. Manag.*, 42:257–276, 2001. 11

[56] J.N. Sanchirico and J.E. Wilen. Bioeconomics of spatial exploitation in a patchy environment. *J. Environ. Econ. Manag.*, 37:129–150, 2005. 11

[57] S. Shin, S. Desai, B. Sah, and J. Clemens. Oral vaccines against cholera. *Clinical Infectious Diseases, Oxford University Press*, 52(11):1343–1349, 2011. 74

[58] J. Simon. Compact sets in the space $l^p(0,t;b)$. *Annali di Matematica pura ed applicata*, CXLVI((IV)):65–96, 1987. 29, 33

[59] J. Tien and D. Earn. Multiple transmission pathways and disease dynamics in a waterborne pathogen model. *Bulletin of Mathematical Biology*, 72:1506–1533, February 2010. 3, 72, 73, 74, 75, 76, 78

[60] J. Tien, Z. Shuai, M. Eisenberg, and P. van den Driessche. Disease invasion on community networks with environmental pathogen movement. *Journal of Mathematical Biology*, (Accepted), 2014. 73, 75, 89, 118, 134, 138, 151, 153

[61] D. Tilman and P. Kareiva, editors. *Spatial Ecology*. Princeton University Press, Princeton, New Jersey, 1997. 1

[62] C. Toropova, I. Meliane, D. Laffoley, E. Matthews, and M. Spalding, editors. *Global Ocean Protection: Present Status and Future Possibilities*. IUCN, The Nature Conservancy, UNEP-WCMC, UNEP, UNU-IAS, Agence des aires marines protégées, Gland, Switzerland, Arlington, USA, Cambridge, UK, Nairobi, Kenya, Tokyo Japan, Brest, France, 2010. 10

[63] G.N. Tuck and H.P. Possingham. Marine protected areas for spatially structured exploited stocks. *Marine Ecology Progress Series*, 192:89–101, 2000. 10

[64] A. Tuite, J. Tien, M. Eisenberg, D. Earn, J. Ma, and D. Fisman. Cholera epidemic in haiti, 2010: Using a transmission model to explain spatial spread of disease and identifiy optimal control interventions. *Ann. Intern. Med.*, 154:593–601, 2011. 71, 72, 73, 75, 76, 102

[65] P. van den Driessche and J. Watmough. Reproduction numbers and sub-threshold endemic equilibria for compartmental models of disease transmission. *Mathematical Biosciences*, 180:29–48, 2002. 84, 87

[66] C.J. Walters and S. J.D. Martell. *Fisheries Ecology and Management*. Princeton University Press, Princeton, New Jerset, 2004. 10

Appendix

Appendix A

Numerical Scheme Explanation

For numerical simulations, we consider the one-dimensional fish stock density model:

$$u_t = (a(x,t)u_x)_x + b(x,t)u_x + f(u) - h(x,t)u \qquad \Omega \times (0,T) \qquad \text{(A.1)}$$

$$\frac{\partial u}{\partial \nu}(x,t) + qu(x,t) = 0 \qquad \partial\Omega \times (0,T) \qquad \text{(A.2)}$$

where $\Omega = (0, L)$.

We assume the initial condition:

$$u(x,0) = u_0(x) \qquad x \in (0,L).$$

The diffusion and advection coefficients, $a(x,t)$ and $b(x,t)$, can be heterogeneous functions. We will solve the state PDE forward in time using the initial conditions.

The adjoint operator L^* and the adjoint PDE for the problem:

$$L^*\lambda = -\lambda_t - (1 - 2u^*)\,\lambda + h\lambda - (a(x,t)\lambda_x)_x + (b(x,t)\lambda)_x \qquad \text{(A.3)}$$

where

$$L^*\lambda + \mu\lambda = h^* \qquad \Omega \times (0,T) \tag{A.4}$$

$$\frac{\partial \lambda}{\partial \nu} + q\lambda - b(x,t)\eta\lambda = 0 \qquad \partial\Omega \times (0,T), \tag{A.5}$$

and

$$\lambda(x,T) = 0.$$

Since we only numerically consider one-dimensional in space, the value of the normal, η, will be 1 or -1 depending on the side of the domain. Also, note that $q > b\eta$ in our cases. We used finite difference schemes to discretize the system of equations.

For the diffusion term, since we consider $a(x,t)$ to be a heterogenous function, we used a scheme described in [30]:

$$\left(a(i,j)\frac{\partial u}{\partial x}\right)_x (i,j) = \frac{a(i+\frac{1}{2},j)u(i+1,j) - \left(a(i+\frac{1}{2},j) + a(i-\frac{1}{2},j)\right)u(i,j) + a(i-\frac{1}{2},j)u(i-1,j)}{(dx)^2}.$$

For the advection term, we used an upwind scheme. The scheme is dependent on the sign of the advection coefficient, $b(x,t)$, in the following way:

If $b(x,t) > 0$, then:

$$\frac{du}{dx}(i,j) = \frac{u(i+1,j) - u(i,j)}{dx}.$$

If $b(x,t) < 0$, then

$$\frac{du}{dx}(i,j) = \frac{u(i,j) - u(i-1,j)}{dx}.$$

Additionally, for the term in the adjoint, $(b(x,t)\lambda)_x$:

If $b(x,t) > 0$, then:

$$(b(i,j)\lambda)_x (i,j) = \frac{b(i+1,j)\lambda(i+1,j) - b(i,j)\lambda(i,j)}{dx}.$$

If $b(x,t) < 0$, then

$$(b(i,j)\lambda)_x (i,j) = \frac{b(i,j)\lambda(i,j) - b(i-1,j)\lambda(i-1,j)}{dx}.$$

We used an Euler method for the time derivative discretization:

$$\frac{du}{dt}(i,j) = \frac{u(i,j+1) - u(i,j)}{dt}.$$

Using the above three schemes, we discretized the state system and solved forward in time using the initial condition. The scheme is written (if $b > 0$):

$$\begin{aligned}
\frac{u(i,j+1) - u(i,j)}{(dt)} &= u(i,j)\left(1 - u(i,j)\right) \\
&+ \frac{1}{(dx)^2}\left(a(i+\frac{1}{2},j)u(i+1,j) + a(i-\frac{1}{2},j)u(i-1,j)\right) \\
&- \frac{1}{(dx)^2}\left(a(i+\frac{1}{2},j) + a(i-\frac{1}{2},j)\right)u(i,j) \\
&- h(i,j)u(i,j) + b(i,j)\left[\frac{u(i+1,j) - u(i,j)}{(dx)}\right].
\end{aligned}$$

After some rewriting, solving for $u(i,j+1)$:

$$\begin{aligned}
u(i,j+1) &= u(i,j) + u(i,j)\left(1 - u(i,j)\right)dt \\
&+ \frac{dt}{(dx)^2}\left(a(i+\frac{1}{2},j)\right)\left(u(i+1,j) - u(i,j)\right) \\
&+ \frac{dt}{(dx)^2}\left(a(i-\frac{1}{2},j)\right)\left(u(i-1,j) - u(i,j)\right) \\
&- h(i,j)u(i,j)dt + b(i,j)\left[u(i+1,j) - u(i,j)\right]\frac{dt}{dx}.
\end{aligned}$$

For the terms at the boundary, $x = 1$ and $x = L$:

$$\frac{du}{d\nu}(1,j) + qu(1,j) = 0 \Rightarrow \left[\frac{u(2,j) - u(0,j)}{2dx}\right]\nu + qu(1,j) = 0$$

and

$$\frac{du}{d\nu}(L,j) + qu(L,j) = 0 \Rightarrow \left[\frac{u(L+1,j) - u(L-1,j)}{2(dx)}\right]\nu + qu(L,j) = 0.$$

We used positions close to the boundary to get the following:

$$\frac{du}{d\nu}(2,j) + qu(2,j) = 0 \Rightarrow \left[\frac{u(3,j) - u(1,j)}{2dx}\right]\nu + qu(2,j) = 0$$

and

$$\frac{du}{d\nu}(L-1,j) + qu(L-1,j) = 0 \Rightarrow \left[\frac{u(L,j) - u(L-2,j)}{2(dx)}\right]\nu + qu(L-1,j) = 0.$$

We then solved for the terms on the boundary (with $\nu = -1$ at $x = 1$ and $\nu = 1$ at $x = L$):

$$u(1,j) = u(3,j) - 2qu(2,j)dx$$

and

$$u(L,j) = u(L-2,j) - 2qu(L-1,j)dx.$$

We discretized the adjoint system and solved the system backward in time using the transversality condition. The scheme is written (if $b > 0$):

$$\begin{aligned}
&-\left(\frac{\lambda(i,j) - \lambda(i,j-1)}{dt}\right) - (1 - 2u(i,j-1))\,\lambda(i,j) \\
&-\frac{1}{(dx)^2}\left(a(i+\frac{1}{2},j)\lambda(i+1,j) + a(i-\frac{1}{2},j)\lambda(i-1,j)\right) \\
&\qquad +\frac{1}{(dx)^2}\left(a(i+\frac{1}{2},j) + a(i-\frac{1}{2},j)\right)\lambda(i,j) \\
&\qquad +\left[\frac{b(i,j)\lambda(i,j) - b(i-1,j)\lambda(i-1,j)}{dx}\right] \\
&\qquad\quad +\mu\lambda(i,j) + (\lambda(i,j) - 1)\,h(i,j-1) \;=\; 0.
\end{aligned}$$

After some rewriting, the code for $\lambda(i, j-1)$ is:

$$\begin{aligned}
\lambda(i,j-1) &= \lambda(i,j) + (1-2u(i,j-1))\,\lambda(i,j)dt \\
&- \mu\lambda(i,j)dt + h(i,j-1)\,(1-\lambda(i,j))\,dt \\
&+ \frac{dt}{(dx)^2}\left(a(i+\frac{1}{2},j)\right)(\lambda(i+1,j)-\lambda(i,j)) \\
&+ \frac{dt}{(dx)^2}\left(a(i-\frac{1}{2},j)\right)(\lambda(i-1,j)-\lambda(i,j)) \\
&- \frac{dt}{dx}\left[b(i,j)\lambda(i,j) - b(i-1,j)\lambda(i-1,j)\right].
\end{aligned}$$

For the terms at the boundary, $x = 1$ and $x = L$:

$$\begin{aligned}
\frac{\partial\lambda}{\partial\nu}(1,j), +q\lambda(1,j) - b(1,j)\eta\lambda(1,j) &= 0 \\
\Rightarrow \left[\frac{\lambda(2,j)-\lambda(0,j)}{2dx}\right]\nu + q\lambda(1,j) - b(1,j)\eta\lambda(1,j) &= 0
\end{aligned}$$

and

$$\begin{aligned}
\frac{\partial\lambda}{\partial\nu}(L,j), +q\lambda(L,j) - b(L,j)\eta\lambda(L,j) &= 0 \\
\Rightarrow \left[\frac{\lambda(L+1,j)-\lambda(L-1,j)}{2dx}\right]\nu + q\lambda(L,j) - b(L,j)\eta\lambda(L,j) &= 0.
\end{aligned}$$

Again, we used positions close to the boundary to get the following:

$$\left[\frac{\lambda(3,j)-\lambda(1,j)}{2dx}\right]\nu + q\lambda(2,j) - b(2,j)\eta\lambda(2,j) = 0$$

and

$$\left[\frac{\lambda(L,j)-\lambda(L-2,j)}{2dx}\right]\nu + q\lambda(L-1,j) - b(L-1,j)\eta\lambda(L-1,j) = 0.$$

We then solved for the terms on the boundary:

$$\begin{aligned}\lambda(1,j) &= \lambda(3,j) - 2\left(q + b(2,j)\right)\lambda(2,j)dx \\ \lambda(L,j) &= \lambda(L-2,j) - 2\left(q - b(L-1,j)\right)\lambda(L-1,j)dx.\end{aligned}$$

We then characterized the control as described in (2.42). We set the control as h_{max}, 0, or $h_{singular}$ depending on the value of the adjoint. The $h_{singular}$ case did not occur in our simulations.

Appendix B

Cholera Simulations

We include several additional plots for the simulations of a cholera outbreak and optimal vaccination strategies.

B.1 Additional Linear Spatial Arrangement Results

The vaccination rates for each patch with an outbreak in Patch 3 or 5 are given in Figures B.1 and B.2.

B.2 Additional Hub Patch 1 Spatial Arrangement Results

Results for when an outbreak begins in Patch 5 are given in Figures B.3-B.5.

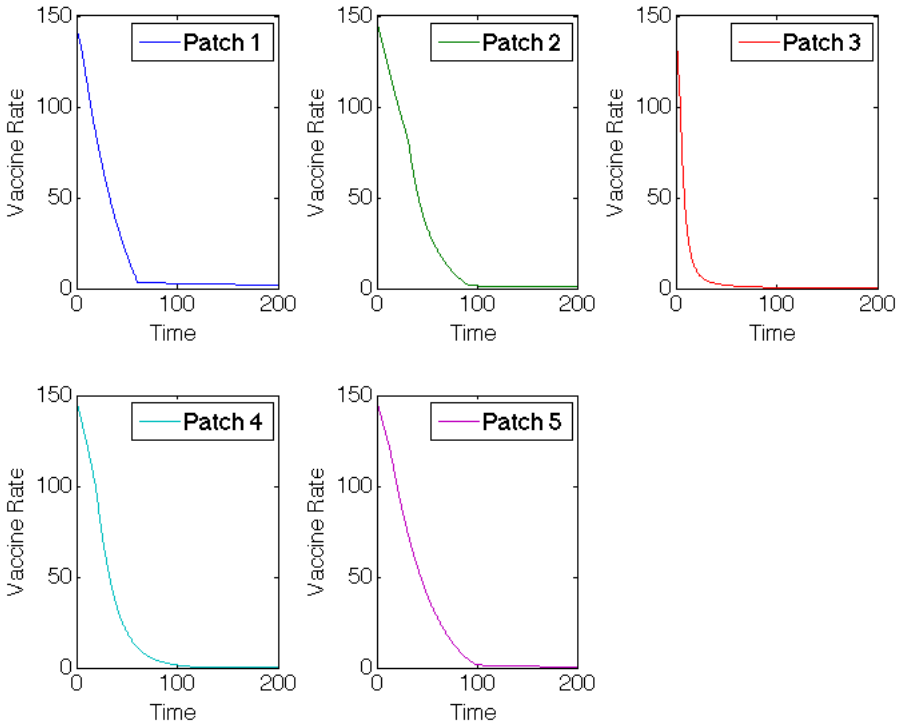

Figure B.1: Linear Arrangement: Vaccination rates of patches with outbreak in Patch 3

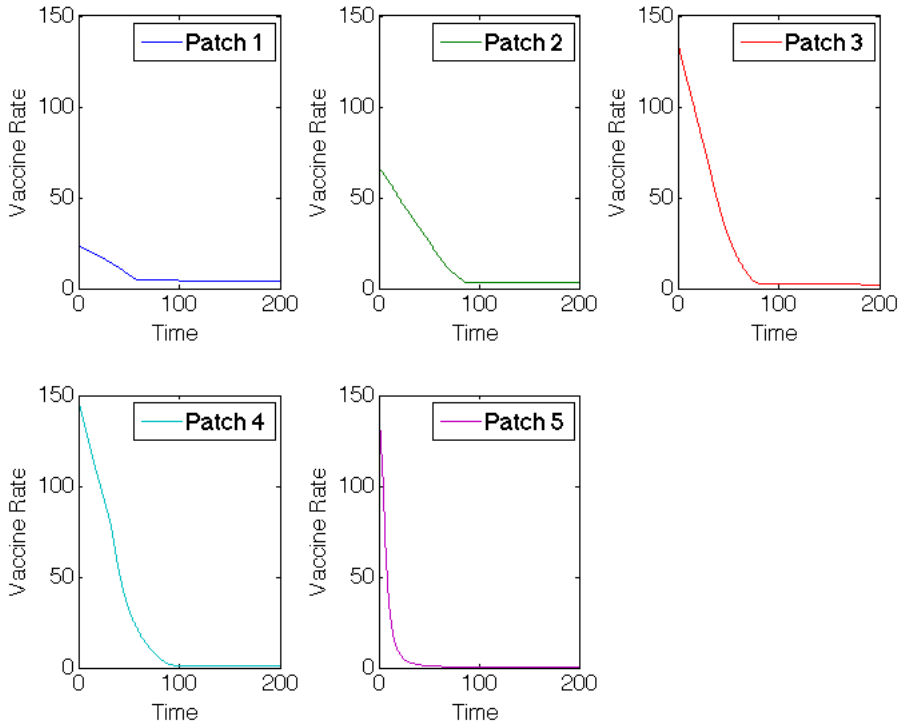

Figure B.2: Linear Arrangement: Vaccination rates of patches with outbreak in Patch 5

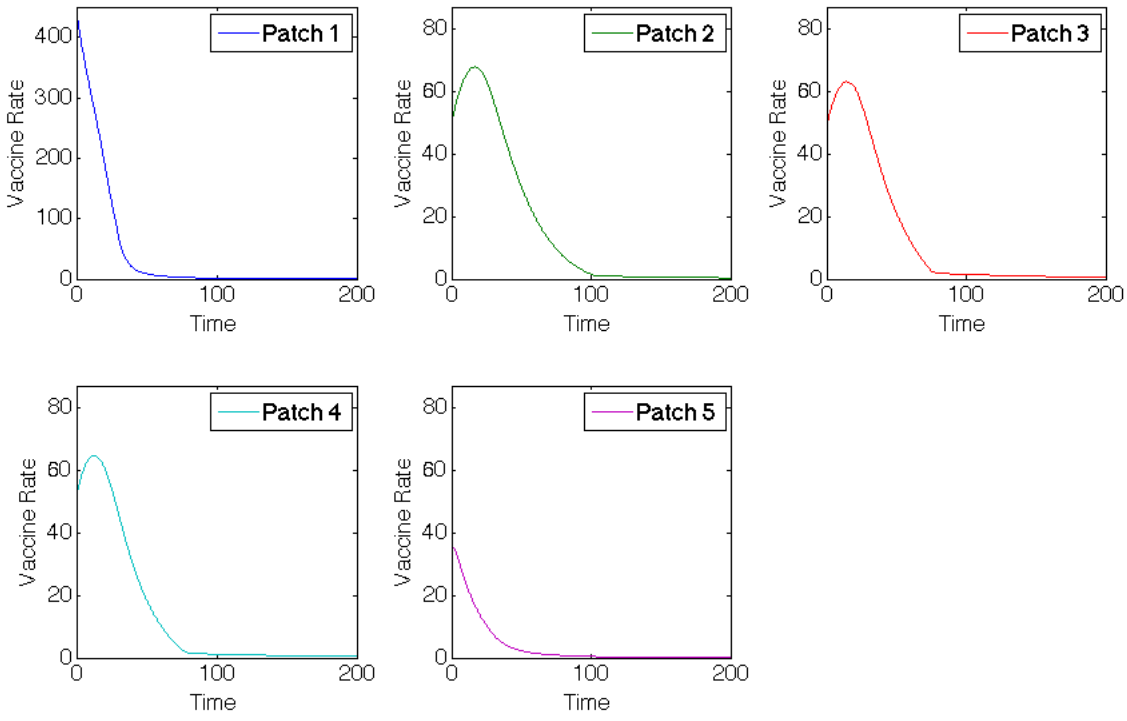

Figure B.3: Hub Patch 1 Arrangement: Vaccination rates of patches with outbreak in Patch 5

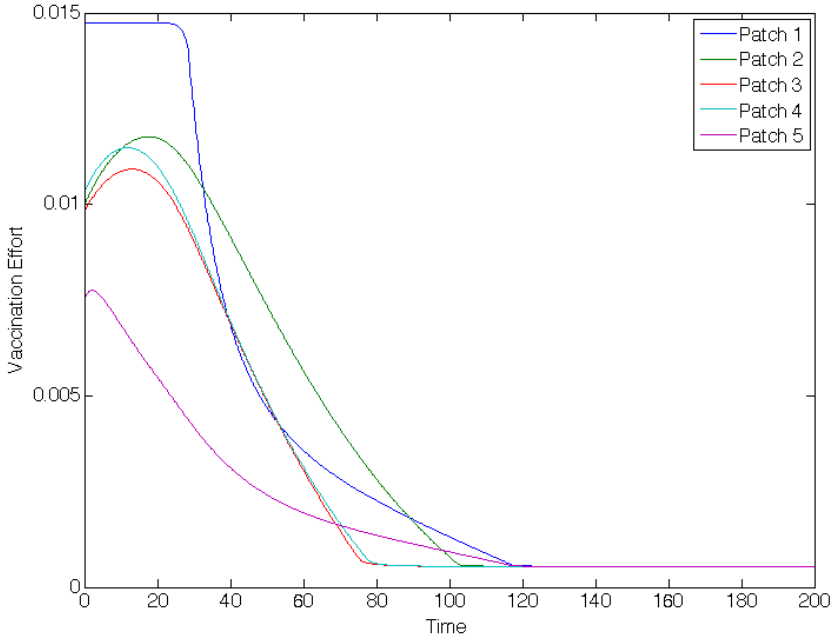

(a) Vaccination

Figure B.4: Hub Patch 1 Arrangement: Vaccination effort of patches with outbreak in Patch 5

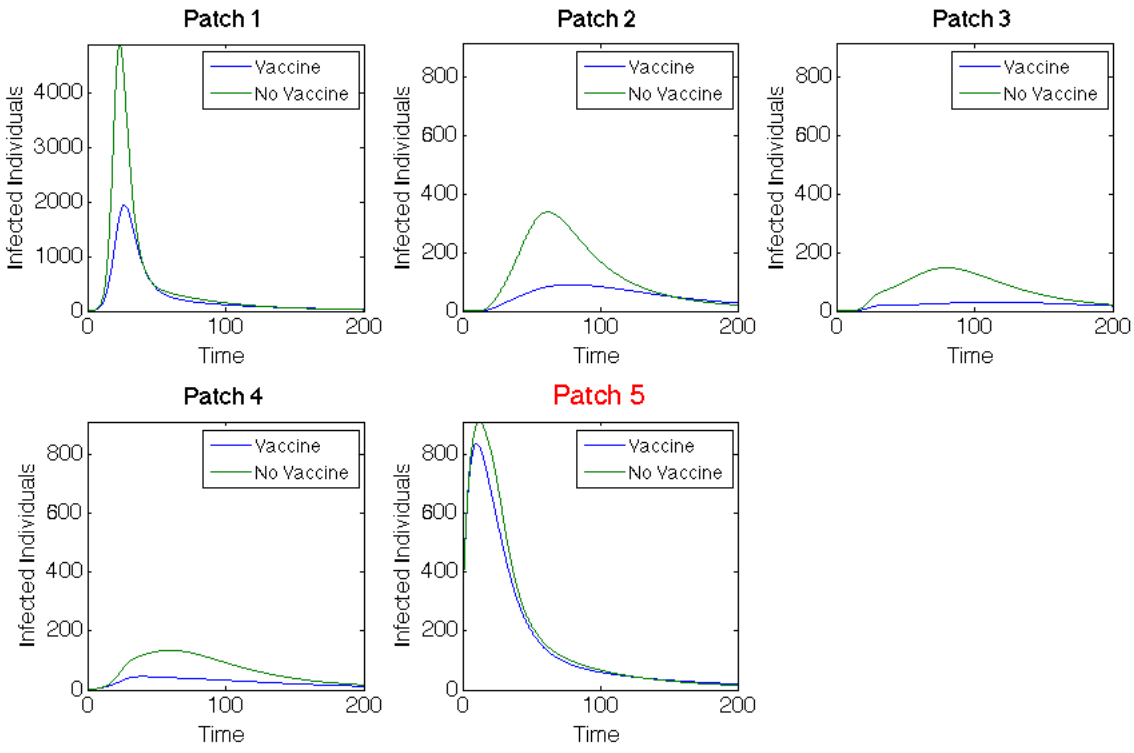

Figure B.5: Hub Patch 1 Arrangement: Infected population dynamics comparison with and without vaccination with outbreak in Patch 5

Table B.1: Hub Patch 3 Arrangement: The basic reproduction number for network and for each patch

Network $\mathbf{R}_0$		Patch 1	Patch 2	Patch 3 (Hub)	Patch 4	Patch 5
13.1942		2.9409	2.9409	17.6457	2.9409	2.9409

Table B.2: Hub Patch 3 Arrangement: Objective functional values for each scenario

Outbreak Patch		J($\mathbf{v}$) (w Vaccine)
1		185,725
2		187,217
3		188,461
4		179,717
5		176,902

B.3 Hub Patch 3 Spatial Arrangement Results

We now consider the hub in the center of the river arrangement in Patch 3 and find optimal vaccination results for the cases when the outbreak occurs in the either Patch 1, 3, or 5 of the metapopulation. The basic reproduction number of each patch in each of the five scenarios with Patch 3 as the hub are recorded in Table B.1. For each scenario, the objective functional values, the total infected with and without vaccination, and the total vaccinated in each patch and metapopulation are listed in Tables B.2, B.3, and B.4. Results for when the outbreak occurs within the hub patch are shown in Figure B.8. Results for when the outbreak occurs outside the hub patch are shown in Figures B.11 and B.14.

Table B.3: Hub Patch 3 Arrangement: Total number of infected individuals in metapopulation, with and without vaccine

Outbreak Patch		Total Infecteds (w/o Vaccine)	Total Infecteds (with Vaccine)
1		196,666	121,298
2		194,466	135,631
3		190,856	158,215
4		191,729	122,275
5		191,485	114,260

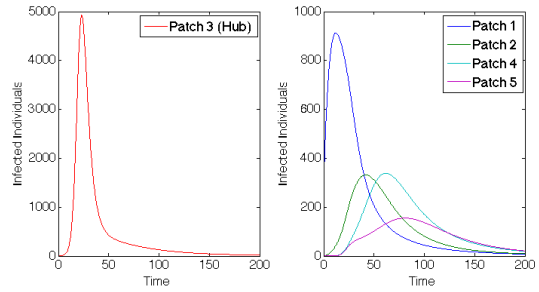

(a) Outbreak in Patch 1

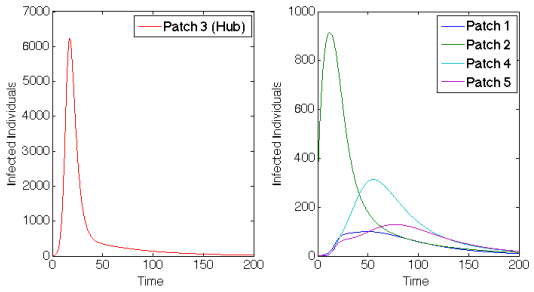

(b) Outbreak in Patch 2

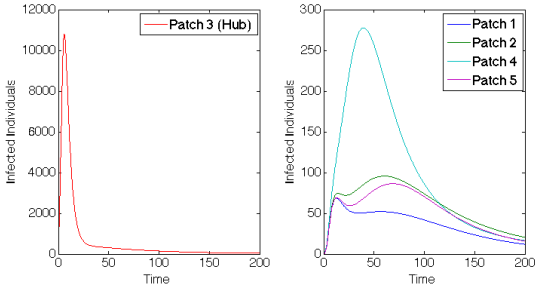

(c) Outbreak in Patch 3

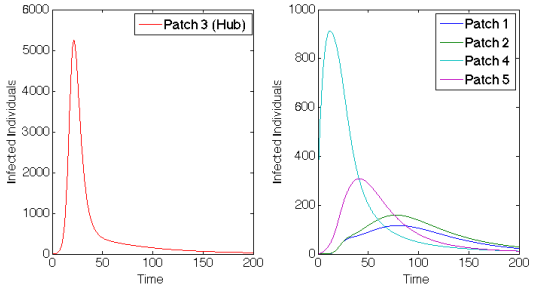

(d) Outbreak in Patch 4

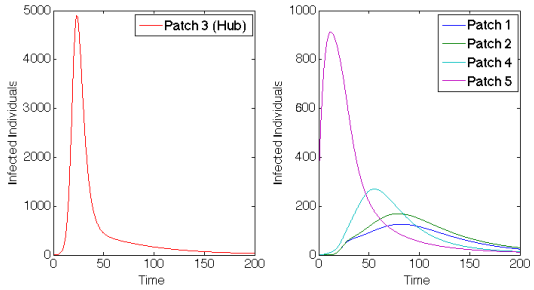

(e) Outbreak in Patch 5

Figure B.6: Hub Patch 3 Arrangement: Infected population dynamics when outbreak occurs in each of the five patches (without vaccination), where plot on left is the hub only, plot on right is surrounding patches

Table B.4: Hub Patch 3 Arrangement: Total individuals vaccinated in each patch for each scenario

		Patch 1	Patch 2	Patch 3	Patch 4	Patch 5	Total Vaccinated
Outbreak 1		714	2,530	8,240	3,380	2,700	17,564
Outbreak 2		2,071	682	6,097	2,809	2,460	14,120
Outbreak 3 (Hub)		1,336	1,555	1,960	1,597	1,751	8,198
Outbreak 4		2,394	2,612	7,666	698	2,437	15,806
Outbreak 5		2,506	2,729	8,359	2,875	736	17,206

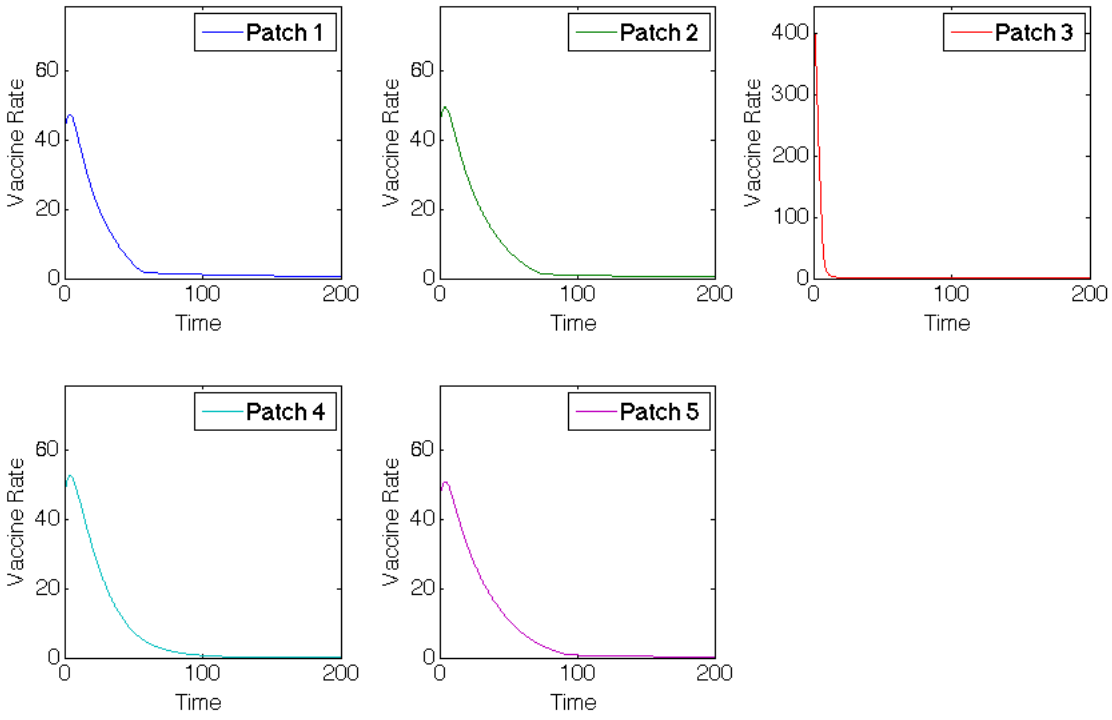

Figure B.7: Hub Patch 3 Arrangement: Vaccination rates of patches with outbreak in hub, Patch 3

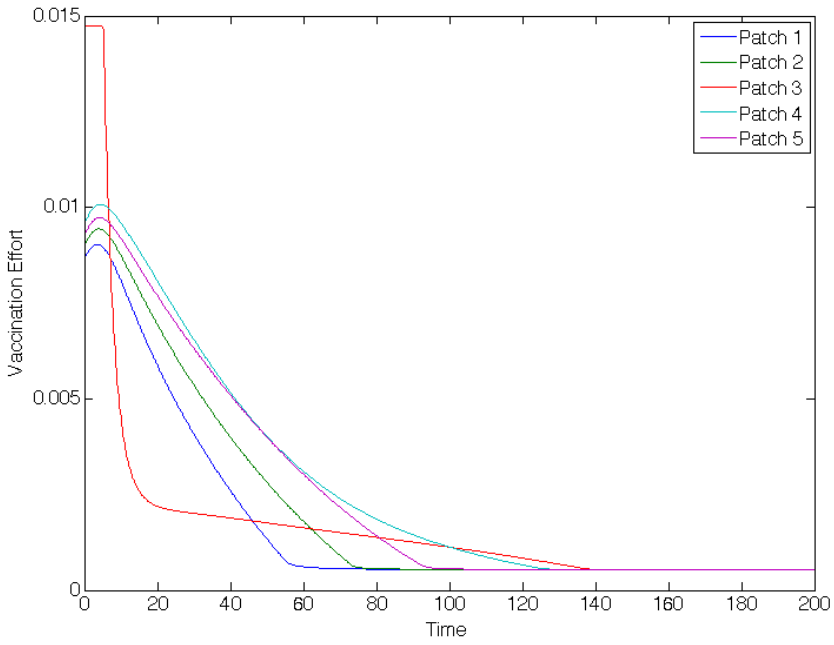

(a) Vaccination

Figure B.8: Hub Patch 3 Arrangement: Vaccination efforts of patches with outbreak in hub, Patch 3

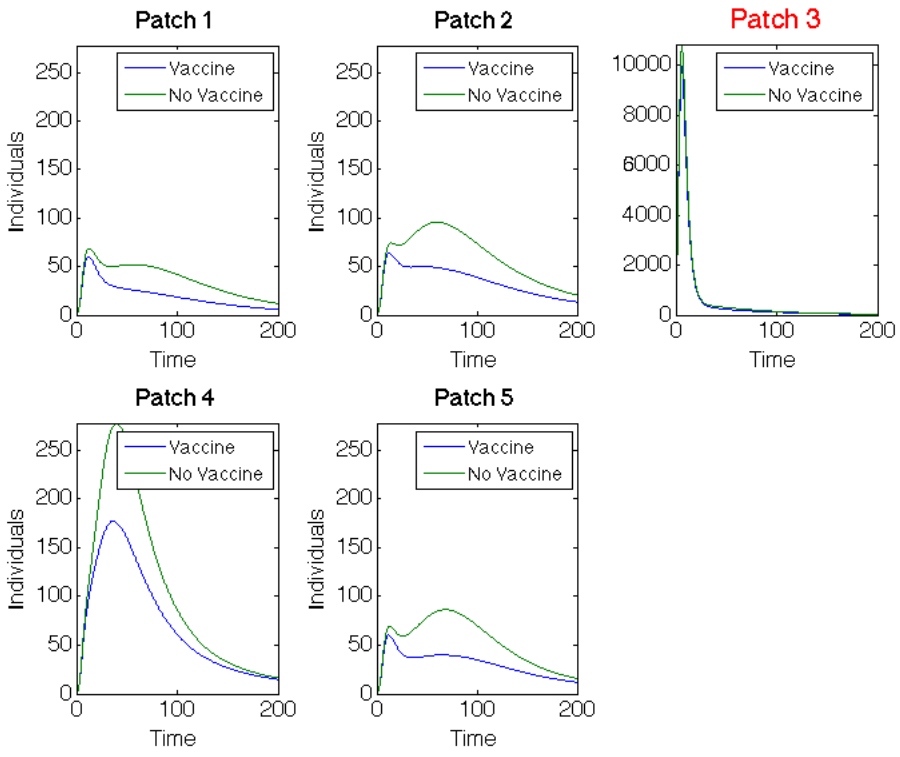

Figure B.9: Hub Patch 3 Arrangement: Infected population dynamics comparison with and without vaccination with outbreak in hub, Patch 3

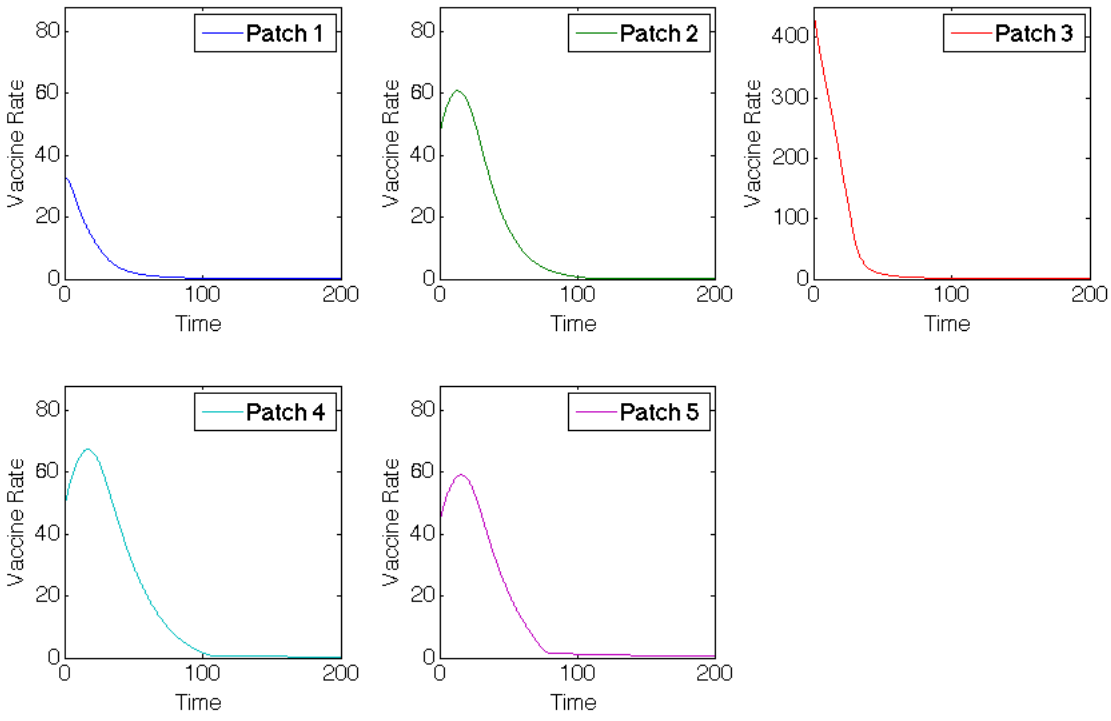

Figure B.10: Hub Patch 3 Arrangement: Vaccination rates of patches with outbreak in Patch 1

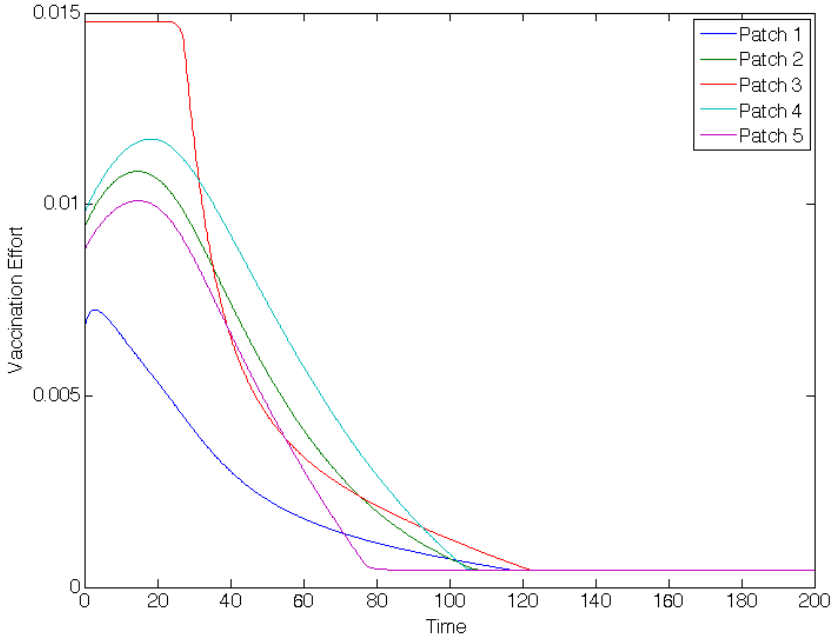

(a) Vaccination

Figure B.11: Hub Patch 3 Arrangement: Vaccination efforts of patches with outbreak in Patch 1

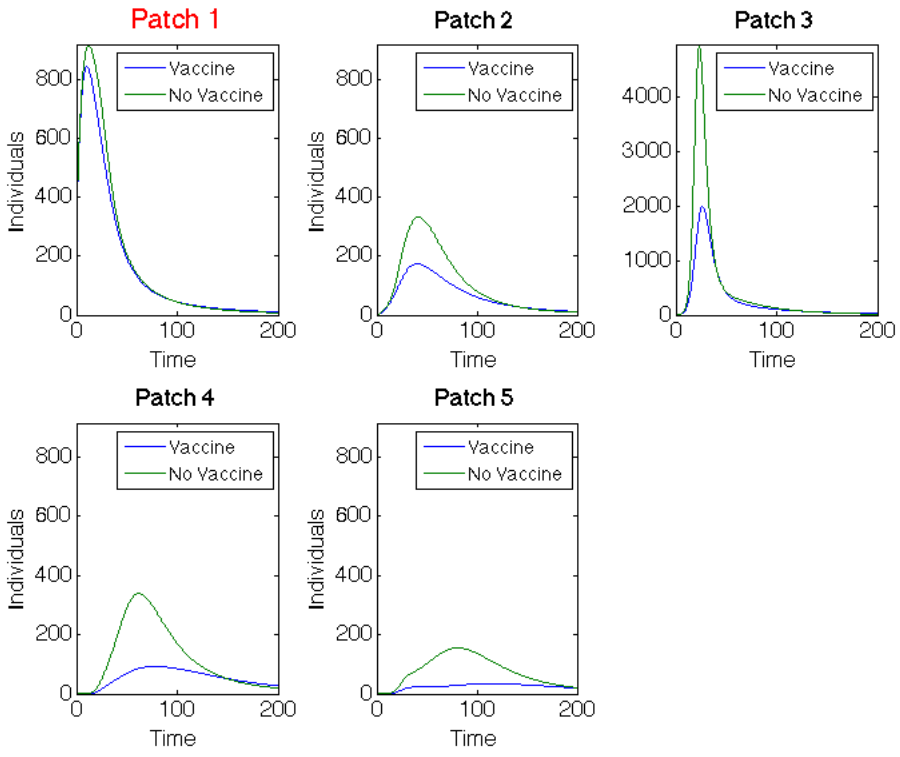

Figure B.12: Hub Patch 3 Arrangement: Infected population dynamics comparison with and without vaccination with outbreak in Patch 1

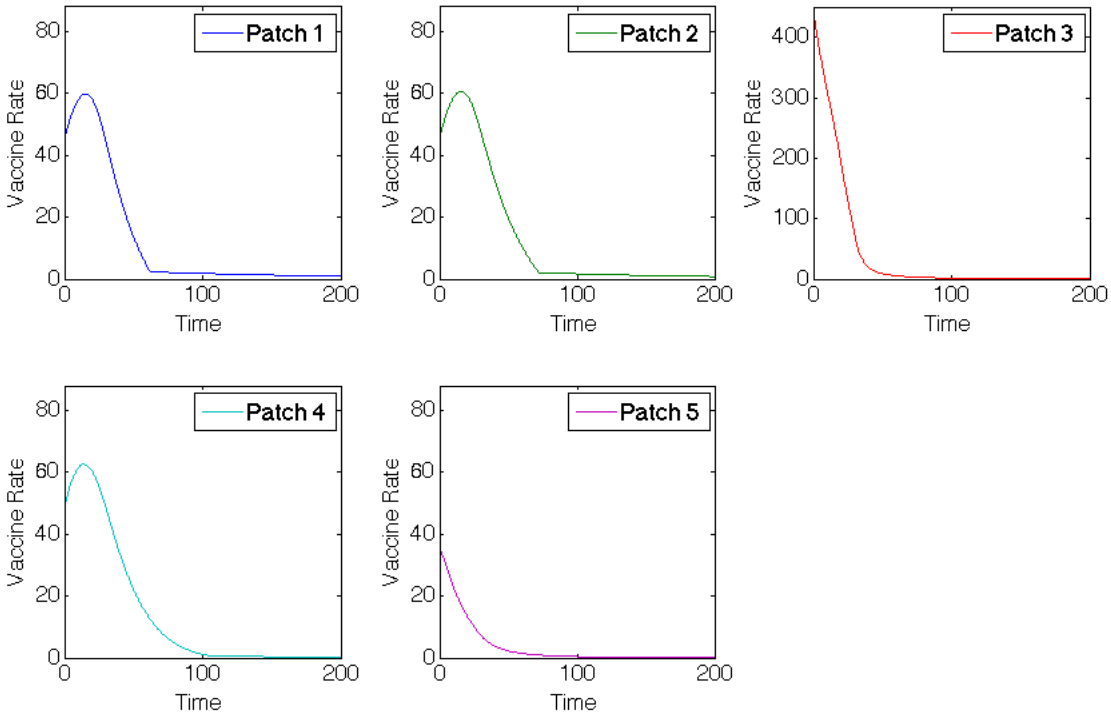

Figure B.13: Hub Patch 3 Arrangement: Vaccination rates of patches with outbreak in Patch 5

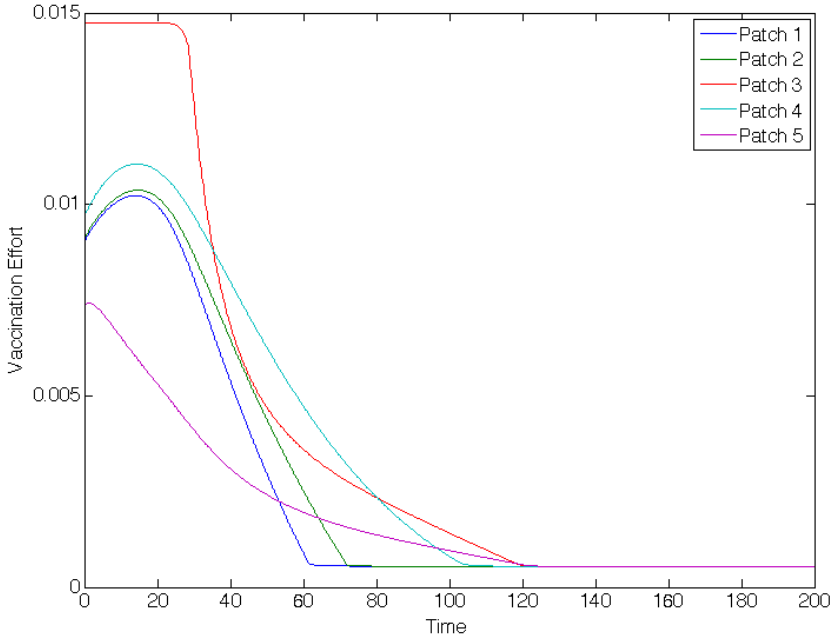

(a) Vaccination

Figure B.14: Hub Patch 3 Arrangement: Vaccination efforts of patches with outbreak in Patch 5

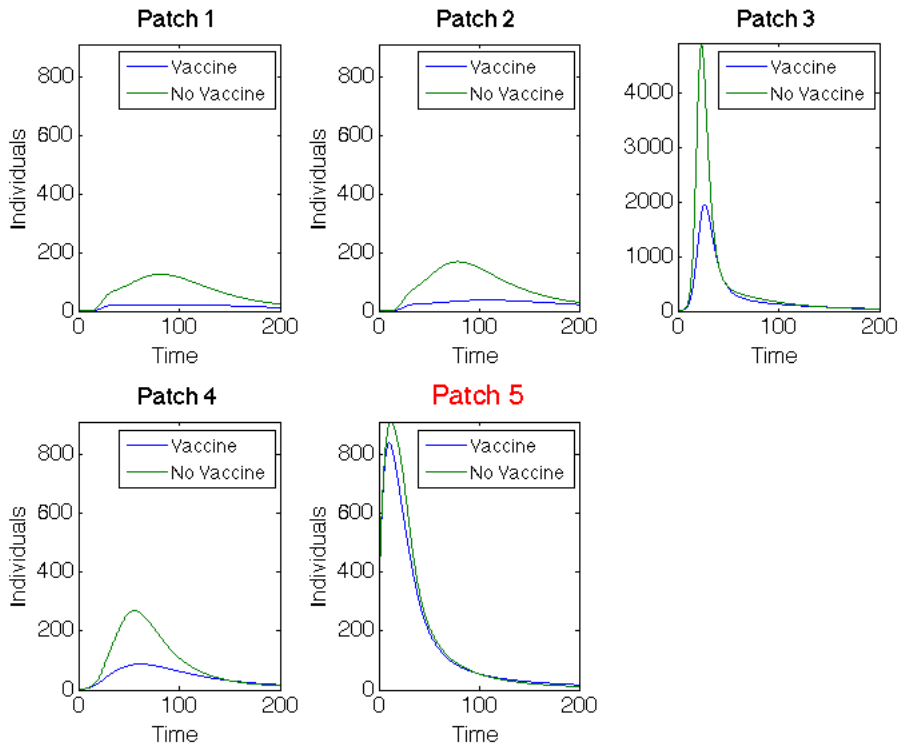

Figure B.15: Hub Patch 3 Arrangement: Infected population dynamics comparison with and without vaccination with outbreak in Patch 5

Table B.5: Hub Patch 5 Arrangement: The basic reproduction number for network and for each patch

Network $\mathbf{R}_0$		Patch 1	Patch 2	Patch 3	Patch 4	Patch 5 (Hub)
16.9561		2.9409	2.9409	2.9409	2.9409	17.6457

Table B.6: Hub Patch 5 Arrangement: Objective functional values for each scenario

Outbreak Patch		J($\mathbf{v}$) (w Vaccine)
1		183,062
2		185,465
3		181,259
4		178,730
5		180,139

B.4 Hub Patch 5 Spatial Arrangement Results

We now consider the hub at the bottom of the river arrangement in Patch 5. Again, we find the optimal vaccination results for when the outbreak occurs in Patches 1, 3, or 5 of the metapopulation. The basic reproduction number of each patch in each of the five scenarios with Patch 5 as the hub are recorded in Table B.5. For each scenario, the objective functional values, the total infected with and without vaccination, and the total vaccinated in each patch and metapopulation are listed in Tables B.6, B.7, and B.8. Results for when the outbreak occurs within the hub patch are shown in Figure B.18. Results for when the outbreak occurs outside the hub patch are shown in Figures B.21 and B.24.

Table B.7: Hub Patch 5 Arrangement: Total number of infected individuals in metapopulation, with and without vaccine

Outbreak Patch		Total Infecteds (w/o Vaccine)	Total Infecteds (with Vaccine)
1		194,093	117,927
2		194,486	122,223
3		191,824	121,276
4		187,749	130,151
5		182,855	151,731

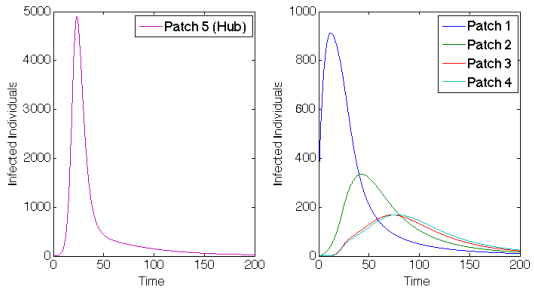

(a) Outbreak in Patch 1

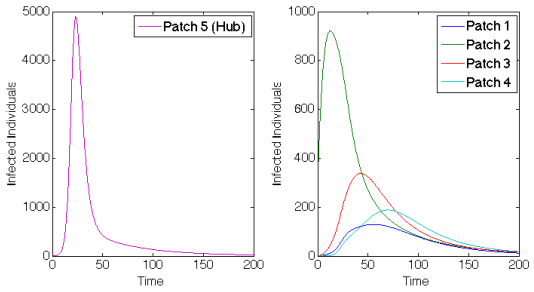

(b) Outbreak in Patch 2

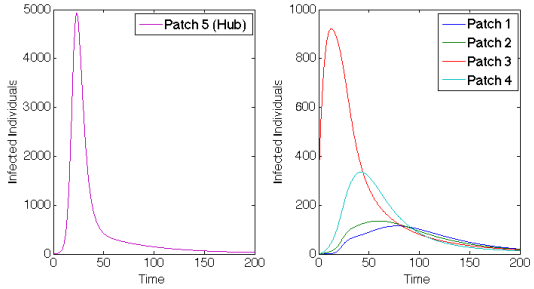

(c) Outbreak in Patch 3

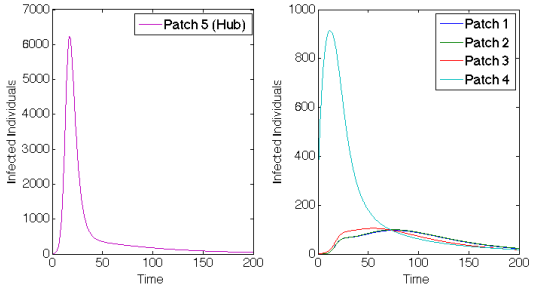

(d) Outbreak in Patch 4

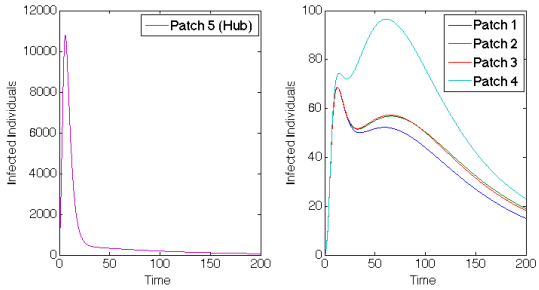

(e) Outbreak in Patch 5

Figure B.16: Hub Patch 5 Arrangement: Infected population dynamics when outbreak occurs in each of the five patches (without vaccination), where plot on left is the hub only, plot on right is surrounding patches

Table B.8: Hub Patch 5 Arrangement: Total individuals vaccinated in each patch for each scenario

		Patch 1	Patch 2	Patch 3	Patch 4	Patch 5	Total Vaccinated
Outbreak 1		765	2,891	3,116	2,699	8,249	17,719
Outbreak 2		2,483	855	2,804	2,932	8,186	17,259
Outbreak 3		2,252	2,691	842	2,535	8,153	16,472
Outbreak 4		2,105	2,194	2,287	705	6,115	13,406
Outbreak 5 (Hub)		1,313	1,437	1,477	1,578	1,998	7,804

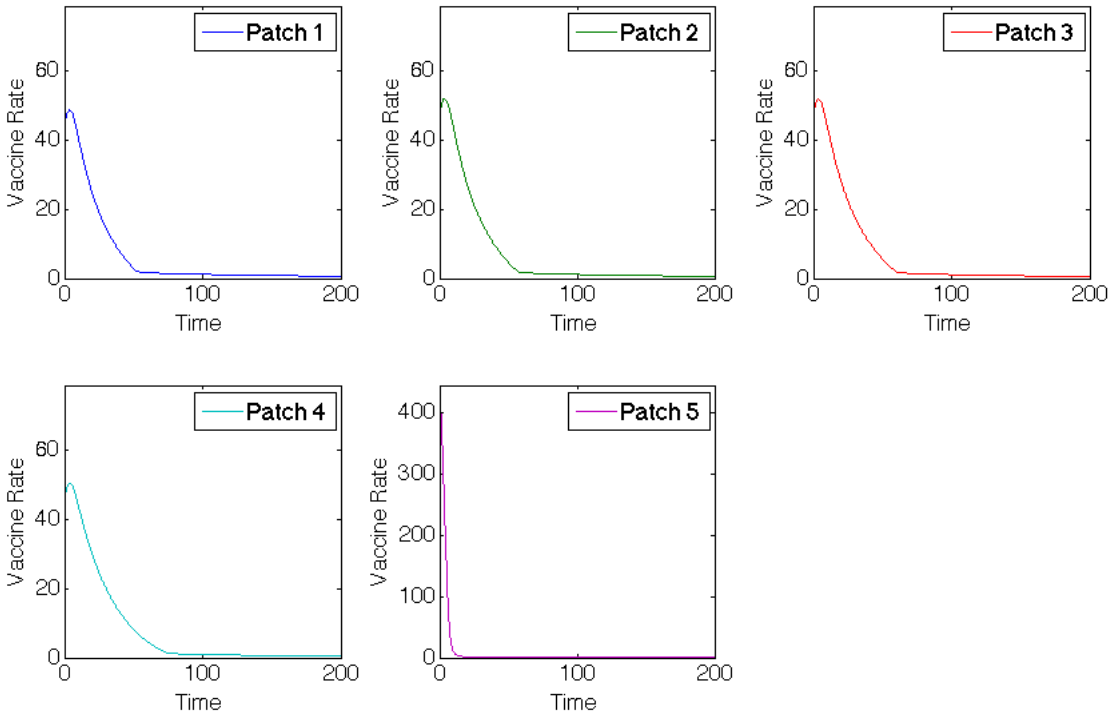

Figure B.17: Hub Patch 5 Arrangement: Vaccination rates of patches with outbreak in hub, Patch 5

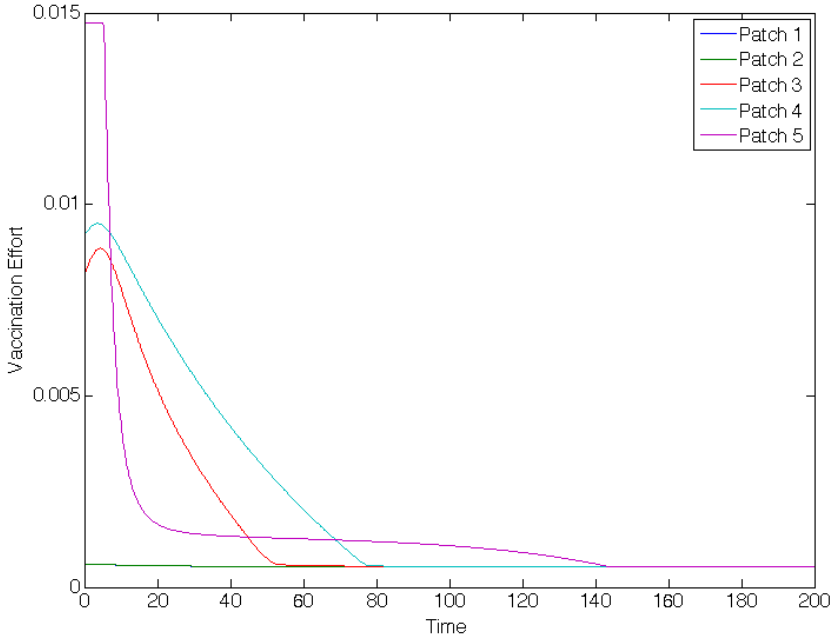

(a) Vaccination

Figure B.18: Hub Patch 5 Arrangement: Vaccination efforts of patches with outbreak in hub, Patch 5

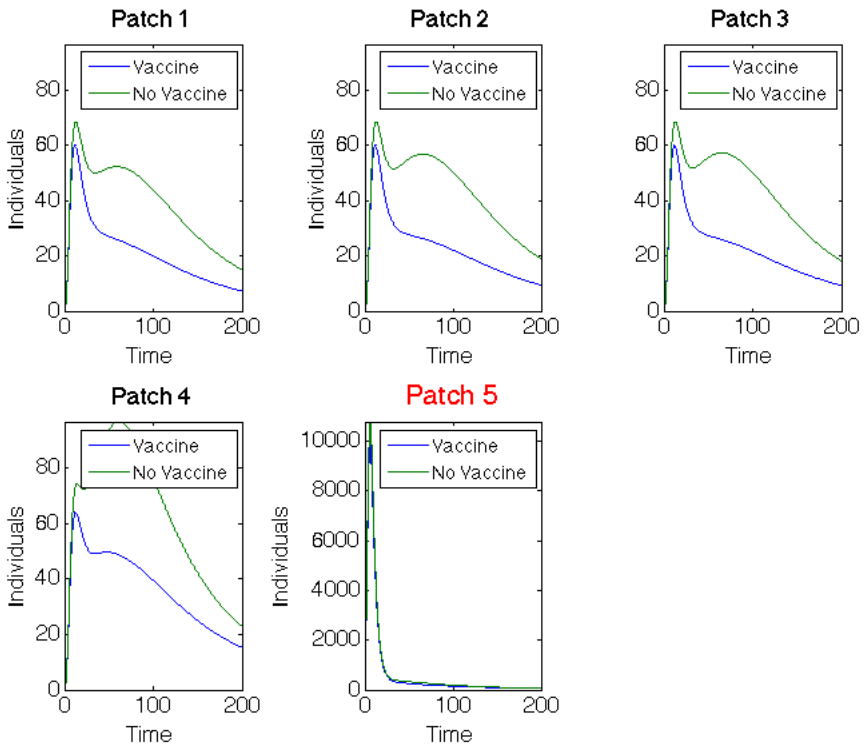

Figure B.19: Hub Patch 5 Arrangement: Infected population dynamics comparison with and without vaccination with outbreak in hub, Patch 5

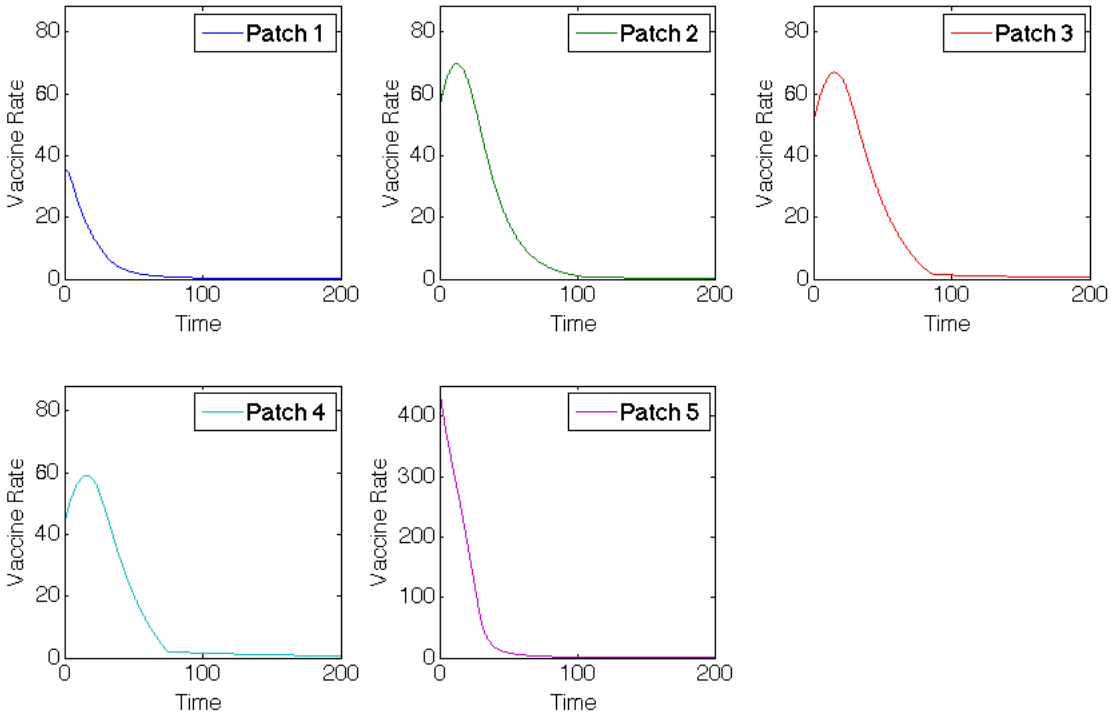

Figure B.20: Hub Patch 5 Arrangement: Vaccination rates of patches with outbreak in Patch 1

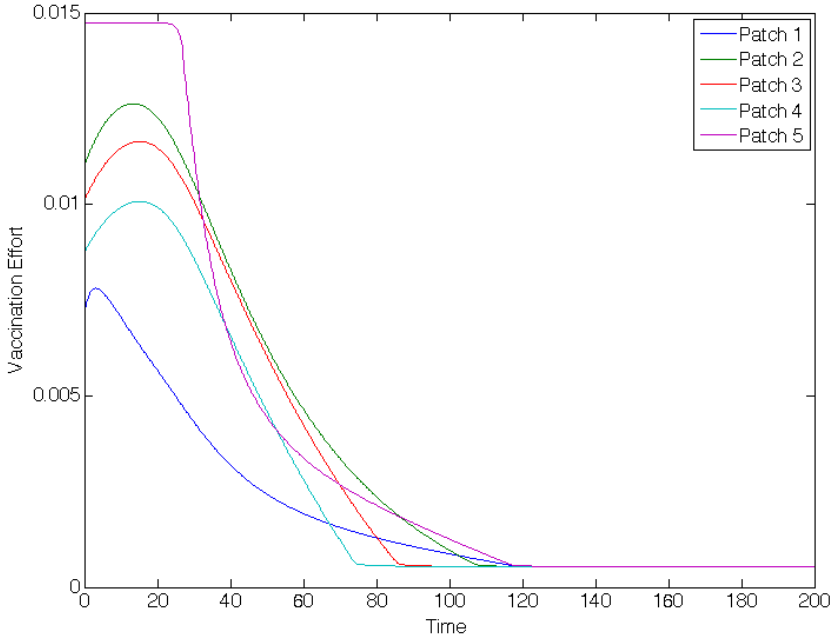

(a) Vaccination

Figure B.21: Hub Patch 5 Arrangement: Vaccination efforts of patches with outbreak in Patch 1

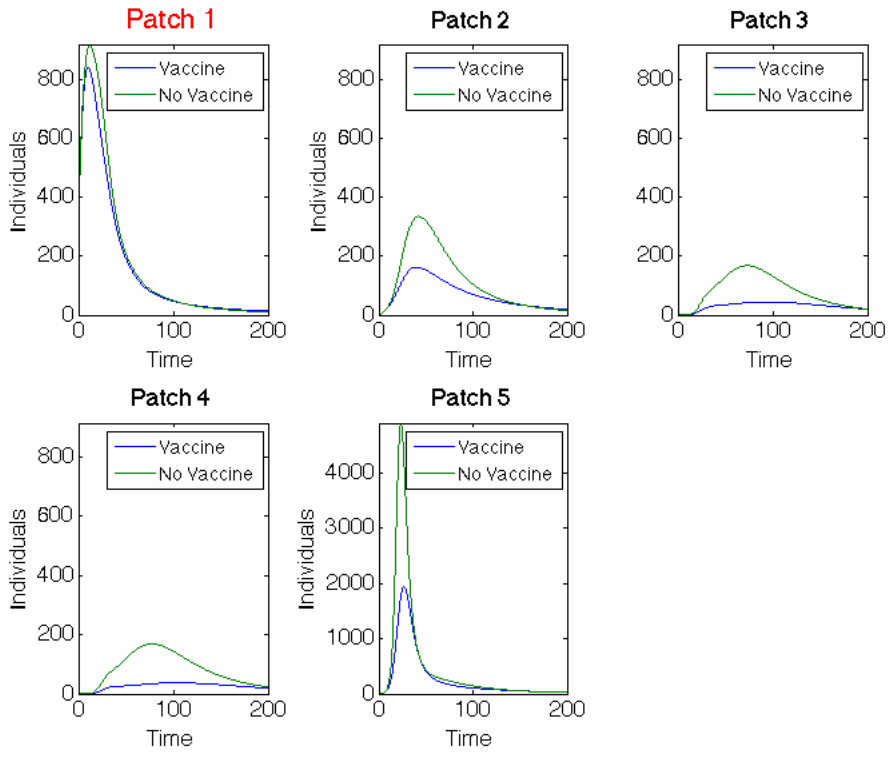

Figure B.22: Hub Patch 5 Arrangement: Infected population dynamics comparison with and without vaccination with outbreak in Patch 1

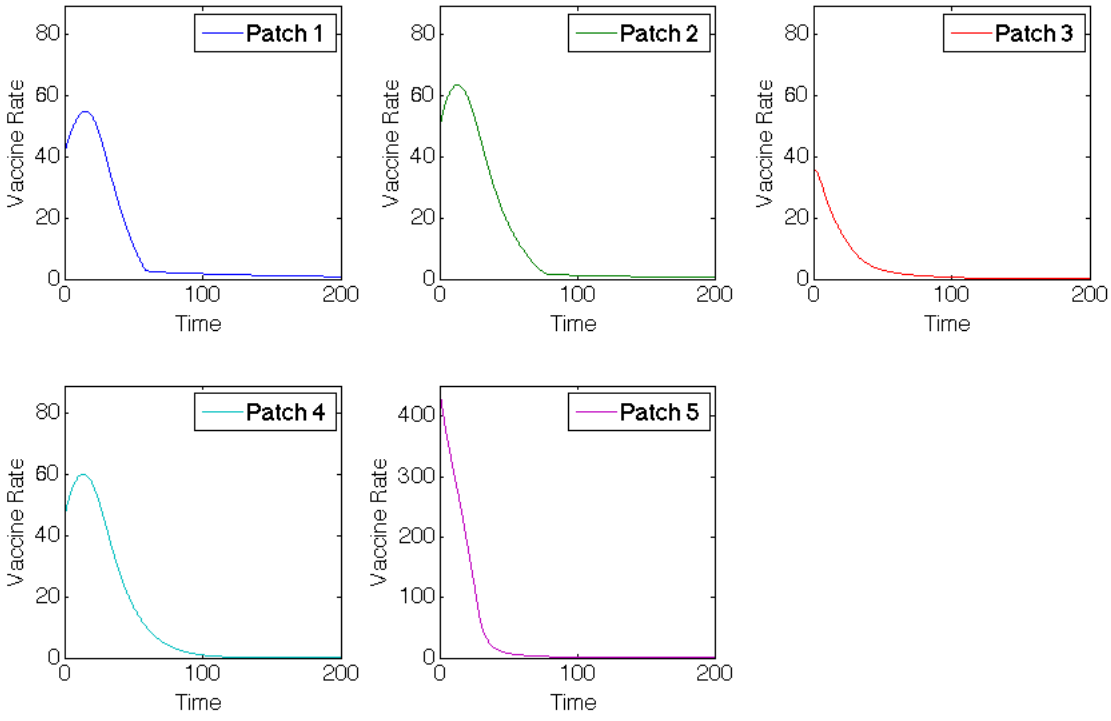

Figure B.23: Hub Patch 5 Arrangement: Vaccination rates of patches with outbreak in Patch 3

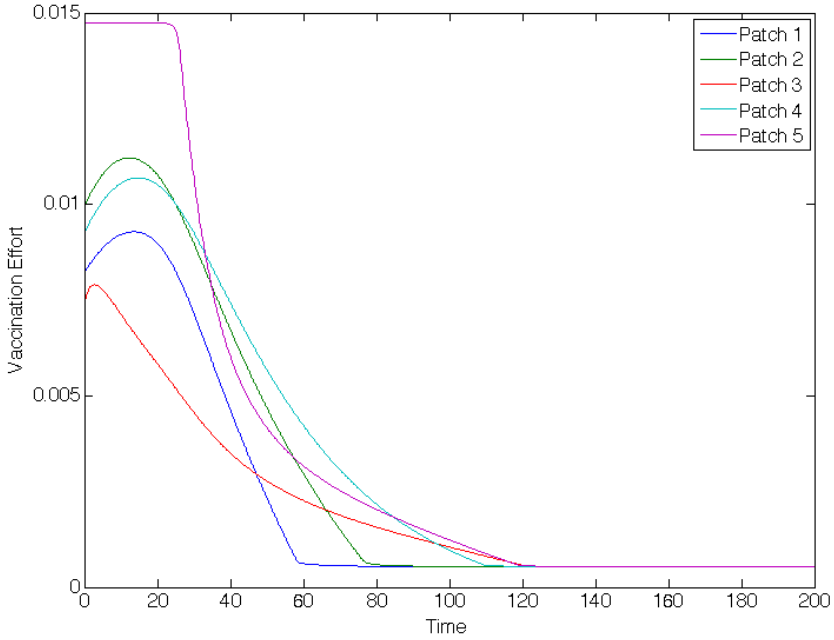

(a) Vaccination

Figure B.24: Hub Patch 5 Arrangement: Vaccination efforts of patches with outbreak in Patch 3

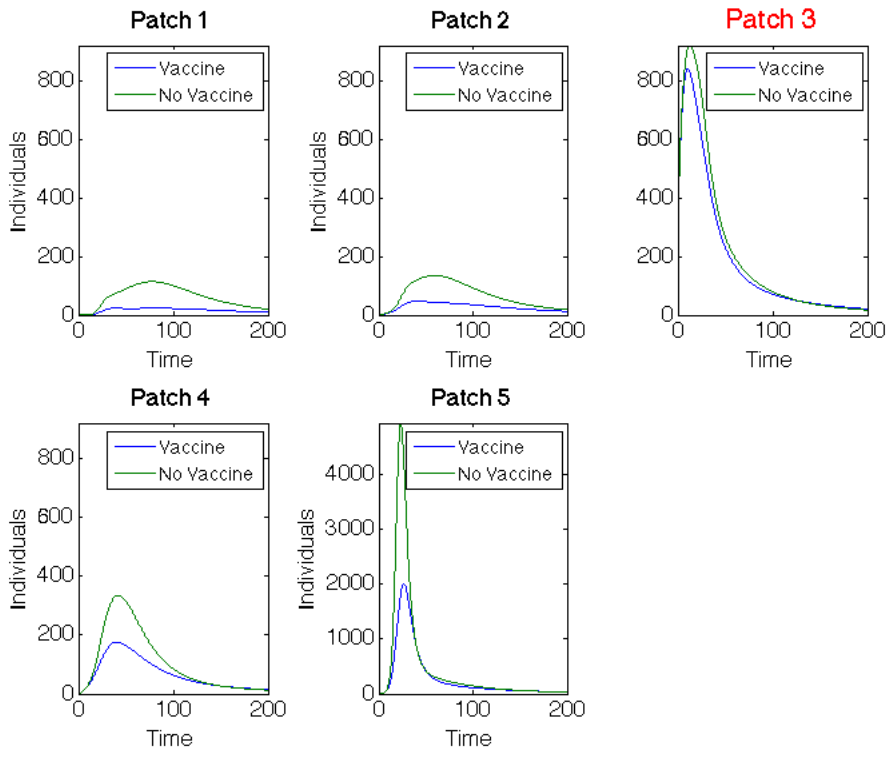

Figure B.25: Hub Patch 5 Arrangement: Infected population dynamics comparison with and without vaccination with outbreak in Patch 3

B.5 Additional Hub Size Comparison Results

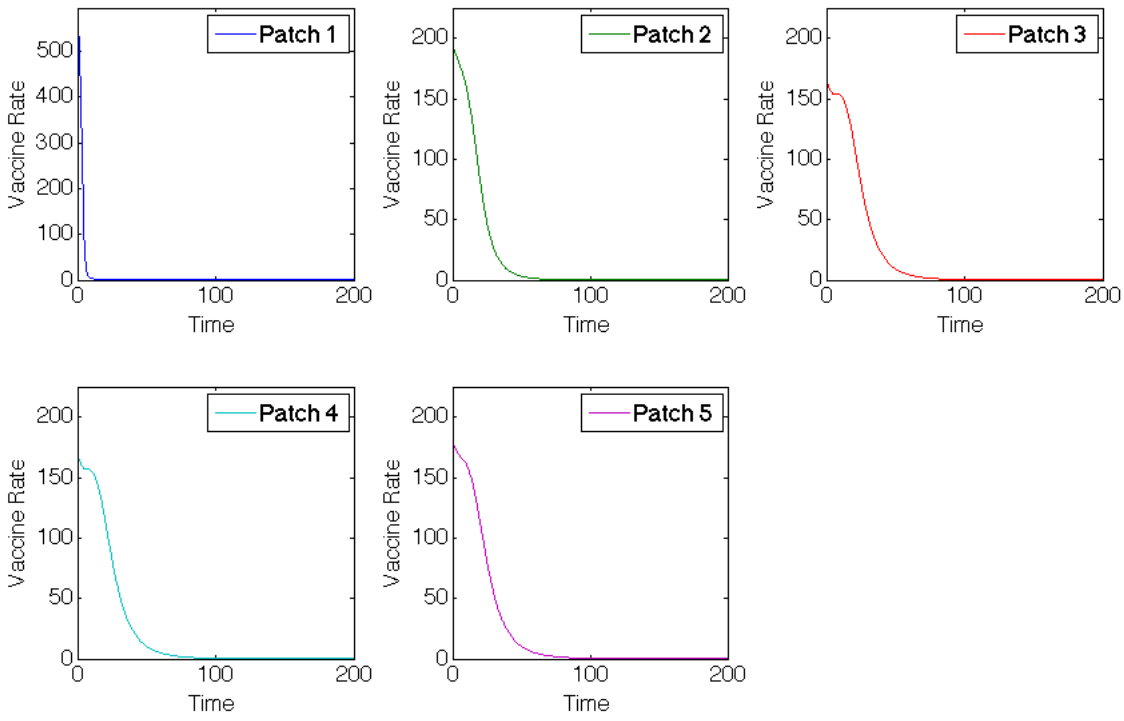

Figure B.26: Hub Patch 1 Arrangement (with 40,000 Individuals): Vaccination rates for patches when outbreak occurs in hub, Patch 1

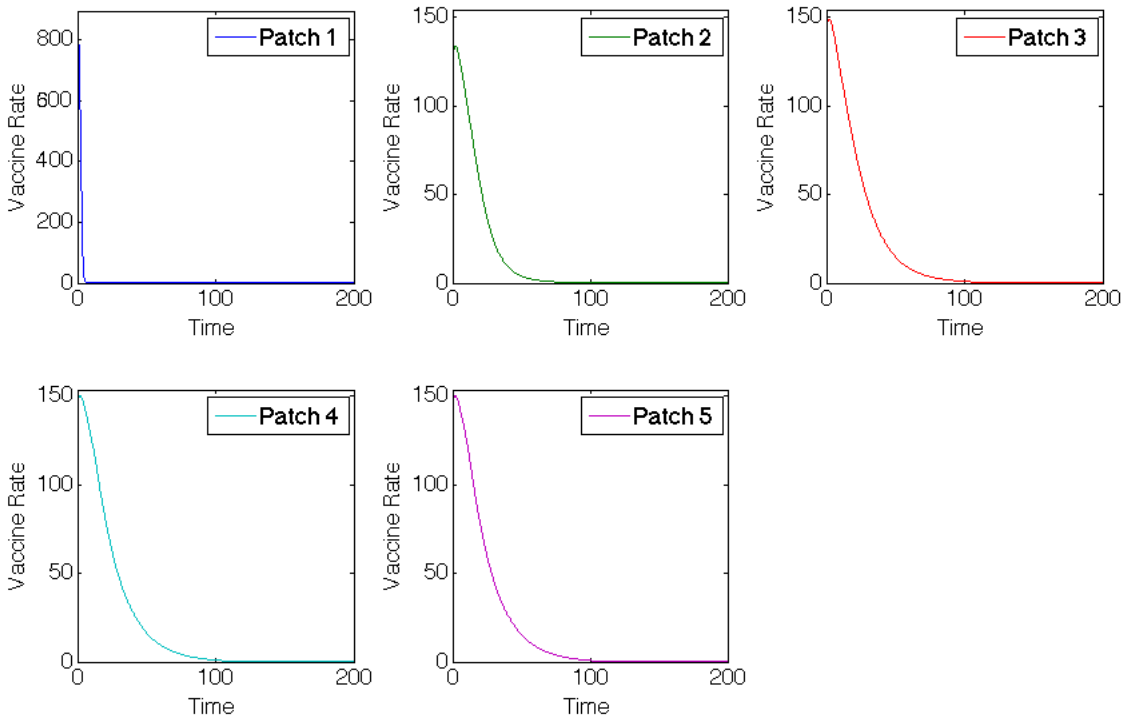

Figure B.27: Hub Patch 1 Arrangement (with 60,000 Individuals): Vaccination rates for patches when outbreak occurs in hub, Patch 1

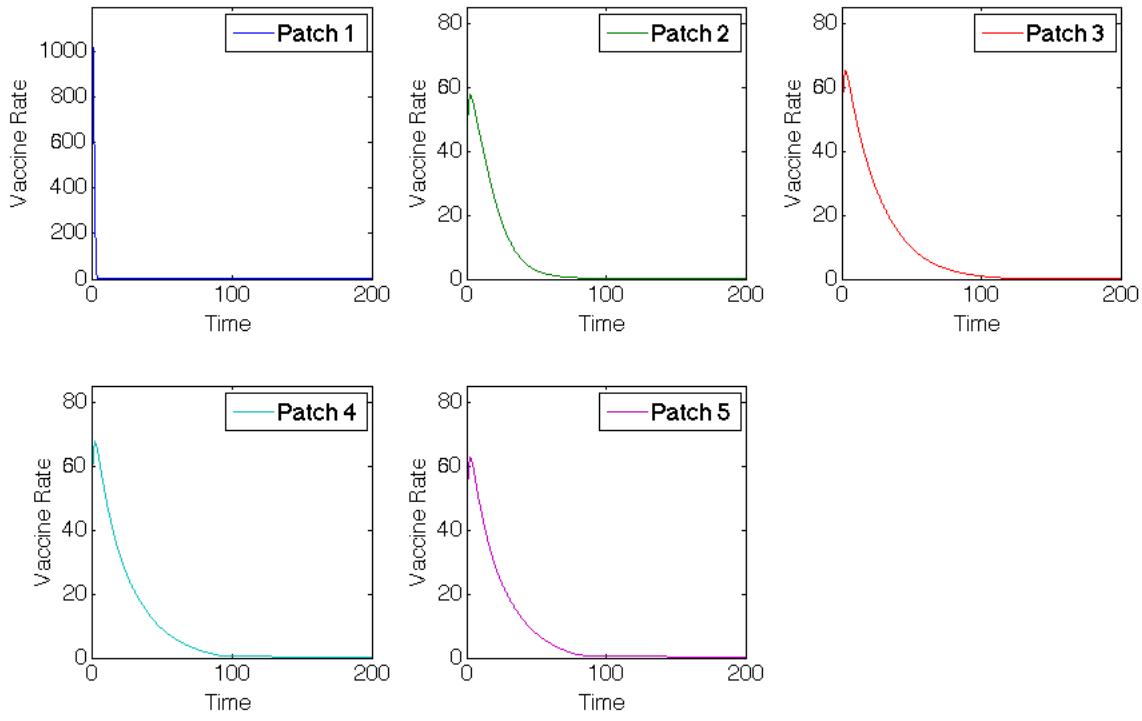

Figure B.28: Hub Patch 1 Arrangement (with $80,000$ Individuals): Vaccination rates for patches when outbreak occurs in hub, Patch 1

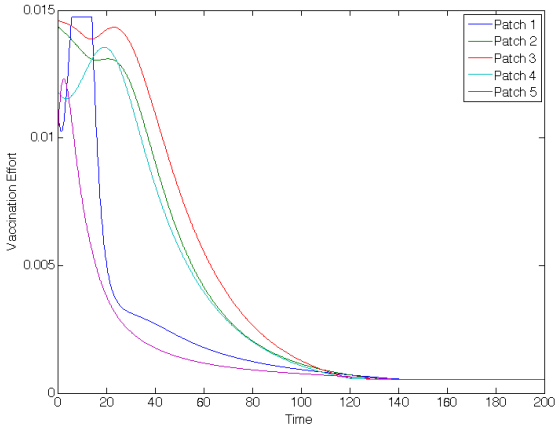

(a) Hub Patch 1 - Hub 40,000 - Vaccine

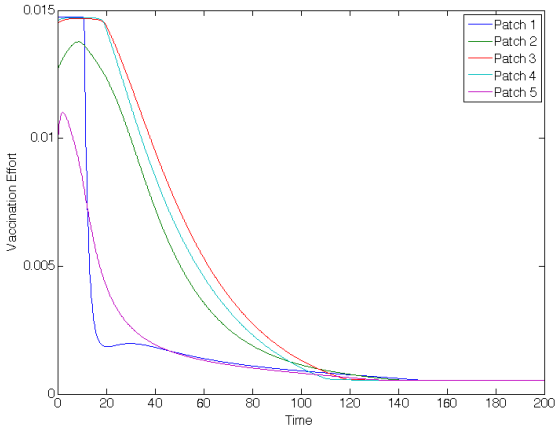

(b) Hub Patch 1 - Hub 60,000 - Vaccine

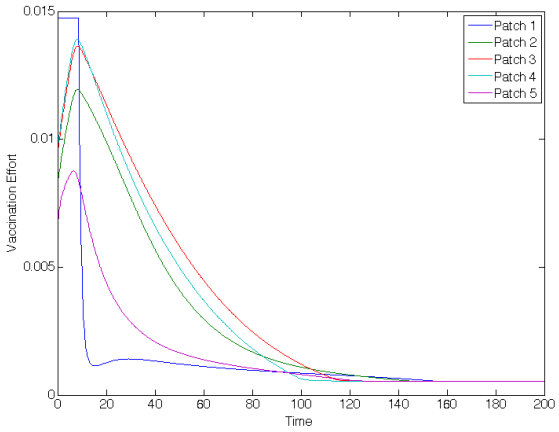

(c) Hub Patch 1 - Hub 80,000 - Vaccine

Figure B.29: Hub Patch 1 Arrangement: Comparison of vaccination effort of metapopulation with varying hub sizes with outbreak in Patch 5

Table B.9: Hot Spot Patch 5: Basic reproduction number for network and for each patch

Network $\mathbf{R}_0$	Patch 1	Patch 2	Patch 3	Patch 4	Patch 5 (HS)
8.6854	5.8819	5.8819	5.8819	5.8819	8.8428

B.6 Additional Linear Spatial Arrangements with Hot Spot Results

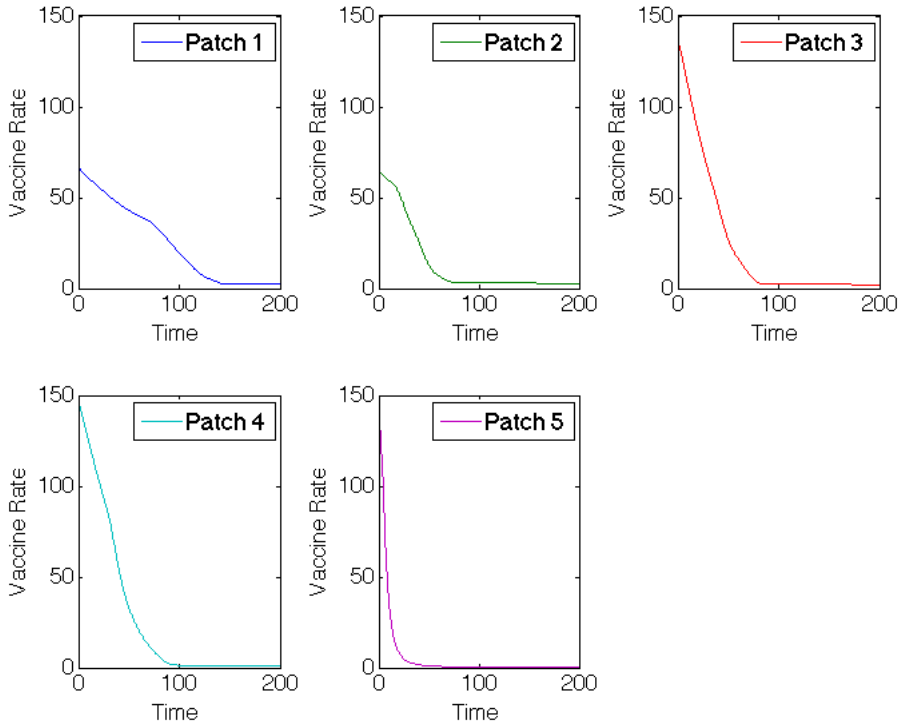

Figure B.30: Hot Spot Patch 1 Arrangement: Vaccination rates for patches in linear arrangement with outbreak in Patch 5

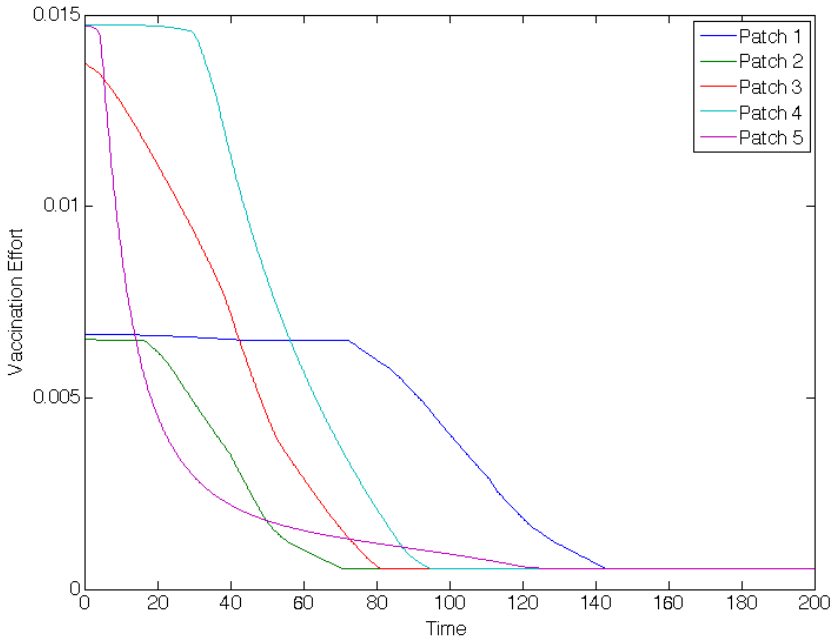

(a) Vaccination

Figure B.31: Hot Spot Patch 1 Arrangement: Vaccination effort for linear arrangement with outbreak in Patch 5

Table B.10: Hot Spot Patch 5: Objective functional values for each scenario

Outbreak Patch		J(**v**) (w Vaccine)
1		169,002
2		181,531
3		174,277
4		153,425
5		124,971

Table B.11: Hot Spot Patch 5: Total number of infected individuals in metapopulation, with and without vaccine

Outbreak Patch	Total Infecteds (w/o Vaccine)	Total Infecteds (with Vaccine)
1	197,920	77,938
2	198,261	93,233
3	196,316	101,437
4	191,601	92,260
5	181,883	64,590

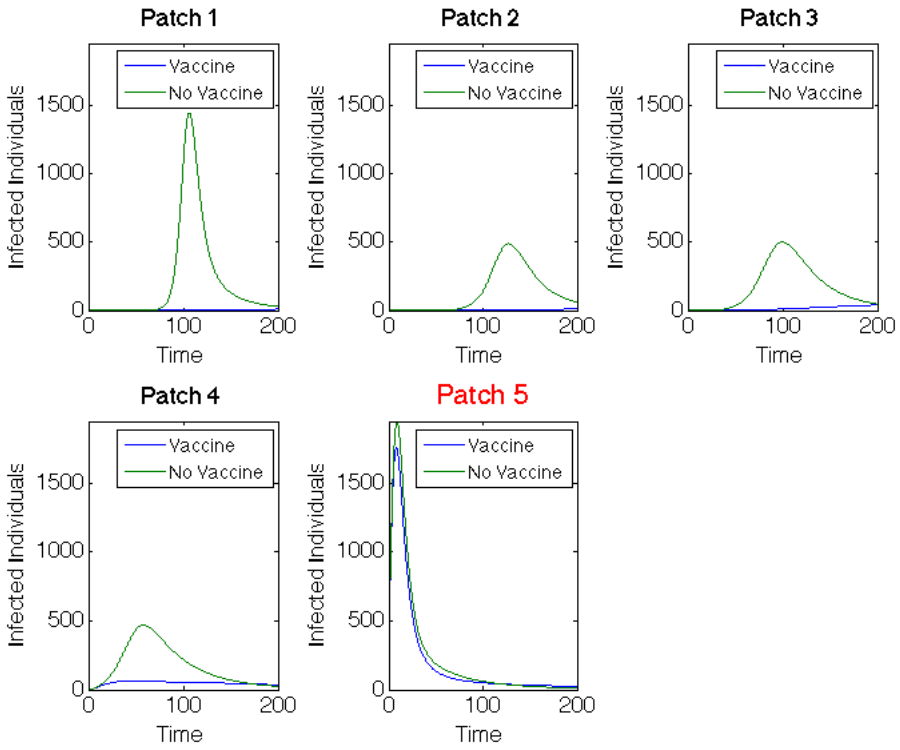

Figure B.32: Hot Spot Patch 1 Arrangement: Infected population dynamics comparison with and without vaccination with outbreak in Patch 5

Table B.12: Hot Spot Patch 5: Total individuals vaccinated in each patch for each scenario

		Patch 1	Patch 2	Patch 3	Patch 4	Patch 5	Total Vaccinated
Outbreak 1		1,178	4,513	6,260	5,764	6,282	23,997
Outbreak 2		4,609	1,293	4,434	6,030	6,749	23,114
Outbreak 3		4,194	5,287	1,283	3,989	4,744	19,497
Outbreak 4		2,781	5,237	5,351	1,262	2,016	16,646
Outbreak 5 (HS)		1,298	4,004	5,341	5,170	745	16,557

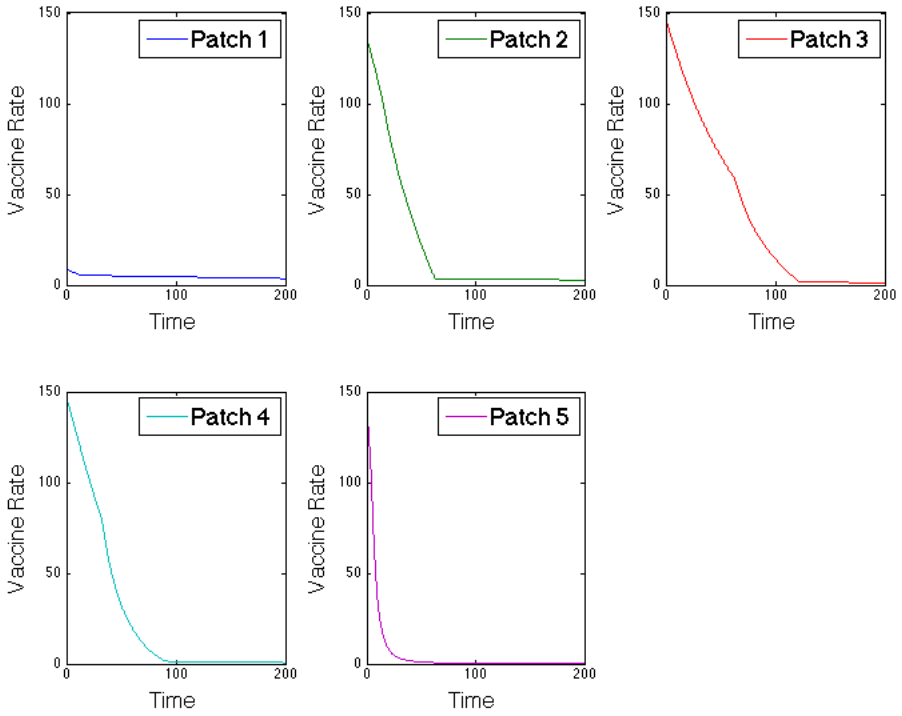

Figure B.33: Hot Spot Patch 3 Arrangement: Vaccination rates for patches in linear arrangement with outbreak in Patch 5

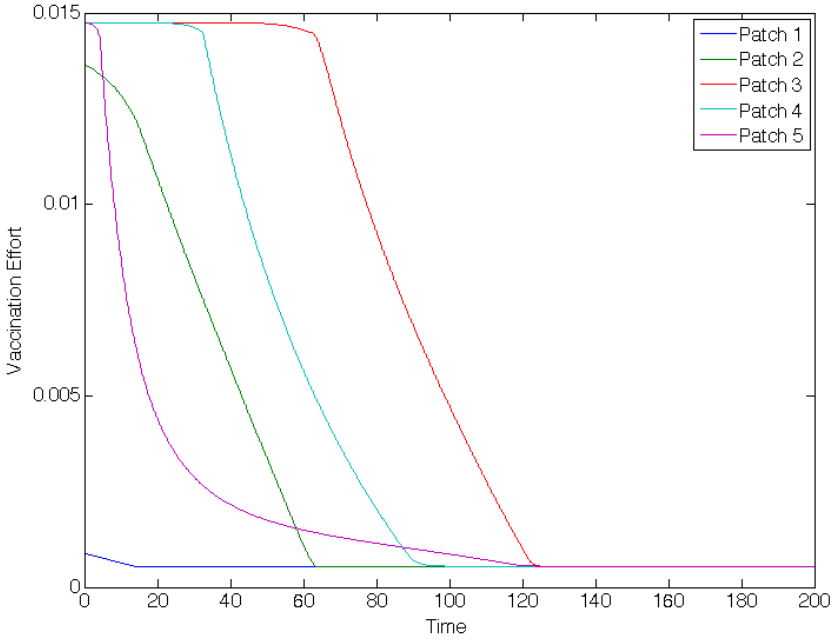

(a) Vaccination

Figure B.34: Hot Spot Patch 3 Arrangement: Vaccination effort for linear arrangement with outbreak in Patch 5

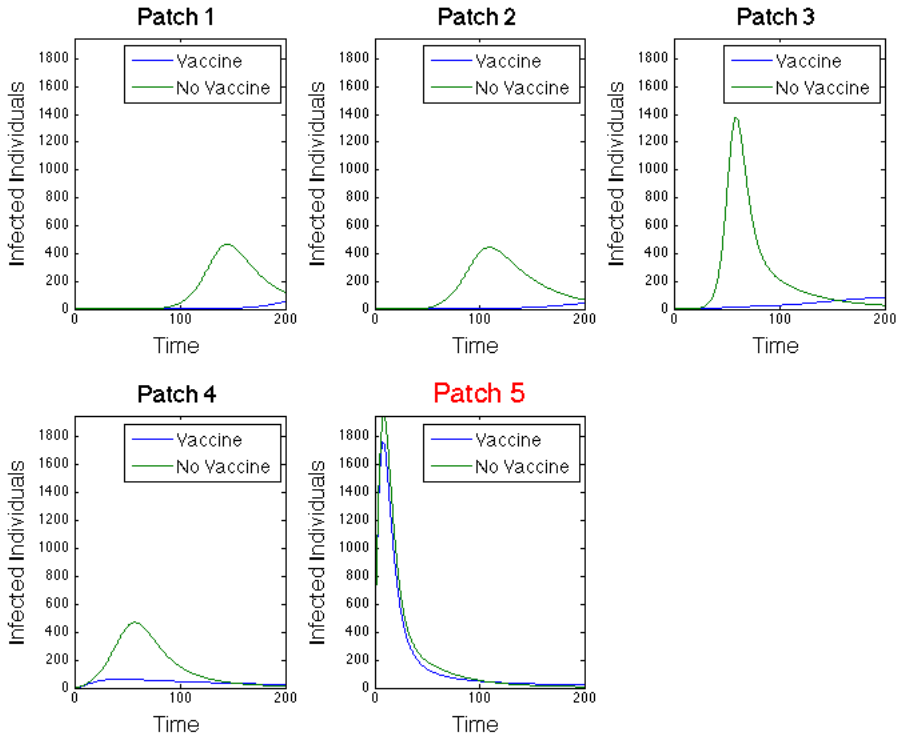

Figure B.35: Hot Spot Patch 3 Arrangement: Infected population dynamics comparison with and without vaccination with outbreak in Patch 5

Vita

Michael Robert Kelly, Jr. was born in Meadowbrook, Pennsylvania, on November 9, 1985. He is the only son of Michael and Linda Kelly. After graduating from Bishop McDevitt High School in 2004, he went on to Franklin and Marshall College in Lancaster, Pennsylvania where he studied mathematics. He received his Bachelor of Arts in May 2008.

In August 2008, Michael began his graduate career at the University of Tennessee, Knoxville, in the Department of Mathematics. From January 2009 to August 2013, Michael was supported by a graduate teaching assistantship from the Department of Mathematics. He was awarded a graduate research fellowship from the National Institute for Mathematical and Biological Synthesis, which supported his graduate studies from August 2013 to July 2014. Michael graduated in August 2014 with his Ph.D. in Mathematics with a concentration in Mathematical Ecology.

Michael Robert Kelly, Jr. will continue his work in mathematical biology and in teaching mathematics as a postdoctoral researcher in the Department of Mathematics at the Ohio State University, in Columbus, Ohio.